CRANFIELD UNIVERSITY
COLLEGE OF AERONOUTICS
Ph.D THESIS

Academic Year 1993/94

Jian Shi

Fully Discrete High Resolution Schemes for Systems of Conservation Laws

Supervisor: E.F.Toro

September 1994

This thesis is submitted in partial submission for the degree of Doctor of Philosophy

Abstract

Effective and robust high resolution schemes are of vital importance for simulation of viscous and inviscid flows. Since second-order high resolution schemes in practice are inadquate for many applications, large efforts have been put towards developing higher-order accurate schemes in the past. Although some progress has been made, the efforts were frustrated by the lack of effective and robust new schemes. Therefore this thesis is aimed at challenging this difficult but very important issue.

Some new theories and methodologies were established during this research, which covers the linear stability analysis for high-order numerical schemes; the fully discrete techniques for model equations; the formulation of conservative high-order schemes and the high-order Total Variation Diminishing (TVD) schemes. According to these theories arbitrary-order high resolution schemes can be developed. To illustrate the methodologies second-, third-, fourth-, and 20th-order schemes are presented. These high resolution schemes were tested and validated by solving some popular test problems for one and two dimensional Euler and incompressible Navier-Stokes equations. The efficiency and robustness are the features of these high-order schemes.

Acknowledgements

I would like to express my sincere thanks to Dr. E. F. Toro, my supervisor, for his guidance during this work.

I would also like to thank Professor J. F. Clarke for his direction, advice, and discussions during the time when Dr. Toro was absent from the Cranfield.

Thanks also go to S. J. Billett for the frequent informal discussions between us, and to all those who helped me in this work.

Special thanks go to the College of Aeronautics who has partly granted me financial support for this study.

Finally, I would like to express my love to my wife and daughter for the support, encouragement and enjoyment they have given me throughout the years.

Contents

List of Figures

Chapter 1

Introduction

1.1 Introductory Remarks

At the present time the majority of unsolved problems in Fluid Dynamics are governed by nonlinear Partial Differential Equations (PDE) which are of three types: elliptic, hyperbolic and parabolic. Classification of the three types is determined by the features of the physical problems. Typical examples in Fluid Dynamics are Euler equations (hyperbolic) and Navier-Stokes equations (parabolic). Since analytical solutions of the most nonlinear PDEs are still not available, their solutions can only be treated by a numerical approach. As a consequence a new branch - Computational Fluid Dynamics (CFD) has been given great attention and growing very fast over last twenty years.

Over the same period the tremendous development of versatile and powerful computers now available are sufficiently advanced to deal with an almost limitless range of problems. All that is needed is to continue the development of accurate, reliable and effective numerical methods and to extend these methods to complex industrial design and analysis applications.

In the last two decades considerable progress has been achieved. In recent years CFD methods have been used to simulate the flow around extremely complicated configurations, such as flow over a complete aircraft [1], unsteady flow through turbomachinery [2], gas flow and combustion in a combustor [3] and many other equally complicated flows [4] - [9]. These achievements have given CFD a central role both in fluid dynamic design and

in scientific research.

Today we have already reached the stage at which CFD is in routine use in fluid dynamic design offices. This results in a great reduction of the design lead time and cost. As far as design time and cost are concerned, the integration of CFD into the design procedure has a significant impact on the success of a fluid dynamic associated industry, since nowadays more complex products, a shorter product life cycle and higher quality make manufacturing far more competitive than in the past, hence, a company must design products and get them to market faster and at lower cost without sacrifying quality.

In the field of scientific research, CFD provides an invaluable means for us to investigate and understand the complex flow features, especially, in the field in which experimental research is difficult, dangerous, or even impossible. For instance, the information given by the direct simulation of turbulent flows for moderate Reynolds numbers offers us a fundamental understanding of the turbulence nature [10].

All these evidences signals that CFD is reaching a mature stage.

1.2 Background Review

The area of CFD is very large indeed. Many real life situations when modelled mathematically give rise to fluid dynamical equations. Since the results obtained by numerical computations are used either in the scientific analysis or in the design process, great emphasis is placed on obtaining accurate results in a cost-effective manner.

In order to achieve this goal essentially two strategies can be adopted. One strategy employs grid adaptation techniques which are able to generate desired computational meshes in the regions of interest, so as to obtain the high resolution of the numerical solution. Another strategy is to develop so called *high resolution* methods. Distinguishing from the standard schemes which can not capture discontinuities properly, the high resolution methods can give satisfactory solutions not only for smooth flows but also for flows with strong gradients. We can expect that combination of the two techniques will give us the best resolution.

This thesis is aimed at investigating the latter strategy, high resolution schemes, for nonlinear systems of conservation laws. By definition high resolution methods have the following

essential characteristics: they are at least second-order accurate in smooth regions of the flow; they sharply resolve discontinuities without generating excessive smearing; they are free or nearly free of spurious oscillations in the computed solution.

The early developed numerical schemes did not satisfy the above properties. They were frustrated by the lack of the ability of simulating discontinuities, such as shock waves and contact discontinuities, without oscillations. However this ability is of significant importance in Fluid Dynamics since the appearance of various forms of discontinuities is a frequent and essential phenomenon of high-speed, low viscosity flows (typically inviscid flows). The physically possible discontinuities are: shocks, where all flow variables undergo a discontinuous variation; contact discontinuities and vortex sheets, across which no mass transfer takes place but where density as well as the tangential velocity may be discontinuous, although pressure and normal velocity remain continuous.

Nevertheless, in spite of the defficiencies, the early numerical methods made a considerable contribution to today's modern high resolution schemes. Among others it is worth mention two groups of early schemes. One group is the space-centered schemes; the other is the upwind schemes. The most important space-centered schemes are the second-order accurate schemes of the Lax-Wendroff family, due to the pioneering work of Lax and Wendroff [12] [13] [14] and the earlier work in the field by Richtmyer and Morton [15], MacCormark [16] [17], Lerat and Peyret [18], and Jameson et al. [19]. The uniqueness and its essential property of the Lax-Wendroff schemes lies in the combination of time and space-centered discretizations or full discretizations, therefore, the simplest schemes of second-order accuracy.

However, the second-order Lax-Wendroff schemes introduced oscillations in the vicinity of discontinuities. To prevent this the idea of *artificial viscosity* methods were developed first by von Neumann and Richtmyer [20] and then by the later developments of [19] [21] [22] and [23]. Although the artificial viscosity approach is easy to implement and can effectively remove the oscillations around discontinuities, usually shocks are over-smeared and even worse, contact discontinuities may be not captured at all. Since the satisfactory results of this approach heavily relied on a good judgement and empirical definition of the dissipation term, the popularity of the artificial viscosity methods is bound to loose its place and replaced by the upwind and centered TVD (Total Variation Diminishing) methods.

The group of upwind schemes can be traced back to as early as Courant et al. [24].

The most remarkable extension in the direction is (a) the flux vector splitting methods of Steger and Warming [25] and Van Leer [26]; (b) the Godunov-type methods originally introduced by Godunov [27] and later generated a series of good schemes based on approximate Riemann solvers, e.g. Engquist and Osher [28], Osher [29], Roe [30] [31] and Toro [32]. Differing from the space-centered schemes upwind schemes introduce the physical properties of the flow into the numerical model by considering the correct direction from which characteristic information propagates. The flux vector splitting methods introduce only information on the sign of the wave speeds, thereby the flux terms are split and discretized according to the sign of the associated propagation speeds. Our interest in the thesis is in development of the Godunov-type schemes.

In 1959, Godunov [27] presented a pioneer work in which he proposed a way to make use of the characteristic information within the framework of a conservative method. Although first-order in the first place the Godunov method has been extended to high order. The starting point in Godunov's method is the solution of the Riemann problem which can be computed exactly. This results in substantial information about the characteristic structure and leads to conservative methods. The drawback of the original Godunov method was inefficiency since Godunov's method requires the solution of Riemann problems at each cell boundary in each time step. In order to overcome this, the idea of efficient exact and approximate Riemann solvers was brought about, which results in a variety of Riemann solvers in the literature.

One of motivations behind the constructing upwind schemes was to prevent the creation of the notorious oscillations in the high-order numerical solutions. Unfortunately this is not true. Godunov [27] have theoretically proved that linear second-order schemes always produce oscillations. On the one hand the conclusion is really dispointing, but on the other hand it provokes a deeper and systematic research of the oscillation-free conditions required by a high-order scheme. This has generated some significant results, leading to a intrinsic understanding of the fundamental properties of the discretization and to the introduction of nonlinear components in the discretizations. The concept of nonlinear limiters first introduced by Boris and Book [35] and Van Leer [47] and later led to the important concept of Total Variation Diminishing schemes named by Harten [37]. These schemes labeled TVD were well generalized by Sweby [38] which characterize today's high resolution schemes.

1.3 The Objectives and Strategy

1.3.1 Problem Definition

As reviewed in the last section research into discontinuous nonlinear hyperbolic systems is difficult, not only by virtue of the complexity of the subject itself, but also because of the emergence of discontinuities or shocks with time evolution during wave propagation.

However difficult it is, a great deal of progress has been made over the last fifteen years since Godunov-type, shock-capturing methods were introduced. Presently, a variety of such second-order methods are available. In recent years, there have been large efforts in developing higher-order shock-capturing schemes since the second-order accurate methods are inadequate for considerable applications. A typical example is the direct simulation of turbulent flows which are of great interests in Fluid Dynamics [39]. In the past, efforts towards developing higher-order accurate methods were frustrated because of the lack of roubustness of the new schemes.

Essentially there are two techniques which can be used to construct high-order schemes: semi-discretization and full-discretization. In the approach of semi-discretization the space operators are discretized separately from the time differentials. This method also called the *method of lines* leads to a system of time dependent Ordinary Differential Equations (ODE) which can be discretized properly by a standard ODE solver. ENO (Essentially Non-oscillatory) schemes belong to this category [40] [41] [42].

Distinguishing from the semi-discretization the fully discrete technique combines the time and space discretizations in a single stage. This property makes Lax-Wendroff schemes very popular. However, the Lax-Wendroff schemes are only second-order accurate. Hence investigation of the fully discrete technique and derivation of higher-order, fully discrete, shock-capturing schemes for nonlinear systems of conservation laws are of both theoretical and practical importance in CFD. This leads to the objectives of the thesis.

1.3.2 The Objectives

Because two level, explicit numerical schemes are simple and easy to implement, this thesis will concentrate on developing two-level explicit schemes. The objectives of the

thesis, therefore, are to

- investigate fully discrete methodologies for linear scalar model equations, i.e. model advection equation and model advection-diffusion equation;
- generate some high-order (greater than second-order) fully discrete finite-difference schemes for the linear model equations;
- find a way to reformulate the finite-difference schemes to conservative forms of the Godunov-types;
- investigate a simple approach for linear stability analysis;
- investigate a high-order TVD theory and present high-order TVD schemes for the model equations;
- extend the high-order TVD schemes to nonlinear systems of hyperbolic conservation laws;
- investigate high-order viscous TVD schemes for viscous flows;
- investigate a new approach for solving the incompressible Navier-Stokes equations using the high-order viscous schemes.

1.3.3 The Strategy

The final goal of this thesis is to produce a method of applying fully discrete, high-order schemes to deal with multi-dimensional nonlinear systems of conservation laws. To achieve this goal a good strategy is needed.

First of all, we start with one-dimensional flows. Collective numerical experiments and theoretical works in the literature have justified that the results generated from the study of the one-dimensional flows can be successfully extended to the multi-dimensional flows.

Then, for one-dimensional flows we concentrate on the study of linear scalar model equations. Our experience has proved that the high-order schemes and information obtained from the model equations, such as linear stability conditions and TVD properties, give substantial guidance in order to extend the high-order schemes to systems of conservation laws.

Finally, we extend the high-order schemes to one- and two-dimensional nonlinear systems of conservation laws.

As will be seen later, this strategy is embodied throughout the thesis.

1.4 Thesis Structure

This thesis consists of ten chapters which cover the following topics.

Chapter 2 investigates the issue of linear stability analysis for two and three level, explicit and implicit, one dimensional finite difference numerical schemes. A new approach which simplifies the von Neumann method is presented. It has been proved that the new technique is simple for a linear stability study. This is especially true for high-order and complicated numerical schemes.

Chapter 3 investigates the fully discrete methodology and establishes a formula from which two-level explicit fully discrete arbitrary-order finite difference schemes for a model advection equation can be derived. To illustrate this approach fully discrete second-, third-, fourth- and 20th-order numerical schemes are presented.

Chapter 4 reformulates the non-conservative finite difference methods to conservative schemes. To illustrate the approach fully discrete second-, third- and fourth-order conservative schemes are formulated.

Chapter 5 investigates high-order TVD schemes for a scalar hyperbolic conservation law using flux limiter functions. Formulae which define Courant number dependent TVD regions for second-, third- and fourth-order TVD schemes are established; a semi-empirical TVD procedure for an H-th-order (H > 4) scheme is proposed. Numerical tests to verify the theory are presented.

Chapter 6 investigates fully discrete high-order accurate solutions for non-linear system of hyperbolic conservation laws. Second-, third- and fourth-order high resolution schemes for systems are presented. Performance of the methods is assessed by solving test problems for the time-dependent Euler equations of Gas Dynamics in one and two space dimensions. Exact solutions and experimental data are used to validate the results.

Chapter 7 describes the fully discrete methodology for the linear scalar advection-diffusion

equation. Based on the theory three-, four- and five-point, two-level, explicit, conservative viscous numerical schemes are presented.

Chapter 8 gives viscous TVD functions for second-, third-, and fourth-order schemes. Viscous flux limiter functions are proposed and tested via numerical experiments. When solving viscous flows with shocks the viscous flux limiter functions might be used in order to obtain a satisfactory solution.

Chapter 9 extends the methods to steady incompressible Navier-Stokes equations formulated via artificial compressibility approach [73].

Chapter 10 gives suggestions for further work and conclusions.

Chapter 2

Linear Stability Analysis and Convergence

2.1 Introductory Remarks

Firstly, the very important issue of linear *convergence* is discussed.

As is well known, a numerical method is useless if the method will not converge to the differential equation. To prove convergence for nonlinear systems of equations is currently impossible for most cases. For the simpler case of a scalar equation, particularly the linear scalar equation, the analysis is possible. Although linear convergence is not a sufficient condition for guaranteeing nonlinear convergence, it is still a necessary condition to achieve nonlinear convergence. To prove convergence, there is a fundamental Lax equivalence theorem [43] for linear finite difference methods, which declares that for a *consistent* linear method *stability* is necessary and sufficient for *convergence* [15]. Here the linear convergence is obtained by two sequential conditions: one, the numerical method has to be consistent with the PDE simulated; two, the numerical method has to be stable for at least smooth initial data. Since the numerical methods which will be introduced in the thesis are generated from Taylor series (see Chaper 3 and 7), these methods are guaranteed to be consistent. Therefore, all that is left for proving convergence is to prove that these methods are linearly stable.

At present, there are several techniques available to analyse linear stability. This includes

the discrete perturbation method, the Hirt method, the matrix method and the von Neumann method [44] [45]. Details of these methods can also be found in [11]. Comparing with other techniques the von Neumann method is the most widely applied technique. However it is by no means an easy task using these methods to analyse linear stability even for constant coefficient initial value problems. For a numerical scheme generated from a complex high-order PDE or for a numerical method which has more than second-order accuracy, the linear stability analysis can be extremely complicated applying these techniques. Normally quite tedious and complicated algebraic functions or matrices will be encountered, which are very difficult to analyse, or even impossible to manipulate. Often, numerical schemes cannot be applied because of lack of stability information. Obviously a simple and reliable method for proving linear stability is desired.

In this chapter this issue is investigated and an approach to the linear stability analysis in a simple manner is developed. The format of this chapter is organized as follows: section 2 introduces the linear stability analysis method for one dimensional numerical schemes; Section 3 illustrates the method via some applications; Section 4 is the summary.

2.2 Linear Stability Analysis

In this section our study is restricted to the initial value problems (IVP) for the simplest cases of one dimensional scalar linear PDEs with the smooth initial data.

The computational half plane is discretised by choosing a uniform mesh with a cell width $h = \Delta x$, a time step $k = \Delta t$ and define the computational grid $x_j = jh, \quad t_n = nk$. U_j^n is used to denote the computed approximation to the exact solution $u(x_j, t_n)$ of the PDEs.

2.2.1 A New Approach for Linear Stability Analysis

For one dimensional linear finite difference numerical methods with smooth initial data

$$\sum_{k^{n+1}} B_{k^{n+1}}^{n+1} U_{j+k^{n+1}}^{n+1} = \sum_{k^n} B_{k^n}^{n} U_{j+k^n}^{n} + \sum_{k^{n-1}} B_{k^{n-1}}^{n-1} U_{j+k^{n-1}}^{n-1} \tag{2.1}$$

if the amplification coefficient $|\lambda(\theta)|$ *of the scheme is a monotone (increases or decreases) function, i.e.* $(\lambda(\theta)\bar{\lambda(\theta)})' \geq 0$ *(or* ≤ 0*), with respect to* θ *in the interval [0,*π*], then the*

linear stability conditions of the scheme can be determined from

$$\lambda = \frac{\sum_{k^n}(-1)^{|k^n|}B^n_{k^n} + \sum_{k^{n-1}}(-1)^{|k^{n-1}|}\frac{1}{\lambda}B^{n-1}_{k^{n-1}}}{\sum_{k^{n+1}}(-1)^{|k^{n+1}|}B^{n+1}_{k^{n+1}}} \tag{2.2}$$

$$\lambda = \frac{-\sum_{k^{n-1}} B^{n-1}_{k^{n-1}}}{\sum_{k^n} B^n_{k^n} + \sum_{k^{n-1}} B^{n-1}_{k^{n-1}}} \tag{2.3}$$

For pure odd grid point or pure even grid point finite difference numerical schemes if the amplification coefficient is a concave or convex function, i.e. $|\lambda(\theta)|'' \geq 0$ *(or* ≤ 0*), in the interval [0,* π*], then an additional stability condition of the scheme is required*

$$\lambda = \frac{\sum_{k^n} sign^n B^n_{k^n} + \sum_{k^{n-1}} sign^{n-1}\frac{1}{\lambda}B^{n-1}_{k^{n-1}}}{\sum_{k^{n+1}} sign^{n+1}B^{n+1}_{k^{n+1}}} \tag{2.4}$$

here

$$\begin{cases} sign^n = sin\frac{k^n\pi}{2} & \forall\ odd\ \ number\ \ k^n \\ sign^n = cos\frac{k^n\pi}{2} & \forall\ even\ \ number\ \ k^n \end{cases} \tag{2.5}$$

where k^n *are the integer grid point numbers at time level n;* $B^n_{k^n}$ *are constant coefficients;* $\lambda(\theta)$ *is the amplification factor of the numerical scheme;* $\lambda(\bar{\theta})$ *is the conjugate of the* $\lambda(\theta)$*. To achieve stability*

$$|\lambda| \leq 1 \tag{2.6}$$

If the amplification coefficient does not satisfy the conditions above, then the stability conditions can be defined by investigation of those phase angles at which the amplification coefficient has extreme values.

PROOF

The von Neumann method (Fourier Series method) is based on assuming that

$$U^n_j = A^n_L e^{iLj\Delta x} \tag{2.7}$$

where A^n_L is the amplitude at time level n; L is the wave number in x-direction, $L = \frac{2\pi}{\tau}$; τ is the wavelength; i is the complex number, $i = \sqrt{-1}$.

Considering the general form of linear numerical methods of equation (2.1), from equation (2.7) we have

$$\begin{cases} U^{n+1}_{j+k^{n+1}} = A^{n+1}_L e^{iL(j+k^{n+1})\Delta x} \\ U^n_{j+k^n} = A^n_L e^{iL(j+k^n)\Delta x} \\ U^{n-1}_{j+k^{n-1}} = A^{n-1}_L e^{iL(j+k^{n-1})\Delta x} \end{cases} \tag{2.8}$$

Substituting equation (2.8) into equation (2.1)

$$\sum_{k^{n+1}} B_{k^{n+1}}^{n+1} A_L^{n+1} e^{iL(j+k^{n+1})\Delta x} = \sum_{k^n} B_{k^n}^n A_L^n e^{iL(j+k^n)\Delta x} + \sum_{k^{n-1}} B_{k^{n-1}}^{n-1} A_L^{n-1} e^{iL(j+k^{n-1})\Delta x} \tag{2.9}$$

Dividing both sides of equation (2.9) by $A_L^n e^{iLj\Delta x}$ and reorganizing it we get the amplification factor at the new time level:

$$\begin{aligned} \lambda^n(\theta) &= \frac{A_L^{n+1}}{A_L^n} \\ &= \frac{\sum_k (B_{k^n}^n e^{ik^n\theta} + \frac{1}{\lambda^{n-1}} B_{k^{n-1}}^{n-1} e^{ik^{n-1}\theta})}{\sum_{k^{n+1}} B_{k^{n+1}}^{n+1} e^{ik^{n+1}\theta}} \\ &= \gamma_r + i\gamma_i \end{aligned} \tag{2.10}$$

Here θ is the phase angle, $\theta = L\Delta x$;

$$\gamma_r = \frac{\left(\sum_k b_1 + \frac{1}{\lambda^{n-1}} \sum_k c_1\right) \sum_k a_1 + \left(\sum_k b_2 + \frac{1}{\lambda^{n-1}} \sum_k c_2\right) \sum_k a_2}{\left(\sum_k a_1\right)^2 + \left(\sum_k a_2\right)^2} \tag{2.11}$$

$$\gamma_i = \frac{\left(\sum_k b_2 + \frac{1}{\lambda^{n-1}} \sum_k c_2\right) \sum_k a_1 - \left(\sum_k b_1 + \frac{1}{\lambda^{n-1}} \sum_k c_1\right) \sum_k a_2}{\left(\sum_k a_1\right)^2 + \left(\sum_k a_2\right)^2} \tag{2.12}$$

where

$$\begin{aligned} a_1 &= B_{k^{n+1}} cos\ k^{n+1}\theta \\ a_2 &= B_{k^{n+1}} sin\ k^{n+1}\theta \\ b_1 &= B_{k^n} cos\ k^n\theta \\ b_2 &= B_{k^n} sin\ k^n\theta \\ c_1 &= B_{k^{n-1}} cos\ k^{n-1}\theta \\ c_2 &= B_{k^{n-1}} sin\ k^{n-1}\theta \end{aligned}$$

For a linear numerical method with smooth initial data, since the Courant number is constant, therefore the amplification factors at different time levels are identical, i.e. $\lambda^n = \lambda^{n-1}$. From now on we write λ instead for simplicity.

The absolute value of the amplification factor $|\lambda|$ is called amplifier coefficient. Obviously if $|\lambda| > 1$, the numerical method will not be stable, otherwise, it is stable. Therefore, for stability

$$|\lambda| = \sqrt{\gamma_r^2 + \gamma_i^2} \leq 1 \tag{2.13}$$

for all phase angles ranging from $\theta = 0$ to $\theta = \pi$.

This is the normal approach of analysing the stability in practice using the Fourier method. But, as you can see, generally equation (2.13) is a very complicated algebra, especially for high order numerical methods, say, over second order. For a method over second order, $|\lambda|$ is very difficult to work out, or even impossible to manipulate.

Here we are going to adopt a new approach.

The difficulty of analysing equation (2.13) lies in the phase angle θ which covers the whole domain from 0 to π associated with all wave numbers. The question here is that as far as the stability of a numerical scheme is concerned, is it necessary to analyse the whole range of the phase angles? If not, which phase angle do we need to analyse?

The instability of a numerical method is caused by the unbounded fast accumulated amplitude error with the time evolution. To limit the amplitude error overgrowing we need first to find out at which phase angles the amplification coefficient have the extreme values in the interval $[0, \pi]$ (here the angles which represent all turning point angles and boundary point angles are called extreme value angles), and then it is sufficient to restrict these values to less than or equal to 1 at these phase angles.

In order to find the angles at which the $|\lambda|$ has extreme values, first we need the first derivative of $|\lambda|$ with respect to θ, i.e. $|\lambda|'$, then by setting $|\lambda|'$ equals to zero the extreme value angles can be defined.

From equation (2.13) we have

$$\begin{aligned} |\lambda|' &= \frac{\gamma_r \gamma_r' + \gamma_i \gamma_i'}{\sqrt{\gamma_r^2 + \gamma_i^2}} \\ &= 0 \end{aligned} \tag{2.14}$$

Equation (2.14) is equivalent to

$$(\gamma_r^2 + \gamma_i^2)' = 0 \tag{2.15}$$

or

$$(\lambda(\theta)\bar{\lambda(\theta)})' = 0 \tag{2.16}$$

Here

$$\gamma_r^2 + \gamma_i^2 = \frac{(\sum_k b_1 + \frac{1}{\lambda}\sum_k c_1)^2 + (\sum_k b_2 + \frac{1}{\lambda}\sum_k c_2)^2}{(\sum_k a_1)^2 + (\sum_k a_2)^2} \tag{2.17}$$

therefore

$$\begin{aligned}(\gamma_r^2+\gamma_i^2)' &= 2\left[(\Sigma\, a_1)^2+(\Sigma\, a_2)^2\right]\left[(\Sigma\, b_2+\frac{1}{\lambda}\Sigma\, c_2)(\Sigma k^n b_1+\frac{1}{\lambda}\Sigma\, k^{n-1}c_1)\right.\\ &\quad\left.-(\Sigma\, b_1+\frac{1}{\lambda}\Sigma\, c_1)+(\Sigma\, k^n b_2-\frac{1}{\lambda}\Sigma\, k^{n-1}c_2)\right]\\ &\quad -2\left[(\Sigma\, b_1+\frac{1}{\lambda}\Sigma c_1)^2+(\Sigma\, b_2+\frac{1}{\lambda}\Sigma\, c_2)^2\right]\left[\Sigma\, a_2\ \Sigma\, k^{n+1}a_1\right.\\ &\quad\left.-\Sigma\, a_1\ \Sigma\, k^{n+1}a_2\right]/\left[(\Sigma\, a_1)^2+(\Sigma\, a_2)^2\right]^2 \qquad (2.18)\end{aligned}$$

For 3-level explicit schemes equation (2.18) is reduced to

$$\begin{aligned}(\gamma_r^2+\gamma_i^2)' &= 2\left[(\Sigma\, b_2+\frac{1}{\lambda}\Sigma\, c_2)(\Sigma\, k^n b_1+\frac{1}{\lambda}\Sigma\, k^{n-1}c_1)\right.\\ &\quad\left.-(\Sigma\, b_1+\frac{1}{\lambda}\Sigma\, c_1)(\Sigma\, k^n b_2-\frac{1}{\lambda}\Sigma\, k^{n-1}c_2)\right] \qquad (2.19)\end{aligned}$$

For 2-level explicit schemes equation (2.18) is further reduced to

$$(\gamma_r^2+\gamma_i^2)' = 2(\Sigma\, b_2\ \ \Sigma\, k^n b_1-\Sigma\, b_1\ \ \Sigma\, k^n b_2) \qquad (2.20)$$

By solving equation (2.15) the obvious Courant number-independent extreme value angles can be easily defined. They are:

$$\theta_1 = 0 \qquad (2.21)$$

$$\theta_2 = \pi \qquad (2.22)$$

$$\theta_3 = \frac{\pi}{2} \quad \forall\ \textit{either odd or even } k \qquad (2.23)$$

since when $\theta = 0$ or π, a_2, b_2 and c_2 equal to zeros, therefore $(\gamma_r^2+\gamma_i^2)' = 0$; when $\theta = \frac{\pi}{2}$, a_1, b_1 and c_1 are zeros $\forall$ odd k and a_2, b_2, and c_2 are zeros $\forall$ even k, resulting in $(\gamma_r^2+\gamma_i^2)' = 0$.

Equation (2.23) means that for pure odd or even number grid point schemes the amplification coefficient $|\lambda|$ has a extreme value at phase angle $\theta = \frac{\pi}{2}$. For example, the Lax-Friedrichs scheme which is a odd number point scheme has a extreme value angle at the angle $\theta = \frac{\pi}{2}$.

There may be other Courant number-dependent extreme value angles between $\theta = 0$ and $\theta = \pi$ depending on the solution of equation (2.15). However there is one important category of schemes for which the amplification coefficient is a monotone function, that means $(\lambda(\theta)\bar{\lambda(\theta)})' \geq 0$ (or ≤ 0) $\forall$ [0,π]. In this case the extreme value angles must be

either at $\theta = 0$ or at $\theta = \pi$, in which cases the linear stability analysis becomes very simple. Actually as we will see later large number of usefull finite difference numerical schemes fall into this category.

For pure odd or even grid point schemes if $|\lambda(\theta)|'' \geq 0$ (or ≤ 0) $\forall$ [0,π], i.e. the function curve of the amplification coefficient is either concave or convex, then the extreme value angle may appear at $\theta = \frac{\pi}{2}$.

Hence we have the following criterion:

Criterion *For finite difference numerical schemes with smooth initial data it is necessary and sufficient to investigate the linear stability at phase angles at which* $|\lambda(\theta)|$ *has extreme values in the interval* [0,π].

If $(\lambda(\theta)\lambda(\bar{\theta}))' \geq 0$ *(or* ≤ 0*) in the interval* [0,π], *it is necessary and sufficient to investigate the linear stability at the phase angle* $\theta = 0$ *and* $\theta = \pi$.

For pure odd or even grid point finite difference schemes if $|\lambda(\theta)|'' \geq 0$ *(or* ≤ 0*), it is necessary and sufficient to investigate the linear stability at phase angle* $\theta = 0$, $\theta = \pi$ *and* $\theta = \frac{\pi}{2}$.

Based on this criterion substituting $\theta = 0$, π and $\theta = \frac{\pi}{2}$ into equation (2.10) we establish the new approach introduced at the begining of the section.

Equations (2.2) and (2.3) are the general form of amplification function which is valid for two and three time levels, explicit and implicit numerical schemes. For convenience here some specific schemes are given as follows.

2.2.2 3-level Explicit Schemes

If we consider 3-level explicit schemes

$$U_j^{n+1} = \sum_{k^n} B_{k^n}^n U_{j+k^n}^n + \sum_{k^{n-1}} B_{k^{n-1}}^{n-1} U_{j+k^{n-1}}^{n-1} \tag{2.24}$$

then, the equations (2.2) and (2.3) become

$$\lambda = \sum_{k^n} (-1)^{|k^n|} B_{k^n}^n + \frac{1}{\lambda} \sum_{k^{n-1}} (-1)^{|k^{n-1}|} B_{k^{n-1}}^{n-1} \tag{2.25}$$

$$\lambda = -\sum_{k^{n-1}} B^{n-1}_{k^{n-1}} \tag{2.26}$$

2.2.3 2-level Explicit Schemes

If we consider 2-level explicit schemes

$$U^{n+1}_j = \sum_{k^n} B^n_{k^n} U^n_{j+k^n} \tag{2.27}$$

then, equation (2.2) is further simplified to

$$\lambda = 1 - 2 \sum_{k^n = \pm 1, \pm 3, \ldots} B^n_{k^n} \tag{2.28}$$

since $\sum_{k^n} B^n_{k^n} = 1$ for consistency.

2.2.4 2-level Implicit Schemes

For 2-level implicit schemes

$$\sum_{k^{n+1}} B^{n+1}_{k^{n+1}} U^{n+1}_{j+k^{n+1}} = \sum_{k^n} B^n_{k^n} U^n_{j+k^n} \tag{2.29}$$

the amplification factor of equation

$$\lambda = \frac{\sum_{k^n} (-1)^{|k^n|} B^n_{k^n}}{\sum_{k^{n+1}} (-1)^{|k^{n+1}|} B^{n+1}_{k^{n+1}}} \tag{2.30}$$

2.2.5 2-level Fully Implicit Schemes

For fully implicit schemes

$$\sum_{k^{n+1}} B^{n+1}_{k^{n+1}} U^{n+1}_{k^{n+1}} = U^n_j \tag{2.31}$$

The amplification factor has the following simple form

$$\lambda = \frac{1}{1 - 2 \sum_{k^{n+1} = \pm 1, \pm 3, \ldots} B^{n+1}_{k^{n+1}}} \tag{2.32}$$

since $\sum_{k^{n+1}} B^{n+1}_{k^{n+1}} = 1$ for consistency.

2.2.6 Procedures of the New Approach

The procedures of linear stability analysis using the new approach can be outlined as follows:

1. calculate the extreme value angles $\theta(c)$ using equation (2.15) with equations (2.18) - (2.20).

2. check whether or not the extreme value angles $\theta(c)$ function conform to the monotone function requirements.

3. if satify the requirements then the stability conditions can be defined applying equations (2.24) - (2.32) (according to the scheme used).

4. if not, using equation (2.13) with equation (2.17), analyse stability conditions only at the extreme value angles $\theta(c)$ defined at stage one.

2.3 Examples of Stability Analysis

In this section we use some numerical schemes some of which the stability conditions are well known to illustrate the procedures and test the stability approach.

Example 1. Modified Lax-Wendroff scheme

Consider the scheme

$$U_j^{n+1} = U_j^n - \frac{c}{2}(U_{j+1}^n - U_{j-1}^n) + \frac{d}{2}(U_{j+1}^n - 2U_j^n + U_{j-1}^n) \tag{2.33}$$

here, c is the Courant number, $c = \frac{a\Delta t}{\Delta x}$, a is the wave speed, d is a variable.

Applying the analytical approach from equation (2.20) we have

$$(\gamma_r^2 + \gamma_i^2)' = 2\left[\left(c^2 - d^2\right) cos\theta - (1-d)d\right] sin\theta \tag{2.34}$$

Two special cases are easily defined from equation (2.34): when $d = c^2$ and $d = |c|$ the amplification coefficient is monotone, since in these cases equation (2.34) keeps the same sign in the interval $[0, \pi]$. In the former case equation (2.33) becomes the second-order Lax-Wendroff scheme. From equation (2.28) the amplification factor is

$$\lambda = 1 - 2c^2 \tag{2.35}$$

Therefore the stability condition is

$$|\lambda| \leq 1 \quad for \quad |c| \leq 1 \tag{2.36}$$

This is identical to the familiar result. In the latter case equation (2.33) reduces to the first-order upwind scheme. The scheme is stable for $|c| \leq 1$.

For d being other values the $|\lambda|$ is not always a monotone function. Its behavior is determined by Courant number and d. In this case we need to find out the extreme value angle function $\theta(c, d)$ by setting equation (2.34) equal to 0, which gives

$$cos\theta = \frac{(1-d)d}{c^2 - d^2} \tag{2.37}$$

Bringing equation (2.37) into equation (2.13) we have

$$\begin{aligned} |\lambda| &= \sqrt{\frac{1}{4}(1+cos\theta)^2 + c^2 sin^2\theta} \\ &= \sqrt{\frac{1}{4}\left(1+\frac{(1-d)d}{c^2-d^2}\right)^2 + c^2\left[1-\left(\frac{(1-d)d}{c^2-d^2}\right)^2\right]} \end{aligned} \tag{2.38}$$

For stability $|\lambda| \leq 1$.

Example 2. Leapfrog Scheme

The leapfrog scheme for the scalar advection equation has the following form

$$U_j^{n+1} = U_j^{n-1} - cU_{j+1}^n + cU_{j-1}^n \tag{2.39}$$

This is a 3-level explicit scheme. It is easy to prove that the scheme has extreme values at $\theta = 0,\ \pi$, and $\frac{\pi}{2}$. Using equation (2.25) we have

$$\lambda = \frac{1}{\lambda} \tag{2.40}$$

That is

$$\lambda^2 = 1 \tag{2.41}$$

From equation (2.26) we have

$$\lambda = -1 \tag{2.42}$$

From equation (2.4)

$$\lambda = -c \pm \sqrt{1+c^2} \tag{2.43}$$

Equation (2.41) and (2.42) mean $|\lambda| = 1$; equation (2.43) means $|\lambda| \leq 1$ for $|c| \geq 0$. Actually this scheme is neutrally stable for $|c| \leq 1$.

Example 3. Crank-Nicolson Scheme

$$U_j^{n+1} + \frac{1}{4}cU_{j+1}^{n+1} - \frac{1}{4}cU_{j-1}^{n+1} = U_j^n - \frac{1}{4}cU_{j+1}^n + \frac{1}{4}cU_{j-1}^n \tag{2.44}$$

This is a 2-level implicit scheme. The scheme has a monotone amplification coefficient function. From equation (2.30)

$$\lambda = \frac{1 + \frac{1}{4}c - \frac{1}{4}c}{1 - \frac{1}{4}c + \frac{1}{4}c} = 1 \tag{2.45}$$

i.e. $|\lambda| = 1$. This scheme is unconditionally stable.

Example 4. Lax-Friedrichs Scheme

$$U_j^{n+1} = (\frac{1}{2} - \frac{c}{2})U_{j+1}^n + (\frac{1}{2} + \frac{c}{2})U_{j-1}^n \tag{2.46}$$

This is a 2-level explicit odd point scheme. The scheme has a concave amplification coefficient function, therefore we need to check both equations (2.28) and (2.4). From equation (2.28)

$$|\lambda| = 1 \tag{2.47}$$

From equation (2.4)

$$|\lambda| = |c| \tag{2.48}$$

Therefore this scheme is stable if $|c| \leq 1$.

Example 5. Explicit Space-centered Scheme for Model Diffusion Equation $\mathbf{u_t = \nu u_{xx}}$

$$U_j^{n+1} = (1 - 2d)U_j^n + dU_{j+1}^n + dU_{j-1}^n \tag{2.49}$$

here, the d is the diffusion number, $d = \frac{\nu \Delta t}{(\Delta x)^2}$; ν is the viscous coefficient.

It has been proved that the scheme has a monotone amplification coefficient function. From equation (2.28) the amplification factor

$$\lambda = 1 - 4d \tag{2.50}$$

The stable condition is

$$|\lambda| \leq 1 \qquad for \quad d \leq \frac{1}{2} \tag{2.51}$$

Example 6. Fully Implicit Scheme for Model Parabolic Equation

Again he scheme has a monotone function.

$$(1+2d)U_j^{n+1} - dU_{j+1}^{n+1} - dU_{j-1}^{n+1} = U_j^n \tag{2.52}$$

From equation (2.32)

$$\lambda = \frac{1}{1+4d} \tag{2.53}$$

Since d is positive the scheme is unconditionally stable for $d > 0$. We get the same conclusion as that proved by using other techniques.

Example 7. Fully Discrete 20th-order Scheme for Model Advection Equation $u_t = au_x$

The fully discrete 20th-order space-centered scheme for the model advection equation is listed in appendix A. The complexity of the scheme makes it impossible to do a stability analysis when applying other techniques. Here let us apply the new approach to define the stability conditions.

From equation (2.28) the amplification factor of the scheme is

$$\begin{aligned}\lambda \;=\; & 1 \;-\; 2\,(-2.1820901E-08\,c \;+\; 1.91839\,c^2 \;+\; 2.2592523E-08c^3 \\ & -\; 1.144243\,c^4 \;-\; 6.8021899E-09\,c^5 \;+\; 0.2509956\,c^6 \\ & +\; 1.1990592E-09\,c^7 \;-\; 2.6645366E-02\,c^8 \;+\; 4.4792958E-11c^9 \\ & +\; 1.5550008E-03\,c^{10} \;+\; 2.3386265E-13\,c^{11} \;-\; 5.3070333E-05c^{12} \\ & -\; 1.5452447E-14\,c^{13} \;+\; 1.0802879E-06\,c^{14} \;+\; 4.9565642E-16c^{15} \\ & -\; 1.2842341E-08\,c^{16} \;-\; 4.3901846E-18\,c^{17} \;+\; 8.1889627E-11c^{18} \\ & +\; 4.1853998E-21\,c^{19} \;-\; 2.1549903E-13\,c^{20})\end{aligned} \tag{2.54}$$

This function is ploted in figure 2.1. As is clearly shown the possibly stable regions of this method are:

$$\begin{aligned} -4 \;&\leq\; c \leq -3.75 \\ -3 \;&\leq\; c \leq -2.58 \\ -2 \;&\leq\; c \leq -1.3 \\ -1 \;&\leq\; c \leq 1 \\ 1.3 \;&\leq\; c \leq 2 \end{aligned} \tag{2.55}$$

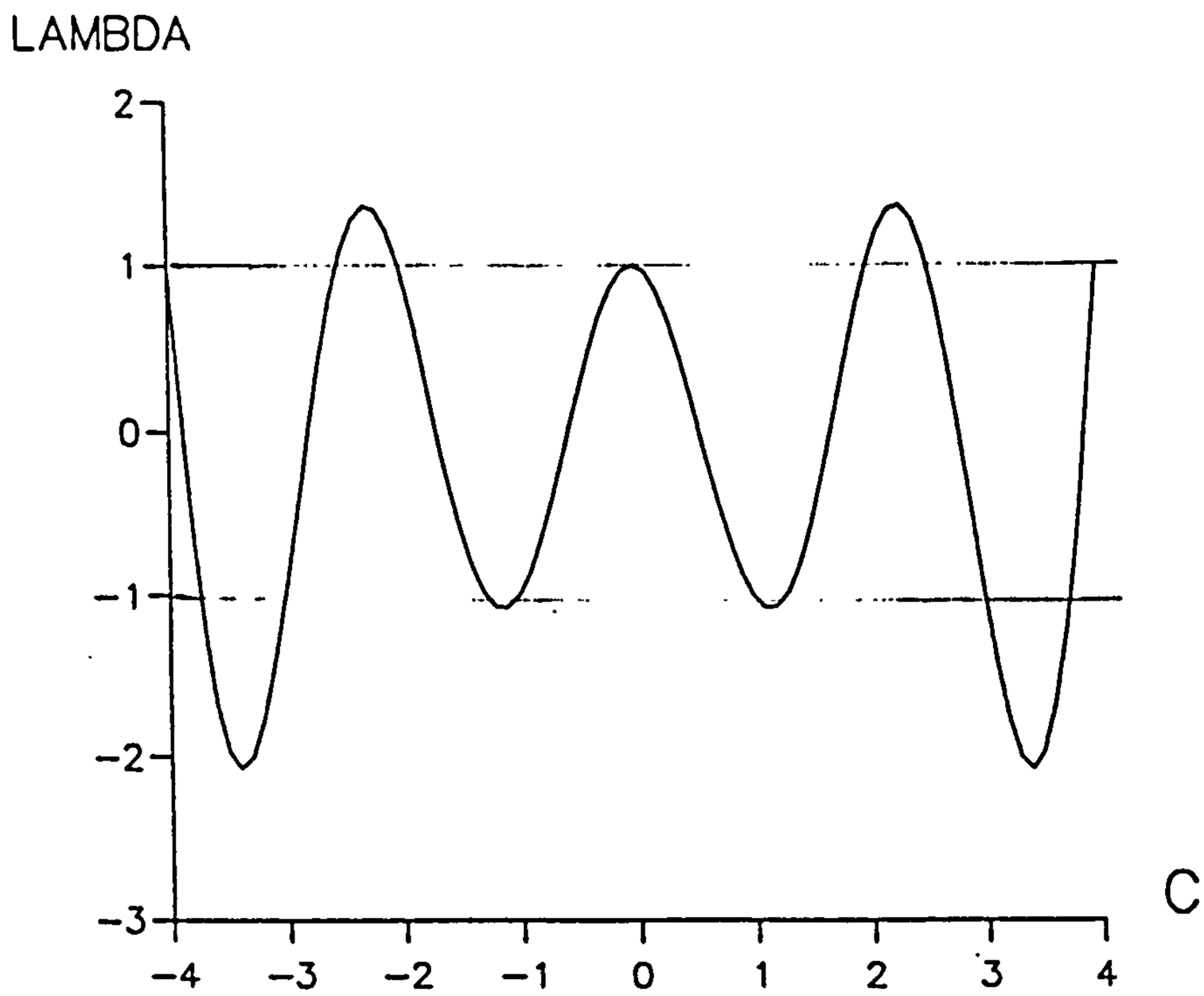

Figure 2.1: Stable Region of the 20th-order Method

$$\begin{aligned} 2.58 &\leq c \leq 3 \\ 3.75 &\leq c \leq 4 \end{aligned}$$

Numerical experiments indicate that the stability condition of the scheme is

$$\begin{aligned} -4 &\leq c \leq -3.85 \\ -3 &\leq c \leq -2.58 \\ -2 &\leq c \leq 2 \\ 2.58 &\leq c \leq 3 \\ 3.85 &\leq c \leq 4 \end{aligned} \tag{2.56}$$

More applications of the linear stability analysis for high-order fully discrete schemes using the new approach can be found in Chapters 3 and 7.

2.4 Summary

In this chapter a linear stability analysis method is presented for one dimensional numerical schemes. This method allows us to study linear stability analytically. To illustrate the method linear stability of a variety of numerical schemes is analysed. This approach offers us a simple means to deal with linear stability study for one-dimensional finite difference schemes.

Chapter 3

Fully Discrete Arbitrary-order Schemes for a Model Advection Equation

3.1 Introductory Remarks

An important research subject in Computational Fluid Dynamics (CFD) concerns the development of high-order numerical schemes for nonlinear hyperbolic conservation laws. There are many application areas for which such research is of vital importance. One example of considerable interest is Acoustics, which needs long time evolution of weak flow features. For this kind of problems low-order methods will produce unacceptable dispersive and diffusive errors in a very short time. Another example concerns problems containing weak shocks in which the physical effects of diffusion and dispersion are important mechanisms. Low-order methods contain large amounts of numerical diffusion and dispersion and are thus totally inaccurate for simulating the propagation of weak shocks. In large computational problems low-order methods would require vast amounts of computer memory (possibly not available in current computers) in order to attain a satisfactory degree of accuracy. A high-order method would attain the same accuracy with coarser meshes requiring less sophisticated hardware and making it possible to actually run the problems.

Essentially, there are two different techniques to construct high-order numerical schemes: semi-discrete and fully discrete methods. In the semi-discrete method (see [46] for description) one divides the discretization process into two separate stages. In the first stage one discretizes in space only leaving the problem continuous in time; in the second stage one has sets of Ordinary Differential Equations (ODE) in time, which can be discretized appropriately. Often this technique is called *the method of lines.* The MUSCL approach introduced by van Leer [47] can be utilised in conjunction with the method of lines. The recently developed ENO schemes [40]-[42] belong to this category. The main idea of the ENO scheme is that the spacial high-order approximations to the flux at a cell interface can be defined using high-order interpolation in space, and then the high-order temporal accuracy can be achieved by another discretization applying a high-order ODE solver. To the author's best knowledge most present high-order numerical schemes rely on the semi-discrete approach.

In this chapter a fully discrete approach is investigated to obtain arbitrary-order numerical methods. The analysis is carried out in the context of a model advection equation. Our experience has proved that designing numerical methods for the solution of the model equation can provide very useful information concerning the properties of schemes and can give substantial guidance for extension of the schemes to nonlinear hyperbolic systems.

This chapter is organized as follows: section 2 establishes an approach from which 2-level, explicit, fully discrete, arbitrary-order non-conservative numerical schemes can be derived. In section 3 we apply the approach to construct some high-order fully discrete numerical schemes and conduct the stability analysis for the schemes. Section 4 contains some numerical experiments and section 5 is the summary.

3.2 Full Discretization of the Model Equation

Let us consider the initial value problem (IVP) for one dimensional linear model advection equation, namely

$$\begin{aligned} u_t + a u_x &= 0 \qquad -\infty < x < \infty, t \geq 0 \\ u(x,0) &= u_0(x) \end{aligned} \tag{3.1}$$

Here, $u(x,t)$ is the unknown function and a is a constant wave propagation speed.

The computational half plane is discretized by choosing a uniform mesh with a mesh width

$h = \Delta x$ and a time step $k = \Delta t$, and define the computational grid $x_j = jh,\ \ t_n = nk$. U_j^n is used to denote the computed approximation to the exact solution $u(x_j, t_n)$ of equation (3.1).

In this section a fully discrete approach for the model equation is investigated. The fully discrete approach is based on a Taylor series expansion in both space and time in a single stage.

Theorem 1 *The fully discrete formula from which a two-level fully discrete explicit $m-th$ order accurate finite difference method can be derived for the model hyperbolic equation, $u_t + au_x = 0$, is defined as*

$$U_j^{n+1} = \sum_{\alpha=1}^{p} B_{k_\alpha}\, U_{j+k_\alpha}^n \tag{3.2}$$

where α is the grid point number; p is the number of grid points used, $p = m+1$; m is the order of accuracy; B_{k_α} are constant coefficients determined by

$$\begin{cases} B_{k_\alpha=0} = 1 - \sum_{\alpha=1, k_\alpha \neq 0}^{m} B_{k_\alpha} \\ \begin{bmatrix} B_{k_1} \\ B_{k_2} \\ \vdots \\ B_{k_m} \end{bmatrix} = \begin{bmatrix} k_1 & k_2 & \dots & k_m \\ k_1^2 & k_2^2 & \dots & k_m^2 \\ \vdots & \vdots & \vdots & \vdots \\ k_1^m & k_2^m & \dots & k_m^m \end{bmatrix}^{-1} \begin{bmatrix} -c \\ c^2 \\ \vdots \\ (-c)^m \end{bmatrix} \\ (k_\alpha \neq 0) \end{cases} \tag{3.3}$$

where c is Courant number, $c = \frac{a\Delta t}{\Delta x}$.

PROOF

In order to prove the theorem, we first analyse the local truncation error of equation (3.2) by Taylor series expansion of both sides of equation (3.2) at (j, n). This can be written as

$$\begin{aligned} E(x,t) &= u(x,t) + \sum_{n=1}^{m} \frac{\Delta t^n}{n!} u_{t^n} + O(\Delta t^{m+1}) \\ &\quad - \sum_{\alpha=1}^{p} B_{k_\alpha} \left[u(x,t) + \sum_{n=1}^{m} \frac{(k_\alpha \Delta x)^n}{n!} u_{x^n} \right] + O(\Delta x^{m+1}) \end{aligned} \tag{3.4}$$

where m is the order of accuracy of the scheme, $1 \leq m < \infty$; $u_{t^n} = \frac{\partial^n u}{\partial t^n}$, $u_{x^n} = \frac{\partial^n u}{\partial x^n}$; $\Delta t^n = (\Delta t)^n$. The relationship between m and p obviously is

$$p = m + 1 \tag{3.5}$$

For the scalar equation in (2.1), it is easy to obtain:

$$u_{t^n} = (-a)^n u_{x^n} \tag{3.6}$$

Substitution of equation (3.6) into equation (3.4) gives

$$\begin{aligned} E(x,t) \;=\; & \left(1 - \sum_{\alpha=1}^{p} B_{k_\alpha}\right) u(x,t) + \sum_{n=1}^{m} \left[\frac{\Delta t^n}{n!}(-a)^n u_{x^n}\right. \\ & \left. - \sum_{\alpha=1}^{p} B_{k_\alpha} \frac{(k_\alpha \Delta x)^n}{n!} u_{x^n}\right] + O(\Delta t^{m+1}) + O(\Delta x^{m+1}) \end{aligned} \tag{3.7}$$

In order to achieve $m-th$ order of accuracy, it is sufficient to require that

$$1 - \sum_{\alpha=1}^{p} B_{k_\alpha} = 0 \tag{3.8a}$$

$$\frac{\Delta t^n}{n!}(-a)^n u_{x^n} - \sum_{\alpha=1}^{p} B_{k_\alpha} \frac{(k_\alpha \Delta x)^n}{n!} u_{x^n} = 0 \tag{3.8b}$$

$$(n = 1, 2, 3, \ldots m)$$

Simplifying equation (3.8b), equations (3.8a) and (3.8b) can be rewritten as

$$\begin{cases} B_{k_\alpha=0} = 1 - \sum_{\alpha=1, k_\alpha \neq 0}^{m} B_{k_\alpha} \\ \sum_{\alpha=1, k_\alpha \neq 0}^{m} k_\alpha^n B_{k_\alpha} = (-c)^n \qquad (n = 1, 2, \cdots, m) \end{cases} \tag{3.9}$$

Equations (3.9) can be transformed into the alternative forms

$$\begin{cases} B_{k_\alpha=0} = 1 - \sum_{\alpha=1, k_\alpha \neq 0}^{m} B_{k_\alpha} \\ k_1 B_{k_1} + k_2 B_{k_2} + \cdots + k_m B_{k_m} = -c \\ k_1^2 B_{k_1} + k_2^2 B_{k_2} + \cdots + k_m^2 B_{k_m} = c^2 \\ \vdots \\ k_1^m B_{k_1} + k_2^m B_{k_2} + \cdots + k_m^m B_{k_m} = (-c)^m \\ (k_\alpha \neq 0) \end{cases} \tag{3.10}$$

or

$$\begin{cases} B_{k_\alpha=0} = 1 - \sum_{\alpha=1, k_\alpha \neq 0}^{m} B_{k_\alpha} \\ \begin{bmatrix} B_{k_1} \\ B_{k_2} \\ \vdots \\ B_{k_m} \end{bmatrix} = \begin{bmatrix} k_1 & k_2 & \ldots & k_m \\ k_1^2 & k_2^2 & \ldots & k_m^2 \\ \vdots & \vdots & \vdots & \vdots \\ k_1^m & k_2^m & \ldots & k_m^m \end{bmatrix}^{-1} \begin{bmatrix} -c \\ c^2 \\ \vdots \\ (-c)^m \end{bmatrix} \\ (k_\alpha \neq 0) \end{cases} \tag{3.11}$$

which is the formula (3.3) and establishes the theorem.

The same result can be found in Roe [48] who derived it in a different manner and utilised it for different purposes to those of his paper. Our ultimate aim is to utilise this result to develop high-order schemes for CFD.

For an $m-th$ order numerical method, according to equation (3.5), p coefficients $B_{k_\alpha}(\alpha = 1,2,\cdots,p)$ are needed in equation (3.2). Equations (3.9), or (3.10), or (3.11), having p equations, are therefore closed so that arbitrary-order numerical methods for the linear scalar equation (3.1) can be obtained.

Some interesting observations can be made. The first one concerns the order of accuracy. This depends on the number of nonlinearly related grid points used, that is, the more grid points are involved the higher the order of accuracy achieved, see equation (3.5). A second aspect relates to the stencil of the scheme. Using the same number of grid points, but in different stencils, different numerical schemes can be obtained. If only integer points are considered, the number of numerical methods (N) which have the same order equal to the number of the points used, i.e. $N = p$. For example, for four-integer-point schemes we can find four third-order numerical methods.

3.3 High-order Numerical Schemes

In this section, some examples are used to demonstrate how to apply the method presented previously to derive high-order numerical schemes.

3.3.1 Fully Discrete Second-order Schemes

From equation (3.5) second-order schemes need at least three grid points. It will be seen that some familiar numerical schemes such as the Lax-Wendroff and Beam-Warming schemes can be derived using our approach.

Space-entered Scheme

Let us denote the 3-point centered scheme as $U_j^{n+1} = f(U_j^n, U_{j-1}^n, U_{j+1}^n)$.

Here, $k_1 = 0,\ k_2 = -1,\ k_3 = 1$ in equation (3.10), which gives

$$\begin{cases} -B_{-1} + B_1 = -c \\ B_{-1} + B_1 = c^2 \\ B_0 = 1 - B_{-1} - B_1 \end{cases}$$

i.e.

$$\begin{cases} B_0 = 1 - c^2 \\ B_{-1} = \frac{c}{2}(c+1) \\ B_1 = \frac{c}{2}(c-1) \end{cases} \tag{3.12}$$

Therefore the numerical scheme is

$$U_j^{n+1} = (1 - c^2)U_j^n + \frac{1}{2}(c^2 + c)U_{j-1}^n + \frac{1}{2}(c^2 - c)U_{j+1}^n \tag{3.13}$$

which is the Lax-Wendroff (L-W) scheme [14].

Applying the stability analysis method introduced in last chapter, from equation (2.28) the amplification factor λ of the scheme is

$$\lambda = 1 - 2c^2 \tag{3.14}$$

For stability one requires $|\lambda| \leq 1$ which is satisfied if

$$|c| \leq 1 \tag{3.15}$$

Upwind Schemes

The upwind scheme is denoted by $U_j^{n+1} = f(U_j^n, U_{j-1}^n, U_{j-2}^n)$ when we assume $a > 0$ in equation (3.1).

Here, $k_1 = 0,\ k_2 = -1,\ k_3 = -2$ in equation (3.10), which gives

$$\begin{cases} -B_{-1} - 2B_{-2} = -c \\ B_{-1} + 4B_{-2} = c^2 \\ B_0 = 1 - B_{-1} - B_{-2} \end{cases}$$

$$\begin{cases} B_0 = 1 + \frac{1}{2}c^2 - \frac{3}{2}c \\ B_{-1} = 2c - c^2 \\ B_{-2} = \frac{1}{2}c^2 - \frac{1}{2}c \end{cases} \tag{3.16}$$

Therefore

$$U_j^{n+1} = (1 + \frac{1}{2}c^2 - \frac{3}{2}c)U_j^n + (2c - c^2)U_{j-1}^n + (\frac{1}{2}c^2 - \frac{1}{2}c)U_{j-2}^n \tag{3.17}$$

which is the Beam-Warming (B-W) scheme [49].

The amplification factor of the scheme is

$$\lambda = 2c^2 - 4c + 1 \tag{3.18}$$

For stability $|\lambda| \leq 1$ which is satisfied if

$$0 \leq c \leq 2 \tag{3.19}$$

For negative speed a in equation (3.1) the corresponding three-point upwind scheme is

$$U_j^{n+1} = (1 + \frac{1}{2}c^2 + \frac{3}{2}c)U_j^n - (c^2 + 2c)U_{j+1}^n + (\frac{1}{2}c^2 + \frac{1}{2}c)U_{j+2}^n \tag{3.20}$$

The amplification factor of the scheme is

$$\lambda = 2c^2 + 4c + 1 \tag{3.21}$$

The stability condition for the scheme is

$$-2 \leq c \leq 0 \tag{3.22}$$

3.3.2 Fully Discrete Third-order Schemes

From equation (3.5) third-order schemes use at least four grid points.

Upwind-biased Schemes

Let us consider a upwind-biased scheme which is denoted as $U_j^{n+1} = f(U_j^n, U_{j-1}^n, U_{j+1}^n, U_{j+2}^n)$.

Here, $k_1 = 0,\ k_2 = -1,\ k_3 = 1,$ and $k_4 = 2$. From equation (3.10) we have

$$\begin{cases} B_0 = 1 - B_{-1} - B_1 - B_2 \\ -B_{-1} + B_1 + 2B_2 = -c \\ B_{-1} + B_1 + 4B_2 = c^2 \\ -B_{-1} + B_1 + 8B_2 = -c^3 \end{cases}$$

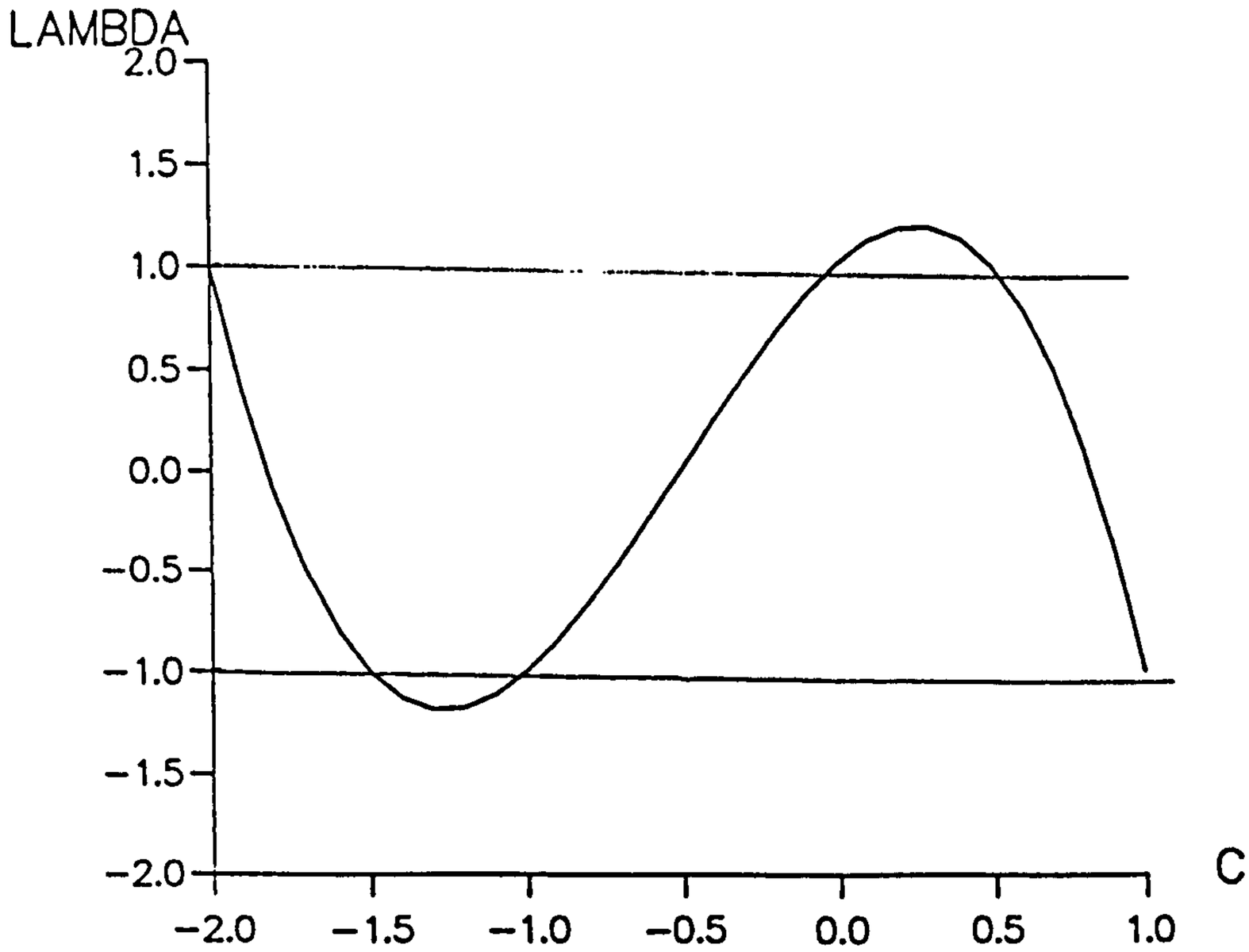

Figure 3.1: Amplification Factor of Third-order Upwind-biased Scheme

or

$$\begin{cases} B_0 = 1 + \frac{1}{2}c - c^2 - \frac{1}{2}c^3 \\ B_{-1} = \frac{1}{6}c^3 + \frac{1}{2}c^2 + \frac{1}{3}c \\ B_1 = \frac{1}{2}c^3 + \frac{1}{2}c^2 - c \\ B_2 = \frac{1}{6}c - \frac{1}{6}c^3 \end{cases} \tag{3.23}$$

Therefore the third-order upwind-biased numerical scheme is

$$\begin{aligned} U_j^{n+1} &= (1 + \frac{1}{2}c - c^2 - \frac{1}{2}c^3)U_j^n + (\frac{1}{6}c^3 + \frac{1}{2}c^2 + \frac{1}{3}c)U_{j-1}^n \\ &\quad + (\frac{1}{2}c^3 + \frac{1}{2}c^2 - c)U_{j+1}^n + (\frac{1}{6}c - \frac{1}{6}c^3)U_{j+2}^n \end{aligned} \tag{3.24}$$

Applying semi-empirical stability analysis approach, the amplification factor of this scheme is

$$\lambda = 1 - \frac{4}{3}c^3 - 2c^2 + \frac{4}{3}c \tag{3.25}$$

Figure 3.1 plotes equation (3.25). When λ moves from -1 to 1, there are three possible regions satisfying the condition of $|\lambda| \leq 1$. Monotonicity analysis indicates that the

amplification factor is monotone only in the region of $-1 \leq c \leq 0$ and it is also proved that other regions are not stable. Therefore, the stability condition for this scheme is:

$$-1 \leq c \leq 0 \tag{3.26}$$

which implies that $a < 0$ in equation (3.1).

For positive speed a in (3.1) the corresponding four-point upwind-biased scheme is

$$\begin{aligned} U_j^{n+1} &= (1 + \frac{1}{2}c^3 - c^2 - \frac{1}{2}c)U_j^n + (\frac{1}{6}c^3 - \frac{1}{6}c)U_{j-2}^n \\ &\quad -(\frac{1}{6}c^3 - \frac{1}{2}c^2 + \frac{1}{3}c)U_{j+1}^n + (c + \frac{1}{2}c^2 - \frac{1}{2}c^3)U_{j-1}^n \end{aligned} \tag{3.27}$$

The amplification factor is

$$\lambda = 1 + \frac{4}{3}c^3 - 2c^2 - \frac{4}{3}c \tag{3.28}$$

The stability condition for this scheme is defined as

$$0 \leq c \leq 1 \tag{3.29}$$

Upwind Schemes

The four-point upwind scheme is denoted as $U_j^{n+1} = f(U_j^n, U_{j+1}^n, U_{j+2}^n, U_{j+3}^n)$

By repeating the same procedure as before, the scheme is

$$\begin{aligned} U_j^{n+1} &= (1 + \frac{11}{6}c + c^2 + \frac{1}{6}c^3)U_j^n - (\frac{1}{2}c^3 + \frac{5}{2}c^2 + 3c)U_{j+1}^n \\ &\quad +(\frac{1}{2}c^3 + 2c^2 + \frac{3}{2}c)U_{j+2}^n - (\frac{1}{6}c^3 + \frac{1}{2}c^2 + \frac{1}{3}c)U_{j+3}^n \end{aligned} \tag{3.30}$$

The amplification factor is

$$\lambda = 1 + \frac{4}{3}c^3 + 6c^2 + \frac{20}{3}c \tag{3.31}$$

The stability condition for this scheme indicates (see figure 3.2)

$$-2 \leq c \leq -1 \tag{3.32}$$

which implies that $a < 0$ in equation (3.1).

For positive speed a in (3.1) the corresponding four-point upwind scheme is

$$\begin{aligned} U_j^{n+1} &= (1 - \frac{1}{6}c^3 + c^2 - \frac{11}{6}c)U_j^n + (\frac{1}{2}c^3 - \frac{5}{2}c^2 + 3c)U_{j-1}^n \\ &\quad -(\frac{1}{2}c^3 - 2c^2 + \frac{3}{2}c)U_{j-2}^n + (\frac{1}{6}c^3 - \frac{1}{2}c^2 + \frac{1}{3}c)U_{j-3}^n \end{aligned} \tag{3.33}$$

The amplification factor is

$$\lambda = 1 - \frac{4}{3}c^3 + 6c^2 - \frac{20}{3}c \tag{3.34}$$

The stability condition for this scheme

$$1 \leq c \leq 2 \tag{3.35}$$

is defined.

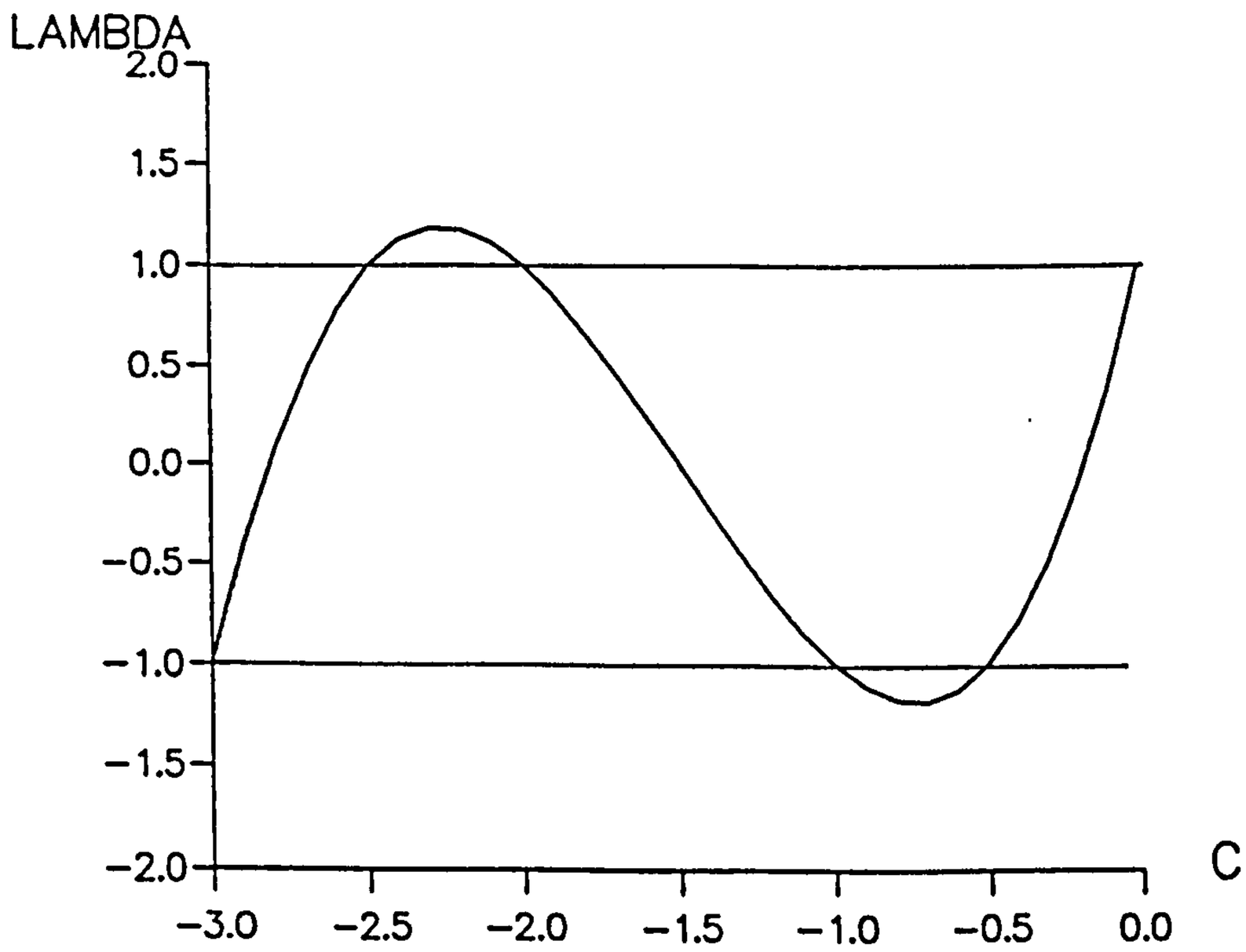

Figure 3.2: Amplification Factor of Third-order Upwind Scheme

3.3.3 Fully Discrete Fourth-order Schemes

From equation (3.5) the fourth-order scheme needs at least five grid points.

Space-centered Scheme

The five-point, space-centered scheme is

$$U_j^{n+1} = (1 + \frac{1}{4}c^4 - \frac{5}{4}c^2)U_j^n + (\frac{1}{24}c^4 + \frac{1}{12}c^3 - \frac{1}{24}c^2 - \frac{1}{12}c)U_{j-2}^n$$

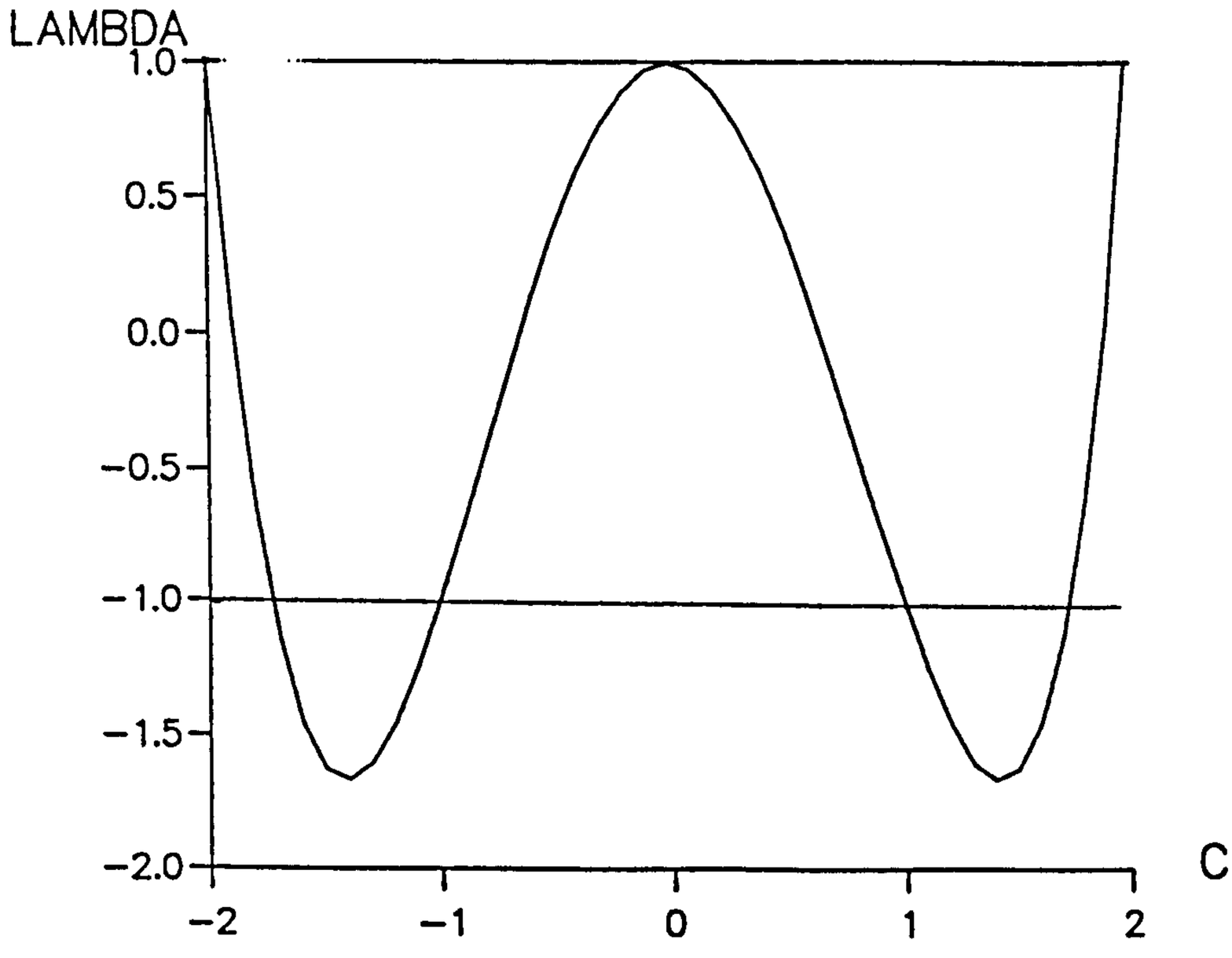

Figure 3.3: Amplification Factor of Fourth-order Space-centered Scheme

$$+(\frac{2}{3}c+\frac{2}{3}c^2-\frac{1}{6}c^3-\frac{1}{6}c^4)U_{j-1}^n+(\frac{1}{6}c^3+\frac{2}{3}c^2-\frac{1}{6}c^4-\frac{2}{3}c)U_{j+1}^n$$
$$+(\frac{1}{12}c-\frac{1}{24}c^2-\frac{1}{12}c^3+\frac{1}{24}c^4)U_{j+2}^n \tag{3.36}$$

The amplification factor of the scheme is

$$\lambda = 1-\frac{8}{3}c^2+\frac{2}{3}c^4 \tag{3.37}$$

The stability condition of this scheme (refer to Figure 3.3)

$$-1 \le c \le 1 \tag{3.38}$$

is defined.

Upwind-biased Schemes

The five-point, upwind-biased scheme is

$$U_j^{n+1} = (1-\frac{1}{6}c^4-\frac{5}{6}c^3-\frac{5}{6}c^2+\frac{5}{6}c)U_j^n+(\frac{1}{24}c^4+\frac{1}{4}c^3+\frac{11}{24}c^2+\frac{1}{4}c)U_{j-1}^n$$

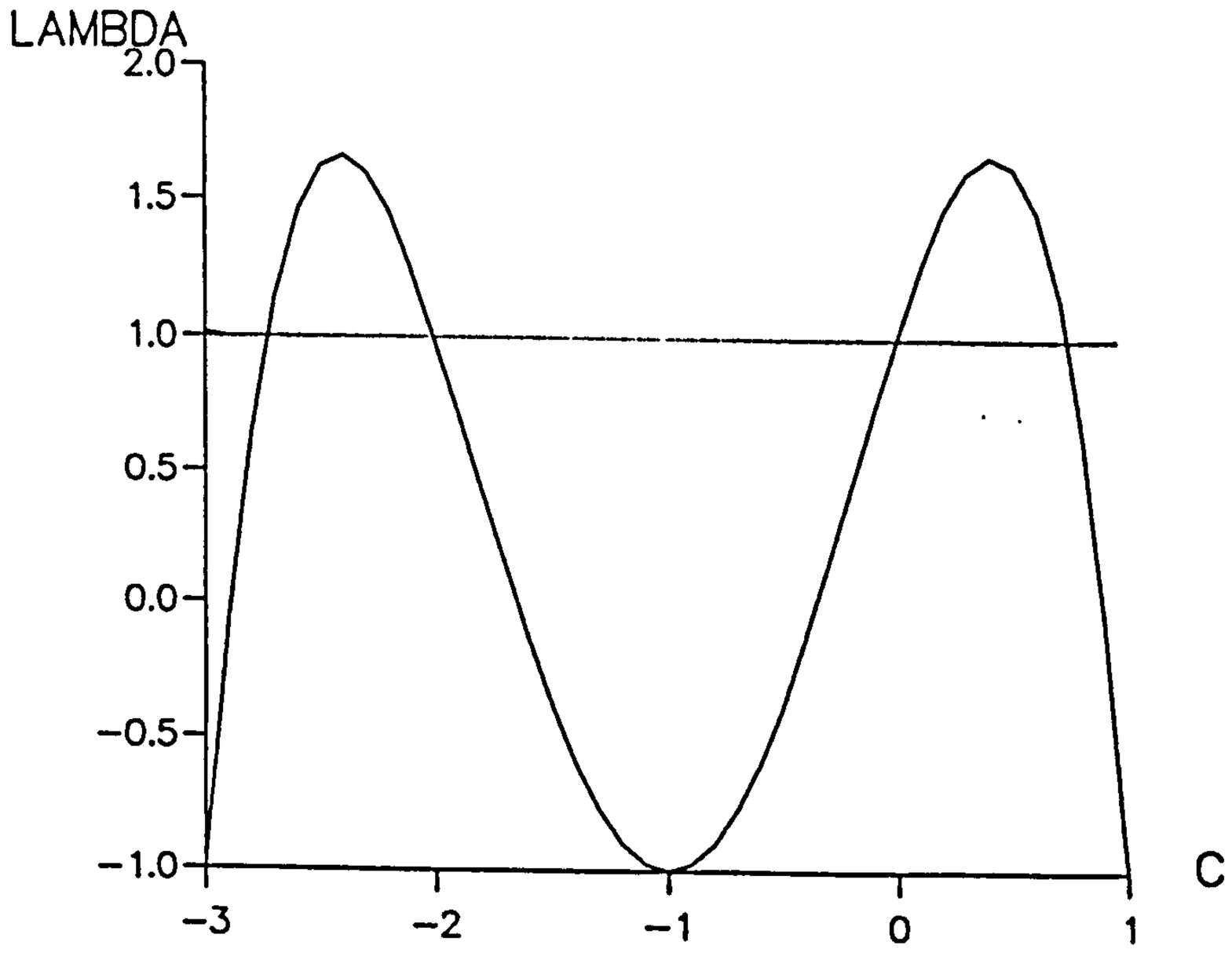

Figure 3.4: Amplification Factor of Fourth-order Upwind-biased Scheme

$$+(\frac{1}{4}c^4+c^3+\frac{1}{4}c^2-\frac{3}{2}c)U^n_{j+1}-\frac{1}{6}(c^4+3c^3-c^2-3c)U^n_{j+2}$$
$$+\frac{1}{24}(c^4+2c^3-c^2-2c)U^n_{j+3} \tag{3.39}$$

The amplification factor of this scheme is

$$\lambda = 1-\frac{2}{3}c^4-\frac{8}{3}c^3-\frac{4}{3}c^2+\frac{8}{3}c \tag{3.40}$$

Figure 3.4 indicates that the stability condition for this scheme is

$$-2 \le c \le 0 \tag{3.41}$$

which implies that $a < 0$ in equation (3.1).

For positive speed a in (3.1) the corresponding five-point, upwind-biased scheme is

$$\begin{aligned} U^{n+1}_j &= (1-\frac{1}{6}c^4+\frac{5}{6}c^3-\frac{5}{6}c^2-\frac{5}{6}c)U^n_j+(\frac{1}{24}c^4-\frac{1}{12}c^3-\frac{1}{24}c^2+\frac{1}{12}c)U^n_{j-3} \\ &+(\frac{1}{2}c^3+\frac{1}{6}c^2-\frac{1}{6}c^4-\frac{1}{2}c)U^n_{j-2}+(\frac{1}{4}c^4-c^3+\frac{1}{4}c^2+\frac{3}{2}c)U^n_{j-1} \\ &+(\frac{1}{24}c^4-\frac{1}{4}c^3+\frac{11}{24}c^2-\frac{1}{4}c)U^n_{j+1} \end{aligned} \tag{3.42}$$

The amplification factor is

$$\lambda = 1 - \frac{2}{3}c^4 + \frac{8}{3}c^3 - \frac{4}{3}c^2 - \frac{8}{3}c \tag{3.43}$$

The stability condition for this scheme is defined as

$$0 \leq c \leq 2 \tag{3.44}$$

Upwind Schemes

The five-point, upwind scheme is

$$\begin{aligned} U_j^{n+1} &= (1 - \frac{25}{12}c + \frac{35}{24}c^2 - \frac{5}{12}c^3 + \frac{1}{24}c^4)U_j^n + (\frac{1}{24}c^4 - \frac{1}{4}c^3 + \frac{11}{24}c^2 - \frac{1}{4}c)U_{j-4}^n \\ &+(\frac{4}{3}c - \frac{7}{3}c^2 + \frac{7}{6}c^3 - \frac{1}{6}c^4)U_{j-3}^n + (\frac{1}{4}c^4 - 2c^3 + \frac{19}{4}c^2 - 3c)U_{j-2}^n \\ &+(4c - \frac{13}{3}c^2 + \frac{3}{2}c^3 - \frac{1}{6}c^4)U_{j-1}^n \end{aligned} \tag{3.45}$$

The amplification factor is

$$\lambda = 1 + \frac{2}{3}c^4 - \frac{16}{3}c^3 + \frac{40}{3}c^2 - \frac{32}{3}c \tag{3.46}$$

The stability condition for this scheme is

$$1 \leq c \leq 3 \tag{3.47}$$

which implies that $a > 0$ in equation (3.1).

For negative speed a in (3.1) the corresponding five-point, upwind scheme is

$$\begin{aligned} U_j^{n+1} &= (1 + \frac{1}{24}c^4 + \frac{5}{12}c^3 + \frac{35}{24}c^2 + \frac{25}{12}c)U_j^n - (\frac{1}{6}c^4 + \frac{3}{2}c^3 + \frac{13}{3}c^2 + 4c)U_{j+1}^n \\ &+(\frac{1}{4}c^4 + 2c^3 + \frac{19}{4}c^2 + 3c)U_{j+2}^n - \frac{1}{6}(c^4 + 7c^3 + 14c^2 + 8c)U_{j+3}^n \\ &+\frac{1}{24}(c^4 + 6c^3 + 11c^2 + 6c)U_{j+4}^n \end{aligned} \tag{3.48}$$

The amplification factor is

$$\lambda = 1 + \frac{2}{3}c^4 + \frac{16}{3}c^3 + \frac{40}{3}c^2 + \frac{32}{3}c \tag{3.49}$$

The stability condition of this scheme (see figure 3.5)

$$-3 \leq c \leq -1 \tag{3.50}$$

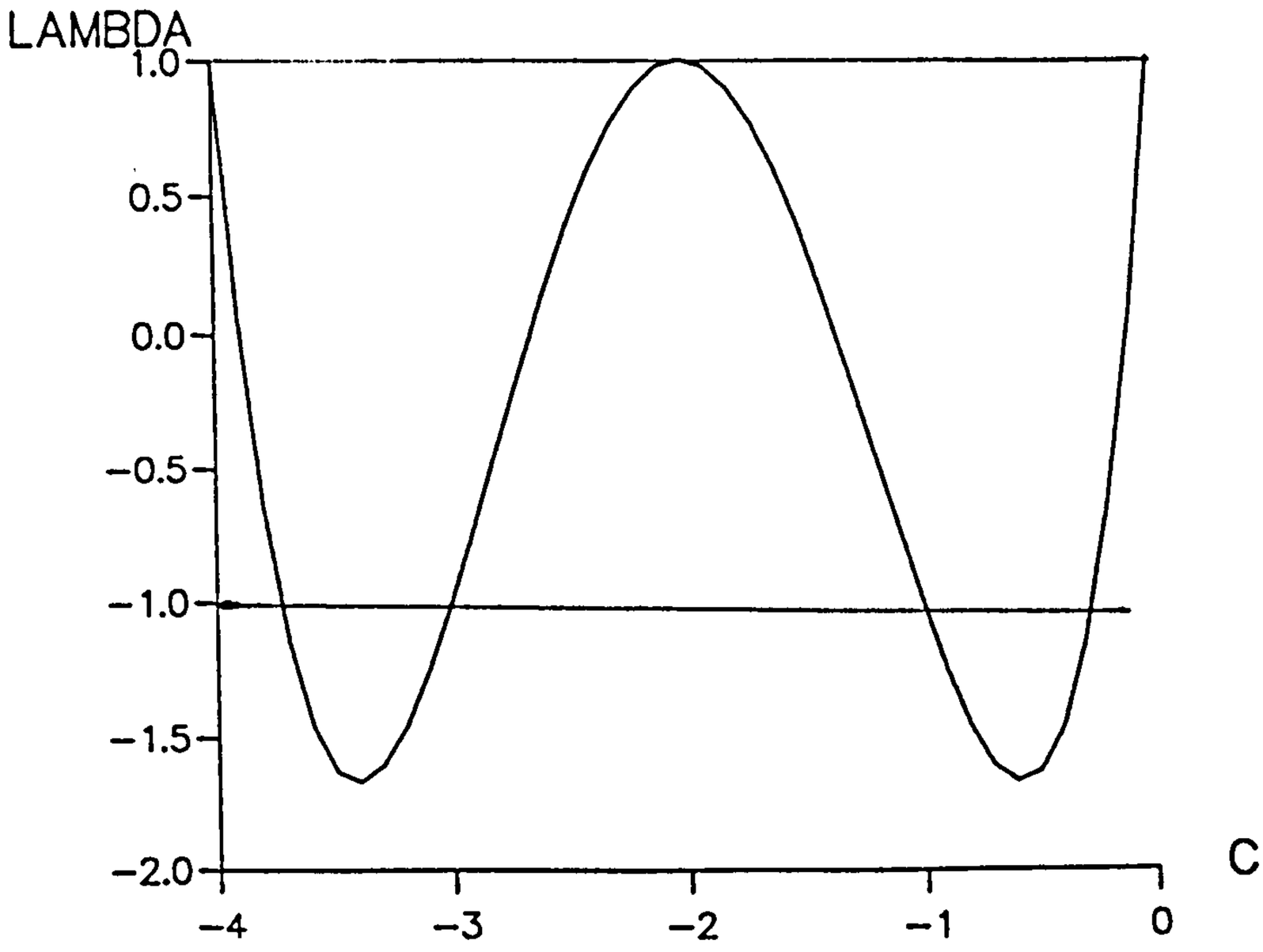

Figure 3.5: Amplification Factor of Fourth-order Upwind Scheme

is fefined.

So far, we have developed second-, third- and fourth-order schemes. We can develop any high-order schemes according to the fully discrete approach. To illustrate this a 20th-order, space-centered numerical method is presented in the appendix.

3.4 Numerical Experiments

In this section some numerical experiments are used to demonstrate the performance of the fully discrete high-order numerical schemes. To this end a smooth initial condition is selected

$$u(x,0) = sin\frac{\pi}{2}x \tag{3.51}$$

We are interested in evolving the solution for long times. The chosen computational domain is therefore large and varies according to the evolution time. A fixed mesh width $\Delta x = 0.1$ and a Courant number coefficient 0.7 are selected.

Figure 3.6 shows a comparison between the numerical solution obtained by the Lax-Wendroff method (boxes) and the exact solution (solid line) after 1000 time steps. The dispersive errors of the method are evident and result in a trailing numerical solution. Clearly second-order methods can be very inaccurate in modelling long time behaviour.

Figure 3.7 shows a comparison between the numerical solution obtained by the third-order upwind-biased method and the exact solution after 6000 time steps. Although the solution looks more acceptable than the Lax-Wendroff solution evolved for only 1000 time steps, the numerical diffusion of the thir-order scheme produces the inaccuracy observed.

Figure 3.8 shows a comparison between the numerical solution obtained by the fourth-order space-centered method and the exact solution after 20000 time steps. The numerical solution still looks accurate at the shown time. This indicates that the accuracy of numerical solutions is improved dramatically by changing from second to fourth order methods.

Figure 3.9 shows a comparison between the numerical solution obtained by the 20th-order space-centered method and the exact solution after 50000 time steps. As expected the numerical solution looks very accurate.

To summarize the situation figure 3.10 shows the comparison of the Lax-Wendroff method (crosses), the fourth-order space-centered scheme (boxes) and the exact solution (solid line) after 10000 time steps. The effects of dispersion and diffusion have made the solution of the Lax-Wendroff method meaningless. This justifies the necessity for higher-order numerical schemes for problems which involve long time evolution.

3.5 Summary

An approach for constructing two-level explicit fully discrete arbitrary-order numerical methods for the one dimensional model advetion equation has been presented. To illustrate the methodology fully discrete second-, third-, fourth-, and 20th-order numerical schemes have been given. Numerical experiments indicate that second-order methods are not accurate enough for problems requiring long time evolution, and a dramatic improvement of the numerical solution is seen when the accuracy changes from second to fourth order.

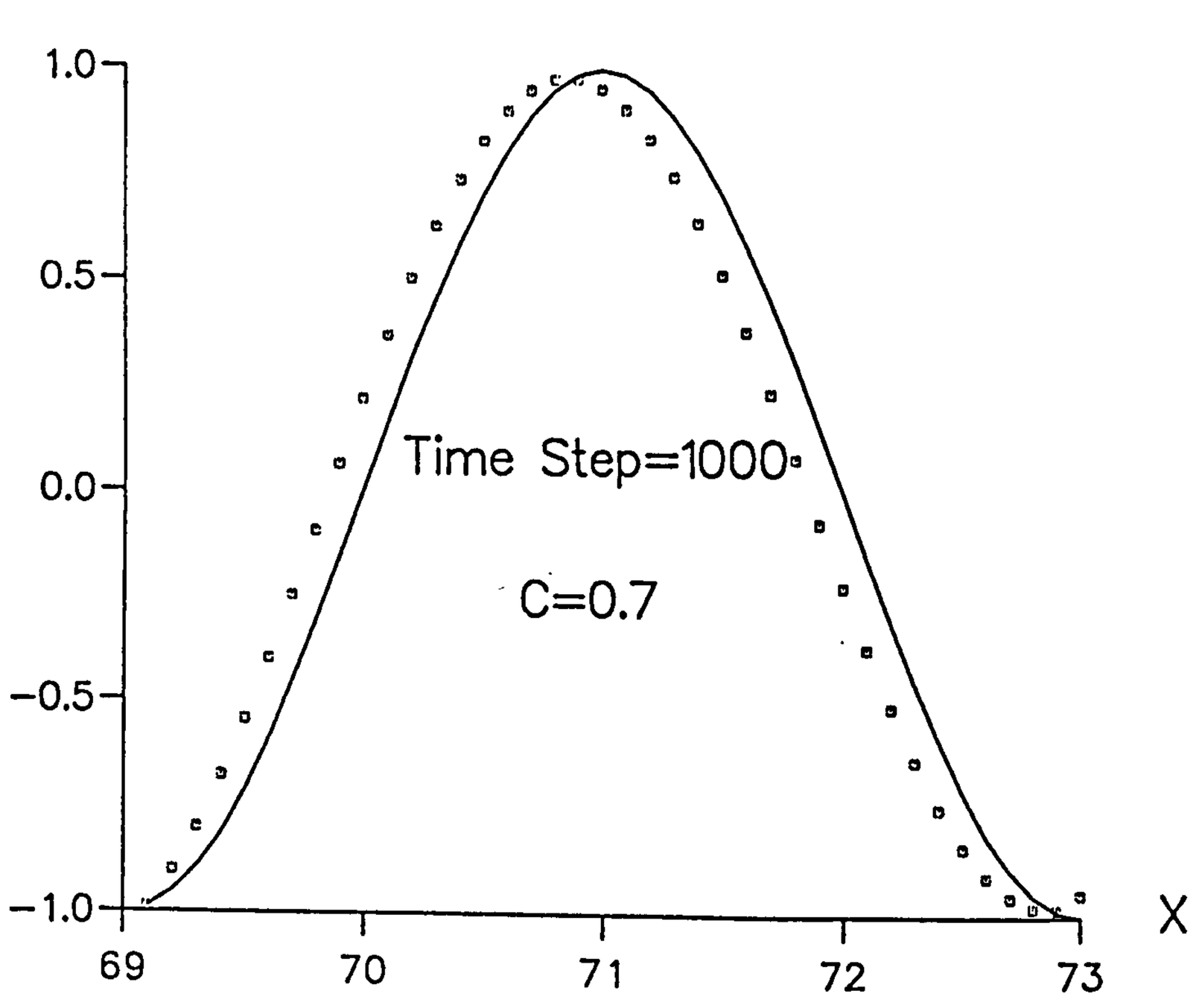

Figure 3.6: Numerical Solution by the Lax-Wendroff Method (symbol) and the Exact Solution (line)

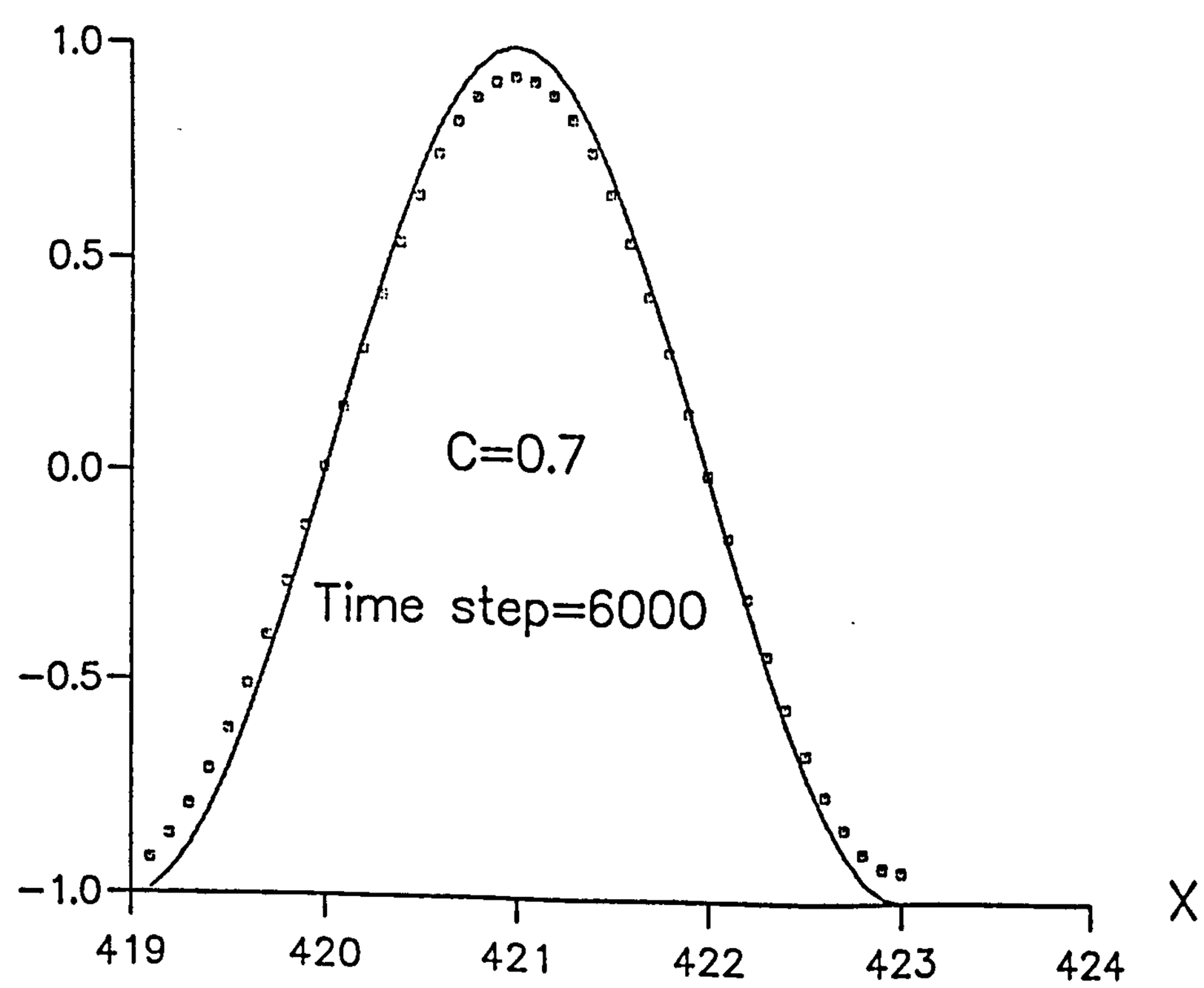

Figure 3.7: Numerical Solution by the 3rd-order, Upwind-biased Method (symbol) and the Exact Solution (line)

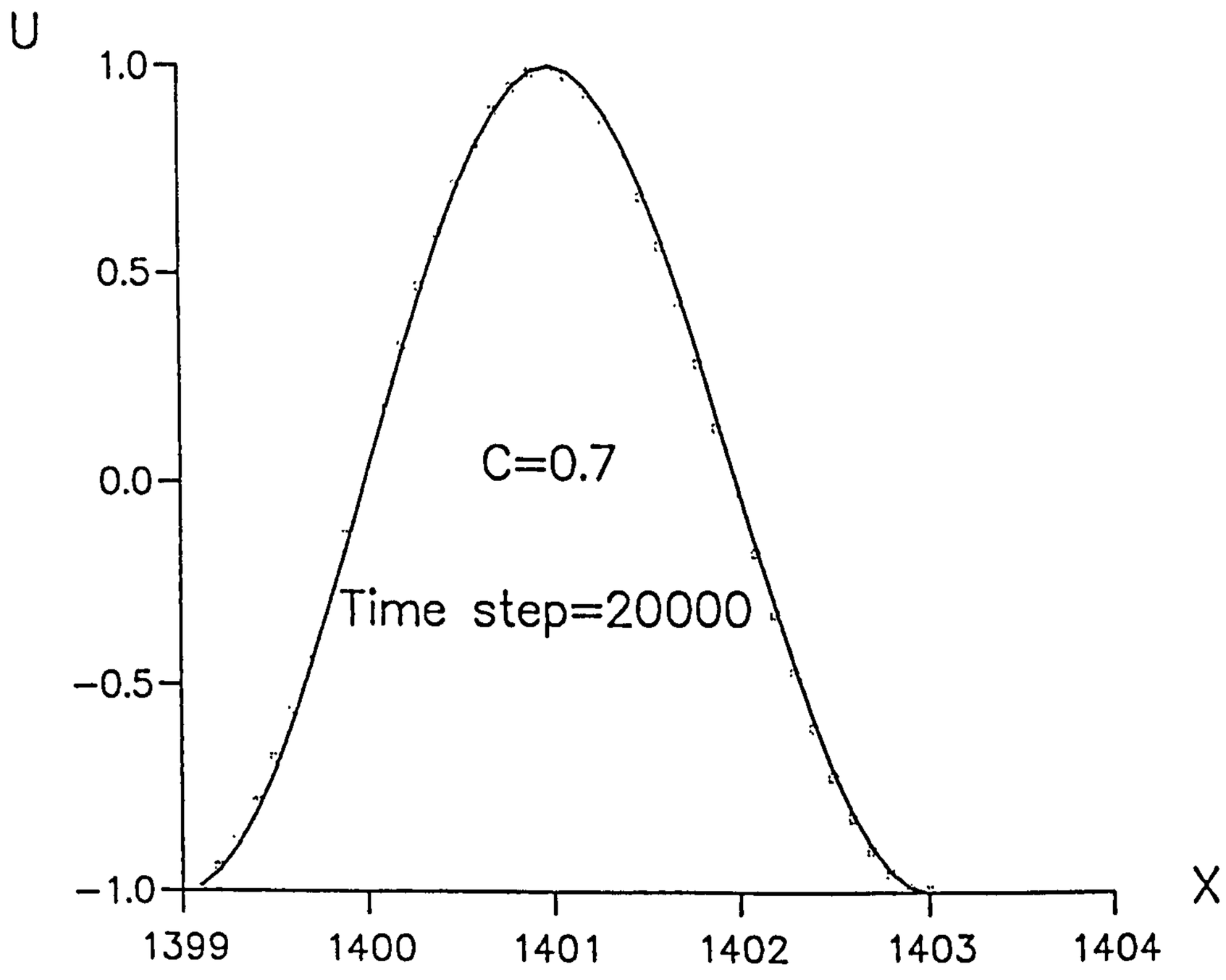

Figure 3.8: Numerical Solution by the 4th-order Space-centered Method (symbol) and the Exact Solution (line)

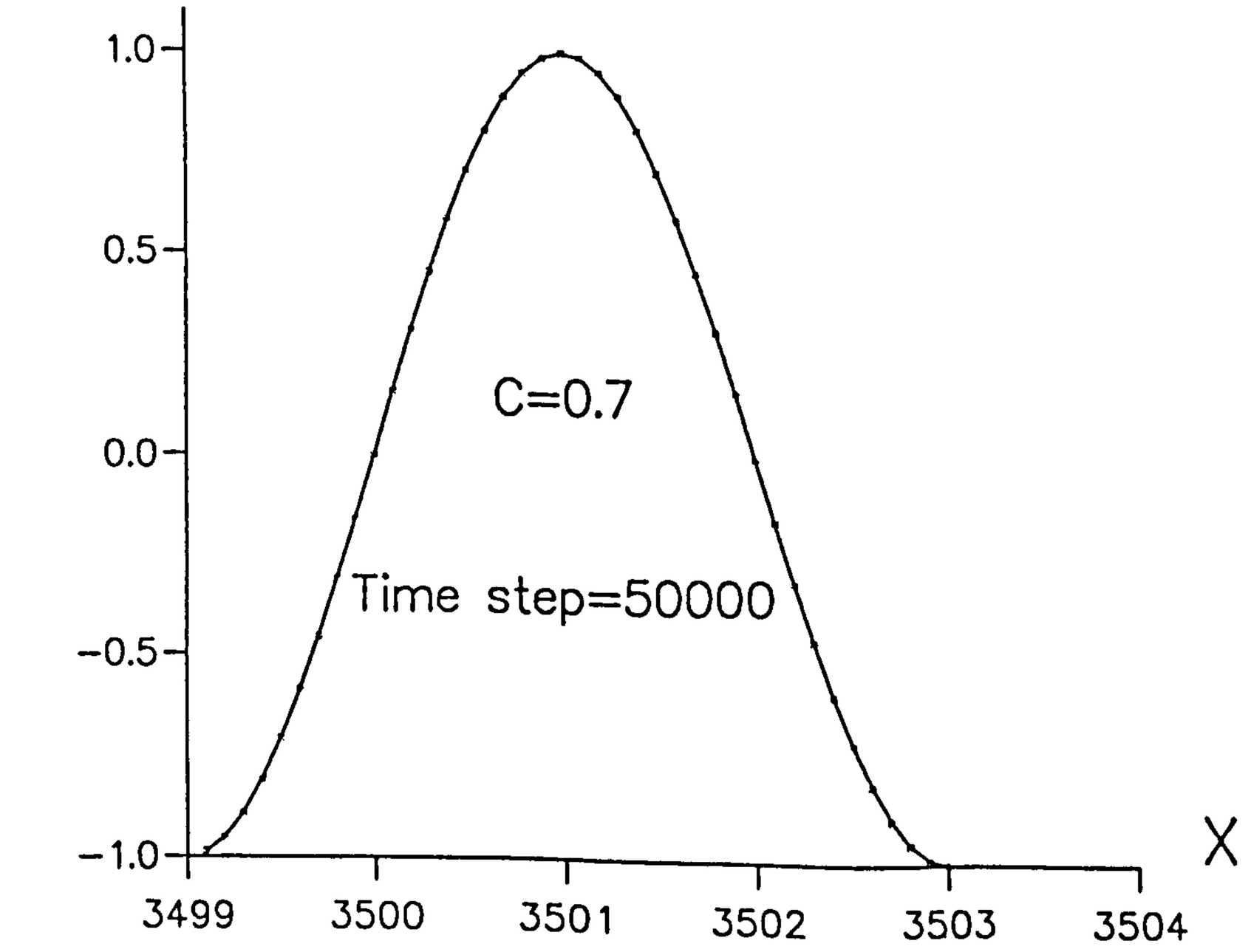

Figure 3.9: Numerical Solution by the 20th-order Space-centered Method (symbol) and the Exact Solution (line)

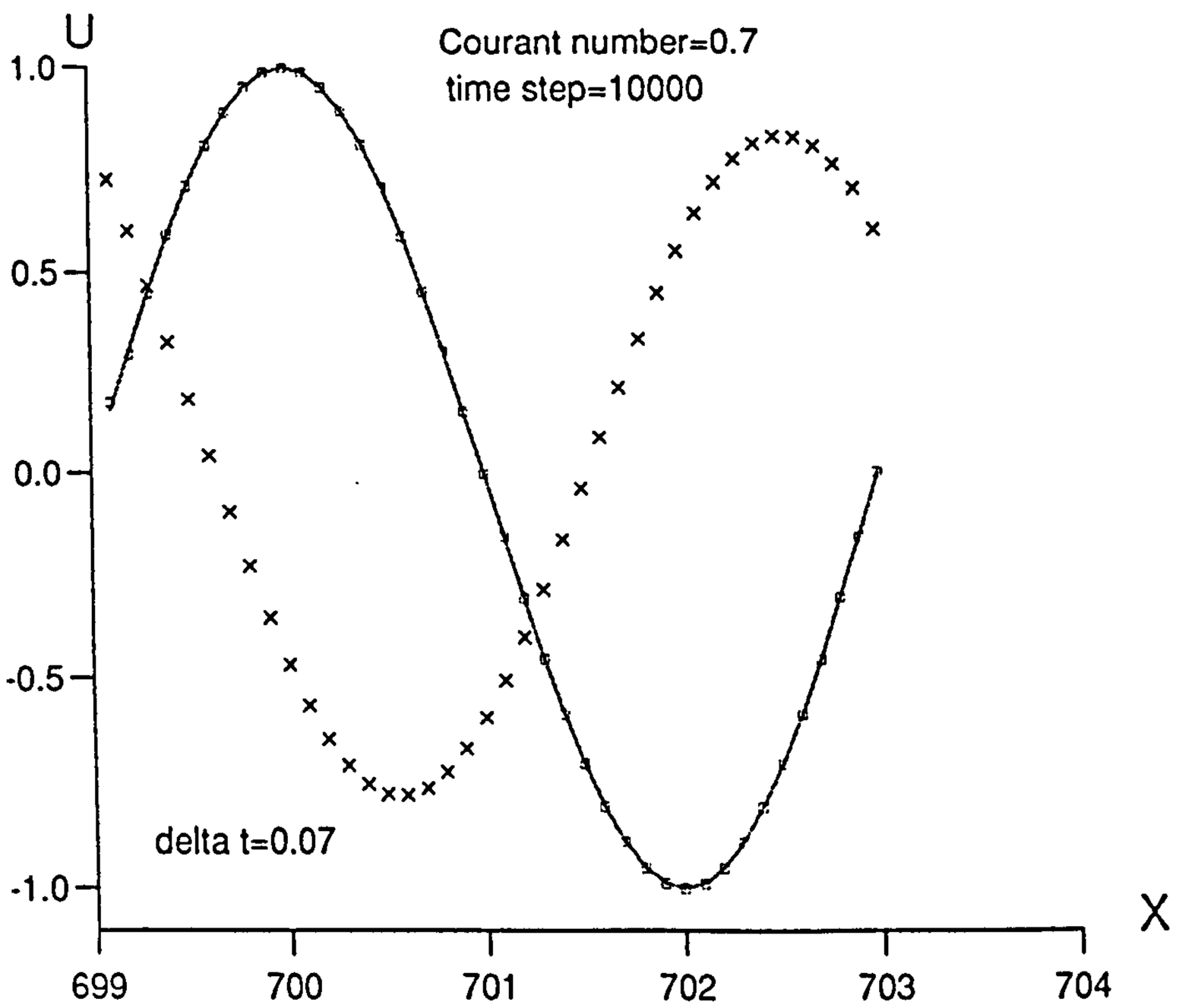

Figure 3.10: Comparision between the Lax-Wendroff Method (crosses), the 4th-order Spaced-centered Method (boxes) and the Exact Solution (line)

Chapter 4

Conservative High-order Schemes and Entropy Condition

4.1 Introductory Remarks

In the last chapter a fully discrete approach was presented from which 2-level, explicit, arbitrary-order, finite-difference numerical methods can be constructed. However these schemes are only suitable for linear systems or non-linear systems with smooth solutions. When extending these methods to nonlinear conservation laws we expect to meet three new problems. First the method might suffer nonlinear instability; second the method might coverge to a function that is not a weak solution at all for the conservation law considered; three the method might coverge to a wrong weak solution. The first problem is often triggered by oscillations and needs special treatment which will be discussed in next chapter.

The problem of converging to a function that is not a weak solution at all lies in the fact that a differential equation of a conservation law can be manipulated to obtain a variety of equations of conservation laws, which implies that a numerical method that is consisitent with one of these conservation laws is also consistent with all of other conservation laws. When applying the method to solve these conservation laws for smooth solutions the method will give exactly the same solutions; however in the context of discontinuities it is impossible for the method to converge to a function that is a weak solution for all of the

conservation laws which actually have different weak solutions.

The root of the problem discussed above stems from the non-conservative formulations of the methods. For discontinuous flows the discretization of the non-conservative form will not lead to the correct solutions. Therefore in order to obtain the correct discontinuities numerically, it is necessary to discretize the conservative form of the flow equations.

To prevent a wrong weak solution the numerical approximations have to satisfy the *entropy* condition, which will pick up the physically meaningfull solution.

In this chapter the conservative, entropy-satisfying schemes will be discussed and a methodology will be investigated from which the arbitrary-order finite-difference schemes of the previous chapter can be reformulated in a conservative form . The rest of the chapter is arranged as follows: section 2 presents an approach for constructing conservative numerical methods; section 3 gives the fully discrete conservative high-order numerical schemes; section 4 discusses the entropy condition that the high-order conservative methods have to satisfy; section 5 is the summary of the chapter.

4.2 Conservative Schemes

We consider the one dimensional integral form

$$\int_{x_{j-1/2}}^{x_{j+1/2}} u(x,t_{n+1})\,dx = \int_{x_{j-1/2}}^{x_{j+1/2}} u(x,t_n)\,dx - \left[\int_{t_n}^{t_{n+1}} f\left(u(x_{j+1/2},t)\right)\,dt - \int_{t_n}^{t_{n+1}} f\left(u(x_{j-1/2},t)\right)\,dt\right] \tag{4.1}$$

of the scalar hyperbolic conservation laws $u_t+f(u)_x=0$. Rather than as an approximation to the pointwise value $u(x_j,t_n)$ in the last chapter, U_j^n is used to denote the computed approximation to a cell average of $u(x,t_n)$ defined by

$$\bar{u}^n(x_j,t_n)=\frac{1}{h}\int_{x_{j-1/2}}^{x_{j+1/2}} u(x,t_n)\,dx \tag{4.2}$$

Substituting equation (4.2) into equation (4.1) given

$$\bar{u}_j^{n+1}=\bar{u}_j^n-\frac{1}{h}\left[\int_{t_n}^{t_{n+1}} f\left(u(x_{j+1/2},t)\right)\,dt-\int_{t_n}^{t_{n+1}} f\left(u(x_{j-1/2},t)\right)\,dt\right] \tag{4.3}$$

Denoting

$$F_{j+\frac{1}{2}}=\frac{1}{k}\int_{t_n}^{t_{n+1}} f\left(u(x_{j+1/2},t)\right)\,dt \tag{4.4}$$

equation (4.3) gives

$$U_j^{n+1} = U_j^n - \frac{k}{h}\left(F_{j+\frac{1}{2}} - F_{j-\frac{1}{2}}\right) \tag{4.5}$$

where F is a numerical flux function which satisfies the consistency condition if

$$F(\bar{u}, \bar{u}, \ldots, \bar{u}) = f(\bar{u}) \tag{4.6}$$

Here $\bar{u}$ is constant.

Since a weak solution $u(x,t)$ satisfies the integral form (4.1), a numerical method in the form of equation (4.5) which is derived from equation (4.1) will guarantee that any discontinuities computed will be in the correct location and therefore converge to the correct weak solutions (if the discontinuities also satisfy the *entropy* condition). In [13] Lax and Wendroff proved this is true. In this sense equation (4.5) is called the conservative method.

However, it is difficult to derive conservative methods, i.e. the numerical flux $F_{j+1/2}$, from the discretization of the integal form of equation (4.1). To get around the difficulty I introduce a way from which the finite-diference methods generated from the differential form of a PDE can be reformulated in a conservative form as follows.

Lemma *Scheme (3.2) can be expressed as*

$$U_j^{n+1} = U_j^n - \frac{k}{h}\left[\frac{1}{c}F_j^n - \sum_{\alpha=1}^{p}\frac{1}{c}B_{k_\alpha}F_{j+k_\alpha}^n\right] \tag{4.7}$$

where the vector B_{k_α} is determined by equation (3.3).

Proof

By manipulating equation (3.2) we have

$$\begin{aligned} U_j^{n+1} &= \sum_{\alpha=1}^{p} B_{k_\alpha}U_{j+k_\alpha}^n \\ &= U_j^n - (1 - B_0)U_j^n + \sum_{\alpha=1,k_\alpha\neq 0}^{p} B_{k_\alpha}U_{j+k_\alpha}^n \\ &= U_n^n - \frac{k}{h}\left[\frac{1}{c}F_j^n - \sum_{\alpha=1}^{p}\frac{1}{c}B_{k_\alpha}F_{j+k_\alpha}^n\right] \end{aligned}$$

which is equation (4.7).

From here we can derive the numerical flux for the conservative form (4.5) of scheme (3.2) by the following theorem.

Theorem 2 *Scheme (3.2) written in conservative form (4.5) has numerical flux*

$$\begin{cases} F_{j+\frac{1}{2}} = \sum_{\alpha=2}^{p} B_\alpha F_{j+k_\alpha}^n \\ F_{j-\frac{1}{2}} = \sum_{\alpha=1}^{p-1} B_{\alpha+1} F_{j+k_\alpha}^n \end{cases} \tag{4.8}$$

the coefficients B_α are defined by

$$\begin{cases} B_p = A_p \\ B_2 = -A_1 \\ B_\alpha - B_{\alpha+1} = A_\alpha \\ (\alpha = 2, 3, \ldots, p-1) \end{cases} \tag{4.9}$$

Proof

If we rewrite the scheme (4.7) as

$$U_j^{n+1} = U_j^n - \frac{k}{h} \sum_{\alpha=1}^{p} A_\alpha F_{j+k_\alpha}^n \tag{4.10}$$

where α is the grid point number, A_α are the coefficients and the p points are arranged as

$$k_1 < k_2 < k_3 < \ldots < k_p \tag{4.11}$$

then

$$F_{j+\frac{1}{2}} - F_{j-\frac{1}{2}} = \sum_{\alpha=2}^{p} B_\alpha F_{j+k_\alpha}^n - \sum_{\alpha=1}^{p-1} B_{\alpha+1} F_{j+k_\alpha}^n$$

$$= B_p F_{j+k_p}^n - B_2 F_{j+k_1}^n + \sum_{\alpha=2}^{p-1} (B_\alpha - B_{\alpha+1}) F_{j+k_\alpha}^n$$

From equation (4.10) we have

$$B_p F_{j+k_p}^n - B_2 F_{j+k_1}^n + \sum_{\alpha=2}^{p-1} (B_\alpha - B_{\alpha+1}) F_{j+k_\alpha}^n = \sum_{\alpha=1}^{p} A_\alpha F_{j+k_\alpha}^n \tag{4.12}$$

Comparing the coefficients on both sides of equation (4.12) we have the following

$$\begin{cases} B_p = A_p \\ B_2 = -A_1 \\ B_\alpha - B_{\alpha+1} = A_\alpha \\ (\alpha = 2, 3, \ldots, p-1) \end{cases}$$

which is equation (4.9) and the proof is complete.

4.3 Conservative High-order Numerical Schemes

In this section, some examples are used to demonstrate how to apply the method presented previously in order to derive conservative high-order numerical schemes.

4.3.1 Conservative Second-order Schemes

Space-centered Scheme

The conservative form of the space-centered scheme, see equation (3.13), according to equation (4.7), is

$$U_j^{n+1} = U_j^n - \frac{k}{h}\left[-\frac{1}{2}(1+c)F_{j-1}^n + cF_j^n + \frac{1}{2}(1-c)F_{j+1}^n\right] \tag{4.13}$$

Note that here, from equation (4.11), $k_1 = -1,\ k_2 = 0,\ k_3 = 1$.

From equation (4.10) we have

$$\begin{cases} A_1 = -\frac{1}{2}(1+c) \\ A_2 = c \\ A_3 = \frac{1}{2}(1-c) \end{cases}$$

and from equation (4.9) we have

$$\begin{cases} B_3 = A_3 = \frac{1}{2}(1-c) \\ B_2 = -A_1 = \frac{1}{2}(1+c) \\ B_2 - B_3 = A_2 = c \end{cases}$$

Therefore the numerical flux of the scheme is

$$F_{j+\frac{1}{2}}^{L-W} = \frac{1}{2}(1+c)F_j^n + \frac{1}{2}(1-c)F_{j+1}^n \tag{4.14}$$

The alternative version of the flux can be written as

$$F_{j+\frac{1}{2}} = \frac{1}{2}(F_j^n + F_{j+1}^n) - \frac{|a|}{2}\Delta U_{j+\frac{1}{2}} + \frac{|a|}{2}(1-|c|)\Delta U_{j+\frac{1}{2}} \tag{4.15}$$

where $\Delta U_{j+1/2} = U_{j+1} - U_j$.

Upwind Scheme

The conservative form of the Beam-Warming scheme, see equation (3.17), according to equation (4.7) is

$$U_j^{n+1} = U_j^n - \frac{k}{h}\left[\frac{1}{2}(3-c)F_j^n - (2-c)F_{j-1}^n - \frac{1}{2}(c-1)F_{j-2}^n\right] \tag{4.16}$$

where from equation (4.11), $k_1 = -2,\ k_2 = -1,\ k_3 = 0.$

From equation (4.10) we have

$$\begin{cases} A_1 = -\frac{1}{2}(1-c) \\ A_2 = c-2 \\ A_3 = \frac{1}{2}(3-c) \end{cases}$$

and from equation (4.9) we have

$$\begin{cases} B_3 = A_3 = \frac{1}{2}(3-c) \\ B_2 = -A_1 = \frac{1}{2}(c-1) \\ B_2 - B_3 = A_2 = c-2 \end{cases}$$

The numerical flux of the scheme is

$$F_{j+\frac{1}{2}} = \frac{1}{2}(c-1)F_{j-1}^n - \frac{1}{2}(c-3)F_j^n \tag{4.17}$$

For negative speed the corresponding flux of the scheme is

$$F_{j+\frac{1}{2}} = \frac{1}{2}(c+3)F_{j+1}^n - \frac{1}{2}(c+1)F_{j+2}^n \tag{4.18}$$

By unifying the two fluxes (4.17) and (4.18) we obtain a second-order, upwind method which can accommodates wave speeds of arbitrary sign and has flux

$$F_{j+\frac{1}{2}} = \frac{1}{2}\left(F_j^n + F_{j+1}^n\right) - \frac{|a|}{2}\Delta U_{j+\frac{1}{2}} + |a|\left(\frac{1}{2} - \frac{|c|}{2}\right)\Delta U_{j+L+\frac{1}{2}} \tag{4.19}$$

where

$$\Delta U_{j+L+\frac{1}{2}} = U_{j+L+1} - U_{j+L} \tag{4.20}$$

$$\begin{cases} L = -1 & if\ a > 0 \\ L = 1 & if\ a < 0 \end{cases} \tag{4.21}$$

The stability condition of the method now becomes:

$$|c| \leq 2 \tag{4.22}$$

4.3.2 Conservative Third-order Schemes

Upwind-biased Scheme

The conservative form of the upwind-biased third-order scheme, see equation (3.24), according to equation (4.7), is

$$\begin{aligned} U_j^{n+1} &= U_j^n - \frac{k}{h}\left[(\frac{1}{2}c^2+c-\frac{1}{2})F_j^n - (\frac{1}{6}c^2+\frac{1}{2}c+\frac{1}{3})F_{j-1}^n\right. \\ &\quad \left.-(\frac{1}{2}c^2+\frac{1}{2}c-1)F_{j+1}^n - (\frac{1}{6}-\frac{1}{6}c^2)F_{j+2}^n\right] \end{aligned} \tag{4.23}$$

where from equation (4.11), $k_1=-1,\ k_2=0,\ k_3=1,\ k_4=2$ and from equation (4.10) we have

$$\begin{cases} A_1 = -(\frac{1}{6}c^2+\frac{1}{2}c+\frac{1}{3}) \\ A_2 = \frac{1}{2}c^2+c-\frac{1}{2} \\ A_3 = -(\frac{1}{2}c^2+\frac{1}{2}c-1) \\ A_4 = \frac{1}{6}c^2-\frac{1}{6} \end{cases}$$

According to equation (4.9) we have

$$\begin{cases} B_4 = A_4 = \frac{1}{6}c^2-\frac{1}{6} \\ B_2 = -A_1 = \frac{1}{6}c^2+\frac{1}{2}c+\frac{1}{3} \\ B_2-B_3 = A_2 = \frac{1}{2}c^2+c-\frac{1}{2} \\ B_3-B_4 = A_3 = 1-\frac{1}{2}c-\frac{1}{2}c^2 \end{cases} \tag{4.24}$$

Hence

$$B_3 = \frac{5}{6}-\frac{1}{3}c^2-\frac{1}{2}c \tag{4.25}$$

and the numerical flux of the scheme is

$$F_{j+\frac{1}{2}} = (\frac{1}{6}c^2+\frac{1}{2}c+\frac{1}{3})F_j^n + (\frac{5}{6}-\frac{1}{3}c^2-\frac{1}{2}c)F_{j+1}^n + (\frac{1}{6}c^2-\frac{1}{6})F_{j+2}^n \tag{4.26}$$

which is for negative wave speed.

For positive wave speed the corresponding four point scheme, see equation (3.27), has flux

$$F_{j+\frac{1}{2}} = (\frac{5}{6}-\frac{1}{3}c^2+\frac{1}{2}c)F_j^n + (\frac{1}{3}+\frac{1}{6}c^2-\frac{1}{2}c)F_{j+1}^n + \frac{1}{6}(c^2-1)F_{j-1}^n \tag{4.27}$$

By unifying the two previous schemes a third-order, upwind-biased method is obtained which can accommodate wave speeds with arbitrary sign and has flux

$$\begin{aligned} F_{j+\frac{1}{2}} &= \frac{1}{2}\left(F_j^n+F_{j+1}^n\right) - \frac{|a|}{2}\Delta U_{j+\frac{1}{2}} + |a|\left(\frac{1}{3}-\frac{|c|}{2}+\frac{c^2}{6}\right)\Delta U_{j+\frac{1}{2}} \\ &\quad +\frac{|a|}{6}\left(1-c^2\right)\Delta U_{j+L+\frac{1}{2}} \end{aligned} \tag{4.28}$$

The stability condition of the method now is:

$$|c| \leq 1 \tag{4.29}$$

Upwind Scheme

By repeating the same procedure as before, the conservative form of the upwind, third-order scheme, refer to equations (3.30) and (3.33), has flux

$$\begin{aligned} F_{j+\frac{1}{2}} &= \frac{1}{2}\left(F_j^n + F_{j+1}^n\right) - \frac{|a|}{2}\Delta U_{j+\frac{1}{2}} + |a|\left(\frac{5}{6} + \frac{c^2}{6} - |c|\right)\Delta U_{j+k_1+\frac{1}{2}} \\ &\quad -|a|\left(\frac{1}{3} - \frac{|c|}{2} + \frac{c^2}{6}\right)\Delta U_{j+k_2+\frac{1}{2}} \end{aligned} \tag{4.30}$$

where

$$\begin{cases} k_1 = -1, \quad k_2 = -2 & if \quad c > 0 \\ k_1 = 1, \quad k_2 = 2 & if \quad c < 0 \end{cases} \tag{4.31}$$

The stability condition of the scheme is:

$$1 \leq |c| \leq 2 \tag{4.32}$$

4.3.3 Conservative Fourth-order Schemes

Space-centered Scheme

The conservative form of the space-centered, fourth-order scheme, see equation (3.36), has flux

$$\begin{aligned} F_{j+\frac{1}{2}} &= \frac{1}{2}\left(F_j^n + F_{j+1}^n\right) - \frac{|a|}{2}\Delta U_{j+\frac{1}{2}} + a\left(\frac{1}{12} + \frac{c}{24} - \frac{c^2}{12} - \frac{c^3}{24}\right)\Delta U_{j-\frac{1}{2}} \\ &\quad +a\left(\frac{1}{2}\,sgn(a) - \frac{7}{12}c + \frac{c^3}{12}\right)\Delta U_{j+\frac{1}{2}} - a\left(\frac{c^3}{24} - \frac{c^2}{12} - \frac{c}{24} + \frac{1}{12}\right)\Delta U_{j+\frac{3}{2}} \end{aligned} \tag{4.33}$$

Upwind-biased Scheme

The conservative form of the upwind-biased, fourth-order scheme, refer to equations (3.39) and (3.42), has flux

$$\begin{aligned} F_{j+\frac{1}{2}} &= \frac{1}{2}(F_j^n + F_{j+1}^n) - \frac{|a|}{2}\Delta U_{j+\frac{1}{2}} + |a|\left(\frac{1}{4} - \frac{11}{24}|c| + \frac{1}{4}c^2 - \frac{1}{24}|c|^3\right)\Delta U_{j+\frac{1}{2}} \\ &+|a|\left(\frac{1}{12}|c|^3 - \frac{1}{3}c^2 - \frac{|c|}{12} + \frac{1}{3}\right)\Delta U_{j+k_1+\frac{1}{2}} \\ &-|a|\left(\frac{1}{24}|c|^3 - \frac{1}{12}c^2 - \frac{1}{24}|c| + \frac{1}{12}\right)\Delta U_{j+k_2+\frac{1}{2}} \end{aligned} \tag{4.34}$$

where

$$\begin{cases} k_1 = -1,\ k_2 = -2 & if\ c > 0 \\ k_1 = 1,\ k_2 = 2 & if\ c < 0 \end{cases} \tag{4.35}$$

The stability condition of the scheme is:

$$|c| \leq 2 \tag{4.36}$$

Upwind Scheme

The conservative form of the upwind, fourth-order scheme, refer to equations (3.45) and (3.48), has flux

$$\begin{aligned} F_{j+\frac{1}{2}} &= \frac{1}{2}(F_j^n + F_{j+1}^n) - \frac{|a|}{2}\Delta U_{j+\frac{1}{2}} + |a|\left(\frac{13}{12} - \frac{35}{24}|c| + \frac{5}{12}c^2 - \frac{1}{24}|c|^3\right)\Delta U_{j+k_1+\frac{1}{2}} \\ &+|a|\left(\frac{|c|^3}{12} - \frac{2}{3}c^2 + \frac{17}{12}|c| - \frac{5}{6}\right)\Delta U_{j+k_2+\frac{1}{2}} \\ &+|a|\left(\frac{1}{4} - \frac{11}{24}|c| + \frac{1}{4}c^2 - \frac{1}{24}|c|^3\right)\Delta U_{j+k_3+\frac{1}{2}} \end{aligned} \tag{4.37}$$

where

$$\begin{cases} k_1 = -1,\ k_2 = -2,\ k_3 = -3 & if\ c > 0 \\ k_1 = 1,\ k_2 = 2,\ k_3 = 3 & if\ c < 0 \end{cases} \tag{4.38}$$

The stability condition of the scheme is:

$$1 \leq |c| \leq 3 \tag{4.39}$$

4.4 Entropy Condition

Applying the conservative methods defined in the last section, we can safely calculate the discontinuities in a correct location, and therefore guarantee that it is a weak solution. However there are situations in which a weak solution for a conservation law is not unique, which means that the weak solution computed might be a wrong weak solution. In order to make sure that the weak solution is the right one, i.e. physically acceptable solution, another condition called *entropy* condition is required.

One property of the entropy is that the quantity of entropy can only increase but never decrease along a particle path, therefore the process of entropy is a inreversible process. It is this property that gives us the entropy conditions. Based on the fact that the entropy keeps constant in smooth flows, however jumps to a higher value in flows with discontinuities, utilising the property of entropy we can easily define the right or entropy-satisfying weak solution for gas dynamics.

There are different versions of entropy condition available (refer to [46]). The general one called entropy function developed by Lax [50] has the following form

$$\eta(u)_t + \psi(u)_x \leq 0 \tag{4.40}$$

here $\eta(u)$ is an entropy function of a conservation law, which is defined as

$$\eta(u) \ \textit{is a convex function of} \ u \tag{4.41}$$

$$\psi'(u) = \eta'(u)\, f'(u) \tag{4.42}$$

$\psi(u)$ is a corresponding entropy flux function; $f(u)$ is a physical flux function of a conservation law.

The equivalent discrete version of entropy function (4.40) has the following form

$$\eta(U_j^{n+1}) \leq \eta(U_j^n) - \frac{k}{h}\left(\Psi_{j+\frac{1}{2}} - \Psi_{j-\frac{1}{2}}\right) \tag{4.43}$$

here $\Psi_{1/2}$ is a numerical entropy flux which is consistent with the entropy flux ψ in the manner

$$\Psi_{j+\frac{1}{2}}(\bar{u}, \bar{u}, \ldots, \bar{u}) = \psi(\bar{u}) \tag{4.44}$$

Here $\bar{u}$ is constant.

It is proved [51] that a numerical solution will converge to the entropy-satisfying weak solution if the conservative numerical scheme in the scalar case is consistent with the entropy condition (4.43). In the later chapters we will discuss a way in which the high-order conservative schemes for nonlinear systems are consistent with the entropy inequality (4.43).

4.5 Summary

When applying non-conservative numerical methods for a scalar conservation law with discontinuities, two new problems are discussed in the chapter. First the shock might be placed in a wrong location, therefore the solution is not a weak solution at all; second the solution might converge to a wrong weak solution. To prevent the first problem, conservative methods are required. An approach is established which gives a way to reformulate the non-conservative methods into conservative schemes. To illustrate the theory, fully discrete second-, third- and fourth-order conservative schemes are presented. To overcome the second problem, a conservative method has to be consistent with the entropy condition which can distinguish the unique entropy-satisfying weak solution from the wrong weak solutions.

Chapter 5

Total Variation Diminishing High-order Schemes

5.1 Introductory Remarks

In this chapter another problem associated with the application of the high-order numerical schemes is addressed. It is well known that when solving shock problems, such as transonic flows with shocks, when applying the high-order schemes it is inevitable that oscillations will be observed in the vicinity of the shocks, which might trigger instabilities. The mechanism behind the oscillations was well discussed by Trefethen [52]. It turns out that the oscillations are caused by the dispersion of the highly oscillatory wave components which are associated with high wavenumbers of Fourier spectrum. This problem had frustrated people for many years until the concept and theory of Total Variation Diminishing (TVD) schemes was introduced [53]. Since then a variety of high-order TVD schemes has been developed [54] - [58] [38].

In this chapter the TVD theory is applied to the conservative high-order schemes presented in the last chapter. These high-order TVD schemes can avoid spurious oscillations and preserve high-order accuracy in smooth parts of the flow. This is achieved by imposing a TVD constraint via the introduction of flux limiter functions [38]. For second-, third- and fourth-order accurate schemes a rigorous TVD analysis that results in Courant-number dependent TVD regions is carried out. Flux limiter functions are constructed and tested.

For methods of higher order of accuracy a semi-empirical TVD approach that works well is proposed. Collective experience with second-order methods suggests that this analysis might provide a useful guide for constructing schemes to solve non-linear hyperbolic systems.

The rest of this chapter is as follows: in section 2 the TVD concept is discussed; in section 3 the TVD theory for fully discrete schemes is investigated; in section 4 the TVD theory is applied to derive Courant-number dependent TVD regions and to construct and test limiter functions for second-order methods; in sections 5 and 6 the TVD theory is applied to third- and fourth-order fully discrete schemes. In section 7 a semi-empirical procedure to develop TVD versions of schemes of arbitrary-order of accuracy is investigated. Conclusions are drawn in section 8.

5.2 Total Variation Stability

The Total Variation, $TV(U^{n+1})$, of the discrete solution is defined as

$$TV(U^{n+1}) = \sum_j \left| U_{j+1}^{n+1} - U_j^{n+1} \right| \tag{5.1}$$

Under the definition a numerical method is called Total Variation Diminishing if the following condition is satisfied.

$$TV(U^{n+1}) \leq TV(U^n) \tag{5.2}$$

which simply states that the total variation is not increased as time evolves, so that the $TV(U^n)$ at any time n is bounded by the $TV(U^0)$ of the initial data.

For a consistent, conservative and entropy-satisfying method for a scalar conservation law, provided the condition of inequality (5.2) is satisfied, the solution will converge to the correct weak solution.

To apply the TVD concept we use Harten' theorem [53] which states that a scheme written as

$$U_j^{n+1} = U_j^n - B_{j-\frac{1}{2}} \Delta U_{j-\frac{1}{2}} + D_{j+\frac{1}{2}} \Delta U_{j+\frac{1}{2}} \tag{5.3}$$

is TVD provided

$$B_{j-\frac{1}{2}} \geq 0 \tag{5.4}$$

$$D_{j+\frac{1}{2}} \geq 0 \tag{5.5}$$

$$B_{j-\frac{1}{2}} + D_{j+\frac{1}{2}} \leq 1 \tag{5.6}$$

Another more convenient and practical criterion for applying the TVD concept is provided by Roe's data compatibility condition [48]

$$0 \leq \frac{U_j^{n+1} - U_j^n}{U_{j-1}^n - U_j^n} \leq 1 \qquad for \;\; 0 \leq c \leq 1 \tag{5.7}$$

$$0 \leq \frac{U_j^{n+1} - U_j^n}{U_{j+1}^n - U_j^n} \leq 1 \qquad for \;\; -1 \leq c \leq 0 \tag{5.8}$$

However conditions (5.7) and (5.8) are only valid for a Courant number in the region $-1 \leq c \leq 1$. In a linear advection, the value of U_j^{n+1} is determined by the Courant number. For example, if the stable region of a numerical method is $1 \leq c \leq 2$, then the value of U_j^{n+1} at the time level $n+1$ lies between U_{j-2}^n and U_{j-1}^n, depending on the value of the Courant number c. Therefore a general form of compatibility condition which applies to an arbitrary region of Courant number is given as follows.

$$0 \leq \frac{U_j^{n+1} - U_{j-k}^n}{U_{j-(k+1)}^n - U_{j-k}^n} \leq 1 \qquad k \leq c \leq k+1 \tag{5.9}$$

$$0 \leq \frac{U_j^{n+1} - U_{j+k}^n}{U_{j+(k+1)}^n - U_{j+k}^n} \leq 1 \qquad -(k+1) \leq c \leq -k \tag{5.10}$$

Here, k is a positive integer, i.e. $k = 0, 1, 2, \ldots$

5.3 TVD Analysis for High-order Schemes

The initial value problem (IVP) for one dimensional scalar hyperbolic conservation laws is considered, namely

$$\begin{aligned} u_t + f(u)_x &= 0 \qquad -\infty < x < \infty, t \geq 0 \\ u(x,0) &= u_0(x) \end{aligned} \tag{5.11}$$

Here, u is the unknown function and $f(u)$ is the physical flux.

In this chapter let us take the linear case $f(u) = au$ so that $f'(u) = a$ is a constant wave propagation speed.

We consider the conservative numerical schemes introduced in last chapter

$$U_j^{n+1} = U_j^n - \frac{k}{h}\left(F_{j+\frac{1}{2}} - F_{j-\frac{1}{2}}\right) \tag{5.12}$$

with numerical flux

$$\begin{aligned} F_{j+\frac{1}{2}} &= \frac{1}{2}(F_j^n + F_{j+1}^n) - \frac{1}{2}|a|(U_{j+1}^n - U_j^n) \\ &\quad + |a|\left(D_0\Delta U_{j+\frac{1}{2}} + D_1\Delta U_{j+L+\frac{1}{2}} + D_2\Delta U_{j+M+\frac{1}{2}}\right) \end{aligned} \tag{5.13}$$

where D_0, D_1 and D_2 are coefficients,

$$\Delta U_{j+\frac{1}{2}} = U_{j+1}^n - U_j^n \tag{5.14}$$

$$\Delta U_{j+L+\frac{1}{2}} = U_{j+L+1}^n - U_{j+L}^n \tag{5.15}$$

$$\Delta U_{j+M+\frac{1}{2}} = U_{j+M+1}^n - U_{j+M}^n \tag{5.16}$$

$$\begin{cases} L = -1, \quad M = 1 \quad for \quad c > 0 \\ L = 1, \quad M = -1 \quad for \quad c < 0 \end{cases} \tag{5.17}$$

The above scheme includes three-point second-order space-centered schemes, five-point second-order upwind schemes, five-point third-order upwind-biased schemes and five-point fourth-order space-centered schemes. For example, when D_1 and D_2 are zero the second-order space-centered scheme (4.15) is obtained; when D_0 and D_2 are zero (5.12)-(5.13) gives the second-order upwind scheme (4.19); when D_2 is zero the five-point third-order upwind-biased scheme (4.28) is obtained; for D_0, D_1 and D_2 distincting from zero the five-point fourth-order space-centered scheme (4.33) is obtained.

To impose a TVD constraint on (5.13) via limiter functions, we write the modified scheme

$$\begin{aligned} F_{j+\frac{1}{2}} &= \frac{1}{2}(F_j^n + F_{j+1}^n) - \frac{1}{2}|a|(U_{j+1}^n - U_j^n) \\ &\quad + |a|\left(D_0\Delta U_{j+\frac{1}{2}} + D_1\Delta U_{j+L+\frac{1}{2}}\right)\phi_j + |a|D_2\Delta U_{j+M+\frac{1}{2}}\,\phi_{j+M} \end{aligned} \tag{5.18}$$

where ϕ_j and ϕ_{j+M} are limiter functions.

Theorem 3 *Scheme (5.12), (5.18) is TVD for* $|c| \leq 1$ *if the limiter function is determined by*

$$\phi_j \leq \frac{(1-|c|)\,\theta_j}{\eta\,(D_1\theta_j + D_0 - D_2)} \tag{5.19}$$

$$\phi_j \leq \frac{1-|c|+\eta D_2/\,\theta_j^*}{\eta\,(D_0 + D_1\theta_j)} \tag{5.20}$$

$$\phi_j \geq \frac{D_2}{(D_0 + D_1\theta_j)\,\theta_j^*} \tag{5.21}$$

$$\phi_j \geq 0 \tag{5.22}$$

where θ_j is called local flow parameter and is defined by

$$\theta_j = \frac{\Delta U_{j-\frac{1}{2}}}{\Delta U_{j+\frac{1}{2}}} \quad for \quad c > 0 \tag{5.23}$$

$$\theta_j = \frac{\Delta U_{j+\frac{3}{2}}}{\Delta U_{j+\frac{1}{2}}} \quad for \quad c < 0 \tag{5.24}$$

θ_j^* is called upwind-downwind flow parameter and is given by

$$\theta_j^* = \frac{\Delta U_{j-\frac{1}{2}}}{\Delta U_{j+\frac{3}{2}}} \quad for \quad c > 0 \tag{5.25}$$

$$\theta_j^* = \frac{\Delta U_{j+\frac{3}{2}}}{\Delta U_{j-\frac{1}{2}}} \quad for \quad c < 0 \tag{5.26}$$

η is defined by

$$\begin{cases} \eta = 1 - |c| & for \quad 0 \le |c| < \frac{1}{2} \\ \eta = |c| & for \quad \frac{1}{2} \le |c| \le 1 \end{cases} \tag{5.27}$$

Proof

First consider a method with Courant number of $0 \le c \le 1$. From (5.12) and (5.18), the numerical method is

$$\begin{aligned} U_j^{n+1} = U_j^n - c \Big[& \Delta U_{j-\frac{1}{2}} + D_0 \Delta U_{j+\frac{1}{2}} \, \phi_j + D_1 \Delta U_{j-\frac{1}{2}} \, \phi_j - D_0 \Delta U_{j-\frac{1}{2}} \, \phi_{j-1} \\ & - D_1 \Delta U_{j-\frac{3}{2}} \, \phi_{j-1} - D_2 \Delta U_{j+\frac{1}{2}} \, \phi_j + D_2 \Delta U_{j+\frac{3}{2}} \, \phi_{j+1} \Big] \end{aligned} \tag{5.28}$$

Modifying equation (5.28), we have

$$\begin{aligned} \frac{U_j^{n+1} - U_j^n}{-\Delta U_{j-\frac{1}{2}}} = c \Bigg[& 1 + \left(D_1 + (D_0 - D_2) \frac{1}{\theta_j} \right) \phi_j - (D_0 + D_1 \theta_{j-1}) \, \phi_{j-1} \\ & + D_2 \frac{1}{\theta_j^*} \, \phi_{j+1} \Bigg] \end{aligned} \tag{5.29}$$

We now apply the data compatibility condition of equation (5.7) whereby the sufficient condition

$$0 \le \frac{U_j^{n+1} - U_j^n}{-\Delta U_{j-\frac{1}{2}}} \le 1 \tag{5.30}$$

satisfies the TVD requirement.

This is equivalent to the Harten's theorem (5.3)-(5.6) with the choice

$$B_{j-\frac{1}{2}} = c\left[1+\left(D_1+(D_0-D_2)\frac{1}{\theta_j}\right)\phi_j-(D_0+D_1\theta_{j-1})\,\phi_{j-1}+D_2\frac{1}{\theta_j^*}\,\phi_{j+1}\right]$$
$$D_{j+\frac{1}{2}} = 0$$

We apply condition (5.30) to (5.29), that is

$$0 \le c\left[1+\left(D_1+(D_0-D_2)\frac{1}{\theta_j}\right)\phi_j-(D_0+D_1\theta_{j-1})\phi_{j-1}+D_2\frac{1}{\theta_j^*}\phi_{j+1}\right] \le 1 \qquad (5.31)$$

One way to satisfy these inequalities is by imposing

$$\left(D_1+(D_0-D_2)\frac{1}{\theta_j}\right)\phi_j-\left((D_0+D_1\theta_{j-1})\phi_{j-1}-D_2\frac{1}{\theta_j^*}\phi_{j+1}\right) \le \frac{1-c}{c} \qquad (5.32)$$

$$\left((D_0+D_1\theta_{j-1})\phi_{j-1}-D_2\frac{1}{\theta_j^*}\phi_{j+1}\right)-\left(D_1+(D_0-D_2)\frac{1}{\theta_j}\right)\phi_j \le 1 \qquad (5.33)$$

i.e.

$$0 \le \left(D_1+(D_0-D_2)\frac{1}{\theta_j}\right)\phi_j \le \frac{1-c}{c} \qquad (5.34)$$

$$0 \le (D_0+D_1\theta_{j-1})\phi_{j-1}-D_2\frac{1}{\theta_j^*}\phi_{j+1} \le \frac{1-c}{c} \qquad (5.35)$$

$$0 \le \left(D_1+(D_0-D_2)\frac{1}{\theta_j}\right)\phi_j \le 1 \qquad (5.36)$$

$$0 \le (D_0+D_1\theta_{j-1})\phi_{j-1}-D_2\frac{1}{\theta_j^*}\phi_{j+1} \le 1 \qquad (5.37)$$

This leads to the following conditions on the flux limiter

$$\phi_j \le \frac{(1-c)\,\theta_j}{c(D_1\theta_j+D_0-D_2)} \qquad (5.38)$$

$$\phi_j \le \frac{\theta_j}{D_1\theta_j+D_0-D_2} \qquad (5.39)$$

$$\phi_j \le \frac{1-c+cD_2\,\phi_{j+1}/\,\theta_j^*}{c(D_0+D_1\theta_j)} \qquad (5.40)$$

$$\phi_j \le \frac{1+D_2\,\phi_{j+1}/\,\theta_j^*}{D_0+D_1\theta_j} \qquad (5.41)$$

$$\phi_j \ge \frac{D_2\,\phi_{j+1}}{(D_0+D_1\theta_j)\,\theta_j^*} \qquad (5.42)$$

$$\phi_j \ge 0 \qquad (5.43)$$

The most restrictive conditions of inequalities (5.38) to (5.41) give

$$\phi_j \leq \frac{(1-c)\,\theta_j}{\eta(D_1\theta_j + D_0 - D_2)} \tag{5.44}$$

$$\phi_j \leq \frac{1 - c + \eta D_2\,\phi_{j+1}/\,\theta_j^*}{\eta(D_0 + D_1\theta_j)} \tag{5.45}$$

where η is defined by equation (5.27). The analysis for $-1 \leq c \leq 0$ goes through in exactly the same way but c is replaced by $|c|$ and ϕ_{j+1} is replaced by ϕ_{j-1}. Finally by setting $\phi_{j+1} = 1$ or $\phi_{j-1} = 1$ the theorem is establishes.

In the following sections the theorem will be used to construct second-, third- and fourth-order TVD schemes.

5.4 Second-order TVD Scheme

The fully discrete, second-order numerical flux with limiter (refer to equation (4.15) for the unlimited case) can be written as

$$F_{j+\frac{1}{2}} = \frac{1}{2}(F_j^n + F_{j+1}^n) - \frac{|a|}{2}\Delta U_{j+\frac{1}{2}} + \frac{|a|}{2}(1-|c|)\Delta U_{j+\frac{1}{2}}\,\phi_j \tag{5.46}$$

where in equation (5.18), $D_0 = \frac{1}{2}(1-|c|)$, D_1 and D_2 are zero.

From equations (5.19)-(5.22) the limiter function ϕ_j has to satisfy the constraints

$$\phi_j \leq \frac{2\theta_j}{\eta} \tag{5.47}$$

$$\phi_j \leq \frac{2}{\eta} \tag{5.48}$$

$$\phi_j \geq 0 \tag{5.49}$$

When $\theta_j < 0$ $\phi_j < 0$ and the scheme reduces locally to first-order by setting $\phi_j = 0$.

Equations (5.47), (5.48) indicate that the second-order TVD region is a function of Courant number $|c|$. This conclusion is consistent with that of other researchers such as [55] [59] and [58]. The Courant number dependent TVD regions of (5.47) and (5.48) are shown in figure 5.1. The upper boundary of the TVD region is the maximum for the choice of $|c| = \frac{1}{2}$. Sweby's TVD region [38] is the special case $|c| = 1$ in the Courant number dependent TVD region of figure 5.1.

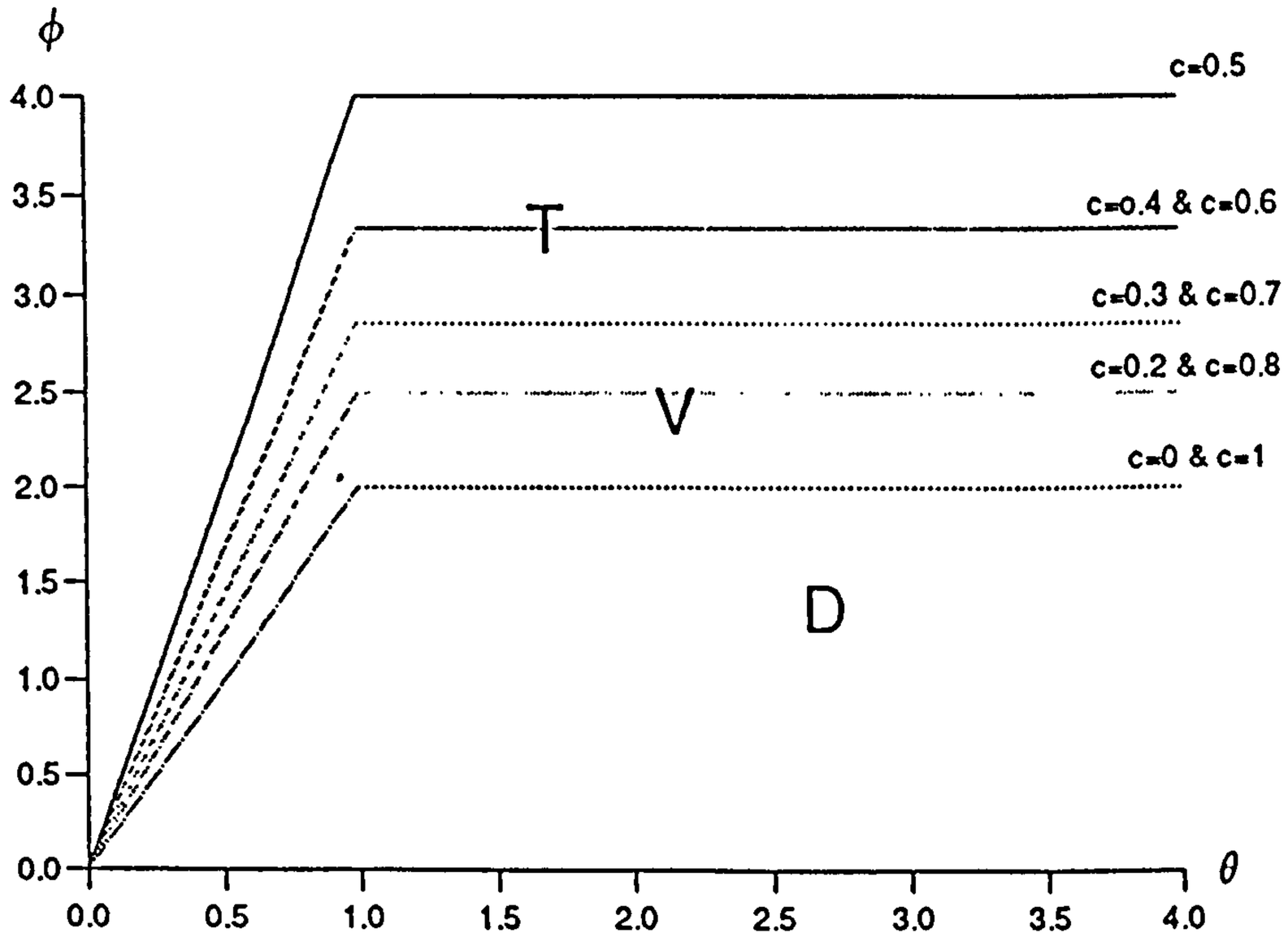

Figure 5.1: Courant Number Dependent Second-order TVD Region

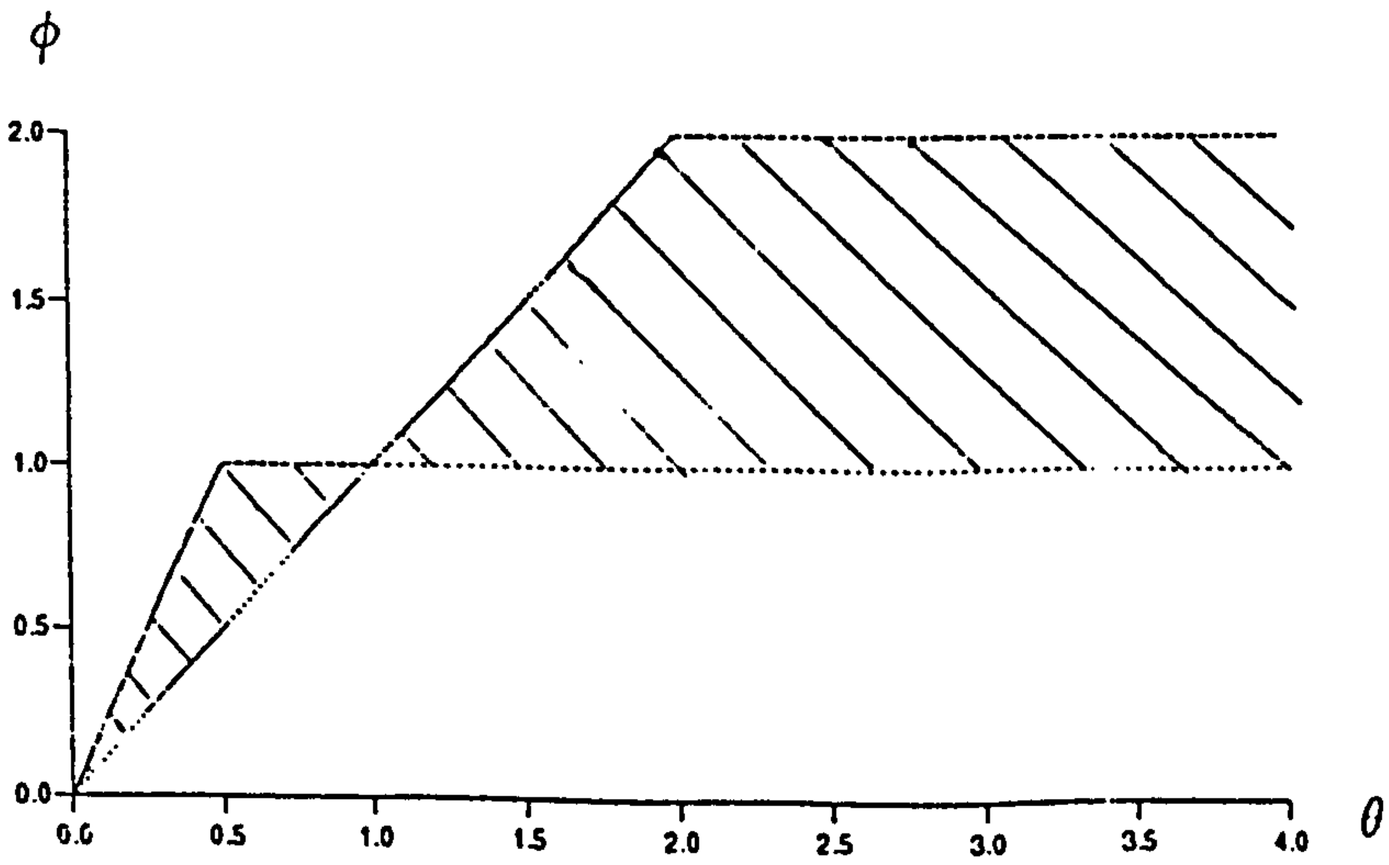

Figure 5.2: FD2A Limiter Function (shaded part)

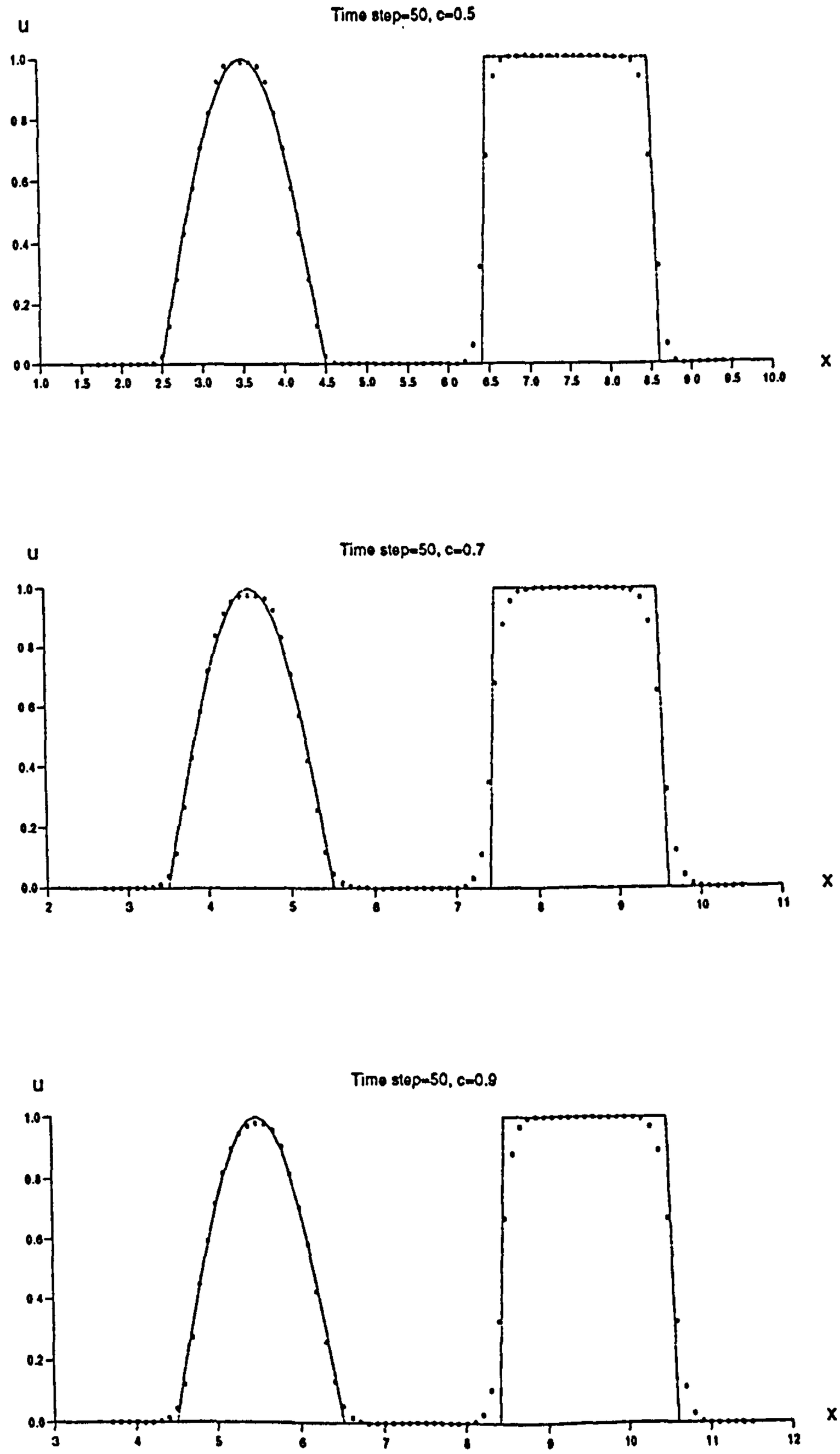

Figure 5.3: Comparision between the Exact Solution (line) and the Numerical Results of FD2A (symbol) after 50 Time Steps

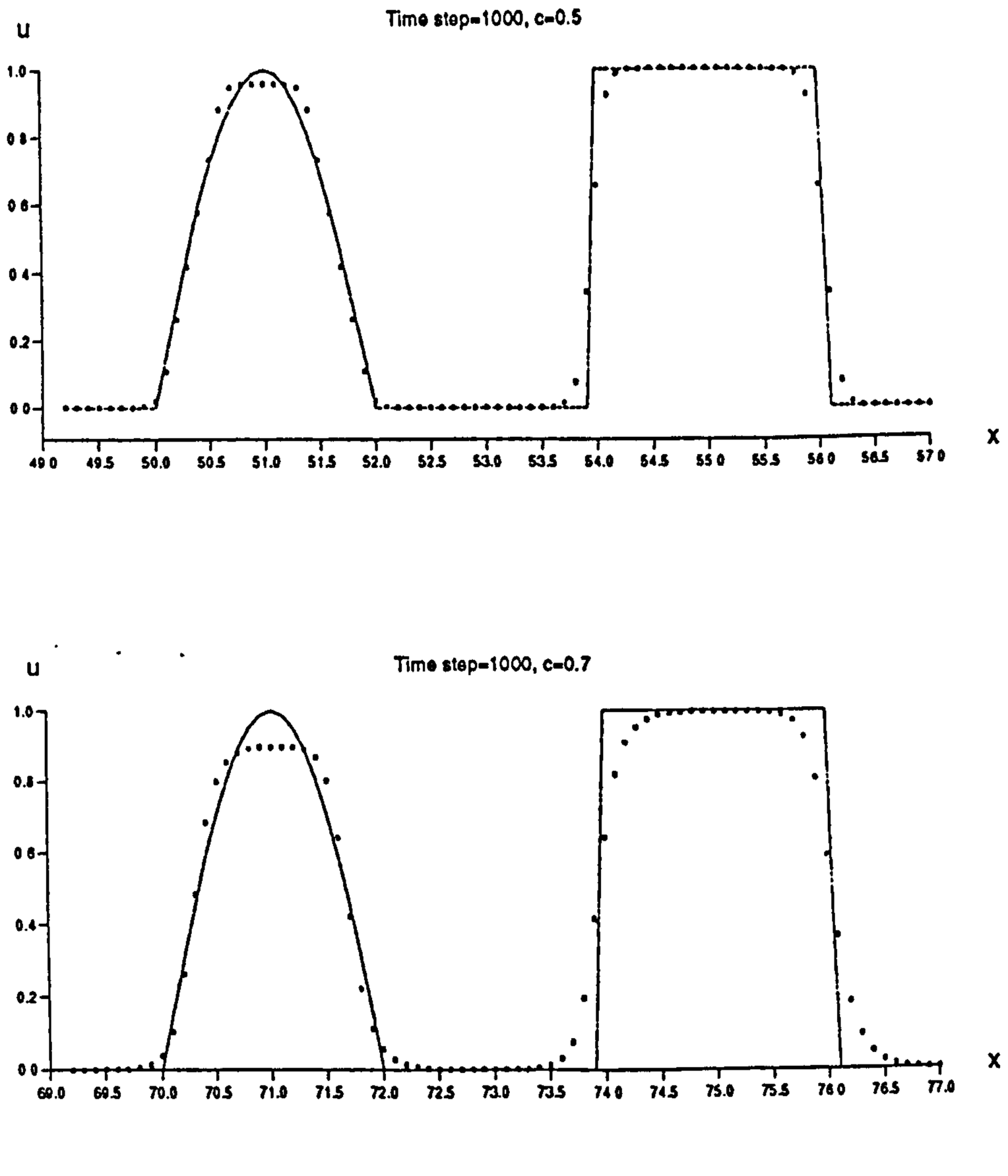

Figure 5.4: Comparision between the Exact Solution (line) and the Numerical Results of FD2A (symbol) after 1000 Time Steps

Using the Courant number dependent TVD region we can develop second-order Courant number dependent limiter functions. One limiter function, called FD2A (Fully Discrete Second-order A) limiter function, has the following form

$$\phi_j(\theta_j) = max\left[0, min\left(1, \frac{\theta_j}{\eta}\right), min\left(\theta_j, \frac{1}{\eta}\right)\right] \tag{5.50}$$

The shaded part in figure 5.2 illustrates the limiter function(5.50). When η is 1/2, the function follows the upper boundary of the area which is Roe's SUPERBEE limiter; when η is 1, the function follows the lower boundary which is the MINMOD limiter; for other values of η the function varies in between the SUPERBEE and MINMOD.

Figure 5.3 and 5.4 show a comparison of the numerical results for linear advection equation $u_t + au_x = 0$ with constant wave speed a using the FD2A (symbol) and the exact solution (line). The initial condition consists of half a *sine* wave and a squared wave. The cell width $\Delta x = 0.1$ is fixed. The Courant numbers used are 0.5, 0.7 and 0.9. The results are shown after 50 time steps (figure 5.3) and 1000 time steps (figure 5.4).

Another limiter function is FD2B given by

$$\phi_j(\theta_j) = max\left[0, min\left(1, \frac{2\theta_j}{\eta}\right), min\left(\theta_j, \frac{2}{\eta}\right)\right] \tag{5.51}$$

This is illustrated by the shaded area of figure 5.5 Note that the lower boundary now is the SUPERBEE limiter.

Figure 5.6 shows a comparison between the numerical results of FD2B (symbol) and the exact solution (line) after 50 time steps. For discontinuities FD2B is superior to FD2A. Clipping of extrema in smooth solution is less severe than that of FD2A. The tendency to square smooth parts is present in both limiter functions and this is typical of very compressive limiters.

To illustrate the long time behaviour of the resulting scheme Figure 5.7 shows a comparison of the numerical results using SUPERBEE (cross), FD2B (box) and the exact solution (line) after 1000 time steps. As seen in the figure the performance of FD2B for the discontinuous part of the solution is superior to that of SUPERBEE; for the smooth part of the solution they both tend to square the profile but FD2B shows less clipping of extrema. The difference between SUPERBEE and FD2B is more noticeable as the Courant number tends to $\frac{1}{2}$.

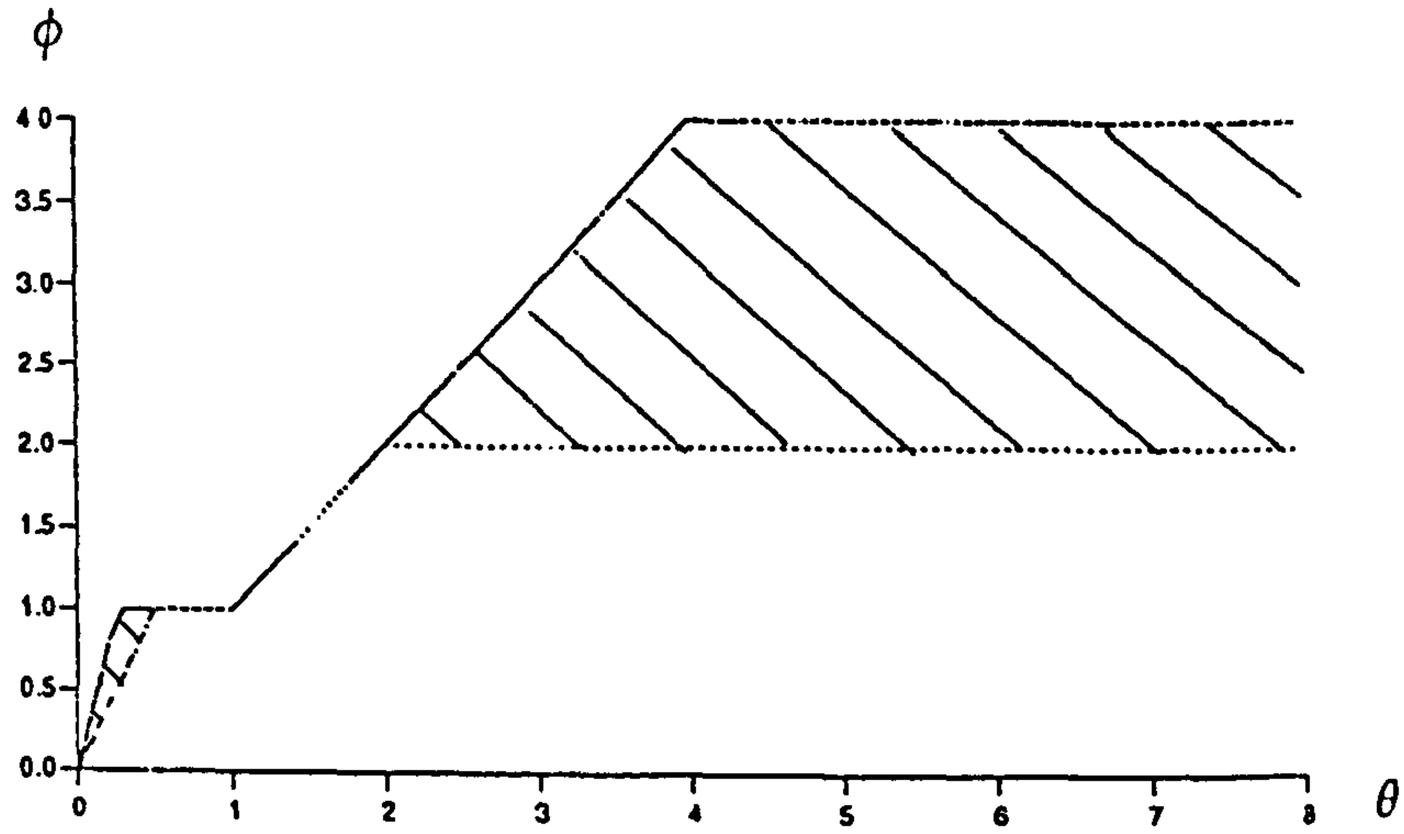

Figure 5.5: FD2B Limiter Function (shaded part)

5.5 Third-order TVD Scheme

The 5-point third-order scheme with limiter function has the following form (refer to equation (4.28) for the unlimited case)

$$F_{j+\frac{1}{2}} = \frac{1}{2}(F_j^n + F_{j+1}^n) - \frac{|a|}{2}\Delta U_{j+\frac{1}{2}} + \left[|a|\left(\frac{1}{3} - \frac{|c|}{2} + \frac{c^2}{6}\right)\Delta U_{j+\frac{1}{2}} + \frac{|a|}{6}(1-c^2)\Delta U_{j+L+\frac{1}{2}}\right]\phi_j \tag{5.52}$$

where

$$|c| \leq 1 \tag{5.53}$$

$$\begin{cases} L = -1 & if \quad c > 0 \\ L = 1 & if \quad c < 0 \end{cases} \tag{5.54}$$

and in equation (5.18)

$$\begin{cases} D_0 = \frac{1}{3} - \frac{1}{2}|c| + \frac{1}{6}c^2 \\ D_1 = \frac{1}{6}(1-c^2) \\ D_2 = 0 \end{cases} \tag{5.55}$$

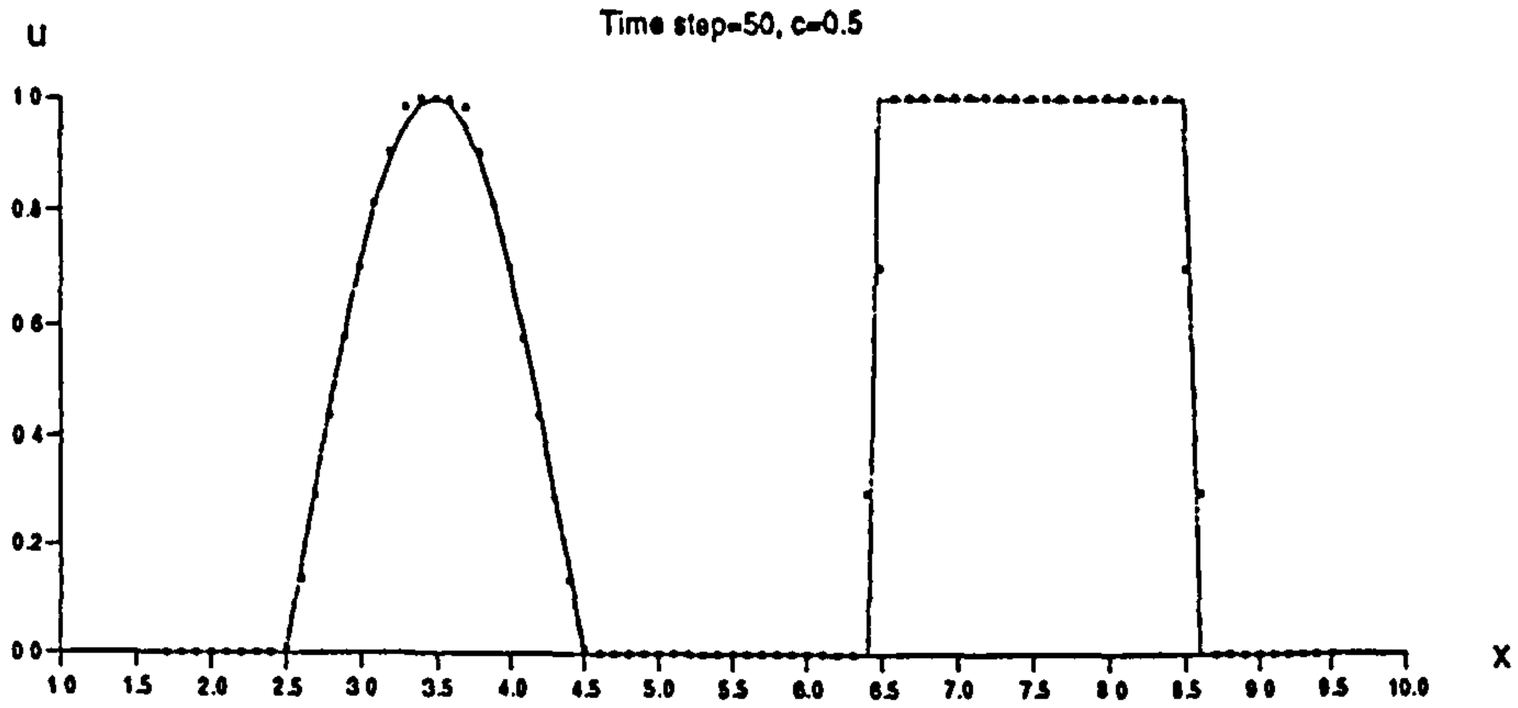

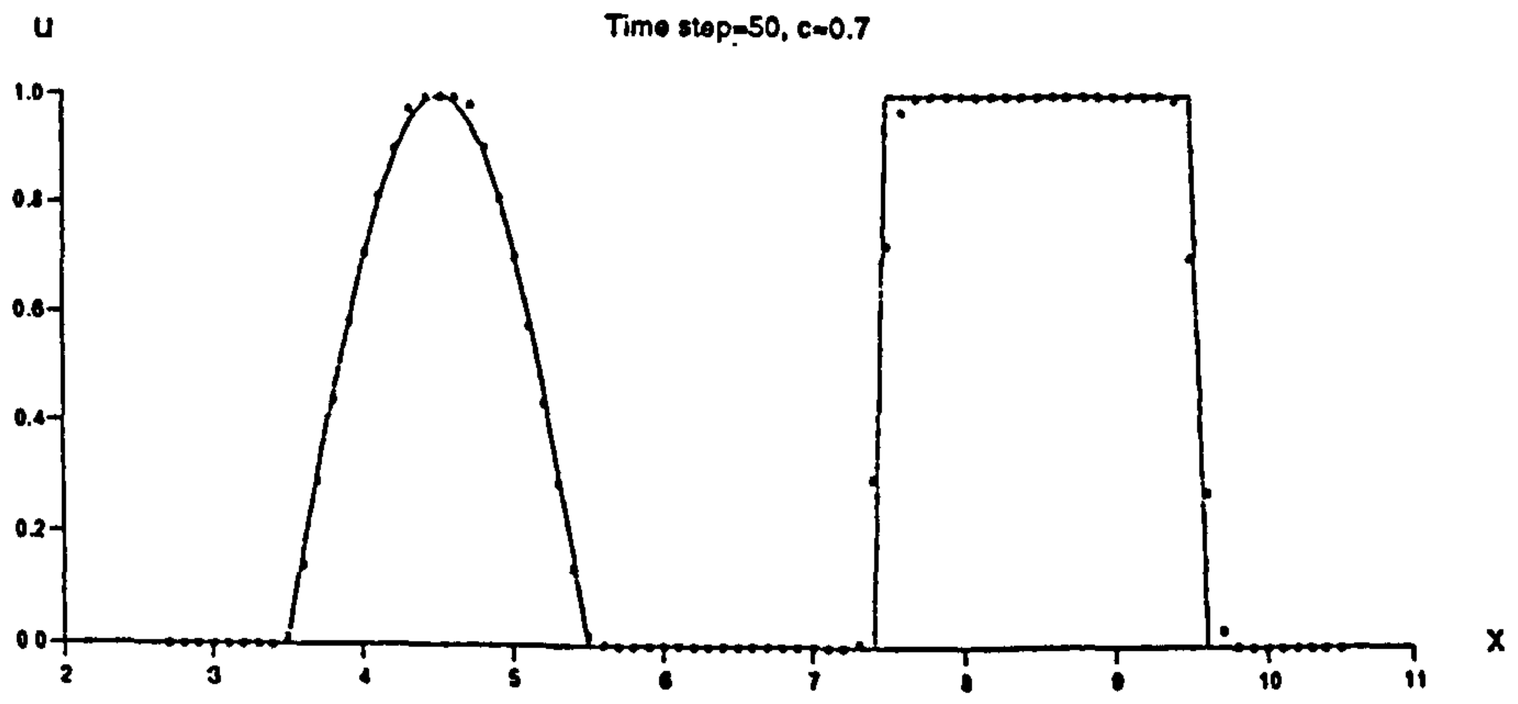

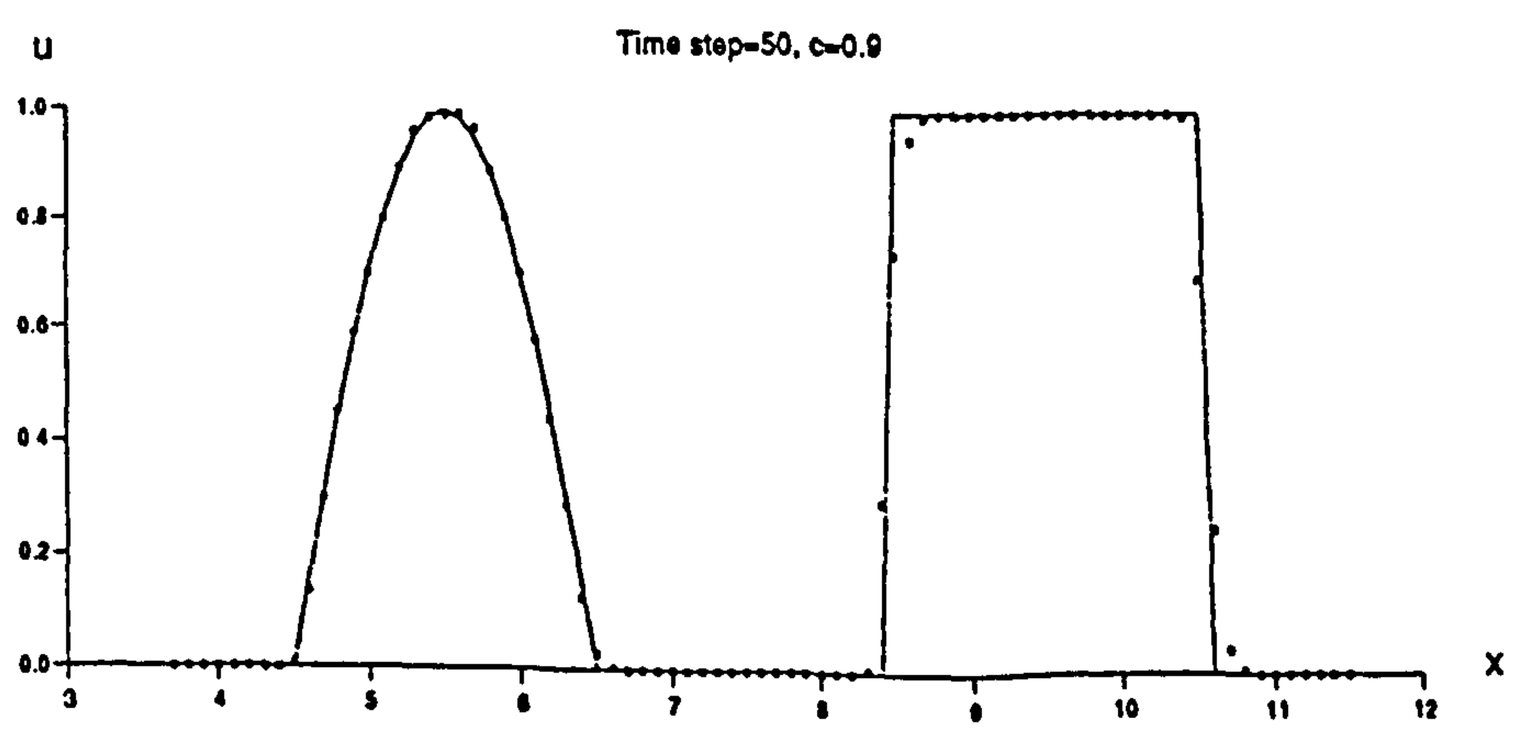

Figure 5.6: Comparision between the Exact Solution (line) and the Numerical Results of FD2B (symbol) after 50 Time Steps

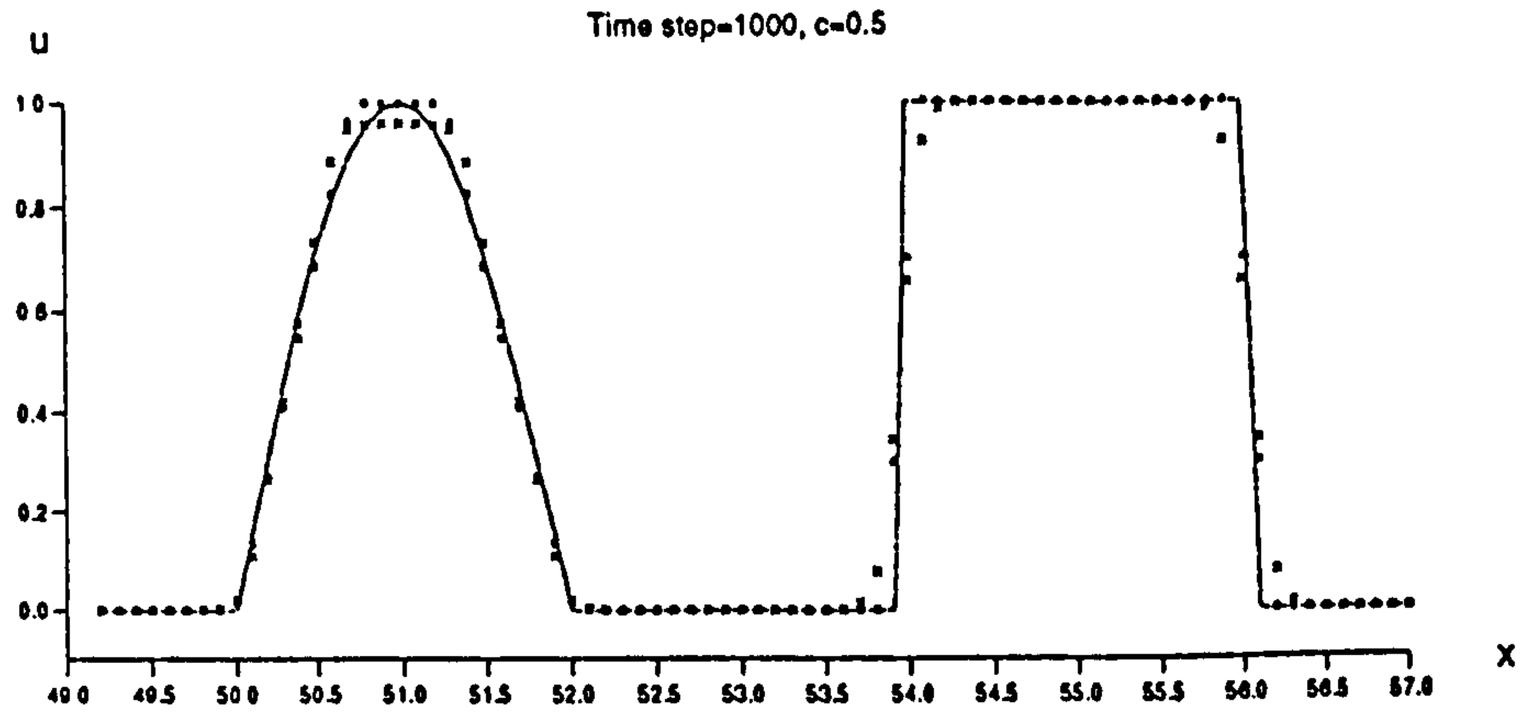

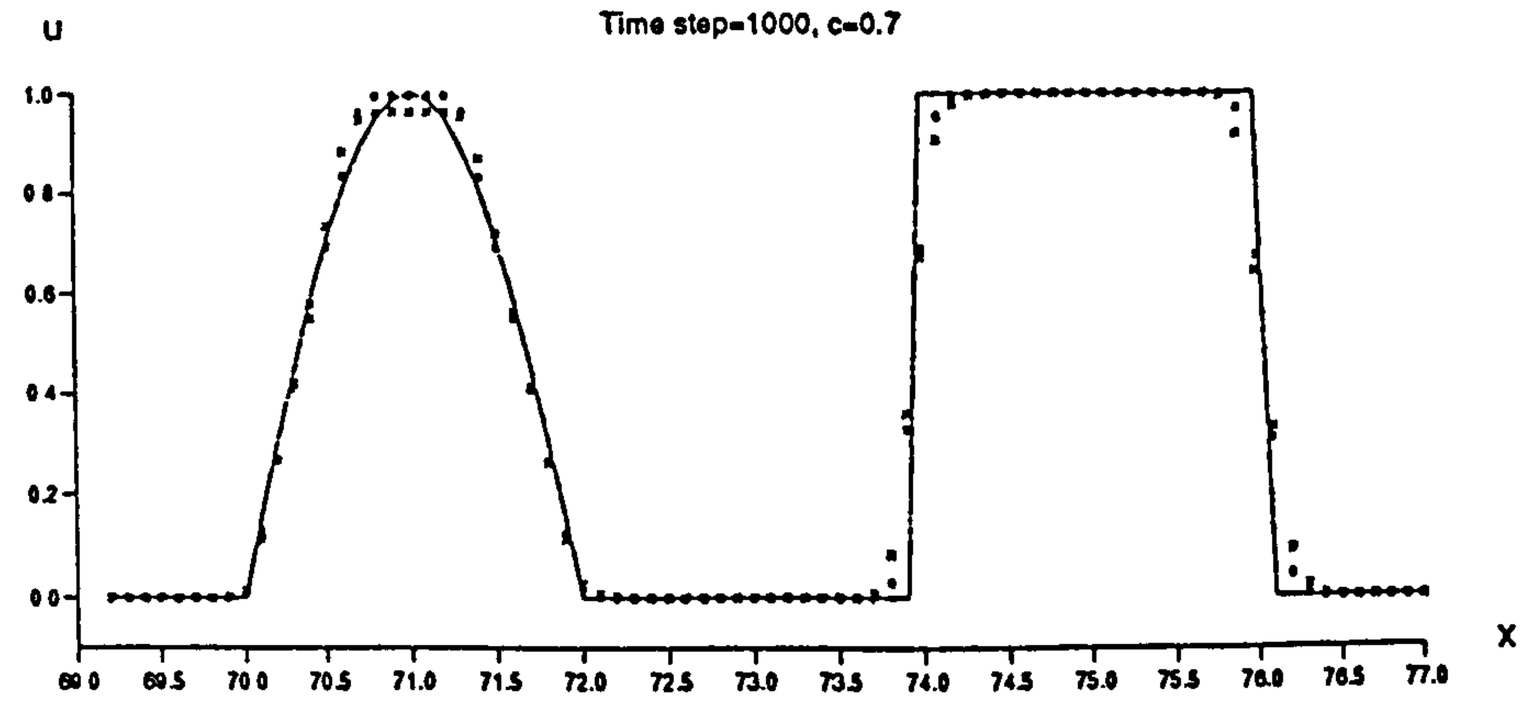

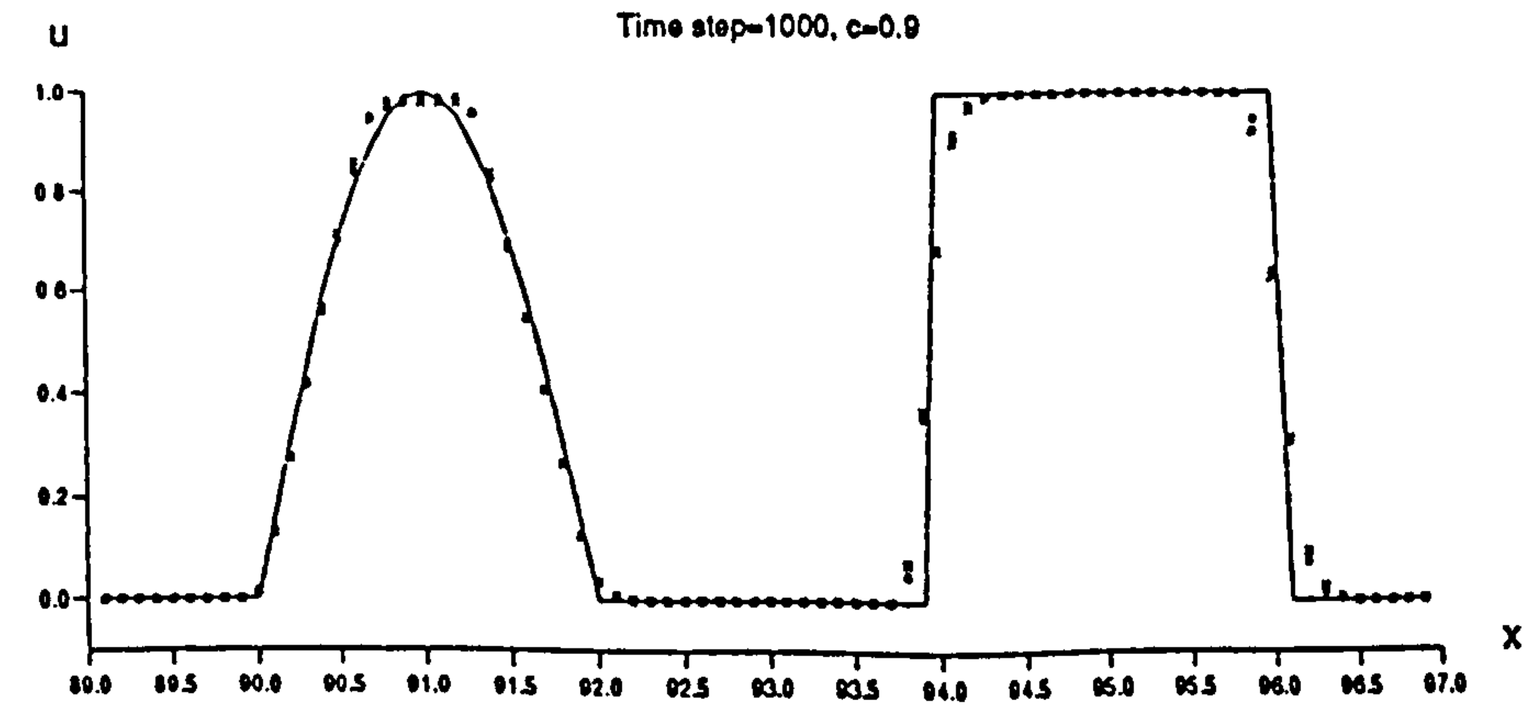

Figure 5.7: Comparison between the Exact Solution (line) and the Numerical Results with SUPERBEE (cross) and FD2B (box) after 1000 Time Steps

Figure 5.8 shows the Courant number dependent TVD regions of this scheme which has similar features to those of the second-order scheme. The upper boundary of the TVD region is maximum when $|c| = \frac{1}{2}$ and minimum when $|c| = 1$. The lower boundary is always $\phi = 0$.

We can define different third-order limiter functions using the Courant number dependent TVD regions. A general limiter function for the third-order scheme called FD3 (Fully Discrete Third-order) has the following form

$$\begin{cases} \phi_j = \frac{6\theta_j}{\eta[\theta_j(1+|c|)+2-|c|]} & if \;\; 0 \le \theta_j < \theta^L \\ \phi_j = 1 & if \;\; \theta^L \le \theta_j \le \theta^R \\ \phi_j = \frac{6}{\eta[\theta_j(1+|c|)+2-|c|]} & if \;\; \theta_j > \theta^R \\ \phi_j = 0 & if \;\; \theta_j < 0 \end{cases} \tag{5.56}$$

In particular a limiter function, called FD3A, is chosen by taking

$$\theta^L = \frac{\eta(2-|c|)}{6-\eta(1+|c|)} \tag{5.57}$$

$$\theta^R = \frac{6-\eta(2-|c|)}{\eta(1+|c|)} \tag{5.58}$$

Figure 5.9 shows the FD3A limiter function for three values of Courant number. They are given by the full lines.

Figure 5.10 shows the performance of the FD3A for the same test problem as before after 50 time steps with 0.5, 0.7 and 0.9. The solid line is the exact solution. The numerical results (symbol) are accurate in the smooth part but discontinuities are smeared with 4-5 interior points. We are interested in the behaviour of the scheme for long time evolution. Figure 5.11 shows the results after 1000 time steps, which shows that this limiter function is not very satisfactory for long times; it introduces too much numerical diffusion. Recall that due to the imposition of the TVD property the scheme reduces locally to first-order accuracy near extrema.

The following limiter function, called FD3B, is suggested

$$\theta^L = 1.1\eta - 0.17 \tag{5.59}$$

$$\theta^R = 2.78 - 1.4\eta \tag{5.60}$$

which is determined by finding the best results for different Courant numbers and then obtaining the function empirically. Figure 5.12 shows the FD3B function for Courant number 0.5.

Figures 5.13 and 5.14 show the comparison of the numerical results of the FD3B (symbol) and the exact solution (line) after 50 and 1000 time steps respectively with Courant numbers 0.5, 0.7 and 0.9. The numerical results of FD3B are superior to those obtained with FD3A. There is virtually no numerical diffusion but some tendency to square the smooth parts is observed. For $|c|$ close to $\frac{1}{2}$ the results are very accurate for both the smooth and discontinuous parts of the solution. We can expect the fully discrete third-order scheme with FD3B to give good performance for most practical flows.

5.6 Fourth-order TVD Scheme

The five-point, fourth-order scheme with limiter function can be written as (refer to equation (4.33) for unlimited version)

$$\begin{aligned} F_{j+\frac{1}{2}} &= \frac{1}{2}(F_j^n + F_{j+1}^n) - \frac{|a|}{2}\Delta U_{j+\frac{1}{2}} + \left(|a|\ D_0\Delta U_{j+\frac{1}{2}} + |a|\ D_1\Delta U_{j+L+\frac{1}{2}}\right)\ \phi_j \\ &\quad + |a|\ D_2\Delta U_{j+M+\frac{1}{2}}\ \phi_{j+M} \end{aligned} \tag{5.61}$$

where

$$\begin{cases} D_0 = \frac{1}{2} - \frac{7}{12}|c| + \frac{1}{12}|c^3| \\ D_1 = \frac{1}{12} + \frac{1}{24}|c| - \frac{1}{12}c^2 - \frac{1}{24}|c^3| \\ D_2 = \frac{1}{12}c^2 + \frac{1}{24}|c| - \frac{1}{12} - \frac{1}{24}|c^3| \end{cases} \tag{5.62}$$

The limiter functions are determined by equations (5.19) to (5.22).

Figure 5.15 shows the TVD regions of the scheme for $\theta_j^* = 1$. The figure has similar features to that of the third-order scheme.

Based on the general TVD condition for the fourth-order scheme we have

$$\begin{cases} \phi_j = \frac{(1-|c|)\ \theta_j}{\eta\ (D_1\theta_j + D_0 - D_2)} & for\ \ 0 \le \theta_j < \theta^L \\ \phi_j = 1 & for\ \ \theta^L \le \theta_j \le \theta^R \\ \phi_j = \frac{1-|c|+\eta D_2\ \phi_{j+M}/\theta_j^*}{\eta\ (D_0 + D_1\theta_j)} & for\ \ \theta_j > \theta^R \\ \phi_j = 0 & for\ \ \theta_j < 0 \end{cases} \tag{5.63}$$

Instead of $\phi_{j+M} = 1$ in equation (5.20) we define

$$\begin{cases} \phi_{j+M} = \eta\ \theta_{j+M} & for\ \ 0 \le \theta_{j+M} < 0.5 \\ \phi_{j+M} = 1 & for\ \ \theta_{j+M} > 0.5 \\ \phi_{j+M} = 0 & for\ \ \phi_j = 0 \end{cases} \tag{5.64}$$

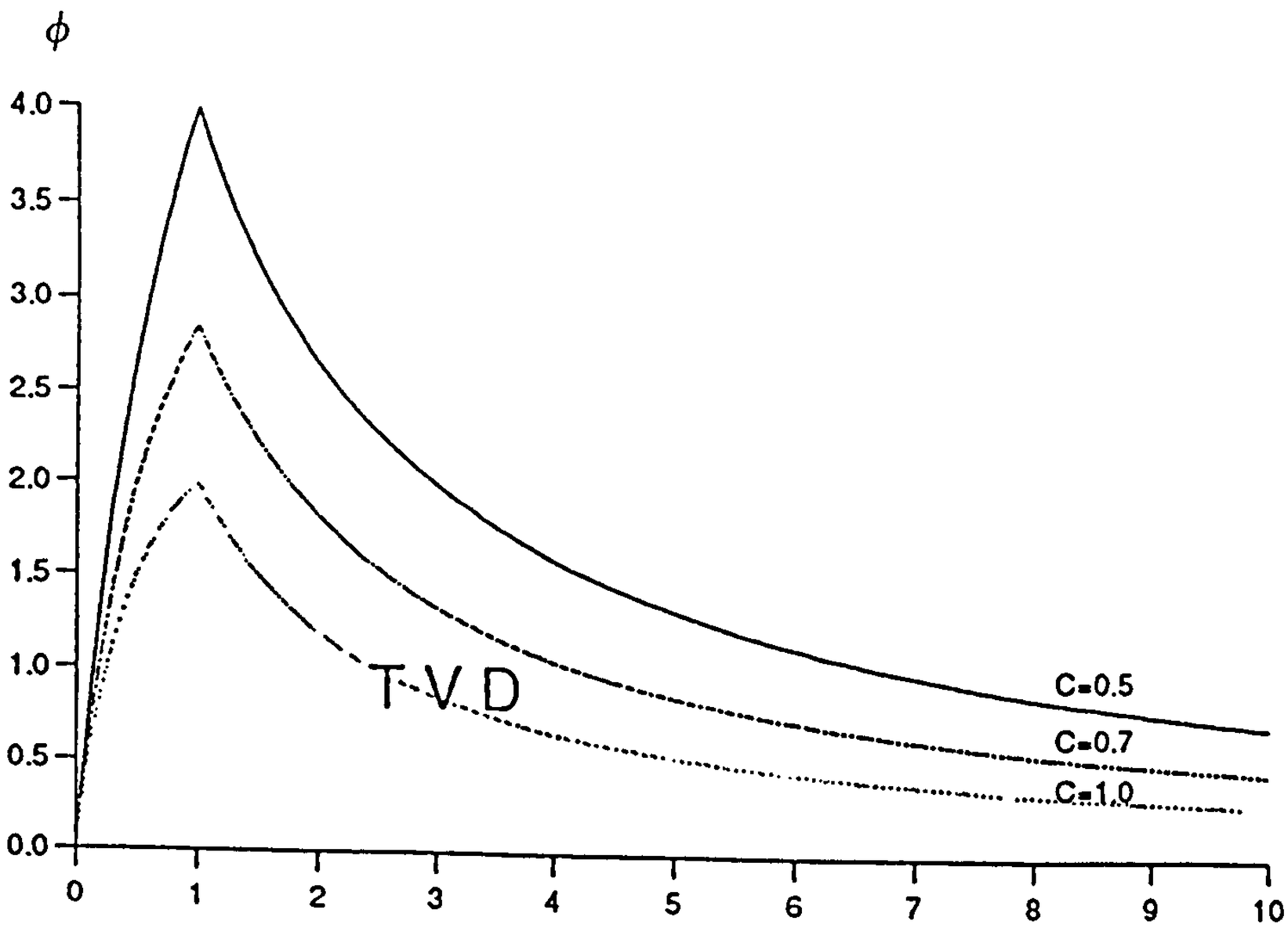

Figure 5.8: Courant Number Dependent Third-order TVD Region

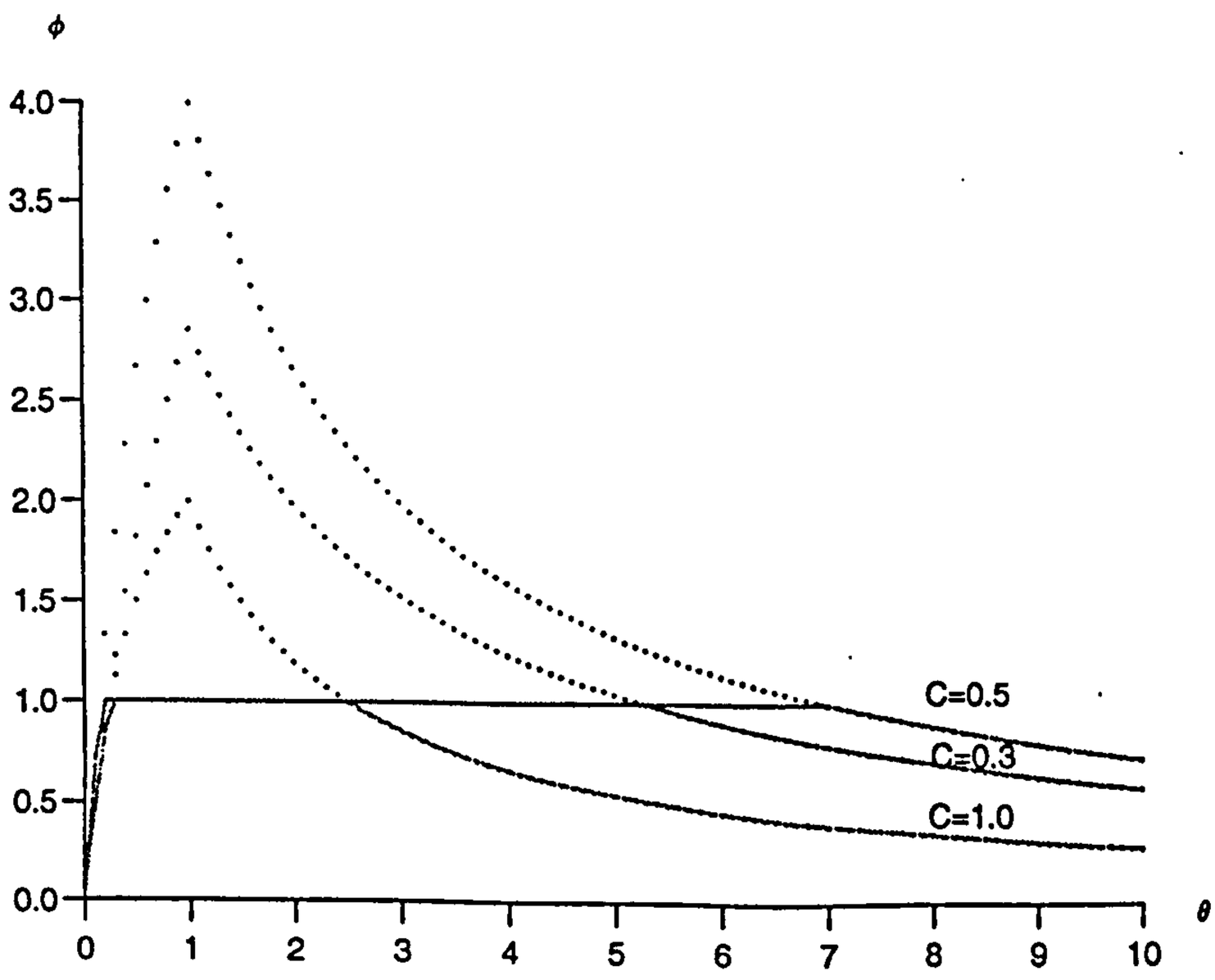

Figure 5.9: FD3A Limiter Function with Courant Number 0.1, 0.3 and 0.5 (lines)

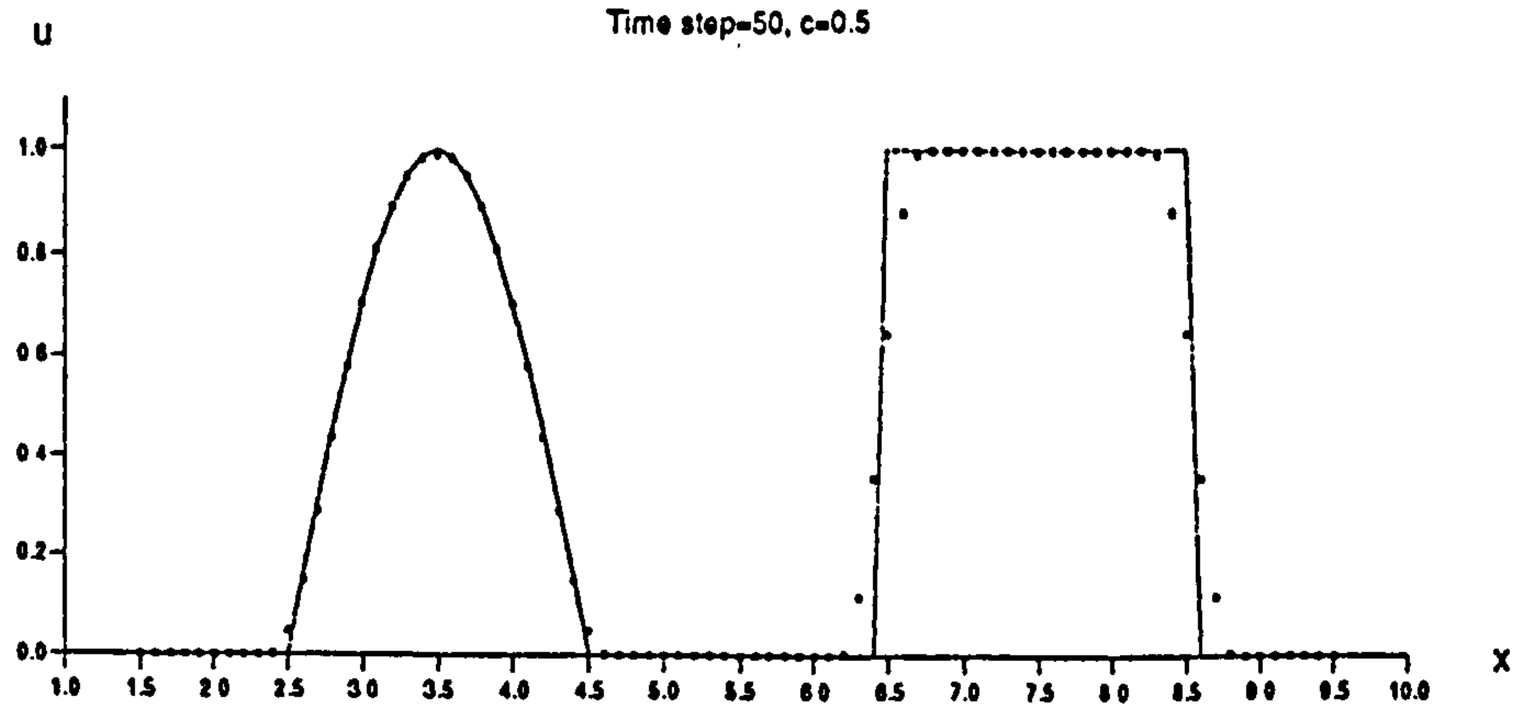

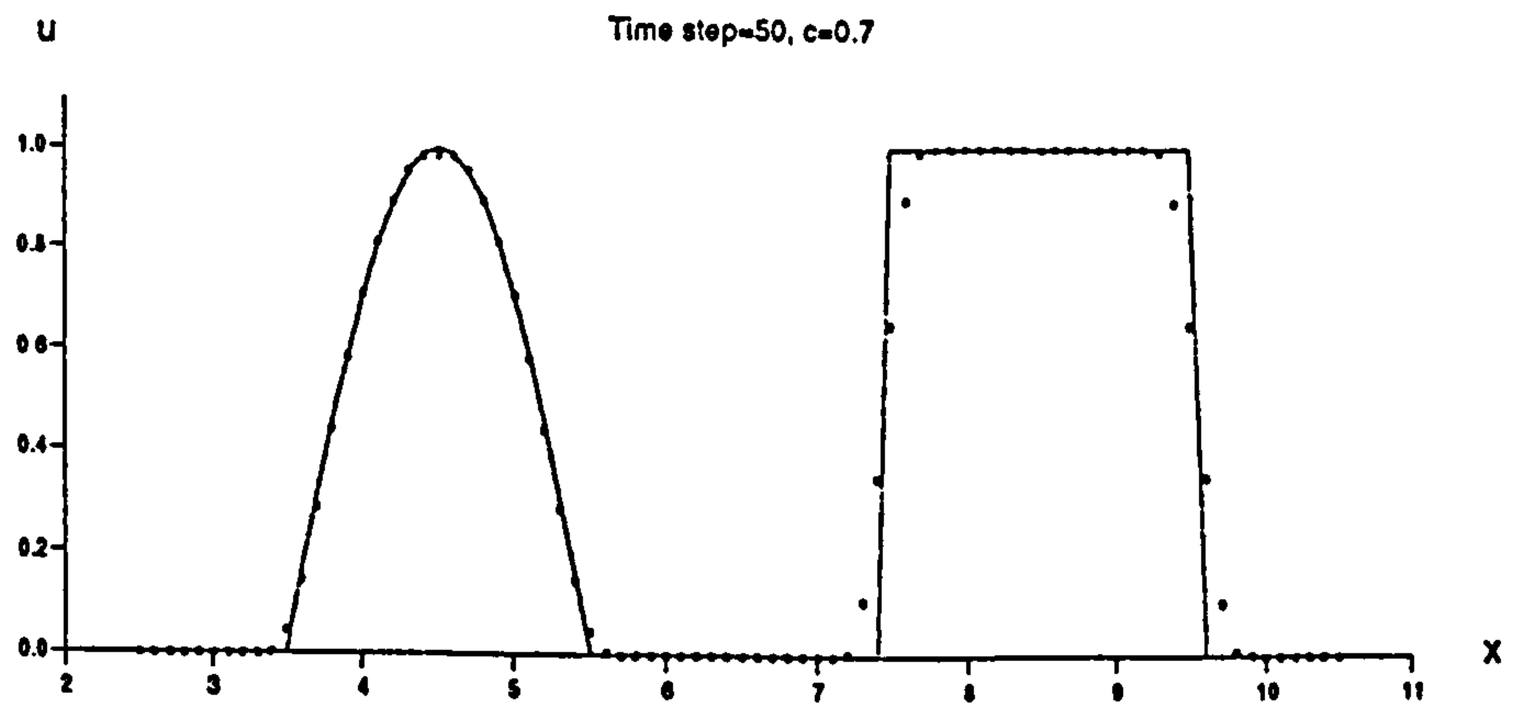

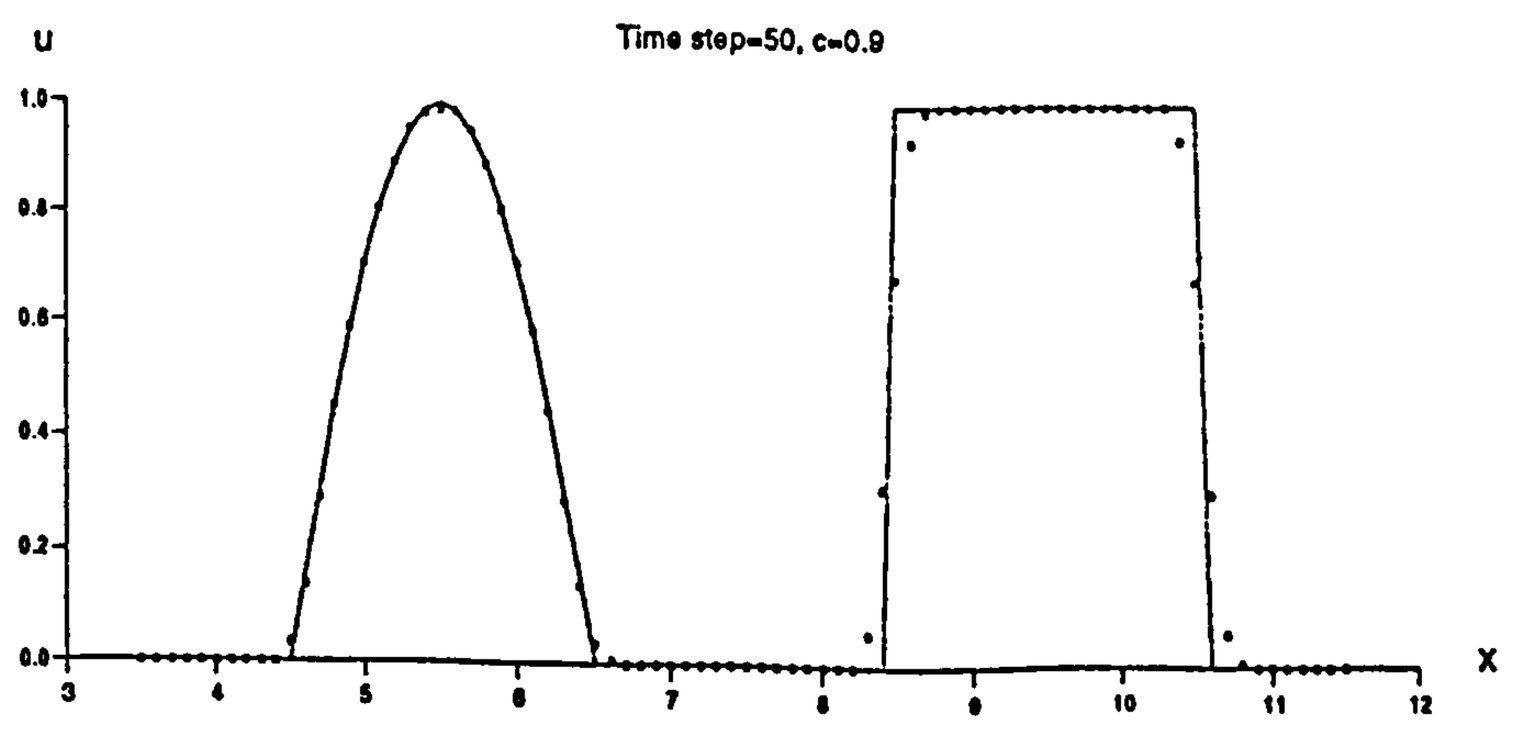

Figure 5.10: Comparision between the Exact Solution (line) and the Numerical Results of FD3A (symbol) after 50 Time Steps

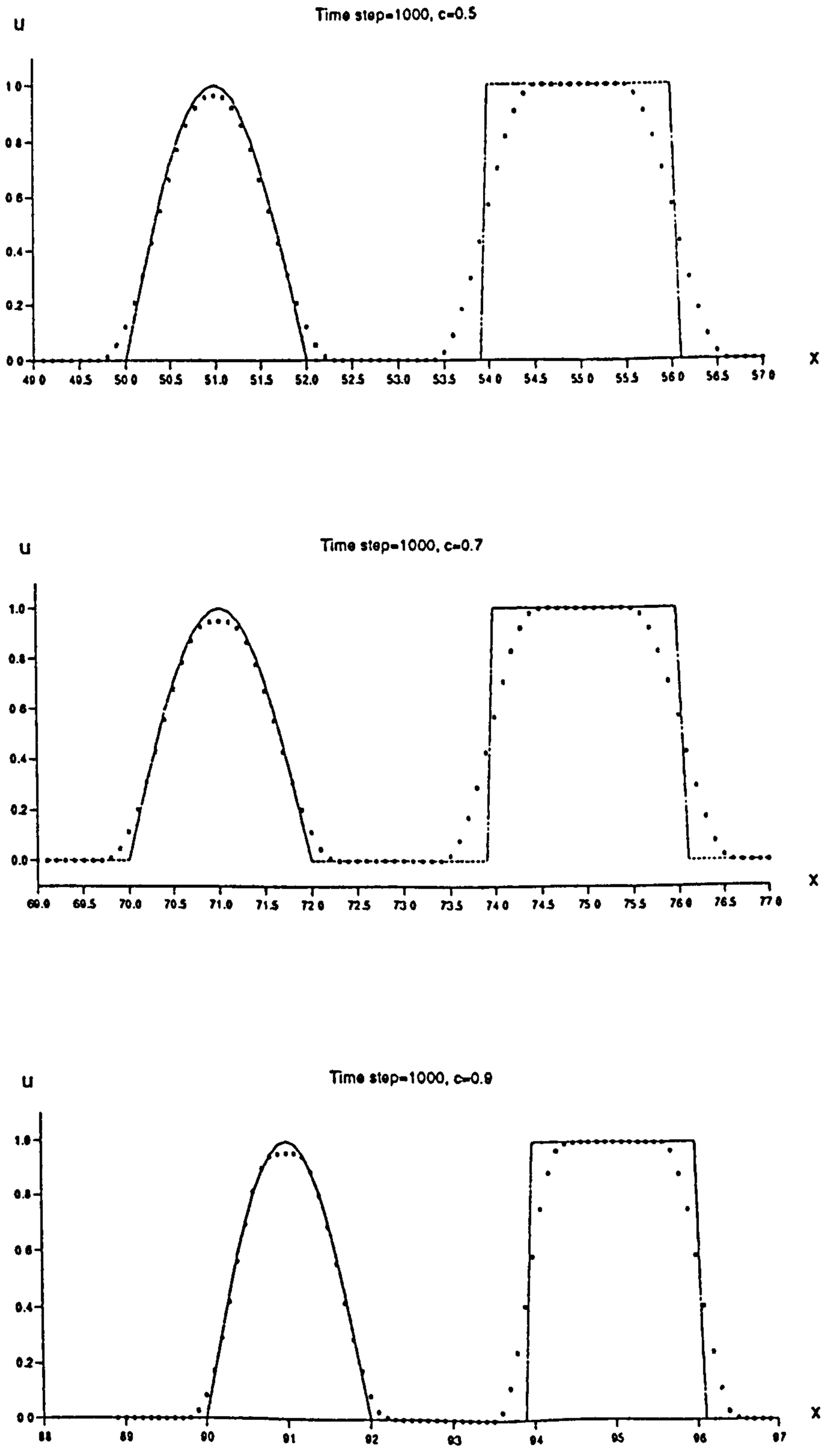

Figure 5.11: Comparision between the Exact Solution (line) and the Numerical Results of FD3A (symbol) after 1000 Time Steps

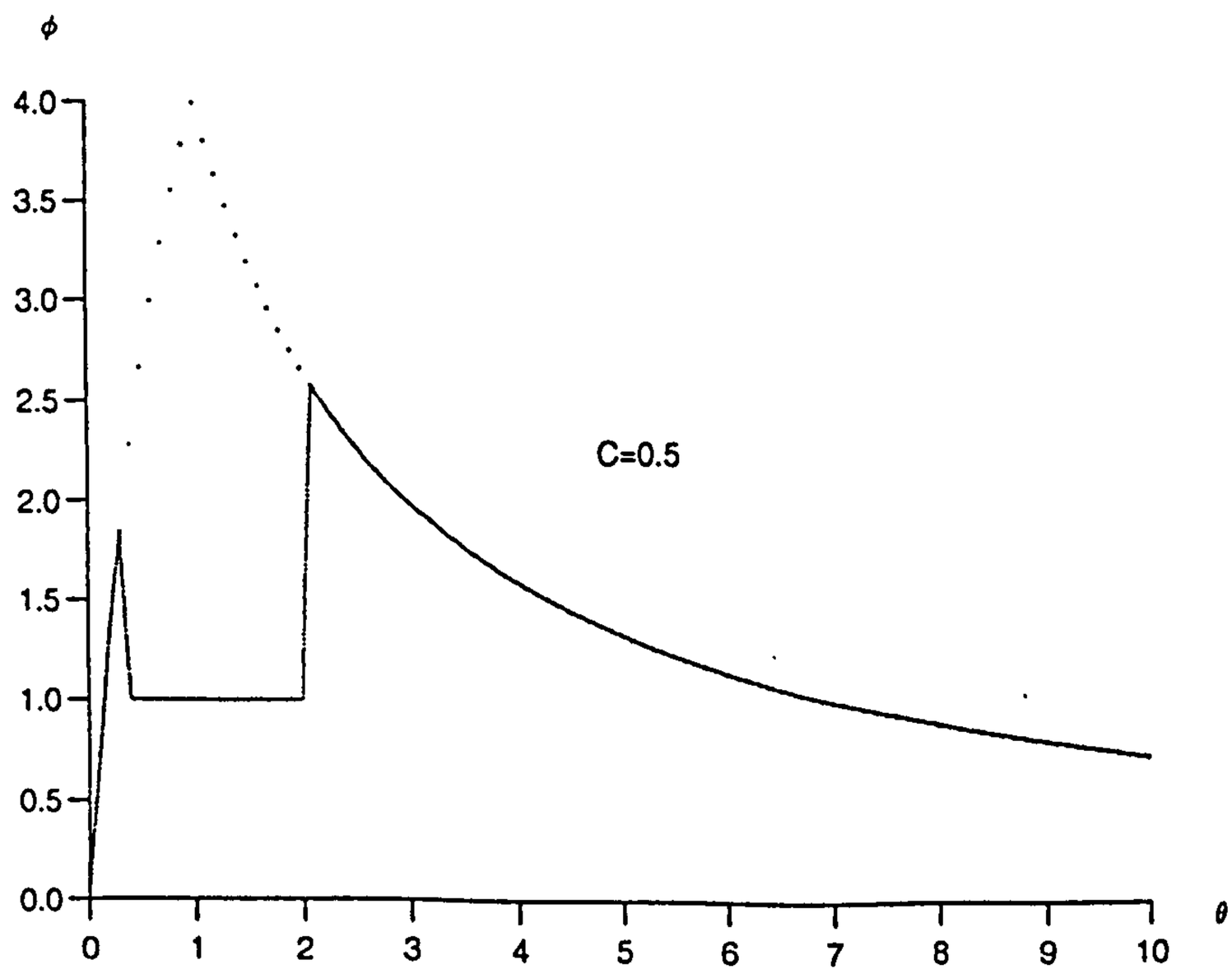

Figure 5.12: FD3B Limiter Function with Courant Number 0.5 (lines)

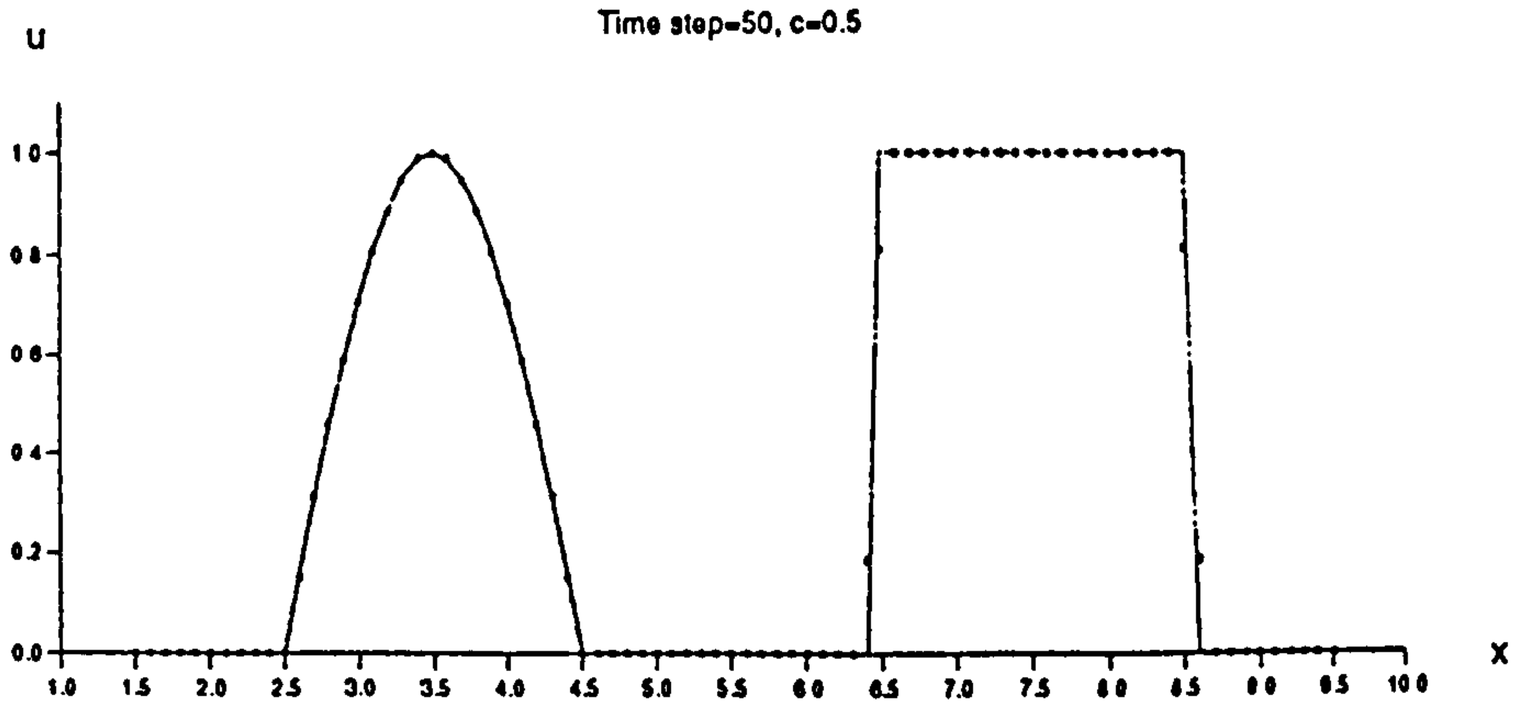

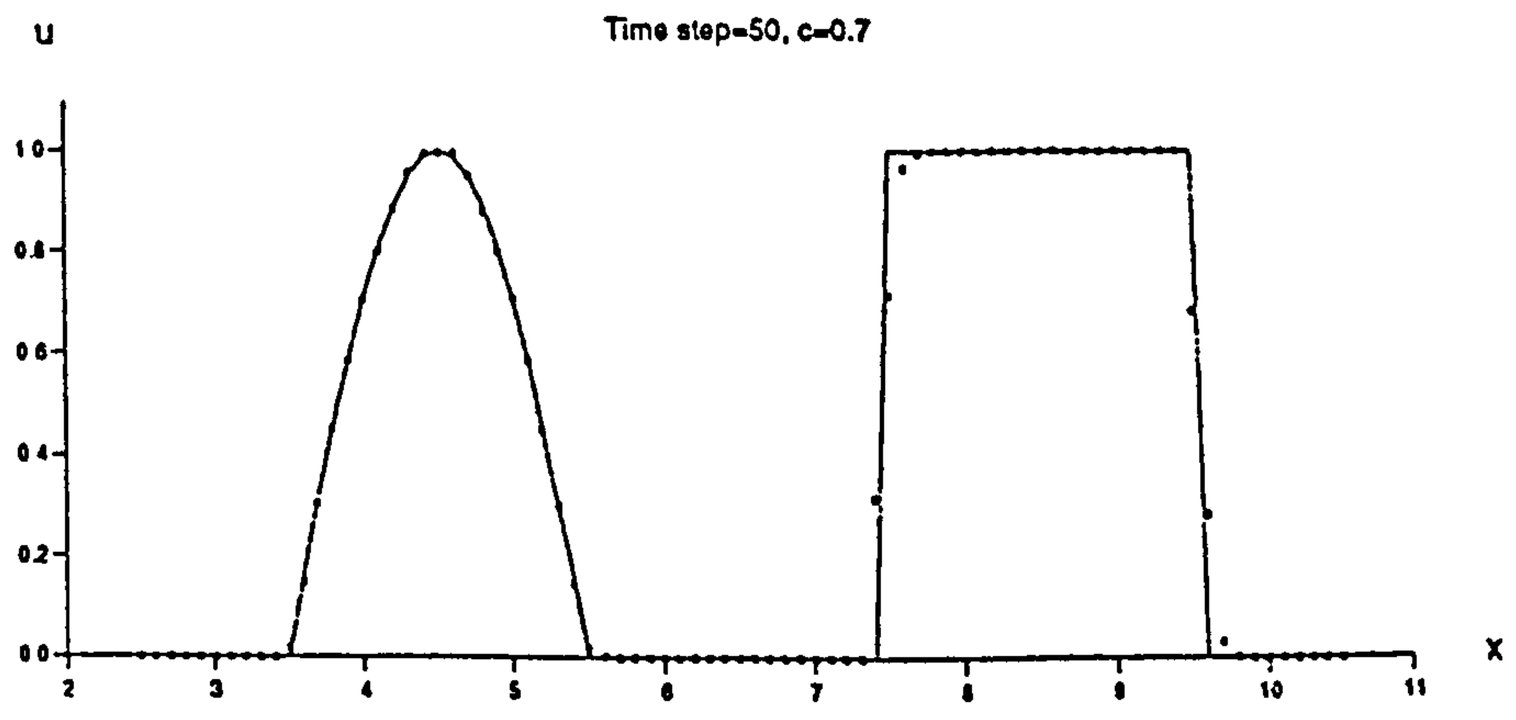

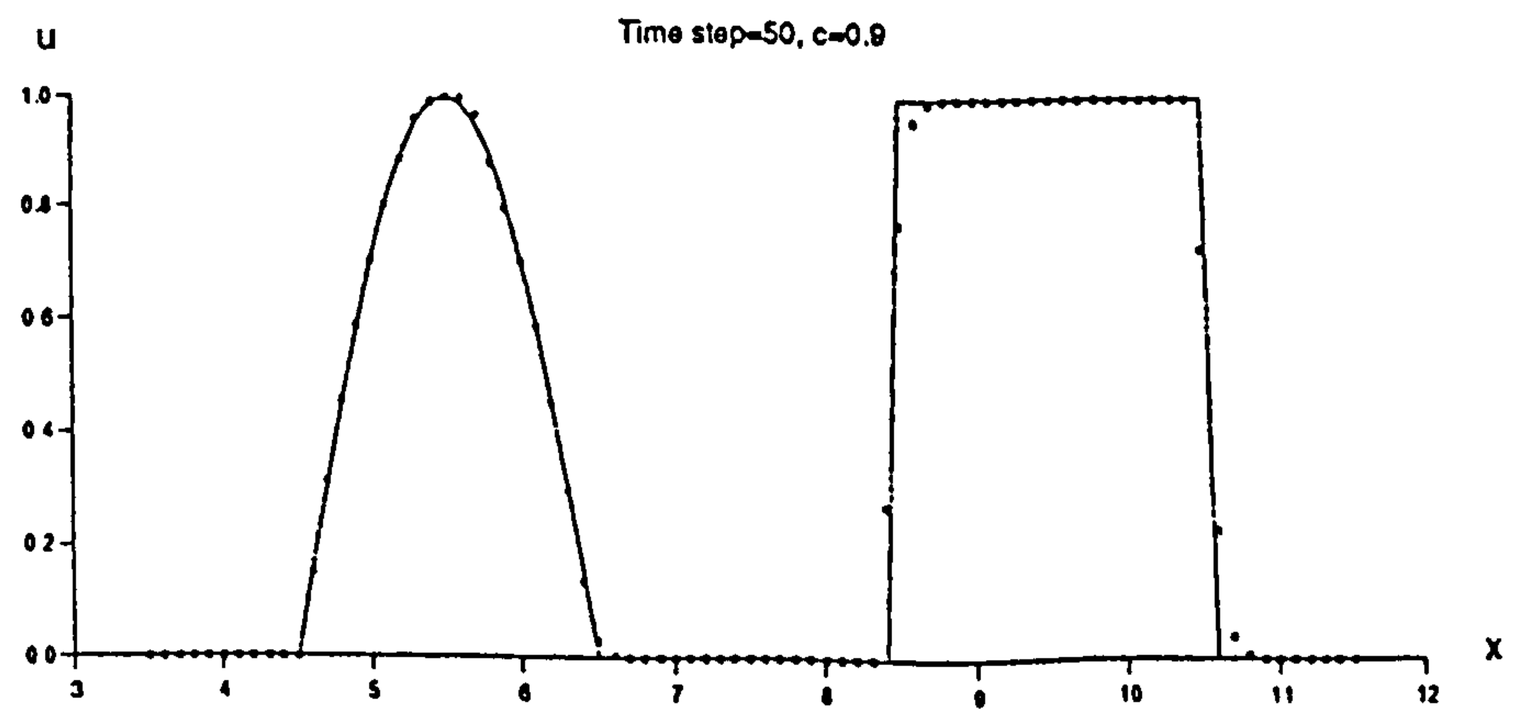

Figure 5.13: Comparison between the Exact Solution (line) and the Numerical Results of FD3B (symbol) after 50 Time Steps

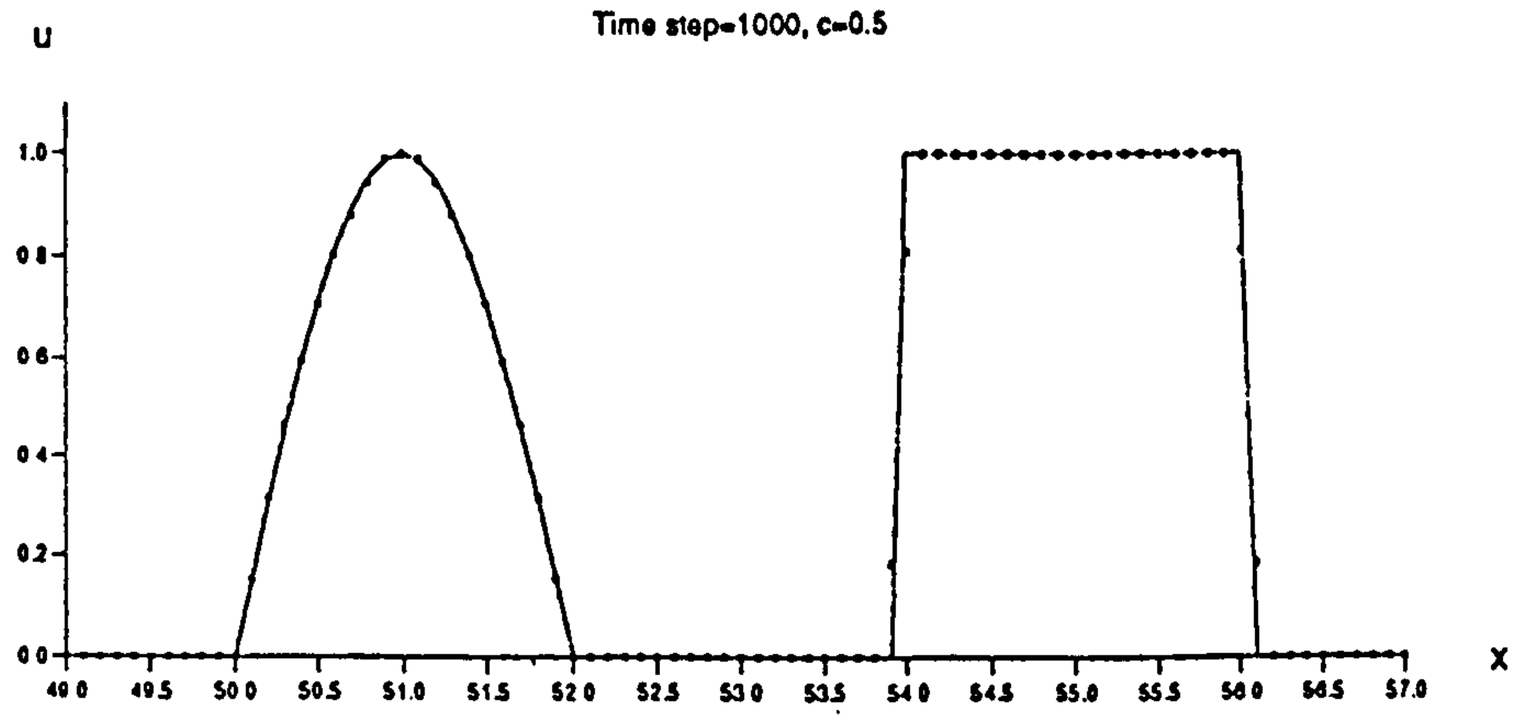

Figure 5.14: Comparison between the Exact Solution (line) and the Numerical Results of FD3B (symbol) after 1000 Time Steps

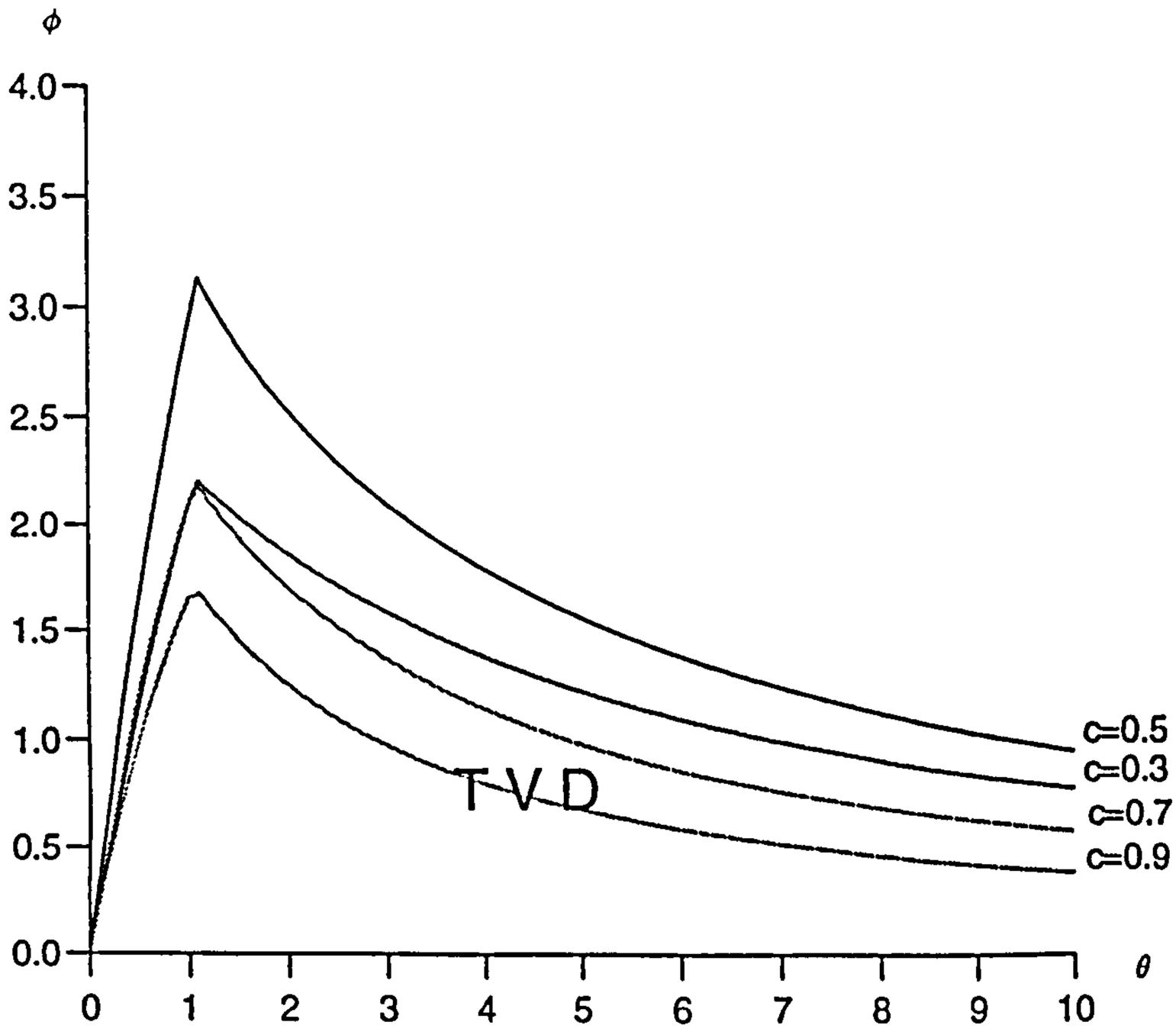

Figure 5.15: Courant Number Dependent Fourth-order TVD Region for $\theta_j^* = 1$

Figure 5.15 shows the TVD regions of the scheme for $\theta_j^* = 1$. The Figure has similar features to that of the third-order scheme.

Based on the general TVD condition for the fourth-order scheme we have

$$\begin{cases} \phi_j = \frac{(1-|c|)\ \theta_j}{\eta\ (D_1\theta_j + D_0 - D_2)} & for\ \ 0 \le \theta_j < \theta^L \\ \phi_j = 1 & for\ \ \theta^L \le \theta_j \le \theta^R \\ \phi_j = \frac{1-|c|+\eta D_2\ \phi_{j+M}/\theta_j^*}{\eta\ (D_0 + D_1\theta_j)} & for\ \ \theta_j > \theta^R \\ \phi_j = 0 & for\ \ \theta_j < 0 \end{cases} \tag{5.69}$$

Instead of $\phi_{j+M} = 1$ in equation (5.20) we define

$$\begin{cases} \phi_{j+M} = \eta\ \theta_{j+M} & for\ \ 0 \le \theta_{j+M} < 0.5 \\ \phi_{j+M} = 1 & for\ \ \theta_{j+M} > 0.5 \\ \phi_{j+M} = 0 & for\ \ \phi_j = 0 \end{cases} \tag{5.70}$$

Our first limiter function, called FD4A, is obtained by setting

$$\theta^L = \frac{\eta(D_0 - D_2)}{1 - |c| - \eta D_1} \tag{5.71}$$

$$\theta^R = \frac{1 - |c| - \eta(D_0 - D_2\ \phi_{j+M}/\ \theta_j^*)}{\eta D_1} \tag{5.72}$$

long time evolution, especially for discontinuities. Also FD4B is simpler than FD4A. Comparing with the results obtained by the third-order schemes (see figures 5.11 and 5.14) although the results obtained by FD4s are not as good as that obtained by FD3s, considering higher-order schemes are more difficult to deal with I am happy with the 4th-order limited results.

5.7 H-th-order TVD Schemes

In order to obtain H-th-order TVD schemes one approach is to use a hybrid flux limiter method following the Flux Corrected Transport approach [35] whereby the H-th-order flux can be written as

$$F_{j+\frac{1}{2}} = F^{(L)}_{j+\frac{1}{2}} + \left(F^{(H)}_{j+\frac{1}{2}} - F^{(L)}_{j+\frac{1}{2}} \right) \phi^*_j \tag{5.69}$$

where $2 \leq L \leq 4$, $H > 4$ and $F^{(L)}_{j+\frac{1}{2}}$ is the L-th-order flux which includes a rigorously derived limiter ϕ_j. Here ϕ^*_j is an empirical flux limiter which is unity in smooth regions and makes the flux (5.69) H-th-order accurate. In regions of high gradients ϕ^*_j is zero, which means that the flux (5.69) reduces to the L-th-order scheme with an appropriate limiter.

In order to determine ϕ^*_j we need first to define the locally smooth regions for flux (5.69). We utilize the information provided by the L-th-order TVD method. For example the third-order method with FD3A limiter function (Fig. 6.9), the smooth region is given by equation (5.56), that is

$$\frac{\eta(2-|c|)}{6-\eta(1+|c|)} \leq \theta_j \leq \frac{6-\eta(2-|c|)}{\eta(1+|c|)}$$

To validate the empirical approach of (5.69) for high-order methods

$$F_{j+\frac{1}{2}} = F^{(3)}_{j+\frac{1}{2}} + \left(F^{(4)}_{j+\frac{1}{2}} - F^{(3)}_{j+\frac{1}{2}} \right) \phi^*_j \tag{5.70}$$

is considered. ($L = 3$, $H = 4$ in equation (5.69)). The results of the scheme can be compared directly with those of the fourth-order TVD schemes of the previous section.

Since the flux (5.70) involves three intercell boundaries ($j-\frac{1}{2}$, $j+\frac{1}{2}$, $j+\frac{3}{2}$), locally smooth regions for the flux (5.70) means that in all of these cells the flow parameters θ^s_j must be

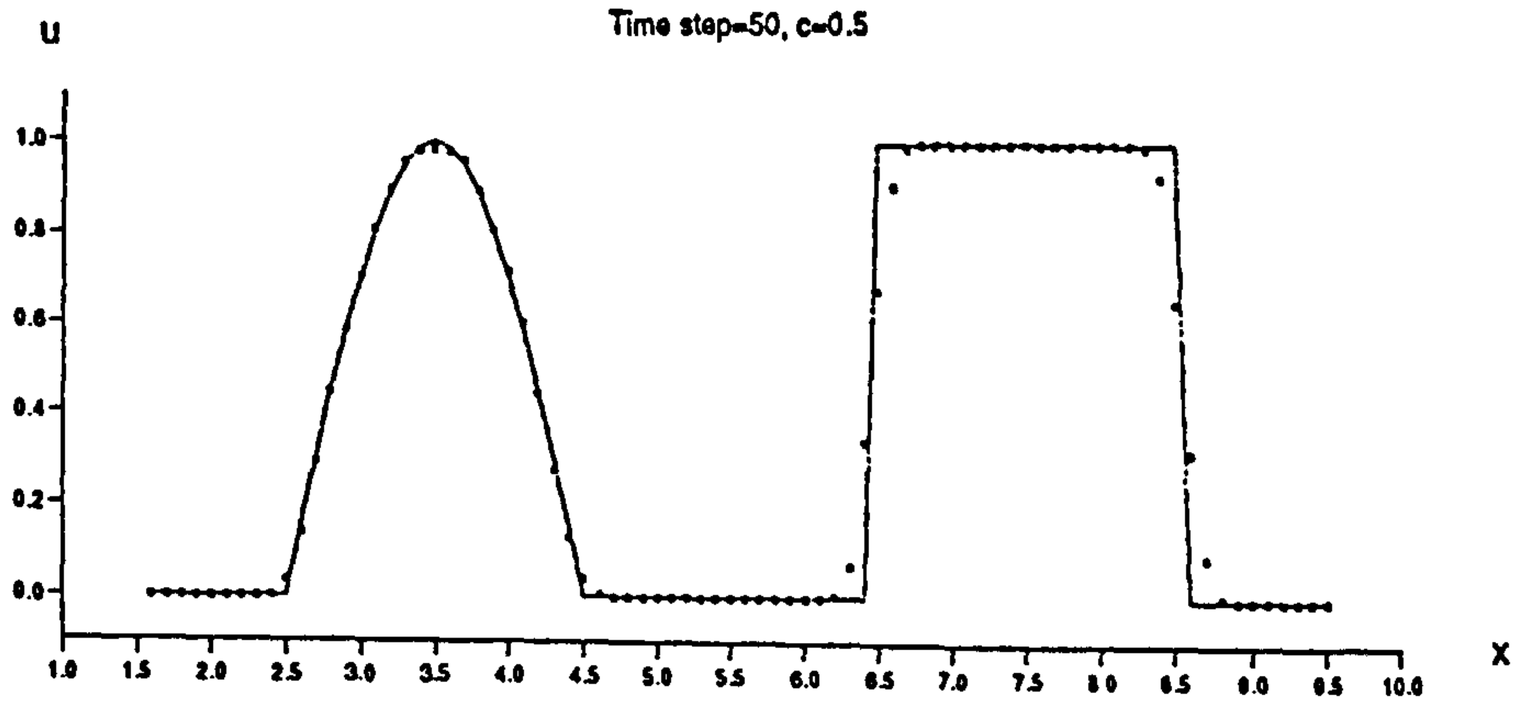

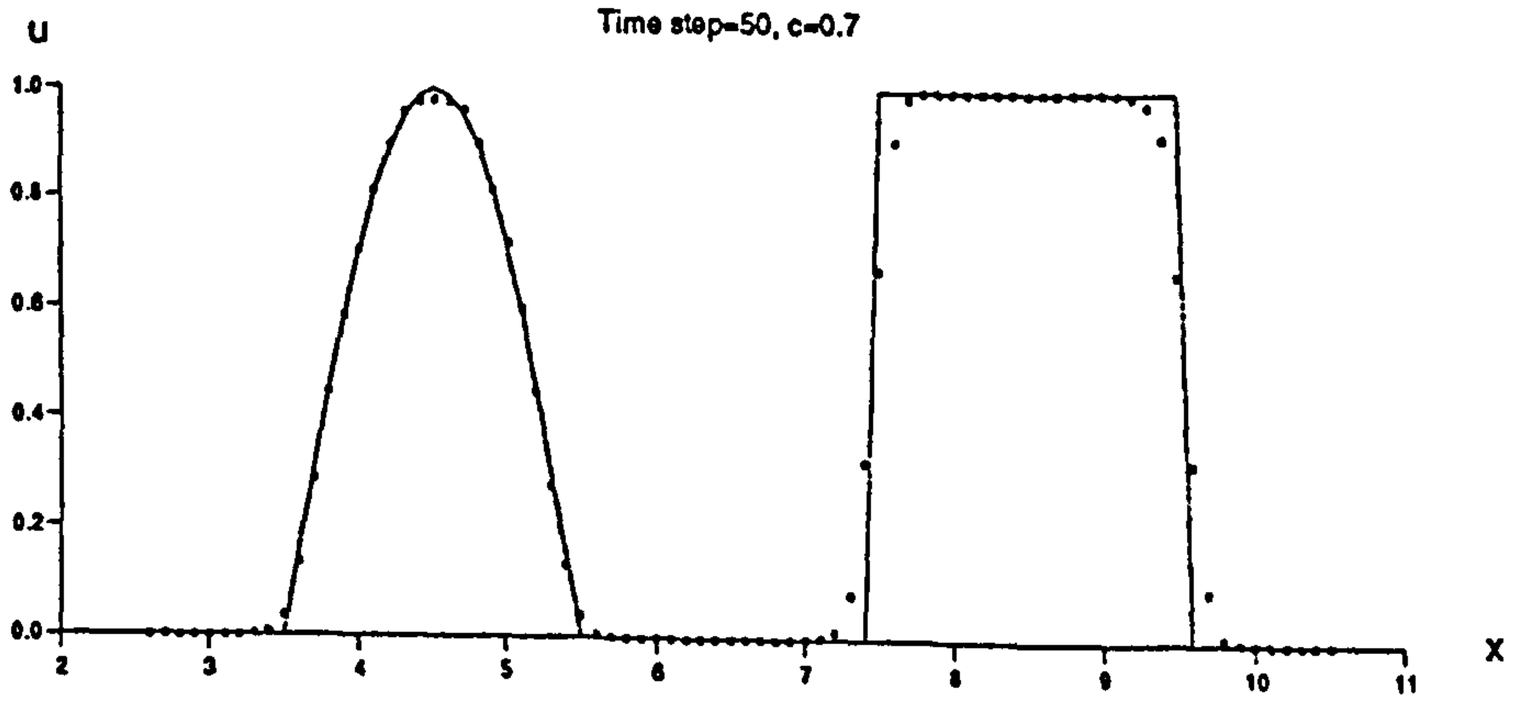

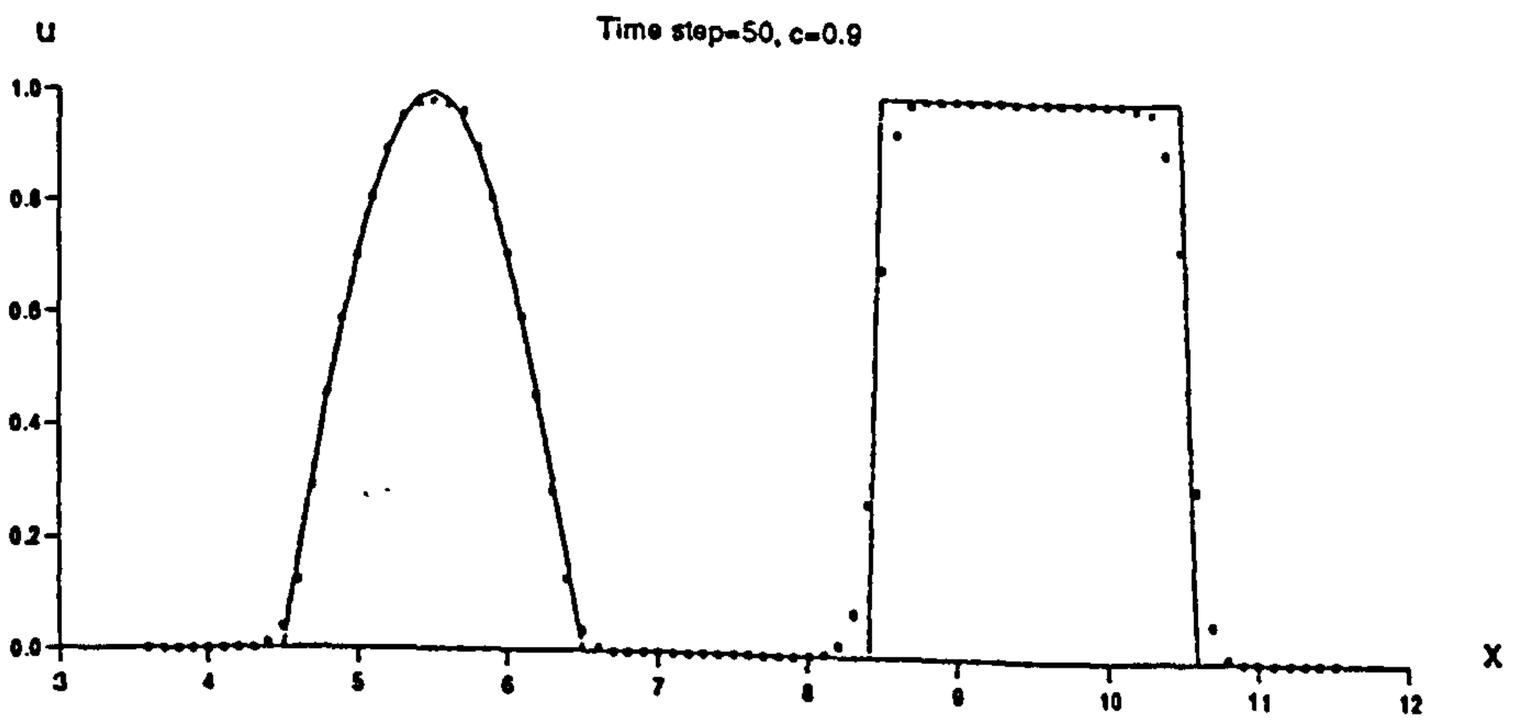

Figure 5.16: Comparison between the Exact Solution (line) and the Numerical Results of FD4A (symbol) after 50 Time Steps

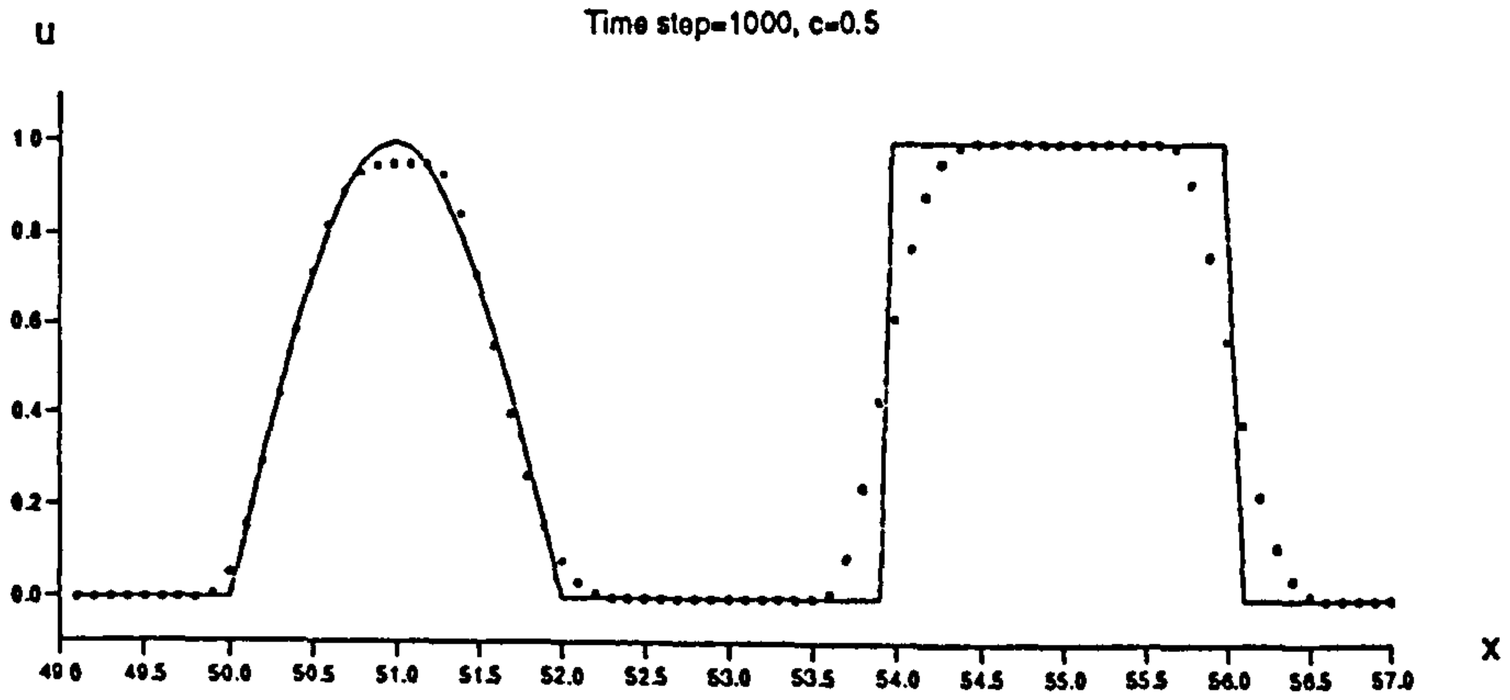

Figure 5.17: Comparison between the Exact Solution (line) and the Numerical Results of FD4A (symbol) after 1000 Time Steps

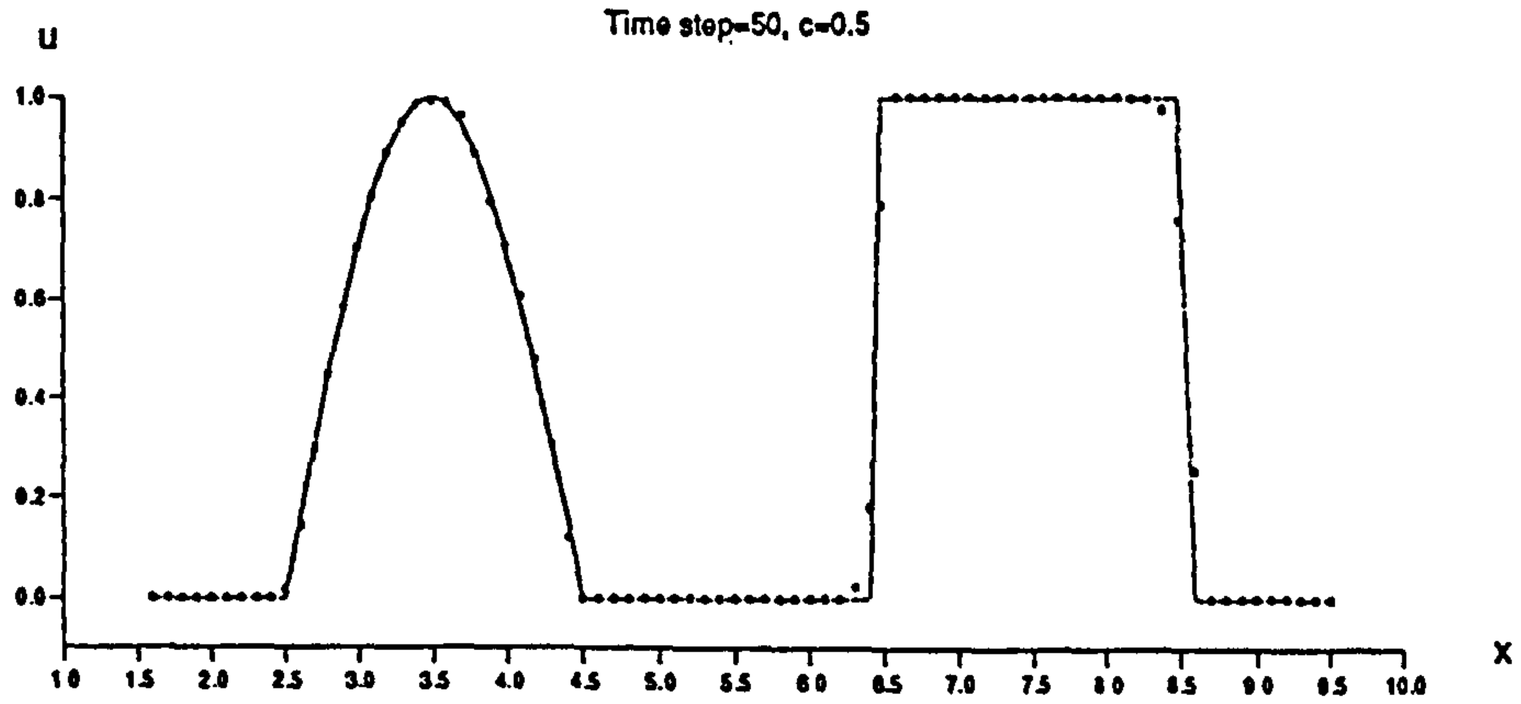

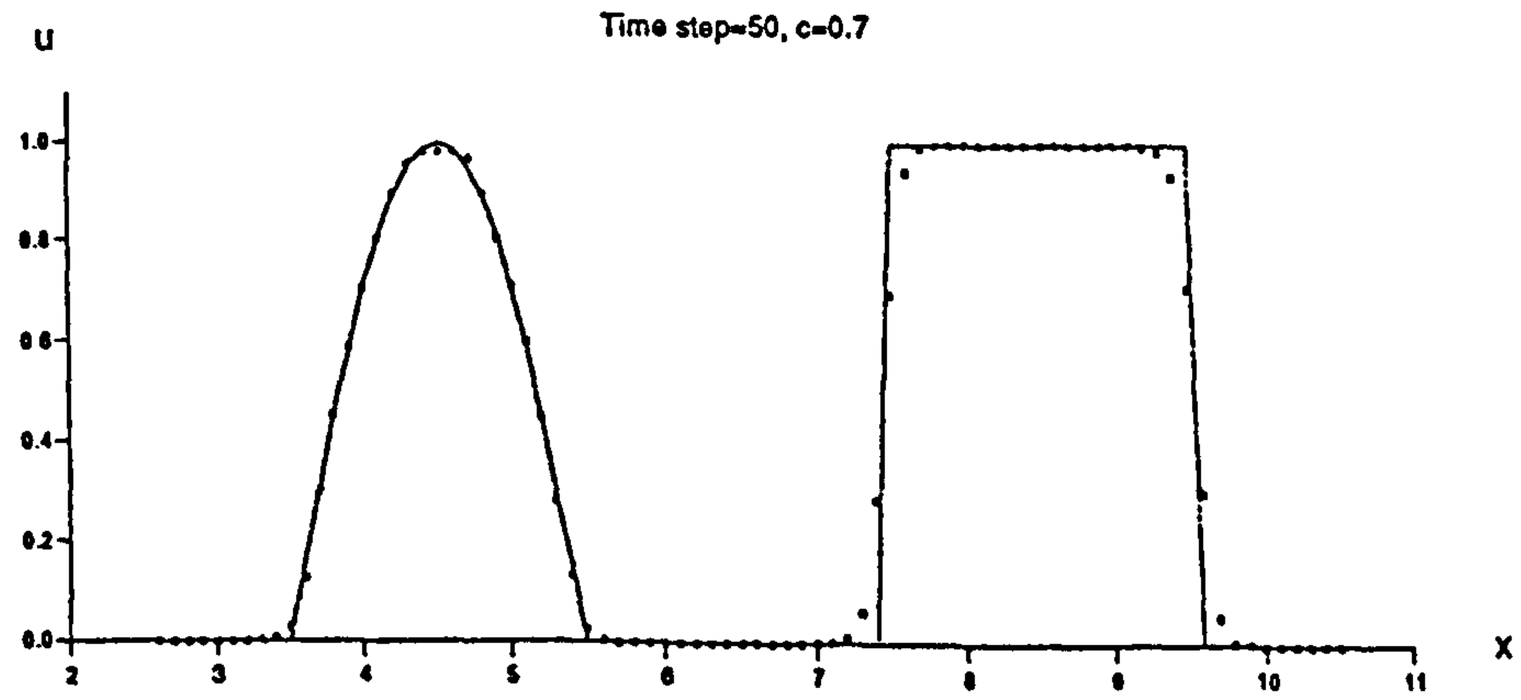

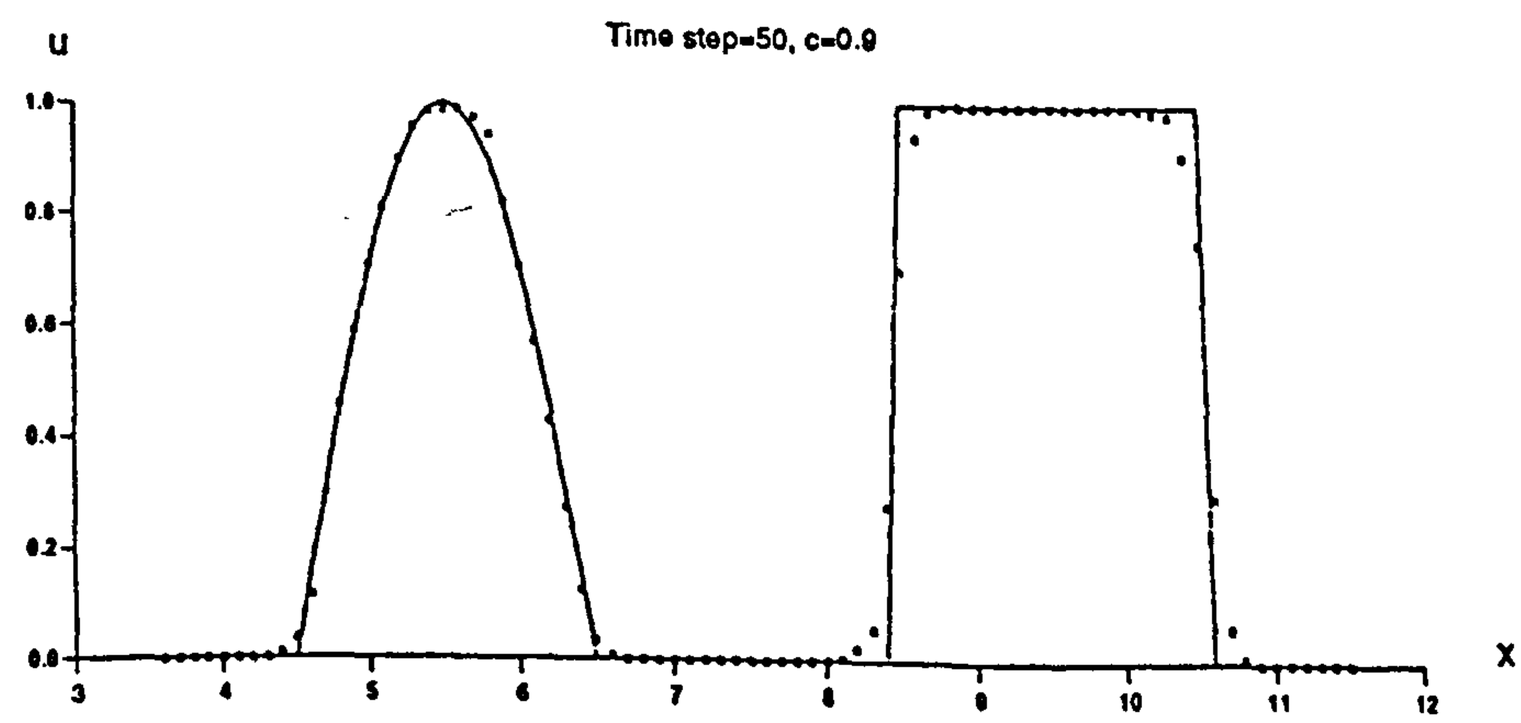

Figure 5.18: Comparison between the Exact Solution (line) and the Numerical Results of FD4B (symbol) after 50 Time Steps

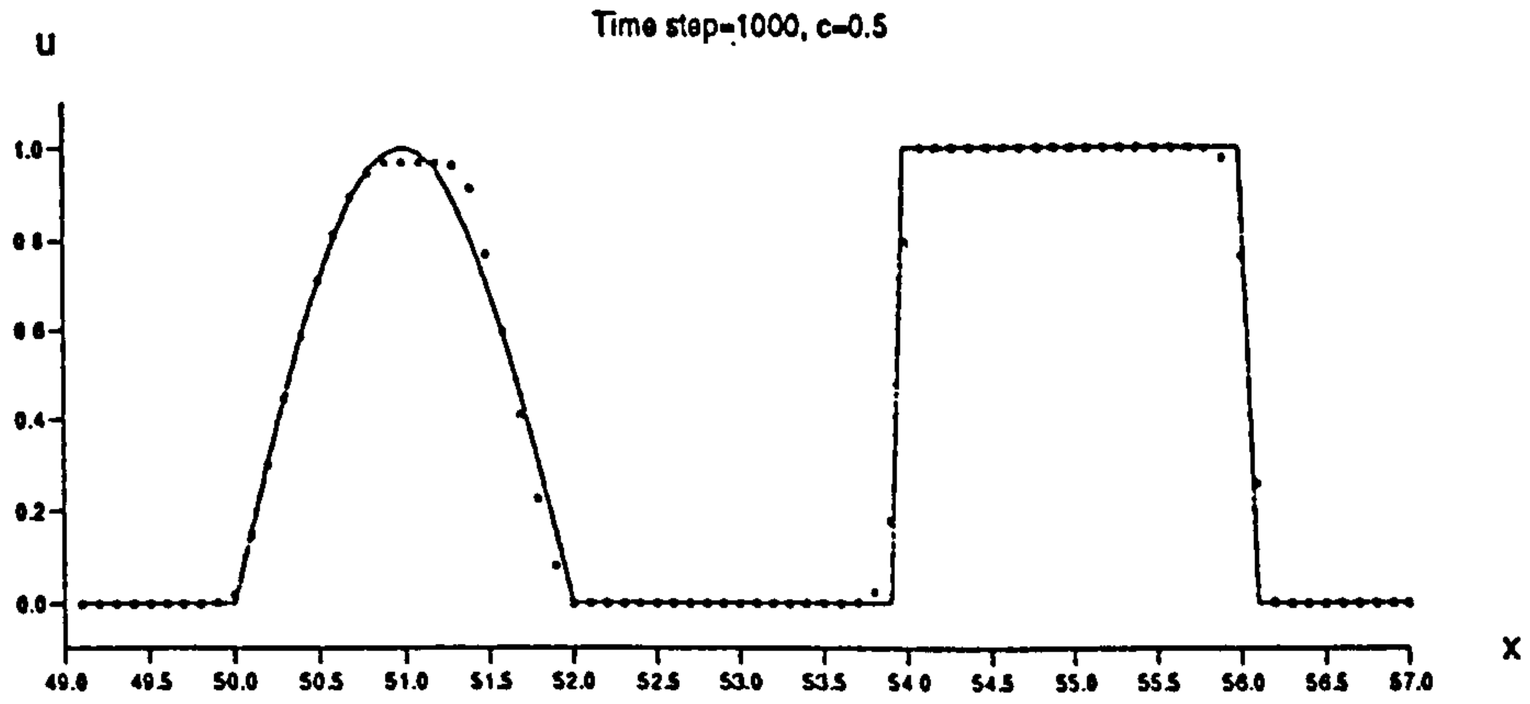

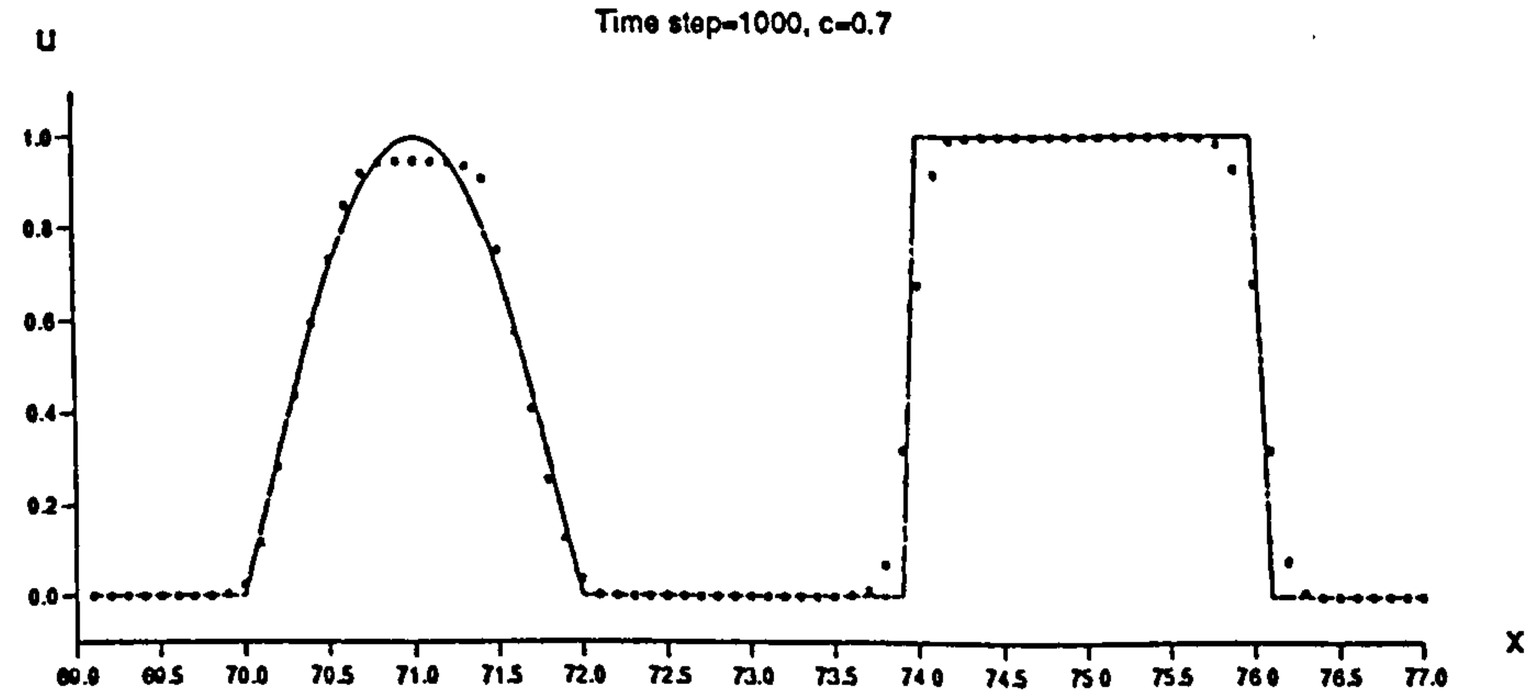

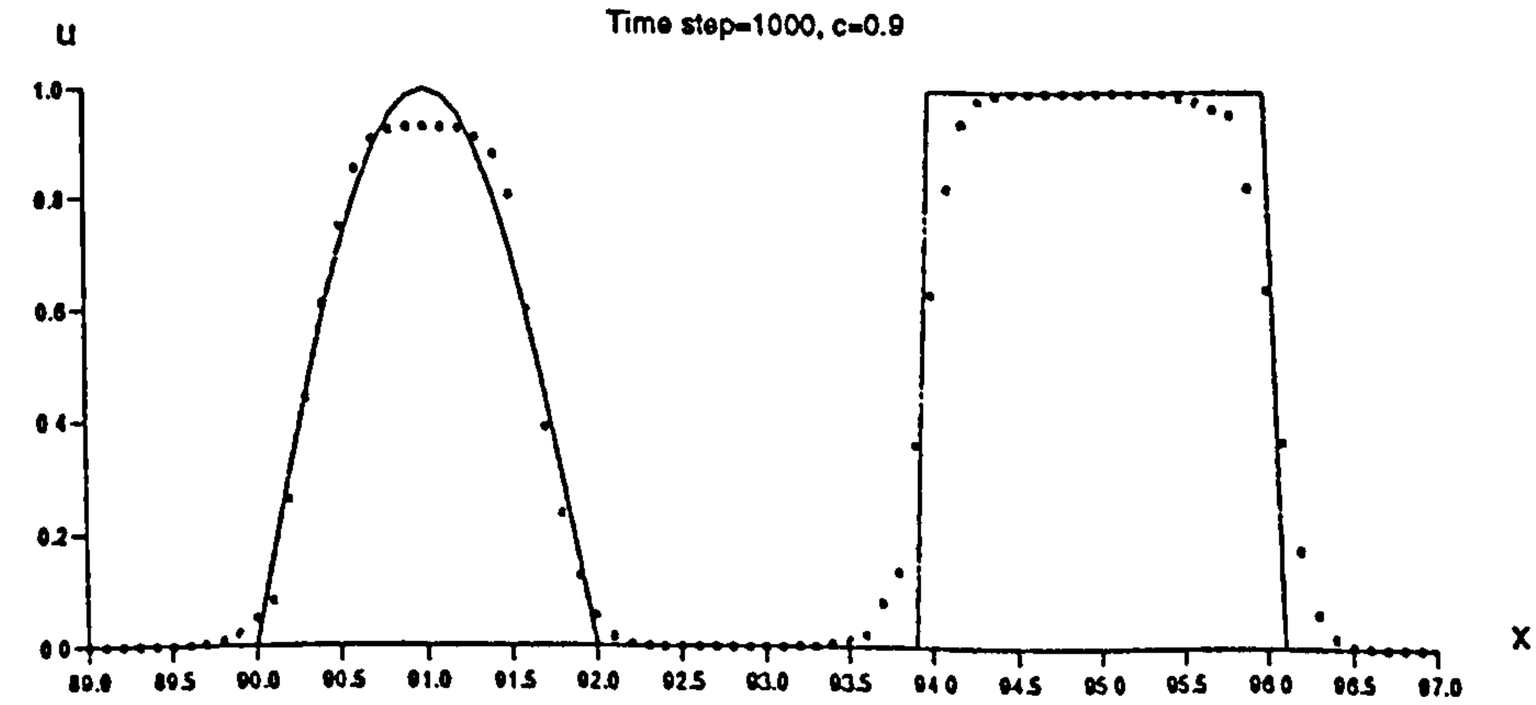

Figure 5.19: Comparison between the Exact Solution (line) and the Numerical Results of FD4B (symbol) after 1000 Time Steps

indicative of smooth flows. Therefore the empirical flux limiter ϕ_j^* is determined by

$$\phi_j^* = 1 \quad if \quad \begin{cases} \frac{\eta(2-|c|)}{6-\eta(1+|c|)} \leq \theta_j^1 \leq \frac{6-\eta(2-|c|)}{\eta(1+|c|)} \\ \frac{\eta(2-|c|)}{6-\eta(1+|c|)} \leq \theta_j^2 \leq \frac{6-\eta(2-|c|)}{\eta(1+|c|)} \end{cases} \tag{5.71}$$

$$\phi_j^* = 0 \quad otherwise \tag{5.72}$$

where

$$\left.\begin{cases} \theta_j^1 = \frac{\Delta U_{j-\frac{1}{2}}}{\Delta U_{j+\frac{1}{2}}} \\ \theta_j^2 = \frac{\Delta U_{j+\frac{1}{2}}}{\Delta U_{j+\frac{3}{2}}} \end{cases} \quad for \quad c > 0 \right\}$$
$$\left.\begin{cases} \theta_j^1 = \frac{\Delta U_{j+\frac{3}{2}}}{\Delta U_{j+\frac{1}{2}}} \\ \theta_j^2 = \frac{\Delta U_{j+\frac{1}{2}}}{\Delta U_{j-\frac{1}{2}}} \end{cases} \quad for \quad c < 0 \right\} \tag{5.73}$$

Figures 5.20 and 5.21 show comparisons between the exact solution (line) and the numerical results (symbol) obtained by the empirical TVD version of the fourth-order scheme with flux (5.70) after 50 and 1000 time steps respectively. It is instructive to compare these results with those obtained by the rigorous TVD fourth-order schemes of figures 5.16 to 5.17 (obtained with FD4A limiter function) and figures 5.18 to 5.19 (obtained with FD4B limiter function). The TVD condition appears to be more restrictive on the fourth-order scheme than on the third-order scheme. The higher-order method has a wider stencil and thus has the potential for becoming first-order accurate (locally) more often than the lower-order scheme.

The hybrid-limiting approach of equation (5.69) provides a satisfactory way of dealing with high-order schemes. The basic scheme $F_{j+\frac{1}{2}}^{(L)}$ is L-th-order accuracy in smooth parts and has a limiter function which is theoretically sound. The only empirical aspect comes in the choice of ϕ_j^*, but the approach suggested utilises the theory for the L-th-order scheme to detect smooth regions, in which ϕ_j^* is set to unity, giving in this way the H-th-order scheme.

5.8 Summary

Courant-number dependent TVD regions for second-, third- and fourth-order schemes have been theoretically established. Flux limiter functions have been proposed and tested via numerical experiments. For methods of H-th-order accuracy ($H > 4$) a semi-empirical

limiting procedure that appears to work well is proposed. Tests on the case $II = 4$ give very satisfactory results.

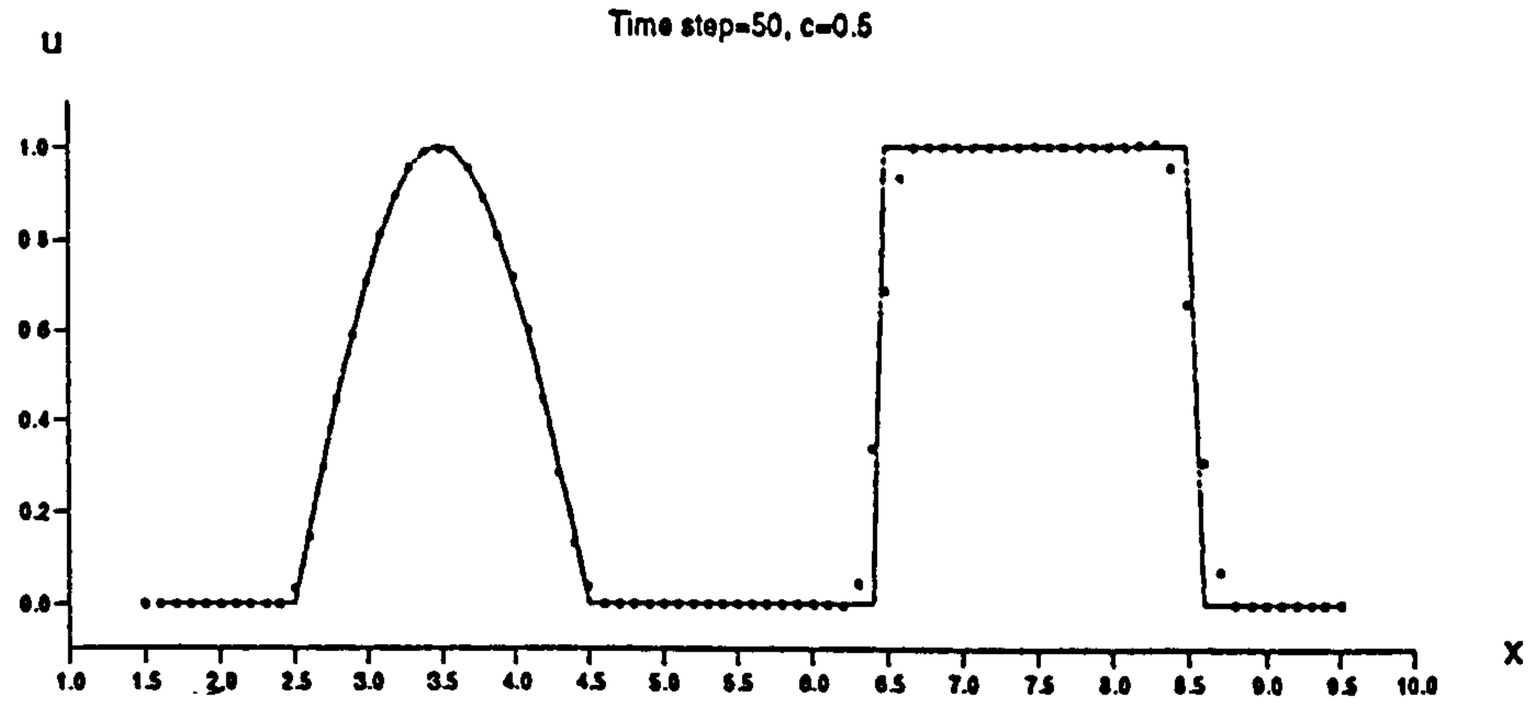

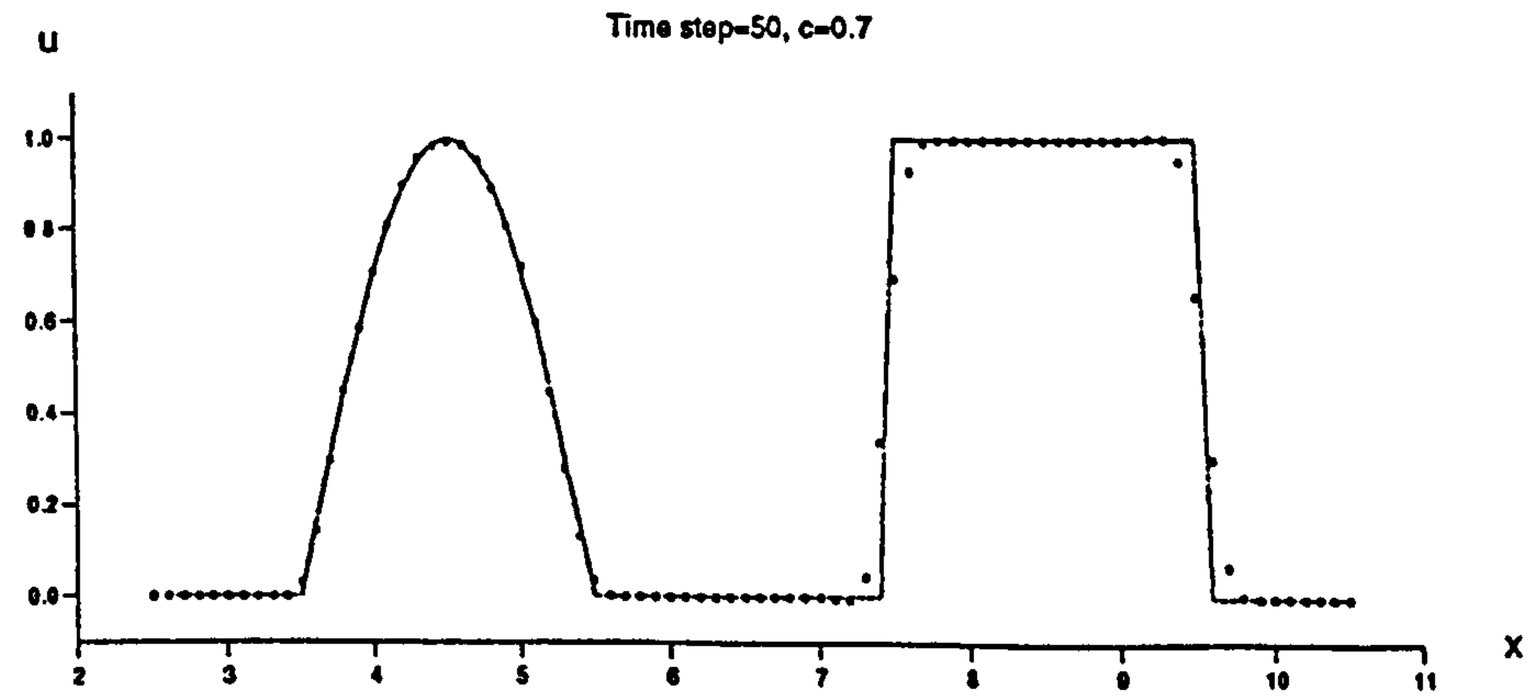

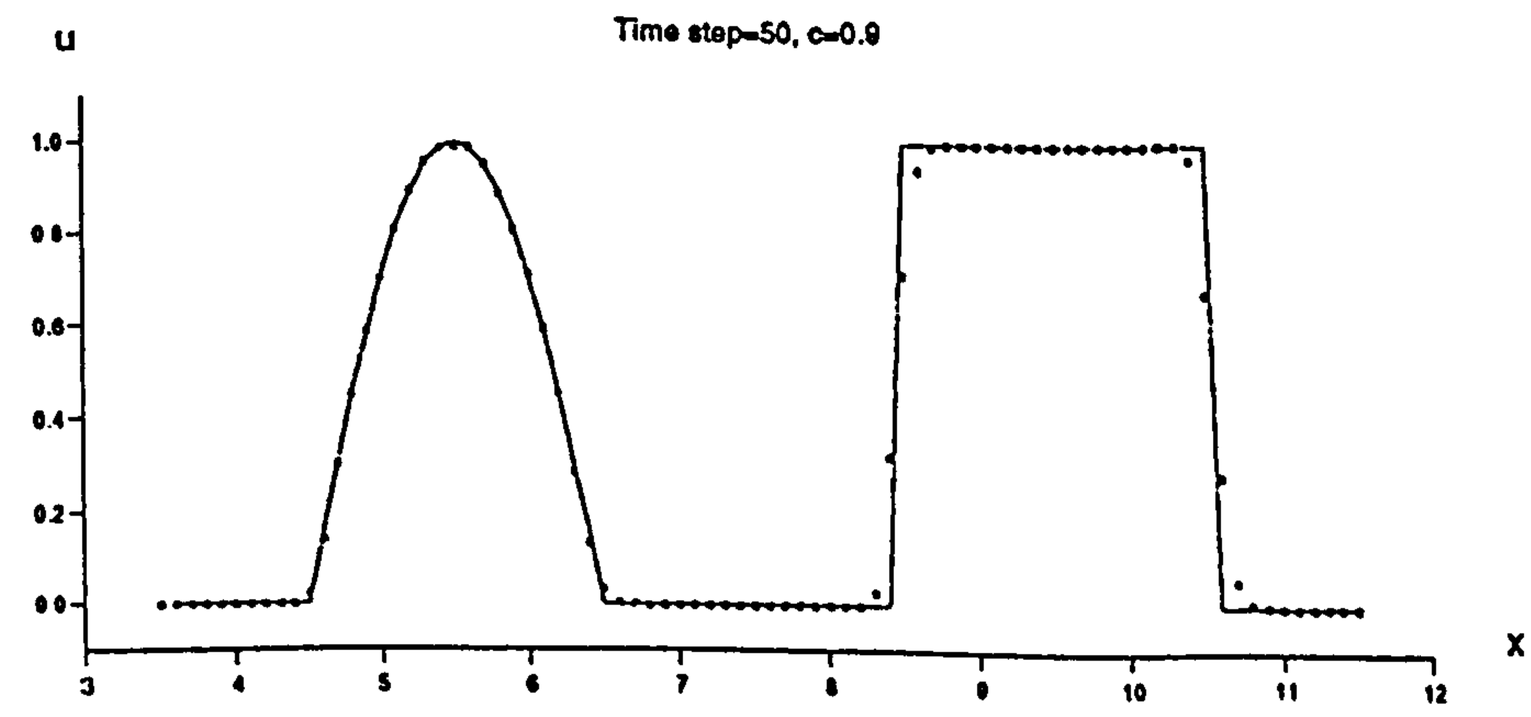

Figure 5.20: Comparison between the Exact Solution (line) and the Numerical Results of the Hybrid Fourth-order Method (symbol) after 50 Time Steps

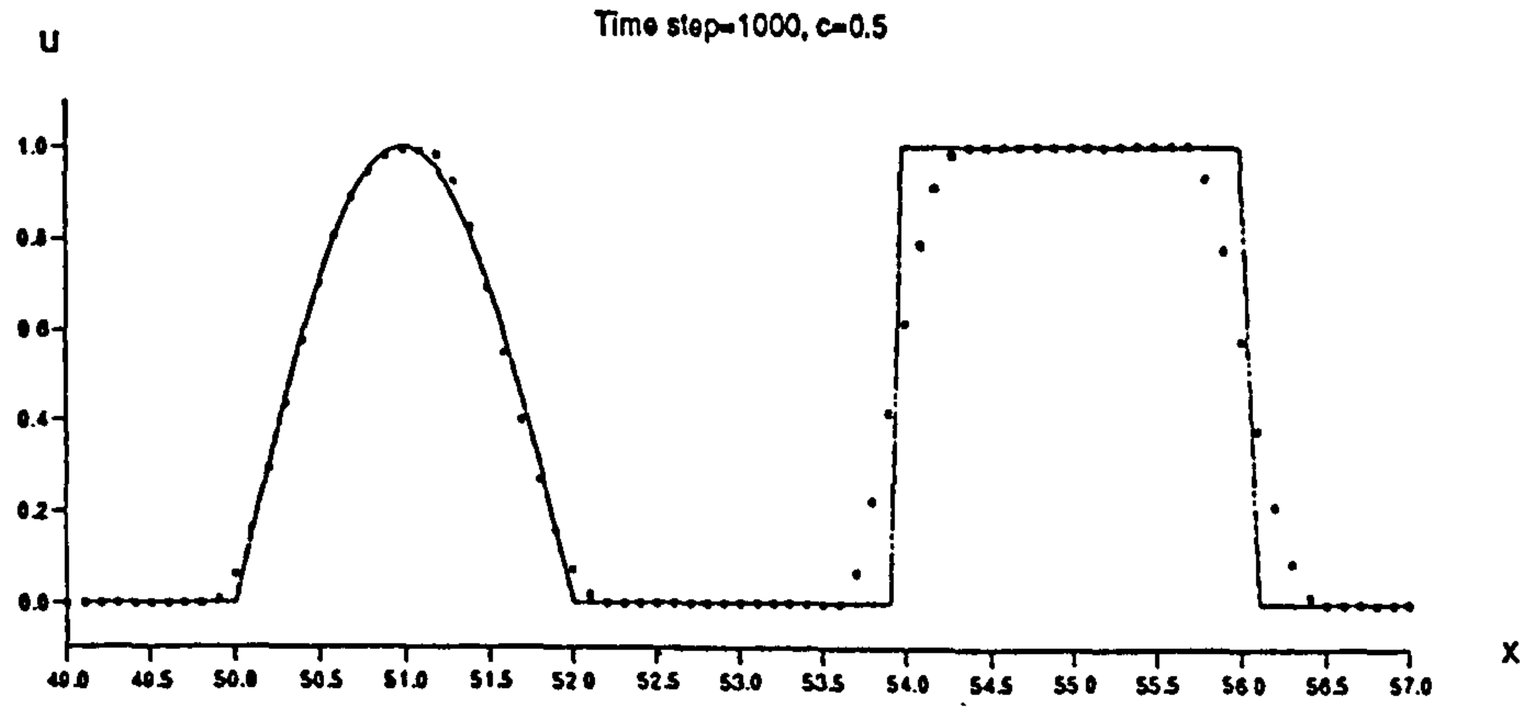

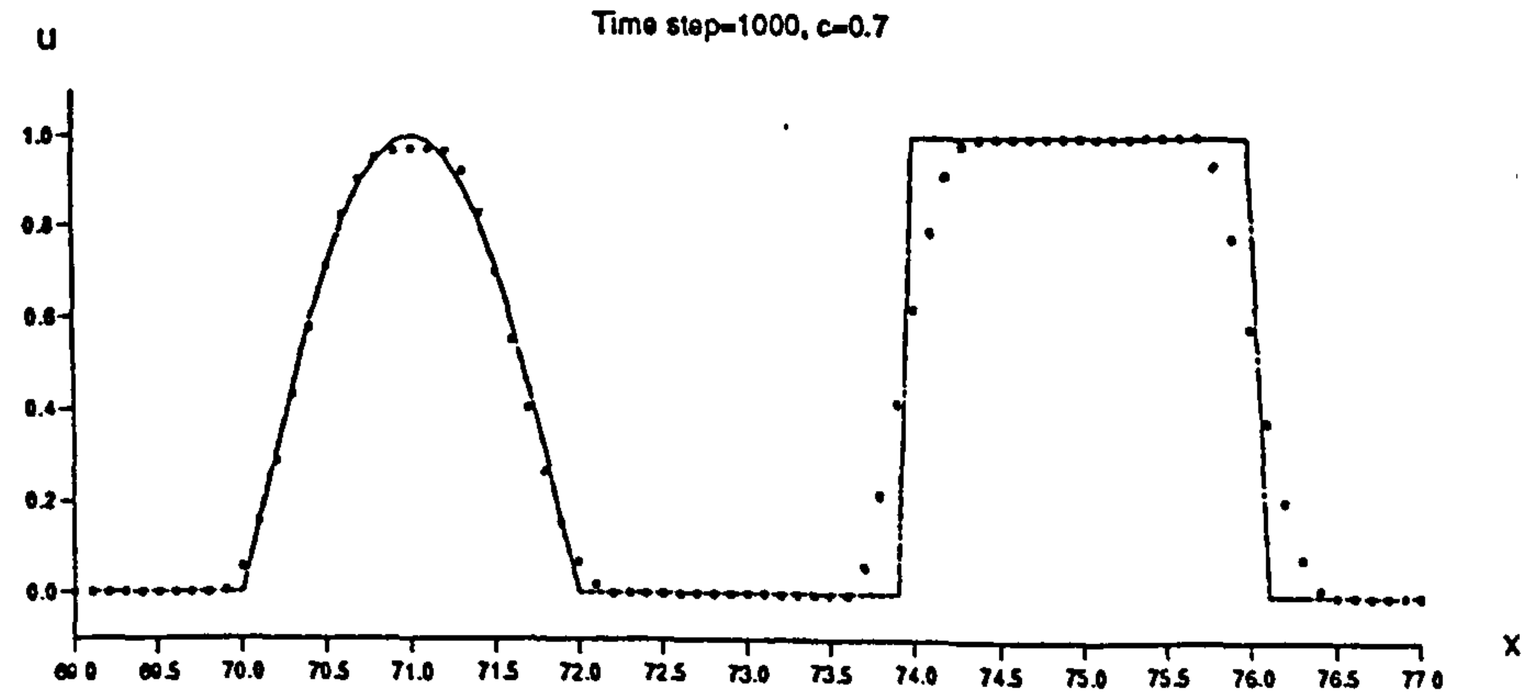

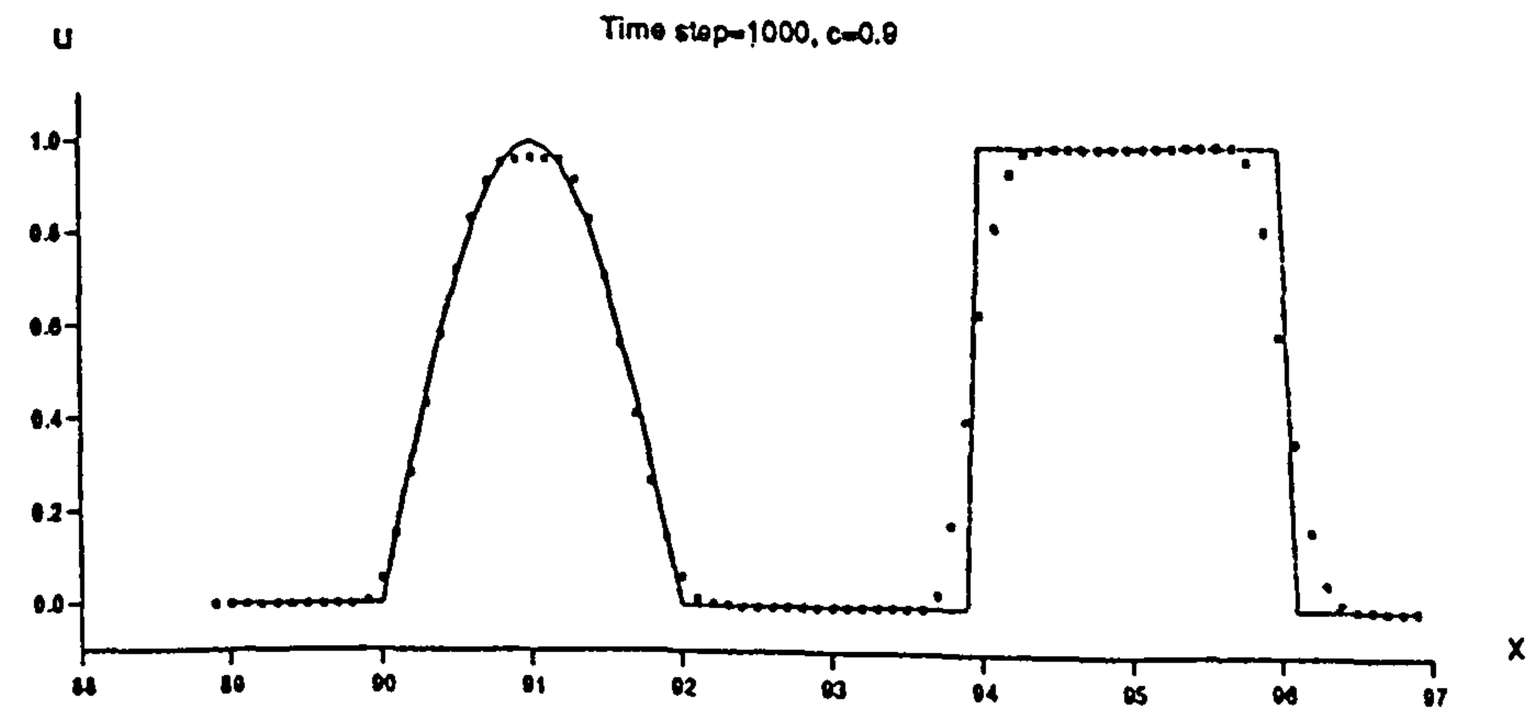

Figure 5.21: Comparison between the Exact Solution (line) and the Numerical Results of the Hybrid Fourth-order Method (symbol) after 1000 Time Steps

Chapter 6

Fully Discrete High Resolution Schemes for Hyperbolic Conservation Laws

6.1 Introductory Remarks

In previous chapters high-order conservative TVD schemes for a linear scalar hyperbolic conservation law are obtained. In this chapter a way to extend the previous work to a general system of conservation laws is discussed.

For constant coefficient linear hyperbolic systems, the extension is straight forward. Recall that the high-order schemes can accommodate arbitrary wave speeds, therefore can automatically deal with linear system of equations with eigenvalues of mixed sign.

For nonlinear hyperbolic systems, however, the matrix of eigenvalues is not constant, which means that the numerical flux can not be defined directly. Hence the approach for linear systems is no longer holds when solving nonlinear systems. Godunov [27] provided a way of dealing with nonlinear systems. Rather than by diagonalizing the Jacobin matrix, Godunov's method employs the solutions of Riemann problems which can be computed exactly and give substantial information about the local characteristic structure. Since Godunov-type methods can be written in conservation form, the Godunov-type methods

are conservative schemes. On the other hand any conservative schemes can be viewed as Godunov-type methods with the interpretation that the Godunov's piecewise constant values at the cell interface $x_{j+1/2}$ are the approximations of the cell averaged values in the conservative schemes. In this sense the high-order conservative schemes developed in previous chapters are Godunov-type high-order schemes, therefore the high-order numerical fluxes could be defined by solving Riemann problems.

In this chapter we first discuss extension of the high-order schemes to linear systems and then extend the discussion to nonlinear system of conservation laws. To illustrate the methodology second-, third- and fourth-order schemes for a system of equations are presented. These schemes are validated by applications to the time-dependent Euler equations in one and two dimensions.

The rest of the chapter is organized as follows: section 2 extends the schemes to linear systems; section 3 discusses nonlinear systems, typically the time dependent Euler equations of Gas Dynamics and present second-, third- and fourth-order solutions to the Euler equations. Sections 4 reports the numerical experiments; section 5 is the summary.

6.2 Linear Hyperbolic Systems

6.2.1 Introduction

Since the solution structure of a linear system can be similiarly extended to that of a nonlinear system, it is worthwile to first study the solution of linear systems although the solution of linear systems can be solved directly.

In this section we extend the scalar schemes (5.46), (5.52) and (5.61) to solve the IVP problem for linear hyperbolic systems with constant coefficients

$$\begin{aligned} U_t + AU_x &= 0 \\ U(x,0) &= U_0(x) \end{aligned} \tag{6.1}$$

where U is a column vector of m conserved variables, and A is an m by m constant matrix.

This is a system of conservation laws with the flux function $F(U) = AU$ which is hyperbolic

if A is diagonalizable with real eigenvalues, i.e. the matrix A can be written as

$$A = R\Lambda R^{-1} \tag{6.2}$$

where Λ= diag $\left(\lambda^{(1)}, \lambda^{(2)}, \ldots, \lambda^{(m)}\right)$ is the diagonal matrix of eigenvalues of A and $R = \left(r^{(1)}, r^{(2)}, \ldots, r^{(m)}\right)$ is the matrix of right eigenvectors of A.

Equation (6.2) means $AR = R\Lambda$, that is

$$Ar^{(p)} = \lambda^{(p)} r^{(p)}, \quad p = 1, 2, \ldots, m \tag{6.3}$$

The natural way to extend the scalar schemes to linear systems is obtained by essentially defining expressions for the flux differences $\Delta F_{j+1/2} = A\Delta U_{j+1/2}$. This can be done by diagonalizing the system, solving local Riemann problems with left and right states U_j^n and U_{j+1}^n, i.e.

$$U(x,0) = \begin{cases} U_j^n & x < 0 \\ U_{j+1}^n & x > 0 \end{cases} \tag{6.4}$$

and letting

$$\alpha_{j+1/2} = R_{j+1/2}^{-1} \Delta U_{j+1/2} \tag{6.5}$$

here $R_{j+1/2}$ is the matrix of right eigenvectors at the interface $j+1/2$, which for the linear constant coefficient case is of course constant; $\alpha_{j+1/2}$ is called the wave strength vector with components $\alpha_{j+1/2}^{(p)}$ $(p = 1, 2, \ldots, m)$ accross the $p-th$ wave traveling at speed $\lambda_{j+1/2}^{(p)}$ in the $(j+1/2)-th$ intercell.

Then we have

$$\Delta U_{j+\frac{1}{2}} = \sum_{p=1}^{m} \alpha_{j+\frac{1}{2}}^{(p)} \; r_{j+\frac{1}{2}}^{(p)} \tag{6.6}$$

Since $F(U) = AU$, this leads to

$$\begin{aligned} \Delta F_{j+\frac{1}{2}} &= A \, \Delta U_{j+\frac{1}{2}} \\ &= \sum_{p=1}^{m} \alpha_{j+\frac{1}{2}}^{(p)} \; A \; r_{j+\frac{1}{2}}^{(p)} \\ &= \sum_{p=1}^{m} \alpha_{j+\frac{1}{2}}^{(p)} \; \lambda_{j+\frac{1}{2}}^{(p)} \; r_{j+\frac{1}{2}}^{(p)} \end{aligned} \tag{6.7}$$

The single jump $\Delta F_{j+1/2} = |a|\Delta U_{j+1/2}$ in the scalar schemes with the appropriate interpretation for $|a|$ is now substituted by a summation of jump (6.7), which gives a natural

extension to linear systems with constant coefficients. For example, considering the scalar first-order upwind scheme, the numerical flux of which can be written as

$$F_{j+\frac{1}{2}} = \frac{1}{2}(F_j + F_{j+1}) - \frac{|a|}{2}\Delta U_{j+\frac{1}{2}} \tag{6.8}$$

By substituting 6.7 in to 6.8 the first-order upwind scheme for linear systems is

$$F_{j+\frac{1}{2}} = \frac{1}{2}(F_j + F_{j+1}) - \frac{1}{2}\sum_{p=1}^{m} |\lambda^{(p)}_{j+\frac{1}{2}}| \;\; \alpha^{(p)}_{j+\frac{1}{2}} \;\; r^{(p)}_{j+\frac{1}{2}} \tag{6.9}$$

Next we discuss the extension of high-order schemes (5.46), (5.52) and (5.61).

6.2.2 Second-order Scheme for Linear Systems

The numerical flux of the second-order scheme for systems is now (refer to equations (5.46), (5.50) and (5.51))

$$\begin{aligned} F_{j+\frac{1}{2}} \;=\; & \frac{1}{2}(F_j + F_{j+1}) - \frac{1}{2}\sum_{p=1}^{m} |\lambda^{(p)}_{j+\frac{1}{2}}| \;\; \alpha^{(p)}_{j+\frac{1}{2}} \;\; r^{(p)}_{j+\frac{1}{2}} \\ & + \frac{1}{2}\sum_{p=1}^{m} \left(1 - |c^{(p)}_{j+\frac{1}{2}}|\right) \; |\lambda^{(p)}_{j+\frac{1}{2}}| \;\; \alpha^{(p)}_{j+\frac{1}{2}} \;\; r^{(p)}_{j+\frac{1}{2}} \;\; \phi^{(p)}_j \end{aligned} \tag{6.10}$$

Here

$$c^{(p)}_{j+1/2} = \frac{\lambda^{(p)}_{j+1/2} \;\; k}{h} \tag{6.11}$$

is the Courant number for the characteristic wave speed $\lambda^{(p)}_{j+1/2}$.

The FD2A limiter function applied to each wave p is now

$$\phi^{(p)}_j = max\left[0, min\left(1, \frac{\theta^{(p)}_j}{\eta^{(p)}_{j+1/2}}\right), min\left(\theta^{(p)}_j, \frac{1}{\eta^{(p)}_{j+1/2}}\right)\right] \tag{6.12}$$

and the FD2B limiter function is

$$\phi^{(p)}_j = max\left[0, min\left(1, \frac{2\theta^{(p)}_j}{\eta^{(p)}_{j+1/2}}\right), min\left(\theta^{(p)}_j, \frac{2}{\eta^{(p)}_{j+1/2}}\right)\right] \tag{6.13}$$

where

$$\theta^{(p)}_j = \frac{\alpha^{(p)}_{j-1/2}}{\alpha^{(p)}_{j+1/2}} \quad if \;\; c^{(p)}_{j+1/2} > 0 \tag{6.14}$$

$$\theta^{(p)}_j = \frac{\alpha^{(p)}_{j+3/2}}{\alpha^{(p)}_{j+1/2}} \quad if \;\; c^{(p)}_{j+1/2} < 0 \tag{6.15}$$

$$\begin{cases} \eta^{(p)}_{j+1/2} = 1 - |c^{(p)}_{j+1/2}| & for \quad 0 \le |c^{(p)}_{j+1/2}| < \frac{1}{2} \\ \eta^{(p)}_{j+1/2} = |c^{(p)}_{j+1/2}| & for \quad \frac{1}{2} \le |c^{(p)}_{j+1/2}| \le 1 \end{cases} \tag{6.16}$$

6.2.3 Third-order Scheme for Linear Systems

The five-point, third-order scheme for linear systems is (refer to equations (5.52) and (5.56))

$$\begin{aligned} F_{j+\frac{1}{2}} &= \frac{1}{2}(F_j + F_{j+1}) - \frac{1}{2}\sum_{p=1}^{m} |\lambda^{(p)}_{j+\frac{1}{2}}| \;\; \alpha^{(p)}_{j+\frac{1}{2}} \;\; r^{(p)}_{j+\frac{1}{2}} \\ &\quad + \sum_{p=1}^{m} \Big[D^{(p)}_{j+\frac{1}{2}} \; |\lambda^{(p)}_{j+\frac{1}{2}}| \;\; \alpha^{(p)}_{j+\frac{1}{2}} \;\; r^{(p)}_{j+\frac{1}{2}} \\ &\quad + D^{(p)}_{j+L+\frac{1}{2}} \; |\lambda^{(p)}_{j+L+\frac{1}{2}}| \;\; \alpha^{(p)}_{j+L+\frac{1}{2}} \;\; r^{(p)}_{j+L+\frac{1}{2}} \Big] \phi^{(p)}_j \end{aligned} \tag{6.17}$$

where

$$D^{(p)}_{j+1/2} = \frac{1}{3} - \frac{1}{2}|c^{(p)}_{j+1/2}| + \frac{1}{6}(c^{(p)}_{j+1/2})^2 \tag{6.18}$$

$$D^{(p)}_{j+L+1/2} = \frac{1}{6}\left(1 - (c^{(p)}_{j+L+1/2})^2\right) \tag{6.19}$$

$$\begin{aligned} \phi^{(p)}_j &= \frac{(1-|c^{(p)}_{j+L+1/2}|)\;\theta^{(p)}_j}{\eta^{(p)}_{j+L+1/2}\;(D^{(p)}_{j+L+1/2}\;\theta^{(p)}_j + D^{(p)}_{j+1/2})} && if \quad 0 \le \theta^{(p)}_j < \theta^L \\ \phi^{(p)}_j &= 1 && if \quad \theta^L \le \theta^{(p)}_j \le \theta^R \\ \phi^{(p)}_j &= \frac{1-|c^{(p)}_{j+L+1/2}|}{\eta^{(p)}_{j+L+1/2}\;(D^{(p)}_{j+L+1/2}\;\theta^{(p)}_j + D^{(p)}_{j+1/2})} && if \quad \theta^{(p)}_j > \theta^R \\ \phi^{(p)}_j &= 0 && if \quad \theta^{(p)}_j \le 0 \end{aligned} \tag{6.20}$$

For the FD3A

$$\theta^L = \frac{\eta^{(p)}_{j+L+1/2}\; D^{(p)}_{j+1/2}}{1 - |c^{(p)}_{j+L+1/2}| - \eta^{(p)}_{j+L+1/2}\; D^{(p)}_{j+L+1/2}} \tag{6.21}$$

$$\theta^R = \frac{1 - |c^{(p)}_{j+L+1/2}| - \eta^{(p)}_{j+L+1/2}\; D^{(p)}_{j+1/2}}{\eta^{(p)}_{j+L+1/2}\; D^{(p)}_{j+L+1/2}} \tag{6.22}$$

and for the FD3B

$$\theta^L = 1.1\;\eta^{(p)}_{j+1/2} - 0.17 \tag{6.23}$$

$$\theta^R = 2.78 - 1.4\eta^{(p)}_{j+1/2} \tag{6.24}$$

with

$$\begin{cases} L = -1 & if \quad c^{(p)}_{j+1/2} > 0 \\ L = 1 & if \quad c^{(p)}_{j+1/2} < 0 \end{cases} \tag{6.25}$$

6.2.4 Fourth-order Scheme for Linear Systems

Following the examples above, the scalar fourth-order scheme (refer to equations (5.61), (5.63) and (5.64)) can be extended to linear hyperbolic systems in the same manner as

$$\begin{aligned} F_{j+\frac{1}{2}} &= \frac{1}{2}(F^n_j + F^n_{j+1}) - \frac{1}{2}\sum_{p=1}^{m} |\lambda^{(p)}_{j+\frac{1}{2}}| \;\; \alpha^{(p)}_{j+\frac{1}{2}} \;\; r^{(p)}_{j+\frac{1}{2}} \\ &\quad + \sum_{p=1}^{m} \left(D^{(p)}_{j+\frac{1}{2}} \;\; |\lambda^{(p)}_{j+\frac{1}{2}}| \;\; \alpha^{(p)}_{j+\frac{1}{2}} \;\; r^{(p)}_{j+\frac{1}{2}} + D^{(p)}_{j+L+\frac{1}{2}} \;\; |\lambda^{(p)}_{j+L+\frac{1}{2}}| \;\; \alpha^{(p)}_{j+L+\frac{1}{2}} \;\; r^{(p)}_{j+L+\frac{1}{2}} \right) \phi^{(p)}_j \\ &\quad + D^{(p)}_{j+M+\frac{1}{2}} \;\; |\lambda^{(p)}_{j+M+\frac{1}{2}}| \;\; \alpha^{(p)}_{j+M+\frac{1}{2}} \;\; r^{(p)}_{j+M+\frac{1}{2}} \;\; \phi^{(p)}_{j+M} \end{aligned} \tag{6.26}$$

where

$$D^{(p)}_{j+L+1/2} = \frac{1}{12} + \frac{1}{24}|c^{(p)}_{j+L+1/2}| - \frac{1}{12}(c^{(p)}_{j+L+1/2})^2 - \frac{1}{24}|(c^{(p)}_{j+L+1/2})^3| \tag{6.27}$$

$$D^{(p)}_{j+1/2} = \frac{1}{2} - \frac{7}{12}|c^{(p)}_{j+1/2}| + \frac{1}{12}|(c^{(p)}_{j+1/2})^3| \tag{6.28}$$

$$D^{(p)}_{j+M+1/2} = \frac{1}{12}(c^{(p)}_{j+M+1/2})^2 + \frac{1}{24}|c^{(p)}_{j+M+1/2}| - \frac{1}{12} - \frac{1}{24}|(c^{(p)}_{j+M+1/2})^3| \tag{6.29}$$

The FD4 limiter functions are now

$$\begin{aligned} \phi^{(p)}_j &= \frac{(1-|c^{(p)}_{j+L+1/2}|)\;\theta^{(p)}_j}{\eta^{(p)}_{j+L+1/2}\;(D^{(p)}_{j+L+1/2}\;\theta^{(p)}_j + D^{(p)}_{j+1/2} - D^{(p)}_{j+M+1/2})} && if \quad 0 \le \theta^{(p)}_j < \theta^L \\ \phi^{(p)}_j &= 1 && if \quad \theta^L \le \theta^{(p)}_j \le \theta^R \\ \phi^{(p)}_j &= \frac{1-|c^{(p)}_{j+L+1/2}| + \eta^{(p)}_{j+L+1/2}\;D^{(p)}_{j+M+1/2}/\;\theta^{*(p)}_j}{\eta^{(p)}_{j+L+1/2}\;(D^{(p)}_{j+L+1/2}\;\theta^{(p)}_j + D^{(p)}_{j+1/2})} && if \quad \theta^{(p)}_j > \theta^R \\ \phi^{(p)}_j &= 0 && if \quad \theta^{(p)}_j \;\; or \;\; \theta^{*(p)}_j \le 0 \end{aligned} \tag{6.30}$$

$$\begin{aligned} \phi^{(p)}_{j+M} &= \eta^{(p)}_{j+M+1/2}\;\theta^{(p)}_{j+M} && for \quad 0 \le \theta^{(p)}_{j+M} < \frac{1}{\eta^{(p)}_{j+M+1/2}} \\ \phi^{(p)}_{j+M} &= 1 && for \quad \theta^{(p)}_{j+M} > \frac{1}{\eta^{(p)}_{j+M+1/2}} \\ \phi^{(p)}_{j+M} &= 0 && for \quad \phi^{(p)}_j = 0 \end{aligned} \tag{6.31}$$

For the FD4A limiter function we have

$$\theta^L = \frac{\eta^{(p)}_{j+L+1/2}\;(D^{(p)}_{j+1/2} - D^{(p)}_{j+M+1/2})}{1 - |c^{(p)}_{j+L+1/2}| - \eta^{(p)}_{j+L+1/2}\;D^{(p)}_{j+L+1/2}} \tag{6.32}$$

$$\theta^R = \frac{1 - |c^{(p)}_{j+L+1/2}| - \eta^{(p)}_{j+L+1/2}\,(D^{(p)}_{j+1/2} - D^{(p)}_{j+M+1/2}/\theta^{*(p)}_j)}{\eta^{(p)}_{j+L+1/2}\, D^{(p)}_{j+L+1/2}} \tag{6.33}$$

and the FD4B limiter function is obtained by setting $\theta^{*(p)}_j = 1$ in equation (6.30) and

$$\theta^L = \eta^{(p)}_{j+1/2} \tag{6.34}$$

$$\theta^R = 3.55 - 1.5\eta^{(p)}_{j+1/2} \tag{6.35}$$

The upwind-downwind flow parameter is now

$$\theta^{*(p)}_j = \frac{\alpha^{(p)}_{j-1/2}}{\alpha^{(p)}_{j+3/2}} \quad if \quad c^{(p)}_{j+1/2} > 0 \tag{6.36}$$

$$\theta^{*(p)}_j = \frac{\alpha^{(p)}_{j+3/2}}{\alpha^{(p)}_{j-1/2}} \quad if \quad c^{(p)}_{j+1/2} < 0 \tag{6.37}$$

with

$$\begin{cases} L = -1, & M = 1 & if & c^{(p)}_{j+1/2} > 0 \\ L = 1, & M = -1 & if & c^{(p)}_{j+1/2} < 0 \end{cases} \tag{6.38}$$

6.3 Nonlinear Hyperbolic Systems

In this section we discuss the extension of the high-order schemes to 2-dimensional non-linear systems of conservation laws, but the same ideals can be applied in 3-dimensions as well.

6.3.1 The Euler Equations

In 2-dimensions a system of conservation laws takes the form

$$U_t + F(U)_x + G(U)_y = 0 \tag{6.39}$$

where, $U(x,t)$ is column vector of m conserved variables; $F(U)$ and $G(U)$ are vector-valued, physical flux function of m components in x and y directions respectively.

The systems of equation (6.39) is assumed to be hyperbolic, that is all eigenvalues $\lambda^{(1)}(U)$, $\lambda^{(2)}(U), \ldots, \lambda^{(m)}(U)$ of any real linear combination of the m by m Jacobian matrix $\alpha A(U) + \beta B(U)$ where

$$A(U) = F'(U), \quad B(U) = G'(U) \tag{6.40}$$

are real for all U and there exists a complete set linearly independent corresponding right eigenvectors.

The Euler equations are taken as a typical nonlinear system of conservation laws to develop the presentation on how to extend our schemes.

The two dimensional Euler equations of Gas Dynamics are

$$U = \begin{pmatrix} \rho \\ \rho u \\ \rho v \\ E \end{pmatrix}, \quad F(U) = \begin{pmatrix} \rho u \\ \rho u^2 + p \\ \rho uv \\ u(E+p) \end{pmatrix}, \quad G(U) = \begin{pmatrix} \rho u \\ \rho uv \\ \rho v^2 + p \\ v(E+p) \end{pmatrix} \tag{6.41}$$

$$p = (\gamma - 1)\left(E - \frac{1}{2}\rho(u^2 + v^2)\right) \tag{6.42}$$

here ρ, u, v, ρu, ρv, p, and E are the density, x and y direction velocities, x and y direction momenta, pressure, and total energy respectively; the γ is the ratio of specific heats.

For the split one dimensional problem the eigenvalues of the Jocabean matrix $F'(U)$ are

$$\lambda^{(1)} = u - a, \quad \lambda^{(2)} = \lambda^{(3)} = u, \quad \lambda^{(4)} = u + a \tag{6.43}$$

The corresponding right eigenvectors are

$$r^{(1)} = \begin{pmatrix} 1 \\ u - a \\ v \\ h - ua \end{pmatrix}, \; r^{(2)} = \begin{pmatrix} 1 \\ u \\ v \\ \frac{1}{2}(u^2 + v^2) \end{pmatrix}, \; r^{(3)} = \begin{pmatrix} 0 \\ 0 \\ 1 \\ v \end{pmatrix}, \; r^{(4)} = \begin{pmatrix} 1 \\ u + a \\ v \\ h + ua \end{pmatrix} \tag{6.44}$$

where h is the specific enthalpy

$$h = \frac{E + p}{\rho} \tag{6.45}$$

The eigenvalues of the Jocabian matrix $G'(U)$ has the same form but the roles of u and v are interchanged.

6.3.2 Operator Splitting Approach

In previous chapters we only considered the one-dimensional problem. However most practical problems are in two or three space dimensions. In this section we discuss a

way in which the one-dimensional methods and theory can be applied to problems in multi-dimensions.

One popular approach to solve multi-dimensional problems is to apply the method of *frectional steps* or *operator splitting* [77]. In this approach the 2-D system (6.39) is split into two augmented one-dimensional systems, then the solution of (6.39) is obtained by solving the two 1-D problems sequencially as follows.

We first solve

$$\begin{aligned} &U_t + F(U)_x = 0 \\ &U(x,y,0) = U_0(x,y) \end{aligned} \tag{6.46}$$

and the solution obtained is $U^*(x,y,t)$, then we solve

$$\begin{aligned} &U_t + G(U)_y = 0 \\ &U(x,y,0) = U^*(x,y,t) \end{aligned} \tag{6.47}$$

and the solution obtained at this stage is the solution of (6.39).

If we denote *pth* order accurate fully discrete 1-D numerical schemes developed in previous chapters as L_k^x and L_k^y over time step k in $x-$ and $y-$directions, respectively, the operator splitting approach gives the following numerical method

$$U^{n+1} = L_k^y L_k^x U^n \tag{6.48}$$

for the 2-D equation (6.39).

However it has been proved that scheme (6.48) has only first-order accuracy in time for the 2-D system (6.39), although L_k^x and L_k^y are *pth* order schemes in the original place. In [77] Strang introduced a new method called *Strang splitting* which increases the temporal accuracy to second-order and has the form

$$U^{n+1} = L_{k/2}^x L_k^y L_{k/2}^x U^n \tag{6.49}$$

In the following chapters the Strang splitting method will be used to deal with 2-D problems. Therefore from now on we turn our attention to study one-dimensional nonlinear systems.

6.3.3 Godunov's Method

From the nature of nonlinear systems the eigenvalues are functions of the unknowns, which means that we can not explicitly define the intercell flux $F_{j+1/2}$ as in the case of linear systems. To deal with the problem Godunov provided a way of utilising the solution of the Riemann problem.

In Godunov's method U_j^n is used to denote a piecewise constant function $\bar{u}(x, t_n)$ at time t_n on the grid cell $x_{j-1/2} < x < x_{j+1/2}$. If we consider that Godunov's piecewise constant function $\bar{u}(x, t_n)$ is an approximation to the cell average as defined in the conservative method (see equation 4.2), then there is no doubt that Godunov's method can be written in conservation form. Therefore the Godunov's numerical flux function is given by

$$F_{j+\frac{1}{2}} = \frac{1}{k}\int_{t_n}^{t_{n+1}} F\left(\bar{u}(x_{j+1/2}, t)\right)\, dt \tag{6.50}$$

Since $\bar{u}$ is constant along the line $x = x_{j+1/2}$ over the time interval (t_n, t_{n+1}), the integral at the right hand side of equation (6.50) can be easily defined.

Godunov used the solution of the local Riemann problem with left and right states U_j^n and U_{j+1}^n to calculate the values of $\bar{u}$. Therefore the constant values depends only on the data U_j^n and U_{j+1}^n. Thus the Godunov's flux (6.50) can be written as

$$F^G_{j+\frac{1}{2}} = F\left(u^*_{j+\frac{1}{2}}(U_j^n, U_{j+1}^n)\right) \tag{6.51}$$

Here $u^*_{j+\frac{1}{2}}(U_j^n, U_{j+1}^n)$ are the cell interface values at $x_{j+1/2}$. However Godunov's method is only first-order accurate. To obtain higher-order accuracy, more grid points are needed, which results in more interface valves $u^*_{j+m+\frac{1}{2}}$ involving in the high-order numerical fluxes

$$F^H_{j+\frac{1}{2}} = F\left(u^*_{j+m+\frac{1}{2}}(U_{j+m}^n, U_{j+m+1}^n)\right) \tag{6.52}$$

where $m = 0, \pm 1, \pm 2, \ldots$ are integers according to a specific scheme.

For example the 4th-order scheme (6.26) has flux

$$F^4_{j+\frac{1}{2}} = F\left(u^*_{j-\frac{1}{2}}(U_{j-1}^n, U_j^n), u^*_{j+\frac{1}{2}}(U_j^n, U_{j+1}^n), u^*_{j+\frac{3}{2}}(U_{j+1}^n, U_{j+2}^n)\right) \tag{6.53}$$

There are essentially two ways of obtaining the values of u^*, therefore, the intercell flux $F_{j+1/2}$ utilising a Riemann problem solution. One way is to obtain the flux function

directly. For nonlinear systems this is always an approximate procedure. We called this the *flux Riemann problem approach* (Flux Riemann Solver). Another way is to find the solution of the Riemann problem for the state variables u^* and then the intercell flux can be obtained by evaluating the physical flux function, i.e. $F_{j+1/2} = F(u^*)$. The solution u^* can be approximate or exact. We call this the *state Riemann problem approach* (State Riemann Solver).

6.3.4 Flux Riemann Solvers

A possible strategy for solving systems of nonlinear conservation laws is to linearize the nonlinear system of equations (6.39) locally at each cell interface by defining an approximate solution to the cell average $\bar{u}$ and then implement the methods of section 6.2 using the linearized systems

$$U_t + \bar{A}\, U_x \;=\; 0 \tag{6.54}$$

Here $\bar{A}$ is a linearized constant matrix depending only on the local data U_j^n and U_{j+1}^n, that is $\bar{A} = \bar{A}(U_j^n, U_{j+1}^n)$.

Popular examples of this approach are Roe's Riemann solver [31] and Osher's Riemann solver [34]. Roe's matrix $\bar{A}(U_j^n, U_{j+1}^n)$ is assumed to satisfy the following properties: (i) $\bar{A}\ \Delta U_{j+1/2} = \Delta F_{j+1/2}$; (ii) $\bar{A}$ is diagonalizable with real eigenvalues; (iii) $\bar{A} \to f'(\bar{U})$ smoothly as $U_j^n,\ U_{j+1}^n \to \bar{U}$. Denoting the Roe eigenvalues, eigenvectors and wave strength as $\bar{\lambda}_{j+1/2}^{(p)}$, $\bar{r}_{j+1/2}^{(p)}$ and $\bar{\alpha}_{j+1/2}^{(p)}$ $(p = 1, 2, \ldots, m)$ then applying the high-order schemes of section 6.2 we solve the original nonlinear systems in a straight-forward manner.

The Roe eigenvalues and eigenvectors are evaluated at the average state $\bar{U}$ which for the one-dimensional case takes the following form

$$\begin{cases} \bar{u} = (\rho_j^{1/2} u_j + \rho_{j+1}^{1/2} u_{j+1})/(\rho_j^{1/2} + \rho_{j+1}^{1/2}), & \bar{\rho} = (\rho_j \rho_{j+1})^{1/2} \\ \bar{h} = (\rho_j^{1/2} h_j + \rho_{j+1}^{1/2} h_{j+1})/(\rho_j^{1/2} + \rho_{j+1}^{1/2}), & \bar{a} = ((\gamma - 1)(\bar{h} - \tfrac{1}{2}\bar{u}^2))^{1/2} \end{cases} \tag{6.55}$$

The average wave strengths $\bar{\alpha}^{(p)}$ are determined by

$$\begin{cases} \bar{\alpha}^{(1)} = \frac{1}{2\bar{a}^2}(\Delta p - \bar{\rho}\bar{a}\Delta u) \\ \bar{\alpha}^{(2)} = \Delta\rho - \frac{\Delta p}{\bar{a}^2} \\ \bar{\alpha}^{(3)} = \frac{1}{2\bar{a}^2}(\Delta p + \bar{\rho}\bar{a}\Delta u) \end{cases} \tag{6.56}$$

here

$$\Delta\rho = \rho_{j+1} - \rho_j, \quad \Delta u = u_{j+1} - u_j, \quad \Delta p = p_{j+1} - p_j \tag{6.57}$$

However it is well known that Roe's Riemann solver under some circumstances can admite non-physical solutions, such as expansion shocks and negative densities. The cure for the first failure will be discussed in section 6.3.6. The second failure afflicts all linearized Riemann solvers. Possible cures to this difficulty were studied by Einfeldt et al. in [61]. A different approach to avoid compromising accuracy and robustness when using approximate Riemann solvers was proposed by Toro [32]. He proposed a hybrid approach in which a very simple linearised solver and an exact Riemann solver are used adaptively.

6.3.5 State Riemann Solvers

These solvers include exact solvers and hybrid solvers which solve the Riemann problem for the state variables. Taking Toro's hybrid solver [32] for example. The hybrid solver includes a linearized solver and an exact solver which are used adaptively. The switch between the two solvers is governed by a simple mechanism. Applications of the solver shows that about 98 percent of all Riemann problems are solved by the fast linearized solver and in the rest of cases the exact solver takes over. The structure of the solution of the Riemann problem contains two intermediate regions between the two nonlinear waves. They are separated by the contact wave and the notation q_L^* and q_R^* is used for quantities to the left and right of the contact respectively.

The *star values* obtained locally by the linearized solver in one dimension has the following form

$$\begin{cases} u^* = \frac{1}{2}(u_j + u_{j+1}) - (p_{j+1} - p_j)/2\bar{\rho}\bar{a} \\ p^* = \frac{1}{2}(p_j + p_{j+1}) - \frac{1}{2}\bar{\rho}\bar{a}(u_{j+1} - u_j) \\ \rho_L^* = \rho_j + (u_j - u^*)\bar{\rho}/\bar{a} \\ \rho_R^* = \rho_{j+1} + (u^* - u_{j+1})\bar{\rho}/\bar{a} \end{cases} \tag{6.58}$$

where

$$\bar{\rho} = \frac{1}{2}(\rho_j + \rho_{j+1}), \quad \bar{a} = \frac{1}{2}(a_j + a_{j+1}) \tag{6.59}$$

are the average values of the desity and sound speed.

Once the star values at each cell interface are calculated the flux jump $\Delta F_{j+1/2}^{(p)}$ for each wave can be easily defined. Then applying the high-order schemes of section 6.2 we can

solve the nonlinear systems to high-order of accuracy. Note that in this approach the flux jump $\Delta F^{(p)}_{j+1/2}$ in the high order schemes is constructed directly.

6.3.6 The Entropy Condition

So far we have not said anything about the entropy condition of the high-order solutions. As discussed in section 4.4, to obtain a physically acceptable right weak solution the high-order conservative schemes for systems must be consistent with the entropy inequality (4.43). It has been proved that the Godunov's method satisfies the entropy function as long as the Riemann solution used is entropy-satisfying [62]. The proof also can be found in [18]. Because the high-order conservative schemes developed in section 6.2 are Godunov-type high-order schemes, which means that provided we apply a entropy-satisfying Riemann solver, then the weak solutions obtained by the high-order schemes will satisfy the entropy condition.

It is well known that under some circumstances Roe's Riemann solver can admite non-physical solutions, i.e. expansion shocks. The failure is due to the fact that Roe's Riemann solver does not satisfy an entropy condition [56]. To remedy this a sonic fix is required. There are several entropy fixes for the Flux Riemann Solvers in the literature. In this chapter the one introduced by Harten and Hyman [60] is applied.

6.4 Numerical Experiments

In this section numerical experiments with fully discrete second-order scheme (6.10), third-order scheme (6.17) and fourth-order scheme (6.26) are reported. The test problems are considered here as the follows:

6.4.1 Sonic Test Problem

Here a sonic test problem with initial data

$$\begin{cases} (\rho,\ u,\ p) = (1,\ 0.75,\ 1) & 0 \le x \le 0.5 \\ (\rho,\ u,\ p) = (0.125,\ 0,\ 0.1) & 0.5 < x \le 1.0 \end{cases} \tag{6.60}$$

is chosen. This problem is a modification of Sod's problem and designed to produce a left sonic rarefaction about $x = 0.5$. Therefore it is a good problem to test the entropy-satifying property of a numerical scheme. Figure 1 and 2 show the performance of these schemes. The computational domain is devided by 100 computational cells. The Courant number used is 0.8. The solid line is the exact solution and the symbol is the numerical result. Figures 6.1 (a) (b) and (c) show the results obtained by the second-, third- and fourth-order schemes respectively with Roe's solver without entropy fix. As clearly shown the second-order scheme (a) automatically satisfies the entropy condition, whereas the solutions of the third- and fourth-order schemes (b) and (c) contain a rarefaction shock which is unphysical. Figure 6.2 shows the corresponding results obtained with Harten and Hyman's entropy fix [60]. The entropy-satisfying condition of the third- and fourth-order schemes is obviously improved.

6.4.2 Sod's Problem

The Sod's problem [63] is one of the most popular test problems for numerical schemes. Therefore this problem is chosen to test all of our limiters presented in the previous sections. Sod's problem consists of initial data:

$$\begin{cases} (\rho,\ u,\ p) = (1,\ 0,\ 1) & 0 \le x \le 0.5 \\ (\rho,\ u,\ p) = (0.125,\ 0,\ 0.1) & 0.5 < x \le 1.0 \end{cases} \tag{6.61}$$

Figures 6.3 to 6.8 show the comparison between the computed results (symbol) and the exact solution (line) with Roe's Riemann solver at time 0.2 units. Again 100 cells and 0.8 for the Courant number were used. Figure 6.3 shows the performance of the second-order scheme with the FD2A limiter. As seen in the figure the numerical results look satisfactory in the smooth parts. The shocks are captured with 2-3 interior points but the contact discontinuities are smeared with 4-5 points. There are no overshoots or undershoots.

Figure 6.4 shows the results of the second-order scheme with the FD2B limiter. Comparing with the results obtained by the FD2A (see Fig. 6.3) the FD2B has an obvious improvement of capturing the contact with 2-3 points, however there are overshoots and undershoots especially in the specific internal energy plot (d).

Figure 6.5 shows the results obtained by the third-order scheme with the FD3A limiter. The results look satisfactory for both smooth parts and shocks. But the contact has 4-5 points and there is a very little overshoot in the internal energy (d).

Figure 6.6 shows the performance of the third-order scheme with the FD3B limiter. Except for a little overshoot and undershoot the results of the limiter are satisfactory. Both shocks and contacts are captured with only 2 points. The overall performance of the third-order scheme is superior to that of the second-order scheme (compare Fig. 6.5 and 6.6 with Fig. 6.3 and 6.4).

Figure 6.7 shows the numerical results of the fourth-order scheme with the FD4A limiter. The smooth part of the solution is satisfactory; shocks are captured with 3 points and the contacts with 5 points. Very small oscillations can be seen. However, it is generally accepted that designing proper dissipation procedure for high-order methods is a very difficulty tasks. I am satisfied with the performance observed.

Figure 6.8 shows the solution of the fourth-order scheme with the FD4B limiter. The results are superior to that obtained by the FD4A limiter (see Fig. 6.7). Both shocks and contacts are presented with 3-5 points. Also the FD4B limiter is simpler than the FD4A. The overall performance of the fourth-order scheme is better than that of the third-order scheme (compare Fig. 6.7 and 6.8 with Fig. 6.5 and 6.6).

6.4.3 Blast-wave Problem

The one-dimensional blast-wave problem introduced by Woodward and Collela [64] involves multiple interactions of strong shocks and rarefactions with each other and with contact discontinuities. This problem is extremely difficult to solve on a uniform Eulerian grid, therefore a good problem to test the robustness of numerical schemes. This problem has initial data:

$$\begin{cases} (\rho,\ u,\ p) = (1,\ 0,\ 1000) & 0 \leq x < 0.1 \\ (\rho,\ u,\ p) = (1,\ 0,\ 0.1) & 0.1 \leq x < 0.9 \\ (\rho,\ u,\ p) = (1,\ 0,\ 100) & 0.9 \leq x \leq 1.0 \end{cases} \tag{6.62}$$

The initial condition consists of three constant stats of a gamma-law gas, with $\gamma = 1.4$, which is at rest between reflecting walls separated by a distance of unity. The density is everywhere unity, while in the far left tenth volume the pressure is 1000, in the far right tenth it is 100, and in between it is 0.1. Two strong blast waves develop and collide, producing a new contect discontinuity. Although there is no exact solution for this test problem there are several good numerical results available.

The computational domain is discretized with 3000 cells. The Courant number used is 0.8.

A hybrid scheme involving Roe's solver and an exact solver used adaptively is applied. The second-order scheme with the FD2B, third-order with the FD3B and fourth-order with the FD4B are chosen to test the robustness of the high-order schemes. Figure 6.9 to 6.11 show the numerical results at time 0.028. The results show that schemes reproduce accurately the known features of the solution.

6.4.4 Shock Reflection Problem

To illustrate the capability of the schemes to solve multi-dimensional problems, solutions to the time dependent, two-dimensional, Euler equations that simulate the flow that results from the reflection of shock wave. The behaviour of shock wave reflection has studied by researchers for many years [64] [65] [66]. Four types of reflection are identified: regular reflection (r.r); single Mach reflection (s.M.r); complex Mach reflection (c.M.r) and double Mach reflection (d.M.r) (see figure 6.12). The type of reflection depends on 1. the Mach number of the incident shock; 2. the angle of the wedge and 3. the ratio of the specific heats for the fluid.

The first reflection problem is to capture a single Mach reflection of plane shock at Mach number 1.7 from a wedge at an angle of 25 degree to the incident flow. The solution to the problem is well studied experimentally in the Shock Wave Research Center, Tohoku University, Japan. Therefore the numerical solutions to the problem have a sound basis to compare with. Figure 6.13 shows a comparison between the numerical solutions of the problem obtained by second-order with the FD2A limiter function (a), third-order with the FD3A limiter function (b), fourth-order with the FD4A limiter function (c) and the experimental result (d) (Courtesy of Professor K. Takayama, Shock Wave Research Center, Tohoku University, Sendai, Japan). These results show a good agreement between the numerical and the experimental results.

The second reflection problem is the present benchmark test problem initiated by the Institute of Fluid Science, Tohoku University, Japan. The benchmark problem is to simulate the process of reflection of a planar shock wave propagating in air from two wedges. The Mach number of the incident shock is 2.0, and the wedge angle is 46 degree in one case and 49 degree in the other. These combinations of incident Mach number and wedge angles result in reflections which are near transition from complex Mach reflection to double Mach reflection. Since accurately defining the starting transition point between reflections has a important interesting in practice, the benchmark problem is designed to compare

results provided by different numerical schemes with experimentally obtained isopycnics. The benchmark problem requires 1. the computational domain is 1 x 1 square; 2. the wedge corner is located at 0.25, and the simulation continued until the position of the incident shock is approximately 0.1 from the boundary towards which it is moving; 3. an Eulerian scheme is used on a 256 x 256 non-adaptive grid; 4. the initial condition is that the undisturbed air is at approximately 30 KPa and 300 K.

Figures 6.14 and 6.15 show the computed results of the benchmark problem using the same numerical schemes as the first problem. Refering to (c) and (d) in figure 6.12 the computed results in figures 6.14 and 6.15 indicate that the transition is just started between c.M.r and d.M.r. As one can see that the top few lines in the figures actually represents the very begining of the double Mach reflection. The results in figure 6.15 is more evident than that in figure 6.14. For example in figure 6.15 the second-order scheme only presents one line d.M.r at the stage (see (a) in the figure), the third-order scheme, however, gives two lines d.M.r (see (b) in the figure), while the fourth-order scheme obtains three lines d.M.r (see (c) in the figure). This clearly shows that the evidence of the transition is most noticeable computed by the fourth-order scheme (c). It also indicates that the third-order scheme (b) has better results than the second-order scheme (a).

6.5 Summary

In this chapter the way to extend scalar fully discrete high-order schemes to systems of conservation laws is discussed. Second-, third-, and fourth-order TVD schemes for nonlinear systems are presented. These schemes are tested and validated by solving the one and two dimensional Euler equations of Gas Dynamics for some well known test problems and a benchmark test problem. The computation was carried out using two different kinds of approximate Riemann solvers which satisfy the entropy condition. The numerical solutions show that these high resolution schemes can give very satisfactory performance.

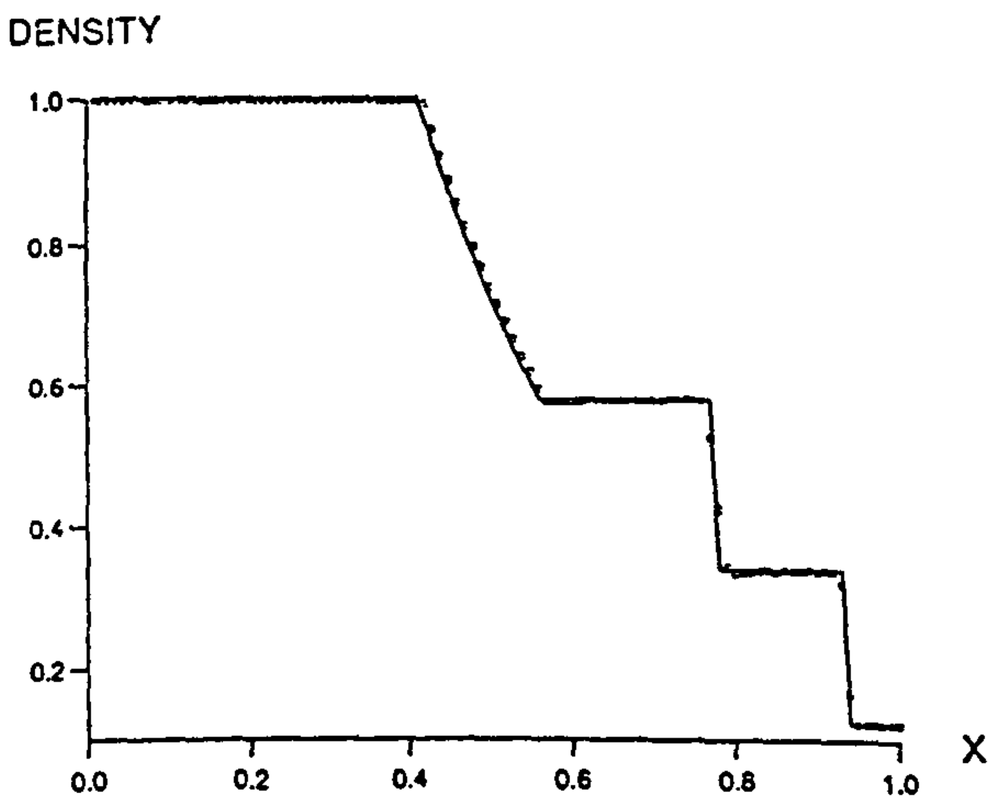

(a) Second-order Scheme with FD2B Limiter

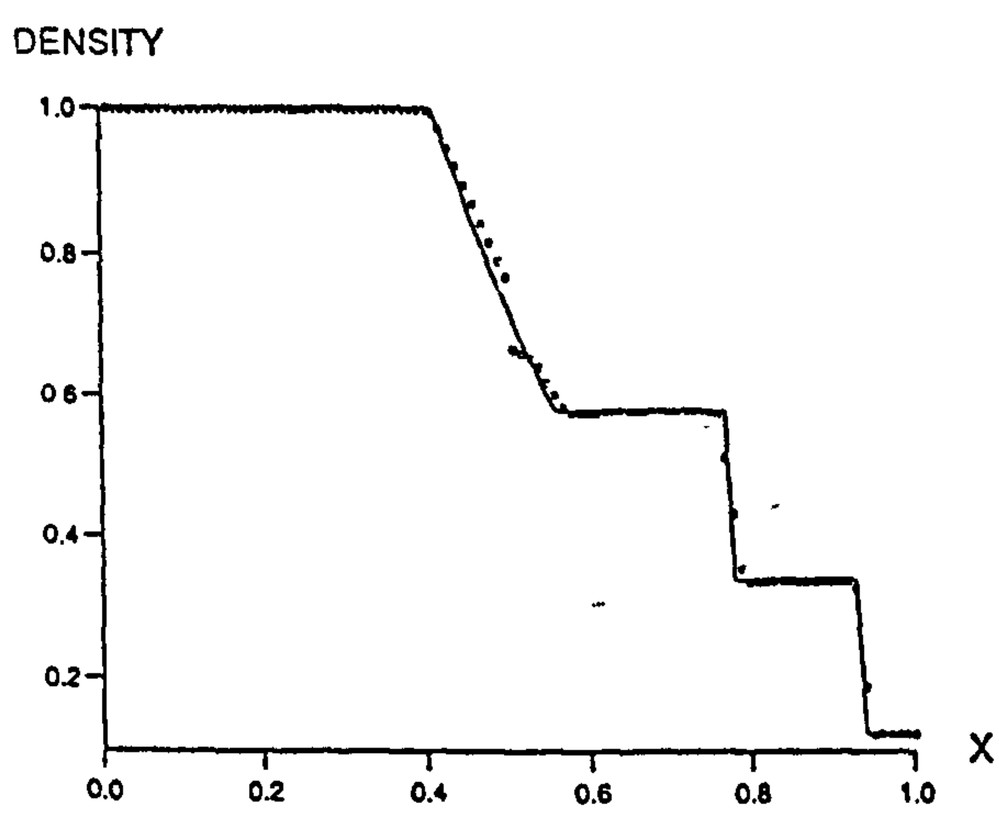

(b) Third-order Scheme with FD3B Limiter

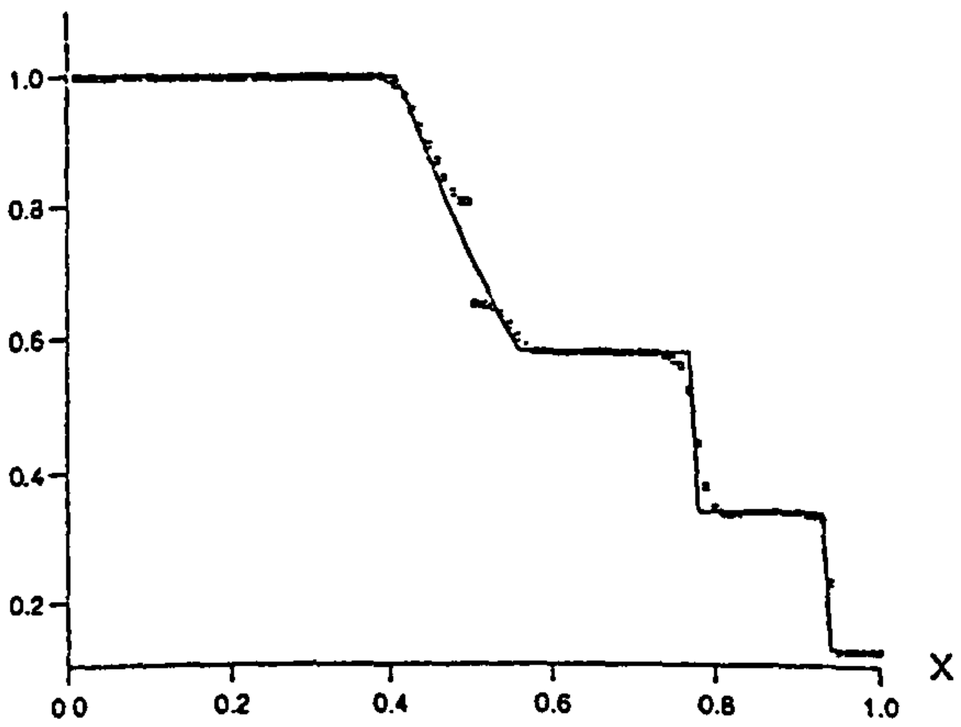

(c) Fourth-order Scheme with FD4B Limiter

Figure 6.1: Sonic Test Problem without Entropy-fixing by the Second-, Third- and Fourth-order Schemes

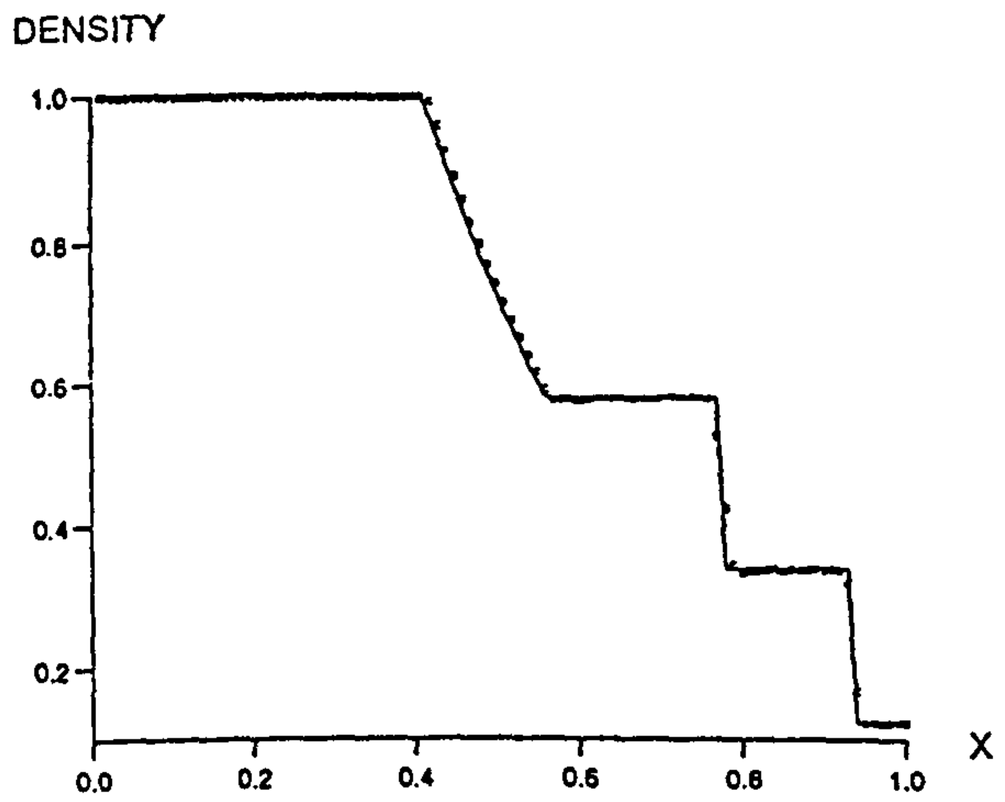

(a) Second-order Scheme with FD2B Limiter

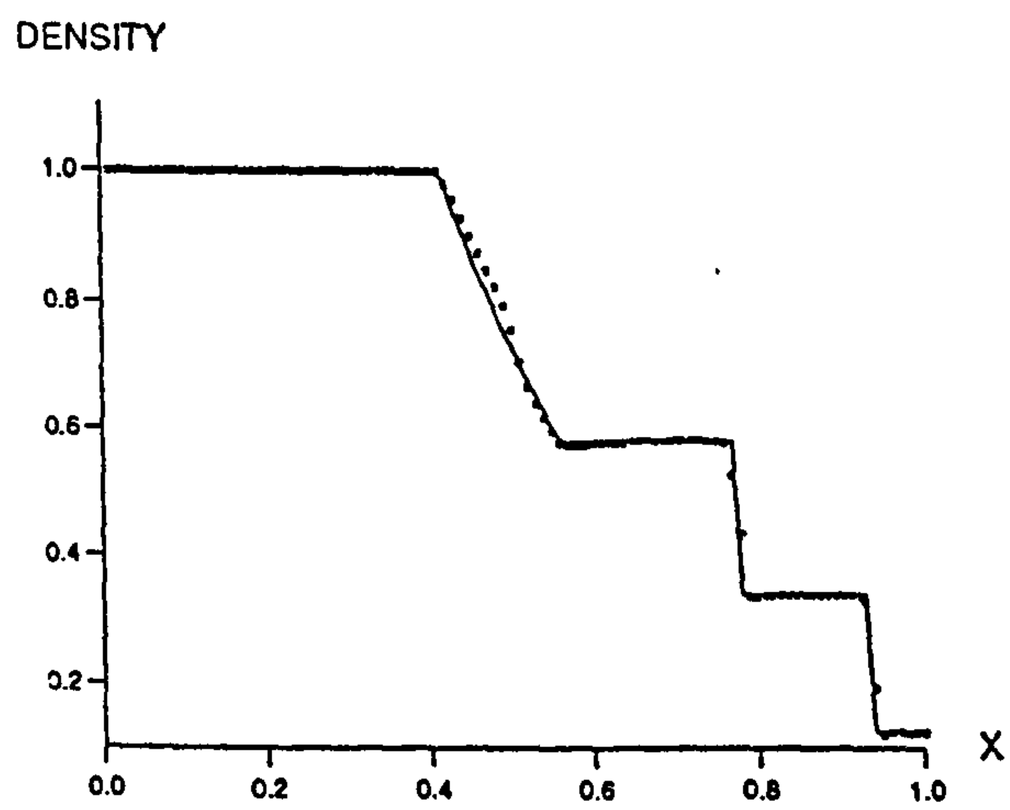

(b) Third-order Scheme with FD3B Limiter

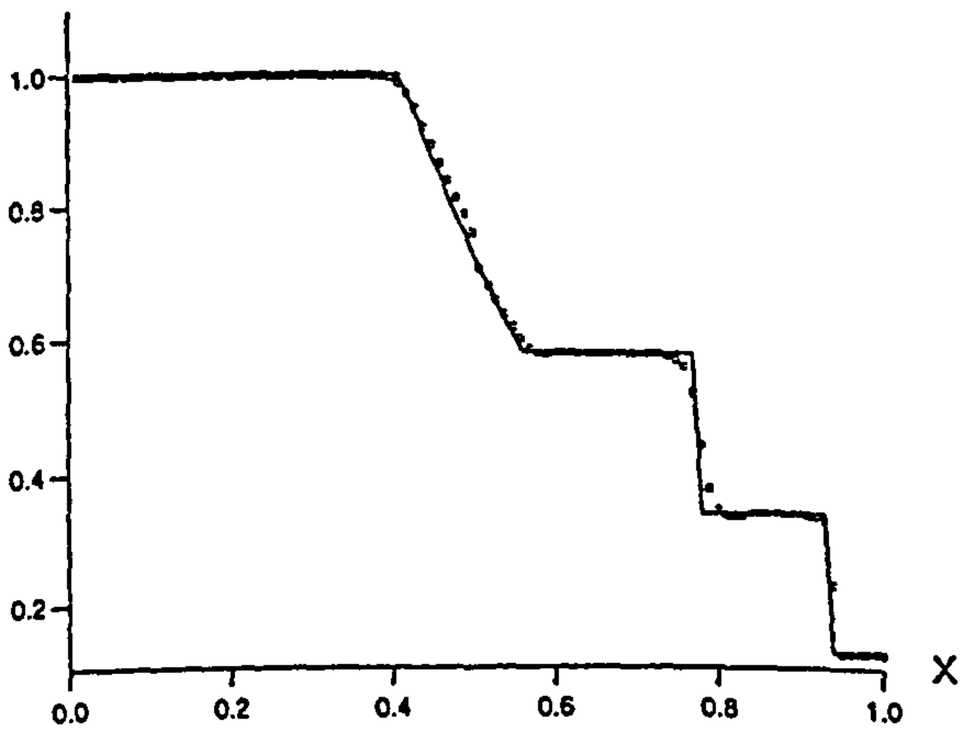

(c) Fourth-order Scheme with FD4B Limiter

Figure 6.2: Sonic Test Problem with Entropy-fixing by the Second-, Third- and Fourth-order Schemes

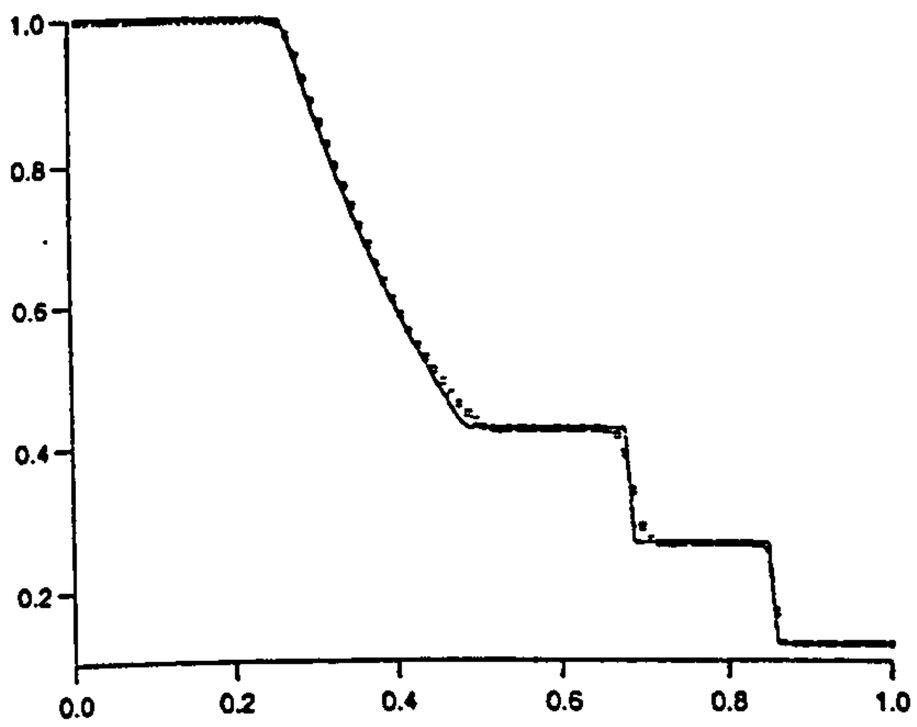

(a)

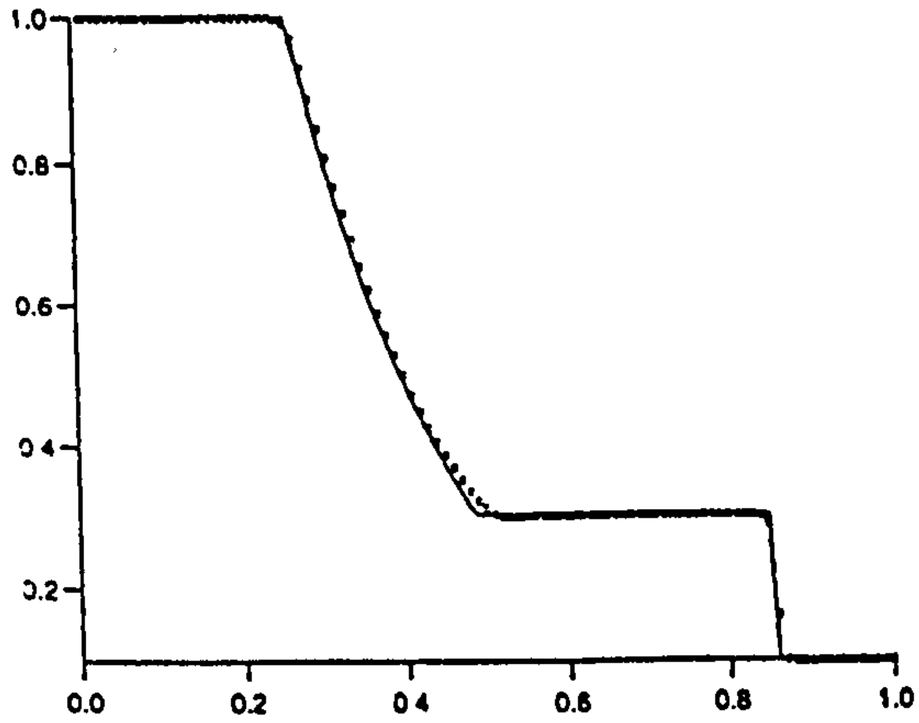

(b)

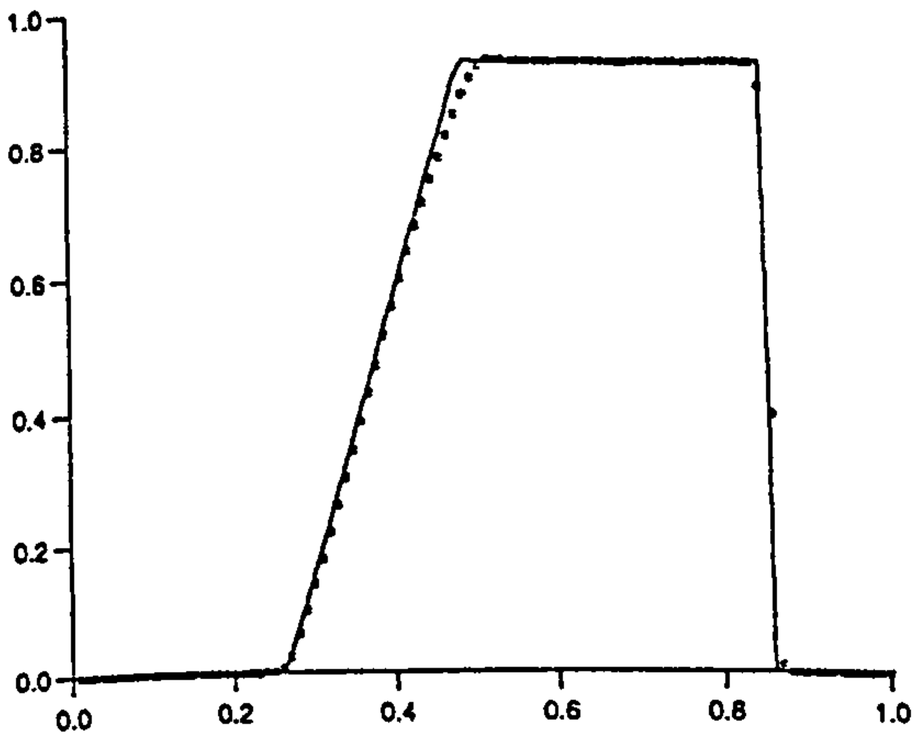

(c)

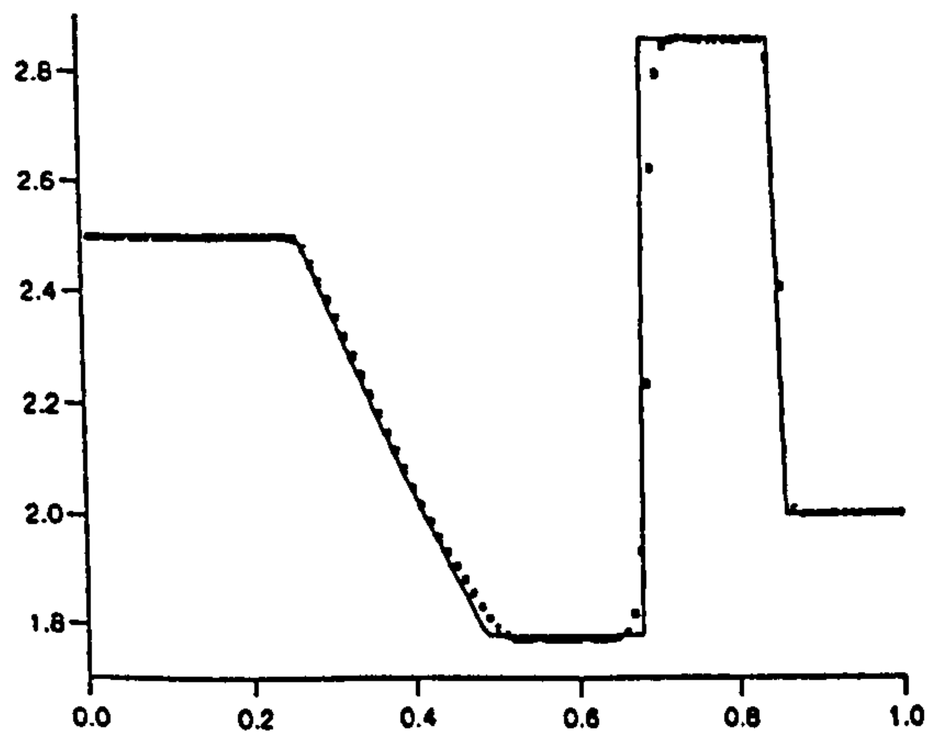

(d)

Figure 6.3: Sod's Problem by the Second-order Scheme with the FD2A Limiter Function: (a) Density, (b) Pressure, (c) Velocity, (d) Specific Internal Energy

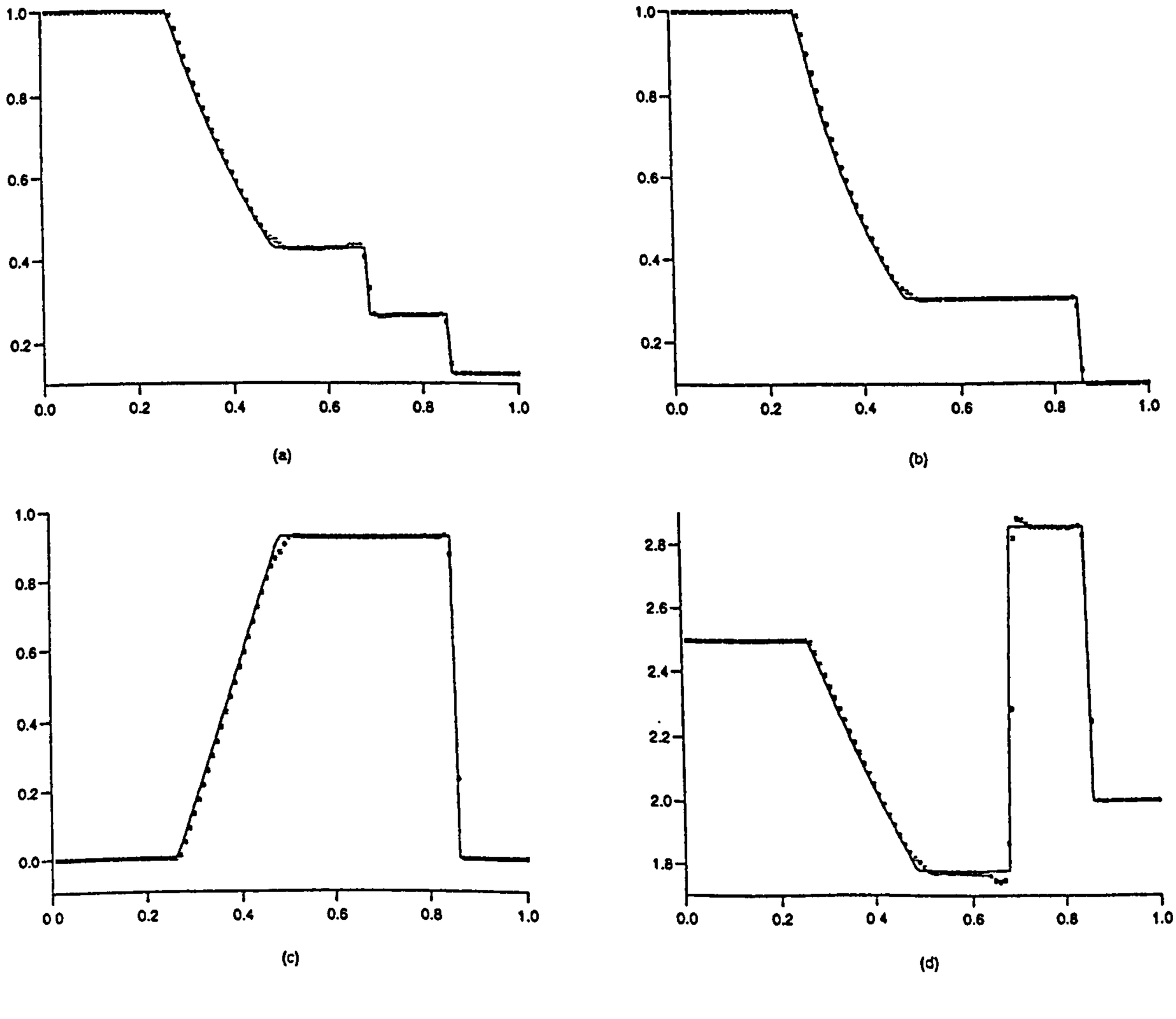

Figure 6.4: Sod's Problem by the Second-order Scheme with the FD2B Limiter Function: (a) Density, (b) Pressure, (c) Velocity, (d) Specific Internal Energy

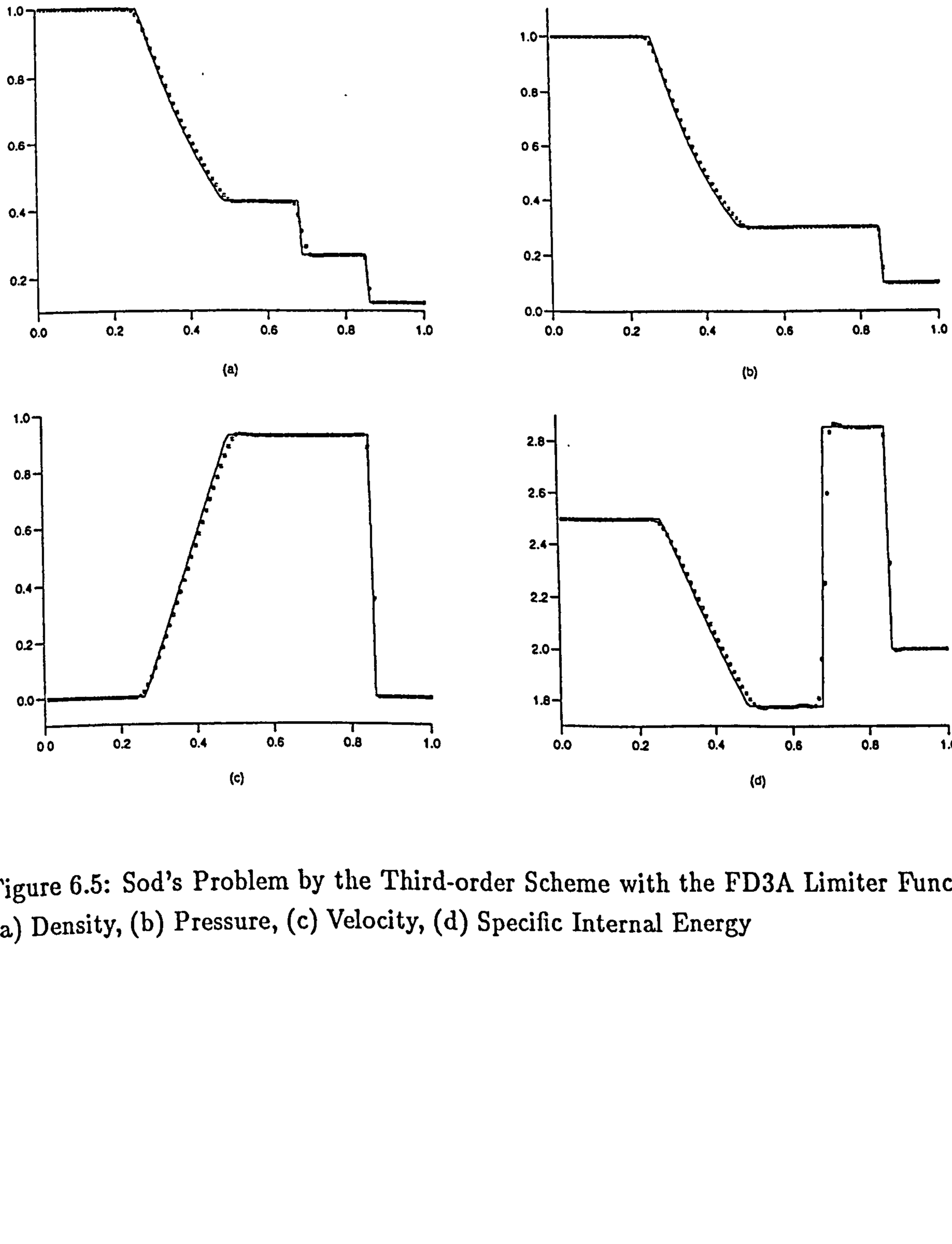

Figure 6.5: Sod's Problem by the Third-order Scheme with the FD3A Limiter Function: (a) Density, (b) Pressure, (c) Velocity, (d) Specific Internal Energy

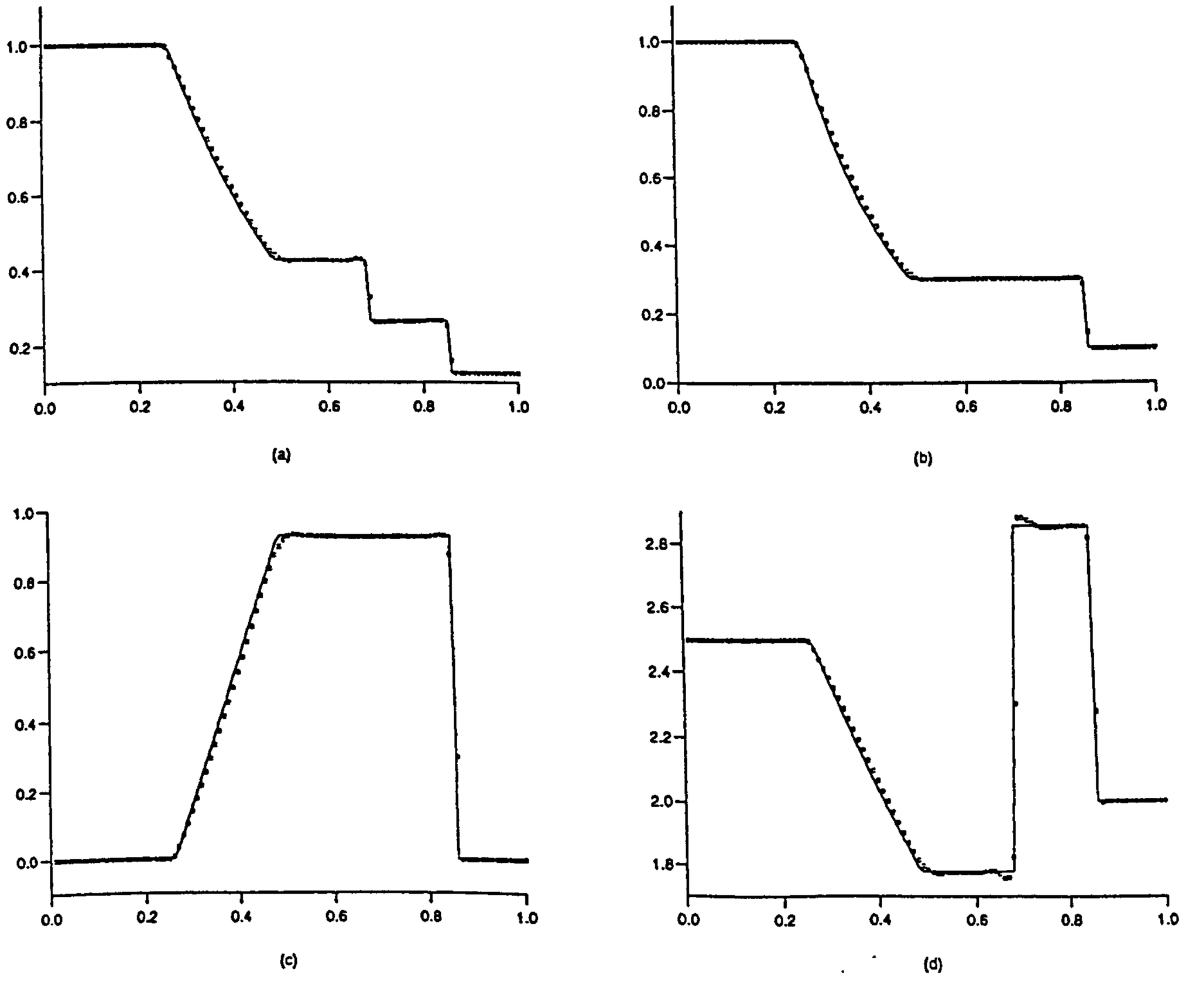

Figure 6.6: Sod's Problem by the Third-order Scheme with the FD3B Limiter Function: (a) Density, (b) Pressure, (c) Velocity, (d) Specific Internal Energy

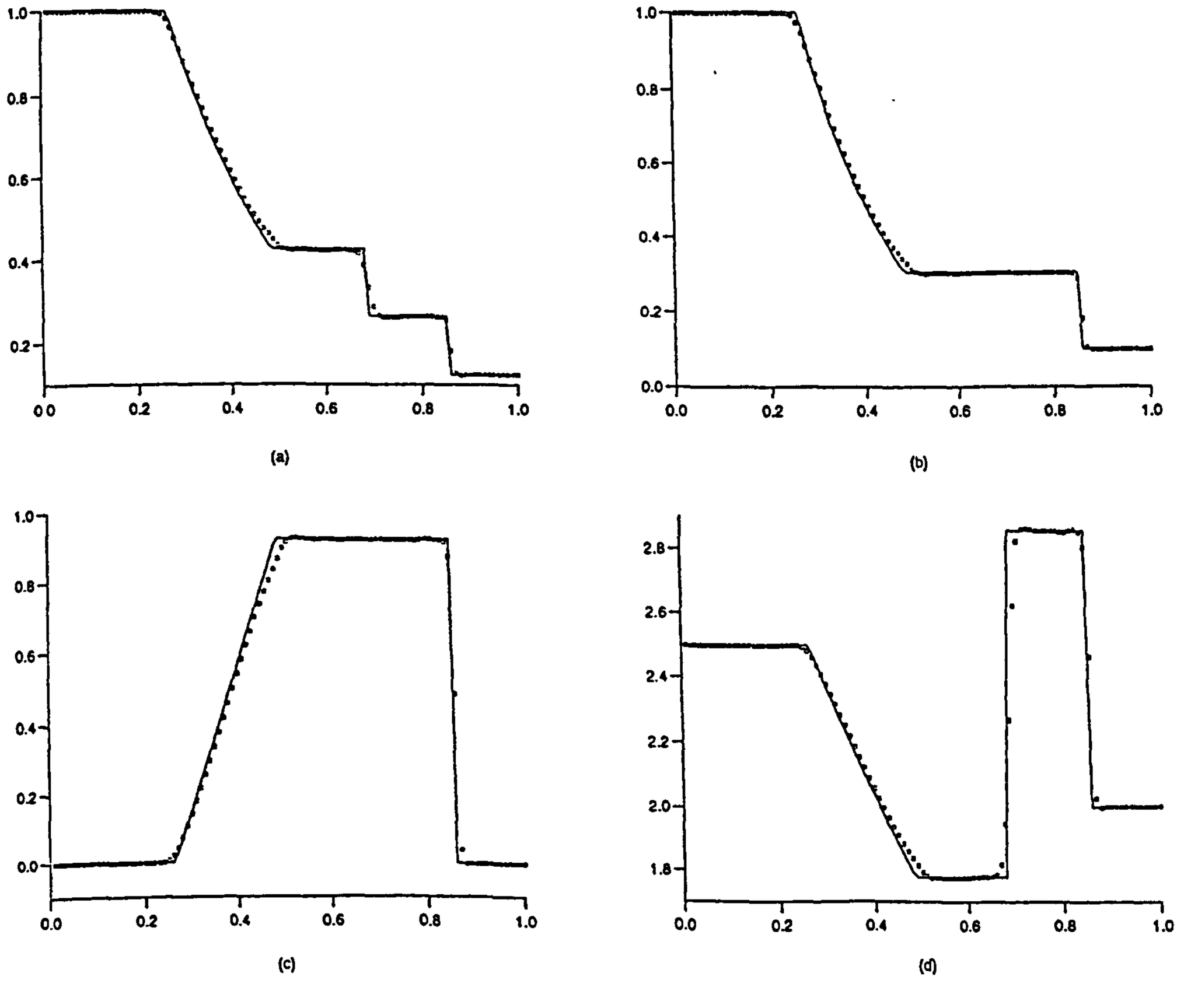

Figure 6.7: Sod's Problem by the Fourth-order Scheme with the FD4A Limiter Function: (a) Density, (b) Pressure, (c) Velocity, (d) Specific Internal Energy

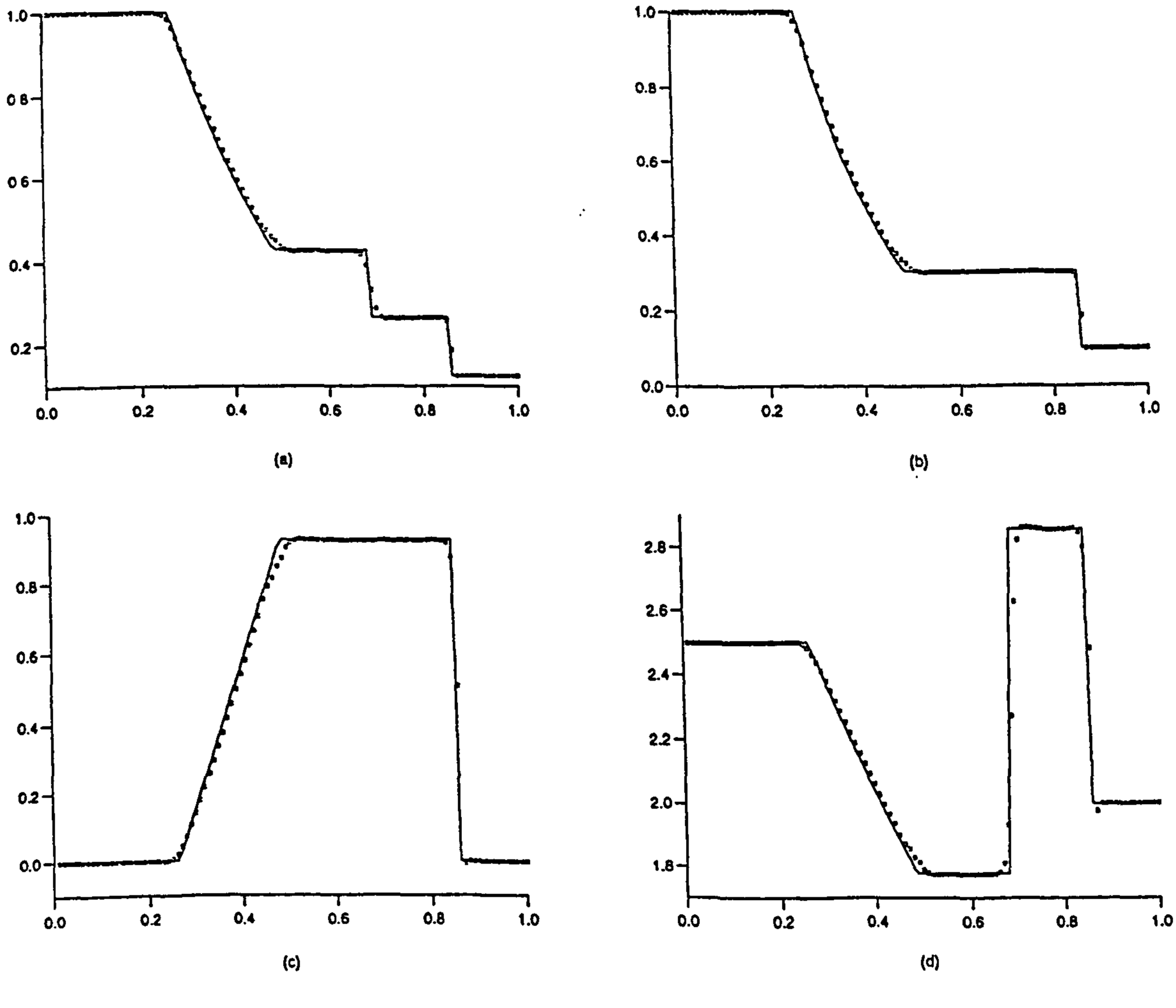

Figure 6.8: Sod's Problem by the Fourth-order Scheme with the FD4B Limiter Function: (a) Density, (b) Pressure, (c) Velocity, (d) Specific Internal Energy

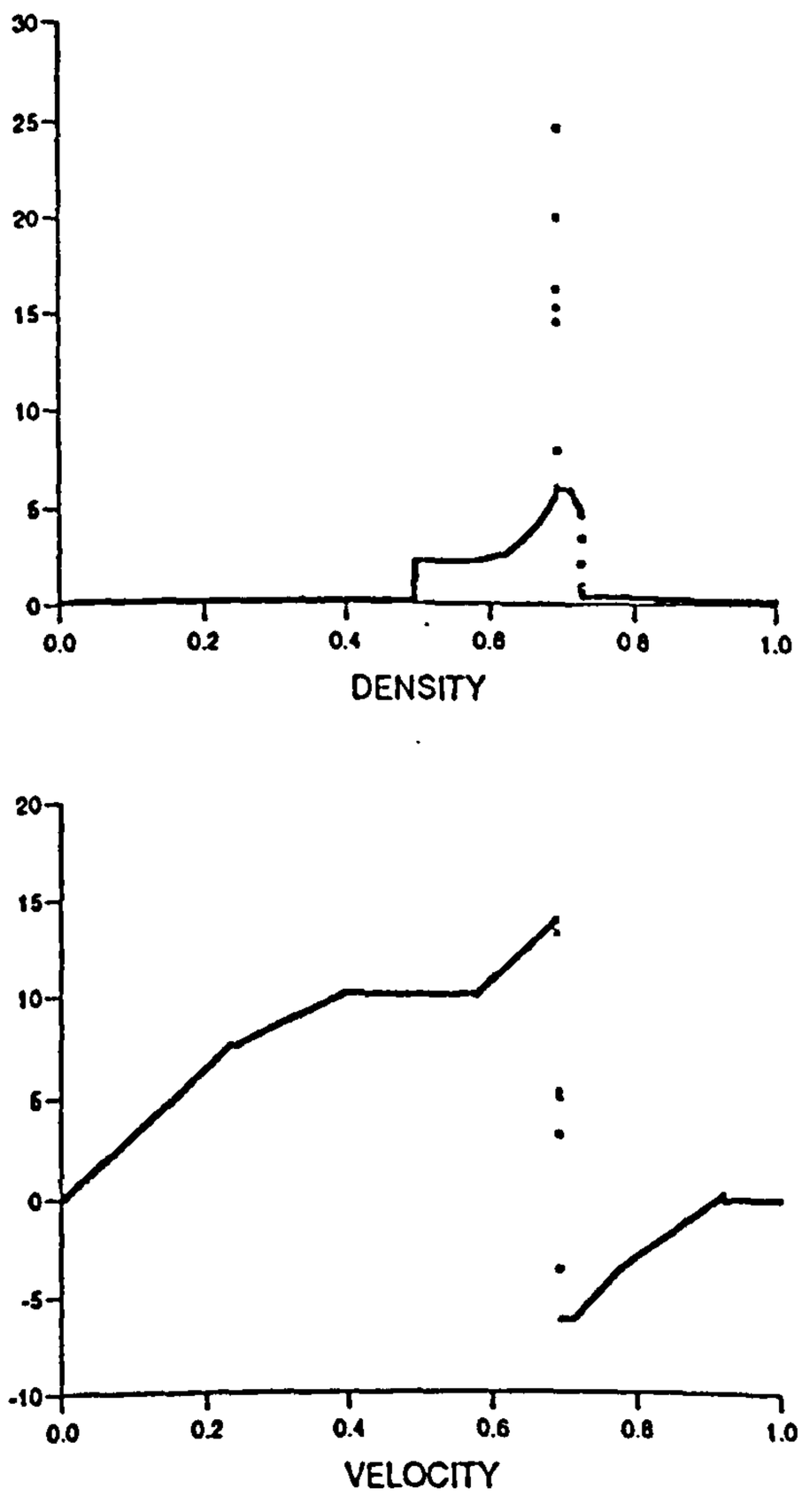

Figure 6.9: Blast-wave Problem by the Second-order Scheme with the FD2B Limiter Function

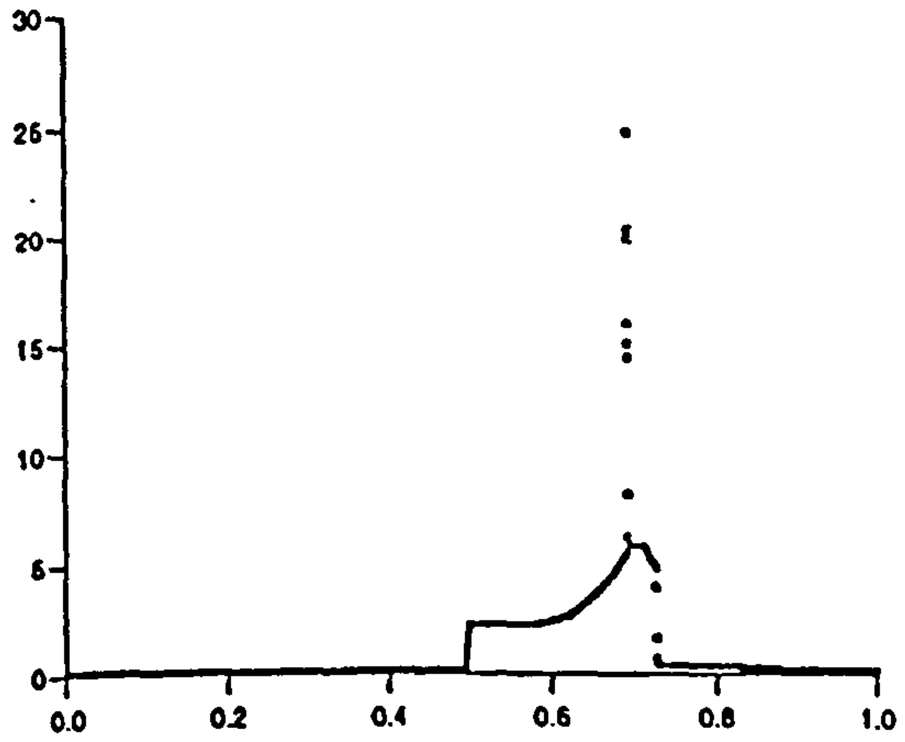

Figure 6.10: Blast-wave Problem by the Third-order Scheme with the FD3B Limiter Function

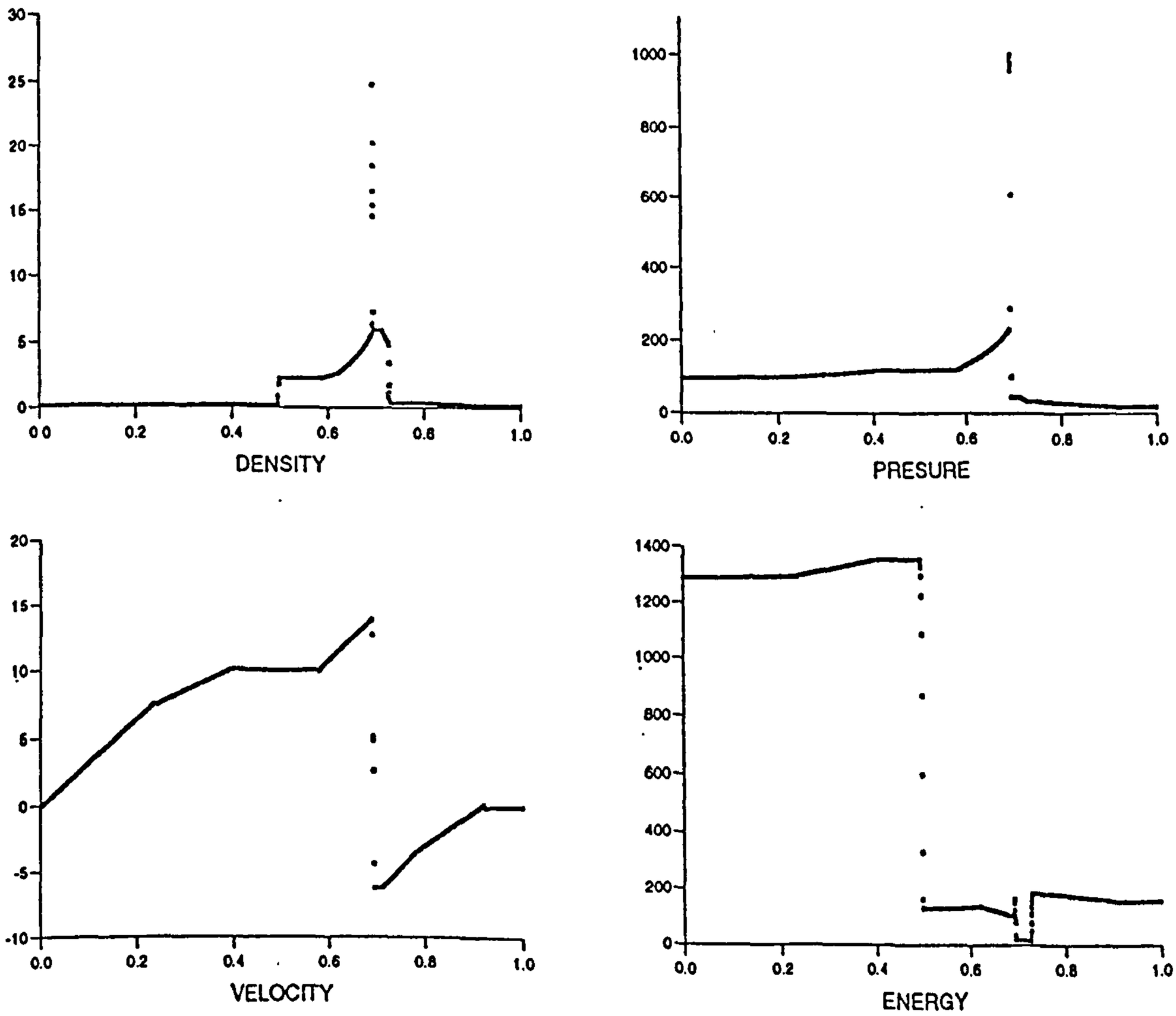

Figure 6.11: Blast-wave Problem by the Fourth-order Scheme with the FD4B Limiter Function

PAGE(S) MISSING

NOT AVAILABLE

P115

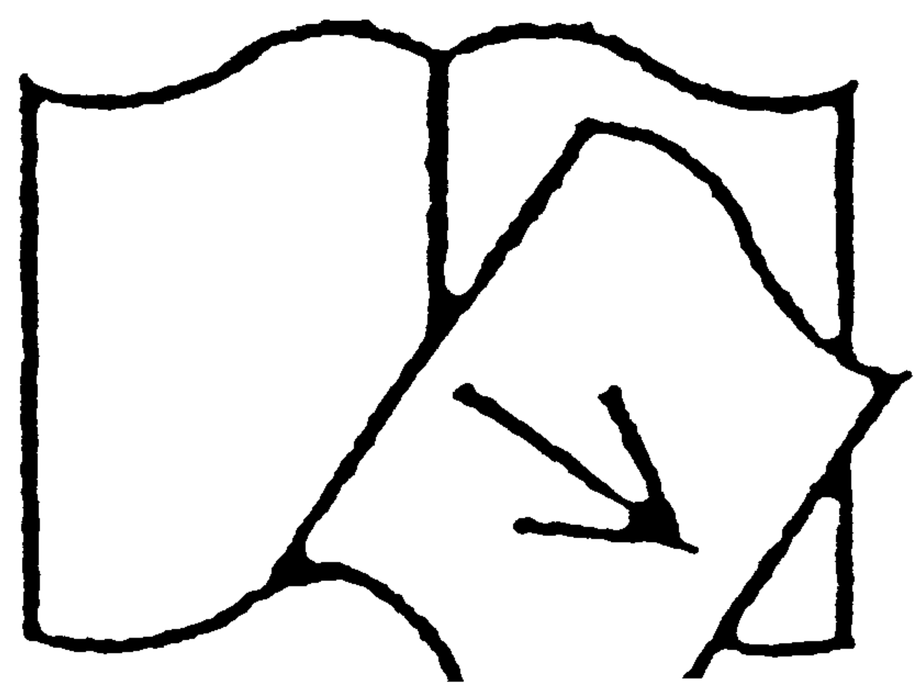

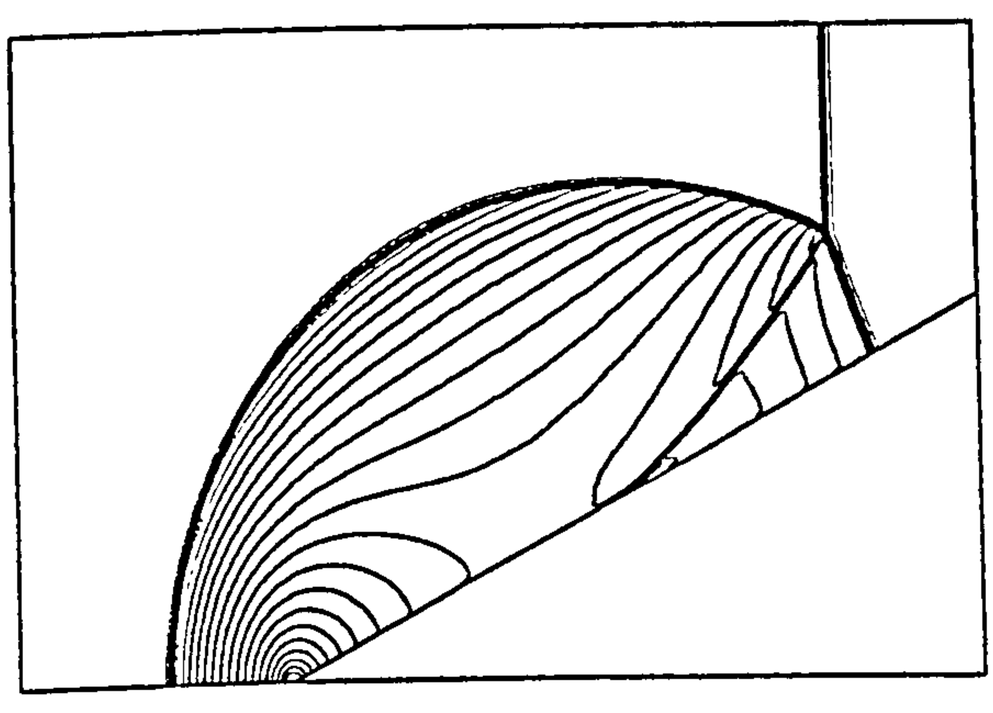

(a)

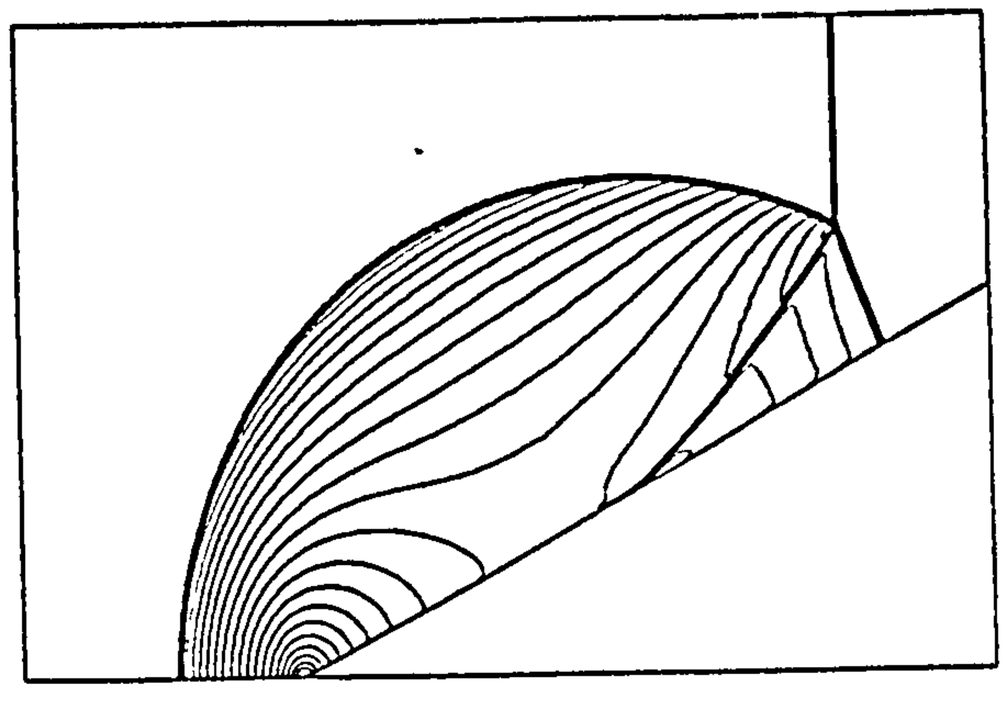

(b)

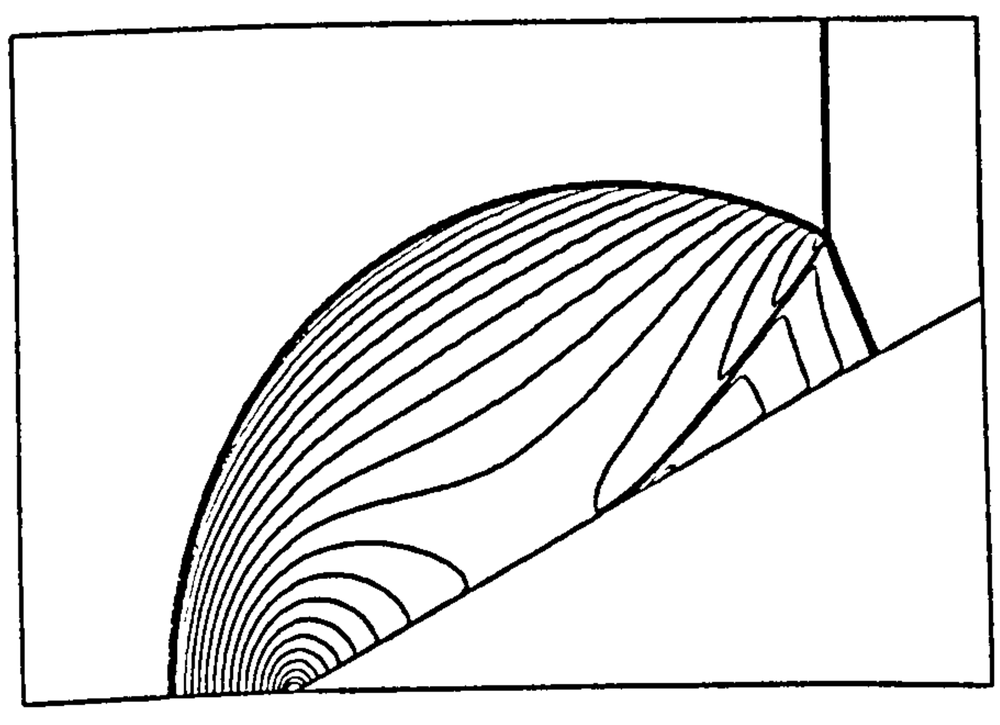

(c)

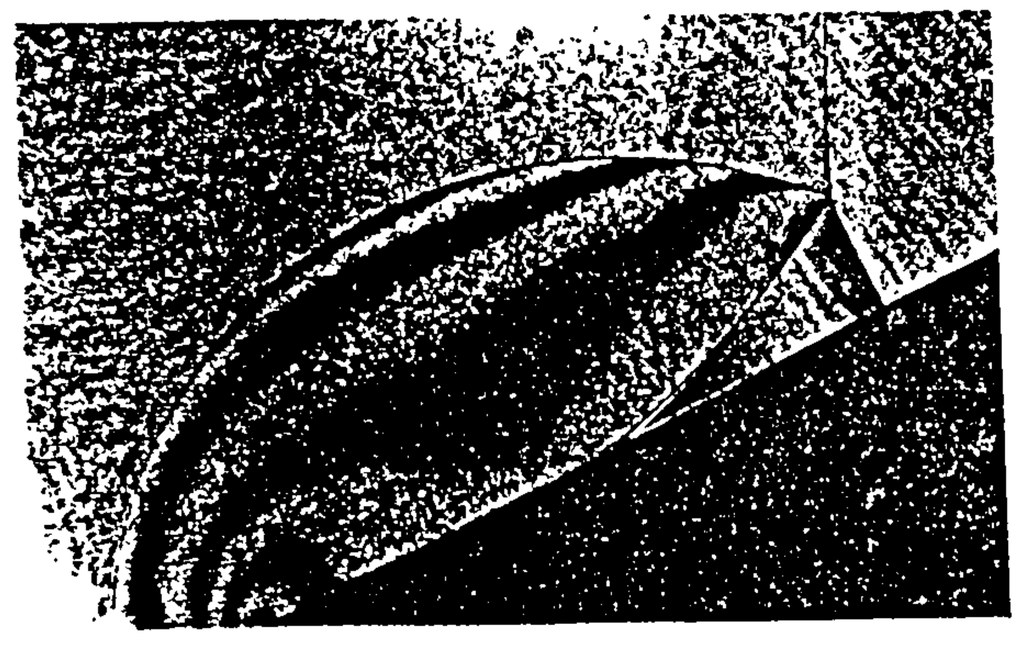

(d)

Figure 6.13: Shock Reflection over 25 Degree Wedge: (a) Computed Result by the Second-order Scheme with the FD2A Limiter Function, (b) Computed Result by the Third-order Scheme with the FD3A Limiter Function, (c) Computed Result by the Fourth-order Scheme with the FD4A Limiter function, (d) The Experimental Result

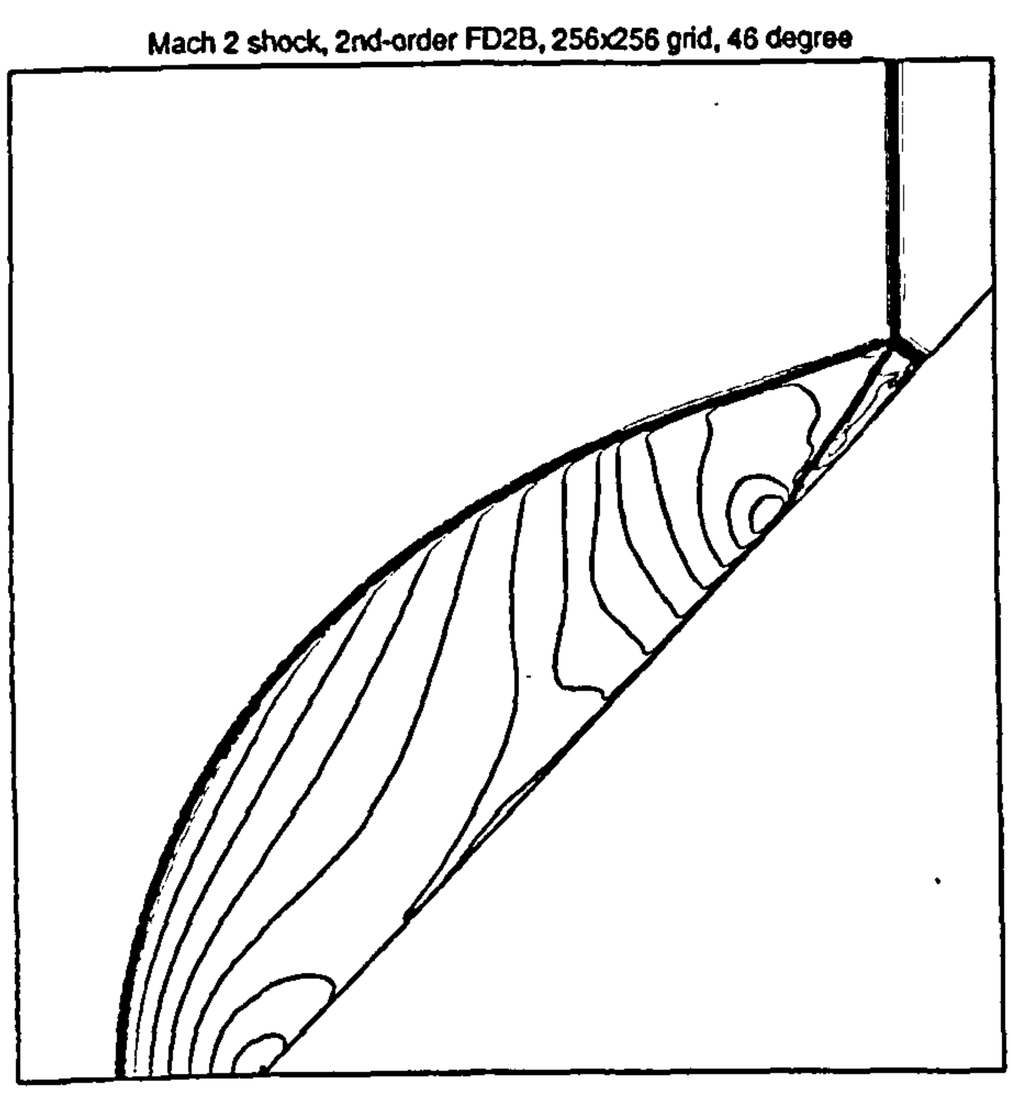

(a)

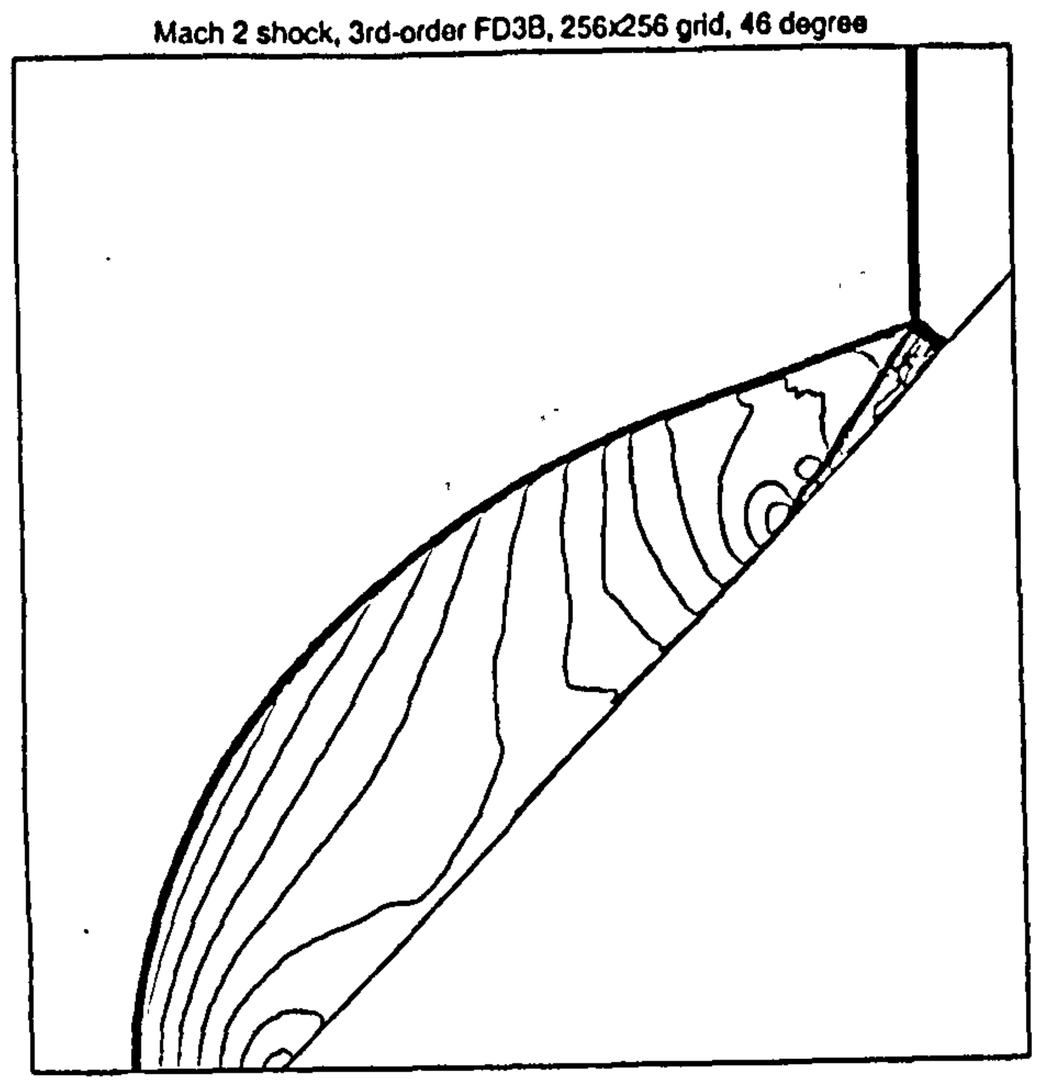

(b)

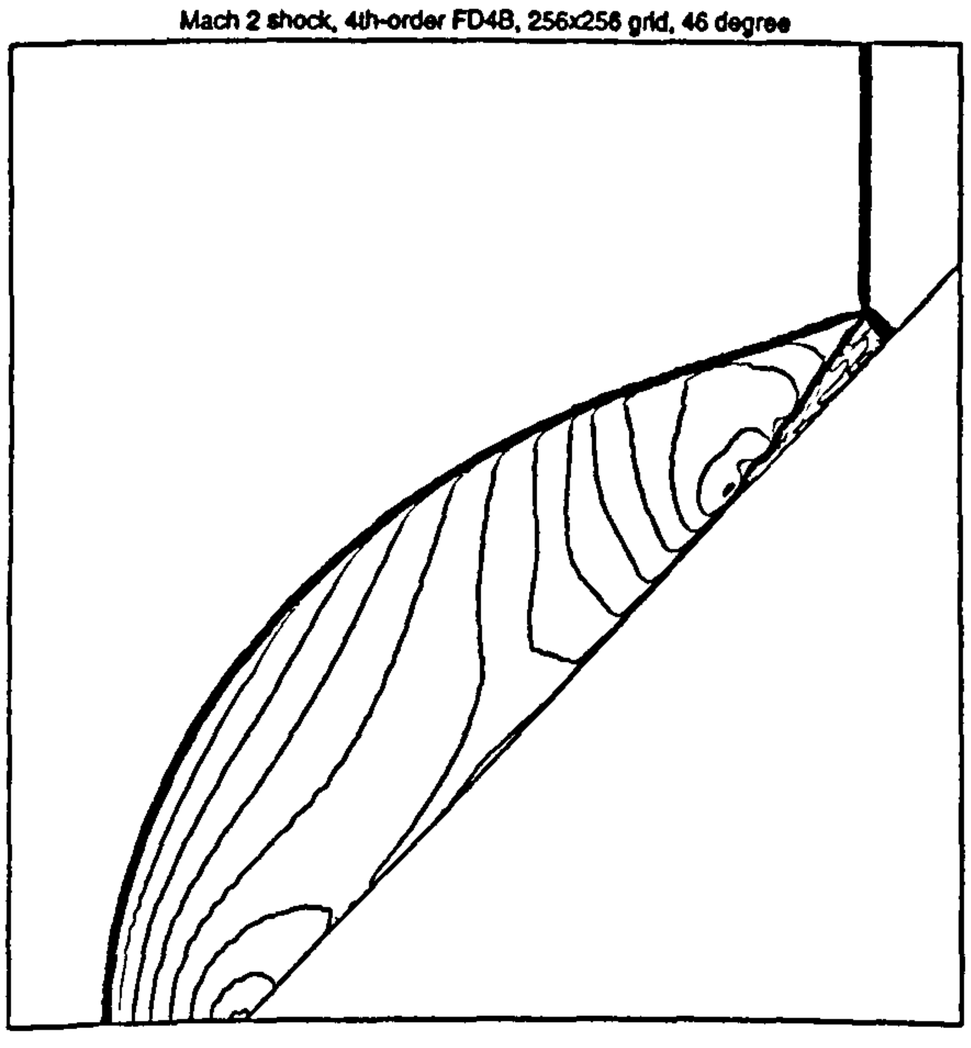

(c)

Figure 6.14: Shock Reflection over 46 Degree Wedge: (a) Computed Result by the Second-order Scheme with the FD2A Limiter Function, (b) Computed Result by the Third-order Scheme with the FD3A Limiter Function, (c) Computed Result by the Fourth-order Scheme with the FD4A Limiter Function

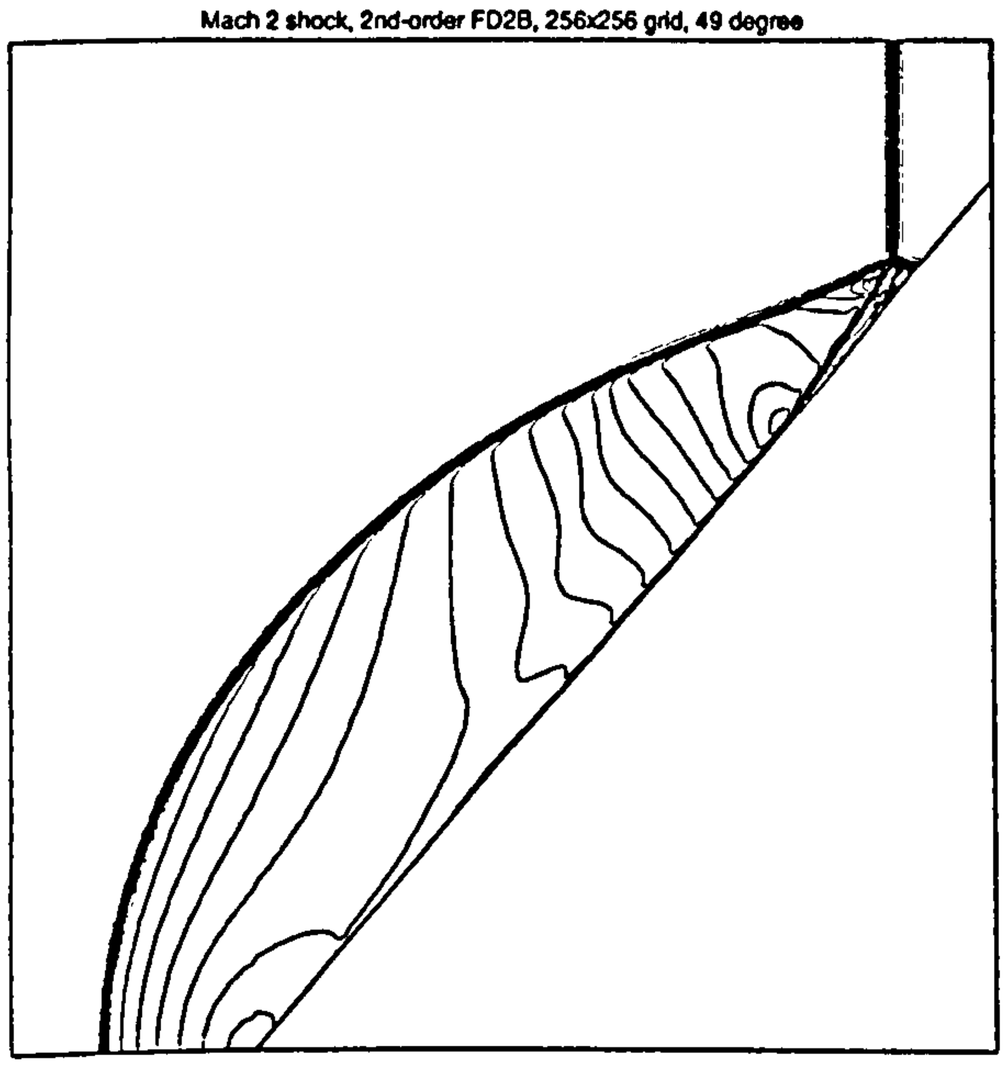

(a)

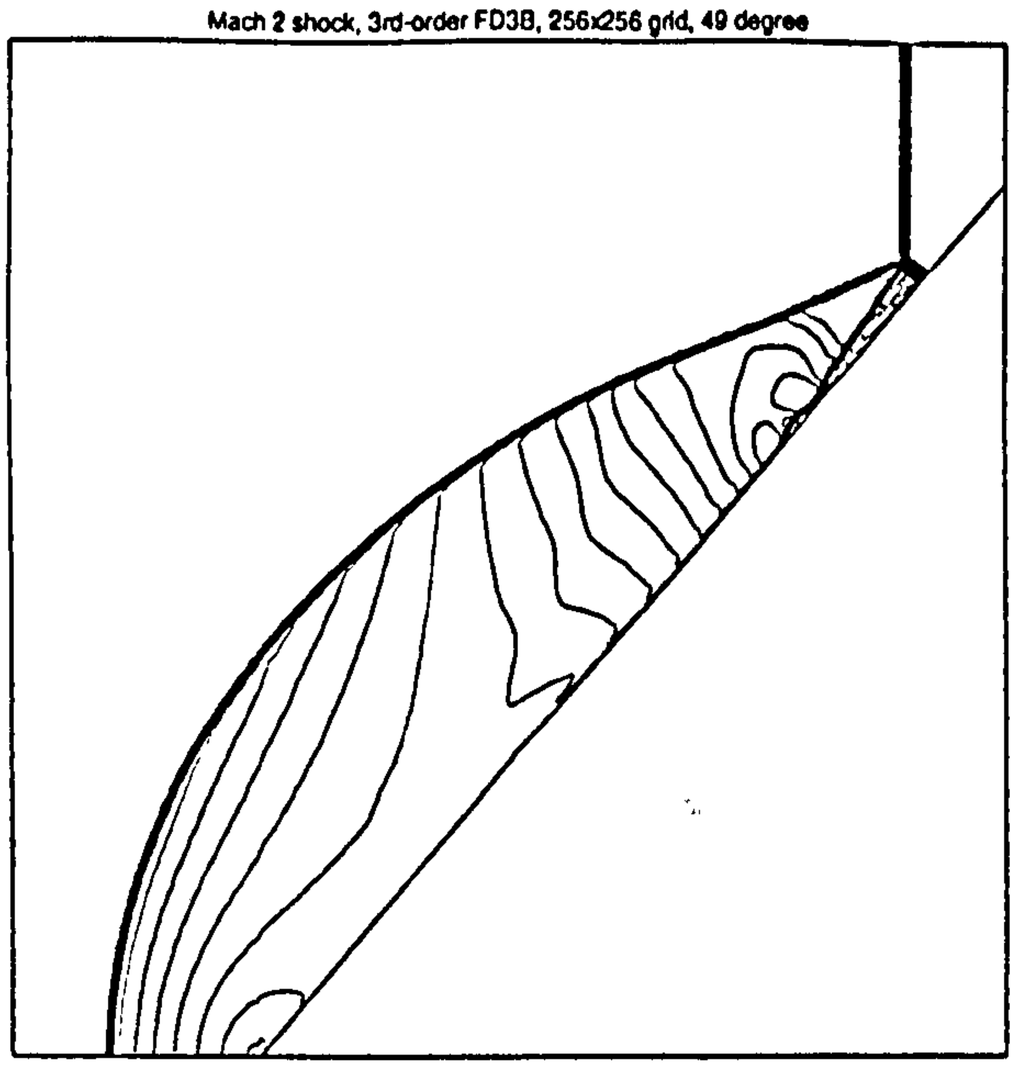

(b)

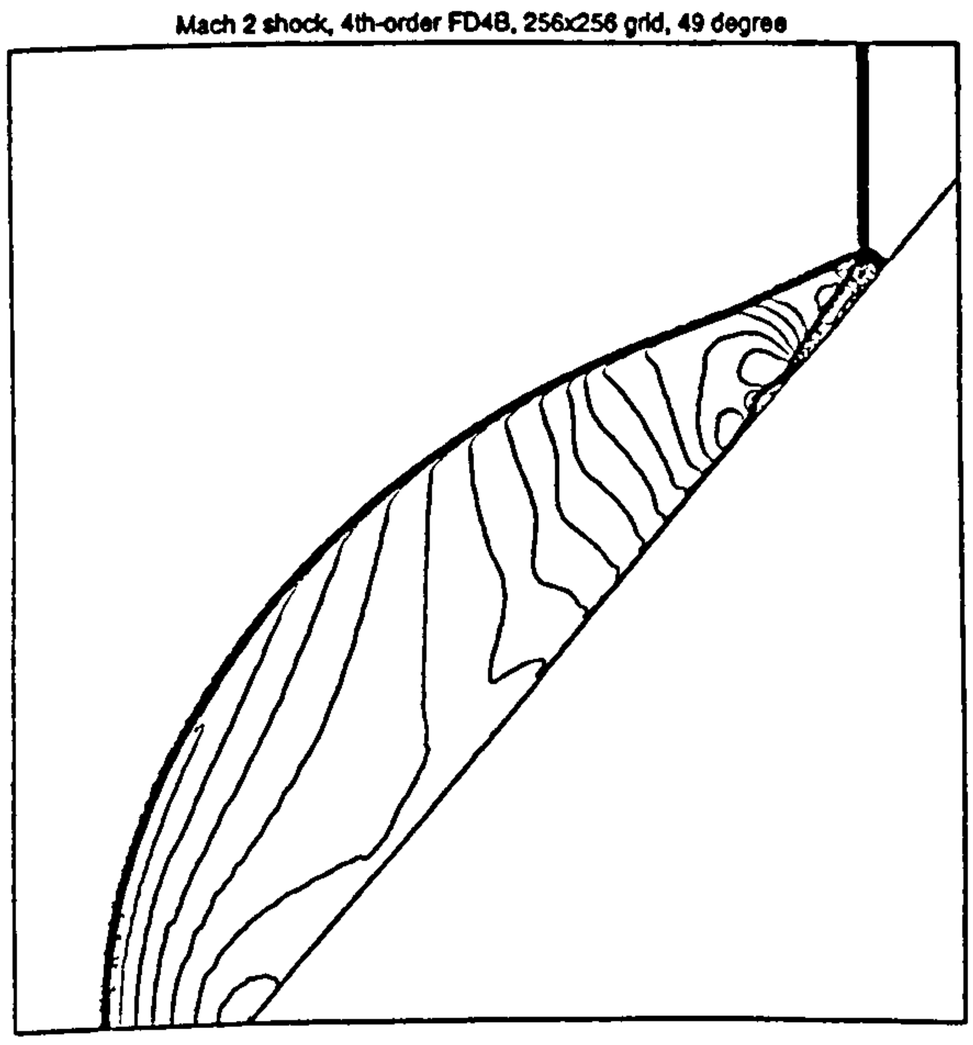

(c)

Figure 6.15: Shock Reflection over 49 Degree Wedge: (a) Computed Result by the Second-order Scheme with the FD2A Limiter Function, (b) Computed Result by the Third-order Scheme with the FD3A Limiter Function, (c) Computed Result by the Fourth-order Scheme with the FD4A Limiter Function

Chapter 7

Fully Discrete Arbitrary-order Schemes for a Model Advection-diffusion Equation

7.1 Introductory Remarks

So far we have discussed high resolution schemes for hyperbolic conservation laws. However most real problems in Fluid Dynamics are viscous flows, which require the solutions of the Navier-Stokes equations. From this chapter on we begin discussing viscous flows. As before let us start with the study of a model equation.

The model equation for the Navier-Stokes (N-S) equations adopted here is the one-dimensional scalar advection-diffusion (A-D) equation. The importance of numerical solutions for the model A-D equation to N-S equations is analogous to that of the model advection equation to the Euler equations. The scalar advection-diffusion equation is also a real model of many true physical phenomena. These phenomena include, for example, particle, momentum, and thermal energy convection and diffusion in gases and liquids.

For the compressible N-S equations, there is an increasing tendency to apply the robust upwind hyperbolic schemes to solve the advection part of the Navier-Stokes equations. However using the flux limiters which are specifically designed for inviscid flows does

not necessarily give satisfactory solutions for viscous flows. Hence viscous problems need viscous flux limiters. These limiters can only be obtained from studying the viscous numerical schemes generated from the model advection-diffusion equation.

In this chapter a fully discrete methodology is investigated for a scalar A-D equation and establish a formula from which two-level, explicit, fully discrete, arbitrary-order numerical schemes can be derived. Some high-order schemes are constructed and tested via numerical experiments. The resulting schemes are expressed in a conservative form, i.e. in a numerical flux function.

The structure of the chapter can be outlined as follows: section 2 establishes a formula defining fully discrete arbitrary-order 2-level explicit numerical schemes for a linear scalar advection-diffusion equation; in section 3 we apply the technique to construct some high-order conservative numerical schemes and analyse linear stability conditions of these schemes; section 4 presents numerical experiments for these high-order schemes; section 5 gives a brief summary.

7.2 Full Discretization of the Model Equation

We consider the initial value problem (IVP) for one dimensional linear scalar advection-diffusion partial differential equation (PDE), namely

$$\begin{aligned} u_t + a u_x &= \mu u_{xx} \quad (-\infty < x < \infty,\ t > 0) \\ u(x,0) &= u_0(x) \end{aligned} \tag{7.1}$$

here a is a constant wave propagation speed and μ is a diffusion coefficient.

In this section a fully discrete technique for the model equation is investigated. The fully discrete approach is based on Taylor series expansion in both space and time in a single stage.

Theorem 4 *The fully discrete formula from which a two-level fully discrete explicit m-th order accurate finite difference method can be derived for the model advection-diffusion equation,* $u_t + a u_x = \mu u_{xx}$, *is defined as*

$$U_j^{n+1} = \sum_{\alpha=1}^{p} B_{k_\alpha}\, U_{j+k_\alpha}^{n} \tag{7.2}$$

where α is the grid point number; p is the number of grid points used, $P = 2m+1$; m is the order of accuracy in time; B_{k_α} are constant coefficients determined by

$$\begin{cases} B_{k_\alpha=0} = 1 - \sum_{\alpha=1,k_\alpha\neq 0}^{2m} B_{k_\alpha} \\ \begin{bmatrix} B_{k_1} \\ B_{k_2} \\ \vdots \\ B_{k_n} \\ \vdots \\ B_{k_{2m}} \end{bmatrix} = \begin{bmatrix} k_1 & k_2 & \dots & k_{2m} \\ k_1^2 & k_2^2 & \dots & k_{2m}^2 \\ \vdots & \vdots & \vdots & \vdots \\ k_1^n & k_2^n & \dots & k_{2m}^n \\ \vdots & \vdots & \vdots & \vdots \\ k_1^{2m} & k_2^{2m} & \dots & k_{2m}^{2m} \end{bmatrix}^{-1} \begin{bmatrix} -c \\ \frac{2}{Re}c + c^2 \\ \vdots \\ \sum_{i=\gamma}^{\frac{n}{2}} \frac{(-1)^{2i}\ n!\ Re^{i-\frac{n}{2}}\ c^{i+\frac{n}{2}}}{(2i)!\ (\frac{n}{2}-i)!} \\ \vdots \\ \sum_{i=\gamma}^{m} \frac{(-1)^{2i}\ (2m)!\ Re^{i-m}\ c^{i+m}}{(2i)!\ (m-i)!} \end{bmatrix} \\ (k_\alpha \neq 0) \end{cases} \tag{7.3}$$

Here we define

$$0! = 1 \tag{7.4}$$

$$\begin{cases} \gamma = \frac{1}{2} & for\ n = 1,3,5,\dots \leq 2m-1 \\ \gamma = 0 & for\ n = 2,4,6,\dots \leq 2m \end{cases} \tag{7.5}$$

c is the Courant number

$$c = \frac{a\Delta t}{\Delta x} \tag{7.6}$$

Re is the cell Reynolds number

$$Re = \frac{c}{d} = \frac{a\Delta x}{\mu} \tag{7.7}$$

and d is the diffusion number given by

$$d = \frac{\mu\Delta t}{(\Delta x)^2} \tag{7.8}$$

Proof

We first analyse the local truncation error of equation (7.2) by Taylor series expansion of both sides of the equation. This can be written as:

$$\begin{aligned} E(x,t) \;=\; & u(x,t) + \sum_{n=1}^{m} \frac{(\Delta t)^n}{n!} u_{t^n} + O\left((\Delta t)^{m+1}\right) \\ & - \sum_{\alpha=1}^{p} B_{k_\alpha} \left[u(x,t) + \sum_{n=1}^{m} \frac{(k_\alpha \Delta x)^n}{n!} u_{x^n} \right] + O\left((\Delta x)^{m+1}\right) \end{aligned} \tag{7.9}$$

where m is the order of accuracy of the scheme, $1 \leq m < \infty$; $u_{t^n} = \frac{\partial^n u}{\partial t^n}$, $u_{x^n} = \frac{\partial^n u}{\partial x^n}$.

Manipulating equation (7.1) we have:

$$u_{t^n} = \sum_{i=0}^{n} A(c,d) u_{x^{n+i}} \tag{7.10}$$

here $A(c,d)$ are constant coefficients that depent on the Courant number c and diffusion number d:

$$A(c,d) = \frac{n!\,(-c)^{n-i}\,d^i\,(\Delta x)^{n+i}}{(n-i)!\,i!\,(\Delta t)^n} \tag{7.11}$$

Substituting (7.10) into (7.9) gives

$$\begin{aligned} E(x,t) \;=\; & \left(1 - \sum_{\alpha=1}^{p} B_{k_\alpha}\right) + \sum_{n=1}^{m} \left[\sum_{i=0}^{n} \frac{(-c)^{n-i}\,d^i\,(\Delta x)^{n+i}}{(n-i)!\,i!}\, u_{x^{n+i}} \right. \\ & \left. - \sum_{\alpha=1, k_\alpha \neq 0}^{m} B_{k_\alpha} \frac{(k_\alpha \Delta x)^n}{n!}\, u_{x^n} \right] + O\left((\Delta t)^{m+1}, (\Delta x)^{2m+1}\right) \end{aligned} \tag{7.12}$$

Note that the order of the truncation error in equation (7.12) is now $m+1$ in time and $2m+1$ in space. Obviously the relationship between m and p is:

$$p = 2m + 1 \tag{7.13}$$

which means that only odd number point schemes can increase the temperal order of accuracy.

Incorporating the right side of equation (7.12), rearranging it, finally in order to obtain $m-th$ order accuracy in time it is sufficient to require that

$$B_{k_\alpha = 0} = 1 - \sum_{\alpha=1, k_\alpha \neq 0}^{2m} B_{k_\alpha} \tag{7.14}$$

$$\sum_{\alpha=1, k_\alpha \neq 0}^{2m} k_\alpha^n B_{k_\alpha} = \sum_{i=\gamma}^{\frac{n}{2}} \frac{n!\,(-c)^{2i}\,d^{\frac{n}{2}-i}}{(2i)!\,(\frac{n}{2}-i)!} \tag{7.15}$$

$$n = 1, 2, \ldots, 2m$$

here we define $0! = 1$ and

$$\begin{cases} \gamma = \frac{1}{2} & for\ n = 1,3,5,\ldots \leq 2m-1 \\ \gamma = 0 & for\ n = 2,4,6,\ldots \leq 2m \end{cases}$$

From equation (7.7) we have

$$d \;=\; Re^{-1} c \tag{7.16}$$

Inserting equation (7.16) into equation (7.15) gives

$$\begin{cases} B_{k_\alpha=0} = 1 - \sum_{\alpha=1,k_\alpha\neq 0}^{2m} B_{k_\alpha} \\ \sum_{\alpha=1,k_\alpha\neq 0}^{2m} k_\alpha^n B_{k_\alpha} = \sum_{i=\gamma}^{\frac{n}{2}} \frac{(-1)^{2i}\ n!\ Re^{i-\frac{n}{2}}\ c^{i+\frac{n}{2}}}{(2i)!\ (\frac{n}{2}-i)!} \\ n = 1,2,\ldots,2m \end{cases} \tag{7.17}$$

Equation (7.17) can be transformed into the alternative forms

$$\begin{cases} B_{k_\alpha=0} = 1 - \sum_{\alpha=1,k_\alpha\neq 0}^{2m} B_{k_\alpha} \\ k_1 B_{k_1} + k_2 B_{k_2} + \cdots + k_{2m} B_{k_{2m}} = -c \\ k_1^2 B_{k_1} + k_2^2 B_{k_2} + \cdots + k_{2m}^2 B_{k_{2m}} = \frac{2}{Re}c + c^2 \\ \vdots \\ k_1^n B_{k_1} + k_2^n B_{k_2} + \cdots + k_{2m}^n B_{k_{2m}} = \sum_{i=\gamma}^{\frac{n}{2}} \frac{(-1)^{2i}\ n!\ Re^{i-\frac{n}{2}}\ c^{i+\frac{n}{2}}}{(2i)!\ (\frac{n}{2}-i)!} \\ \vdots \\ k_1^{2m} B_{k_1} + k_2^{2m} B_{k_2} + \cdots + k_{2m}^{2m} B_{k_{2m}} = \sum_{i=\gamma}^{m} \frac{(-1)^{2i}\ (2m)!\ Re^{i-m}\ c^{i+m}}{(2i)!\ (m-i)!} \\ (k_\alpha \neq 0) \end{cases} \tag{7.18}$$

or

$$\begin{cases} B_{k_\alpha=0} = 1 - \sum_{\alpha=1,k_\alpha\neq 0}^{2m} B_{k_\alpha} \\ \begin{bmatrix} B_{k_1} \\ B_{k_2} \\ \vdots \\ B_{k_n} \\ \vdots \\ B_{k_{2m}} \end{bmatrix} = \begin{bmatrix} k_1 & k_2 & \ldots & k_{2m} \\ k_1^2 & k_2^2 & \ldots & k_{2m}^2 \\ \vdots & \vdots & \vdots & \vdots \\ k_1^n & k_2^n & \ldots & k_{2m}^n \\ \vdots & \vdots & \vdots & \vdots \\ k_1^{2m} & k_2^{2m} & \ldots & k_{2m}^{2m} \end{bmatrix}^{-1} \begin{bmatrix} -c \\ \frac{2}{Re}c + c^2 \\ \vdots \\ \sum_{i=\gamma}^{\frac{n}{2}} \frac{(-1)^{2i}\ n!\ Re^{i-\frac{n}{2}}\ c^{i+\frac{n}{2}}}{(2i)!\ (\frac{n}{2}-i)!} \\ \vdots \\ \sum_{i=\gamma}^{m} \frac{(-1)^{2i}\ (2m)!\ Re^{i-m}\ c^{i+m}}{(2i)!\ (m-i)!} \end{bmatrix} \\ (k_\alpha \neq 0) \end{cases} \tag{7.19}$$

which is the formula (7.3) and establishes the theorem.

For a temporal $m-th$ order numerical method, according to equation (7.13), p coefficients $B_{k_\alpha}(\alpha = 1,2,\cdots,p)$ are needed in equation (7.2). Equations (7.18) or (7.19), having $p = 2m+1$ equations, are therefore closed so that arbitrary-order numerical methods for the linear scalar equation (7.1) can be obtained.

7.3 Fully Discrete High-Order Schemes

In this section we will use some examples to illustrate how to apply the formulae to derive high-order numerical schemes. We first derive non-conservative schemes, then present the corresponding conservative schemes, and finally conduct stability analysis for these schemes.

7.3.1 Fully Discrete Three-point Schemes

From equation (7.13), three-point schemes are first-order in time and second-order in space, i.e. order (1,2).

Space-Centered Scheme

Let us denote the 3-point centered stencil scheme as $U_j^{n+1} = f(U_j^n, U_{j-1}^n, U_{j+1}^n)$. Here, $k_1 = 0,\ k_2 = -1,\ k_3 = 1$ in equation (7.18).

1. Non – conservative Form

Applying equation (7.18) gives

$$\begin{cases} -B_{-1} + B_1 = -c \\ B_{-1} + B_1 = \frac{2}{Re}c + c^2 \\ B_0 = 1 - B_1 - B_{-1} \end{cases}$$

i.e.

$$\begin{cases} B_0 = 1 - \frac{2}{Re}c - c^2 \\ B_1 = \left(\frac{1}{Re} - \frac{1}{2}\right)c + \frac{1}{2}c^2 \\ B_{-1} = \left(\frac{1}{2} + \frac{1}{Re}\right)c + \frac{1}{2}c^2 \end{cases} \tag{7.20}$$

Substituting equation (7.20) into equation (7.2) we have

$$\begin{aligned} U_j^{n+1} &= \left(1 - \frac{2}{Re}c - c^2\right)U_j^n + \left[\left(\frac{1}{2} + \frac{1}{Re}\right)c + \frac{1}{2}c^2\right]U_{j-1}^n \\ &\quad + \left[\left(\frac{1}{Re} - \frac{1}{2}\right)c + \frac{1}{2}c^2\right]U_{j+1}^n \end{aligned} \tag{7.21}$$

Recall $c = Re\ d$, therefore equation(7.21) can also be expressed as:

$$\begin{aligned} U_j^{n+1} &= (1-2d-Re^2d^2)U_j^n + \left[\left(1+\frac{1}{2}Re\right)d+\frac{1}{2}Re^2d^2\right]U_{j-1}^n \\ &\quad + \left[(1-\frac{1}{2}Re)d+\frac{1}{2}Re^2d^2\right]U_{j+1}^n \end{aligned} \tag{7.22}$$

Note that as Reynold number approaches infinity, equation (7.21) reduces to Lax-Wendrof scheme in the hyperbolic case; on the other extreme, as Reynolds number becomes zero, equation (7.22) turns to the centered diffusion scheme for model difusion equation $u_t = \nu u_{xx}$.

2. Conservative Form

According to the theorem 2 introduced in chapter 4, the numerical flux of this scheme is defined as

$$F_{j+\frac{1}{2}} = \frac{1}{2}(F_j^n + F_{j+1}^n) - \frac{|a|}{2}\Delta U_{j+\frac{1}{2}} + |a|\left(\frac{1}{2} - \frac{1}{|Re|} - \frac{|c|}{2}\right)\Delta U_{j+\frac{1}{2}} \tag{7.23}$$

Note here, F_j^n is the local physical advection flux.

3. Stability

Applying the stability analysis technique developed in chapter 2 from equation (2.28) the amplification factor for the 3-point centered scheme λ is defined as

$$\lambda = 1 - \frac{4c}{Re} - 2c^2 \tag{7.24}$$

The amplifier factor $\lambda(c, Re)$ is not only a function of Courant number c, but also a function of cell Reynold number Re. We define an explicit stability function $c \leq f(Re)$ as follows.

For stability $|\lambda| \leq 1$, equation (7.24) gives

$$\left|1 - \frac{4c}{Re} - 2c^2\right| \leq 1 \tag{7.25}$$

i.e.

$$1 - \frac{4c}{Re} - 2c^2 \leq 1 \tag{7.26}$$

$$1 - \frac{4c}{Re} - 2c^2 \geq -1 \tag{7.27}$$

From Equation (7.26) we have

$$c \geq -\frac{2}{Re} \tag{7.28}$$

Equation (7.28) indicates that c and Re have different sign. However, physically c and Re must keep the same sign. Therefore, solution of equation (7.28) is physically meaningless and we will not consider it.

From equation (7.27), we have

$$c \leq \frac{-1+\sqrt{1+Re^2}}{Re} \tag{7.29}$$

$$c \leq \frac{-1-\sqrt{1+Re^2}}{Re} \tag{7.30}$$

Due to the same reason as equation (7.28) we discard equation (7.30). Considering Re can be both positive and negative, finally the stability condition is defined by

$$|c| \leq \frac{\sqrt{1+Re^2}-1}{|Re|} \tag{7.31}$$

here $|Re| \leq \infty$, and correspondingly c is bounded by $|c| \leq 1$.

Upwind Scheme

We denote the scheme by $U_j^{n+1} = f(U_j^n, U_{j-1}^n, U_{j-2}^n)$ in the case of $a > 0$ in equation (7.1). Here, $k_1 = 0,\ k_2 = -1,\ k_3 = -2$ in equation (7.18).

1. Non – conservative Form

Applying equation (7.18) gives

$$\begin{cases} -B_{-1} - 2B_{-2} = -c \\ B_{-1} + 4B_{-2} = \frac{2}{Re}c + c^2 \\ B_0 = 1 - B_{-1} - B_{-2} \end{cases}$$

i.e.

$$\begin{cases} B_0 = 1 + \left(\frac{1}{Re} - \frac{3}{2}\right)c + \frac{1}{2}c^2 \\ B_{-1} = \left(2 - \frac{2}{Re}\right)c - c^2 \\ B_{-2} = \left(\frac{1}{Re} - \frac{1}{2}\right)c + \frac{1}{2}c^2 \end{cases} \tag{7.32}$$

Substitution of equation (7.32) into equation (7.2) we have

$$\begin{aligned} U_j^{n+1} &= \left[1+\left(\frac{1}{Re}-\frac{3}{2}\right)c+\frac{1}{2}c^2\right]U_j^n+\left[\left(2-\frac{2}{Re}\right)c-c^2\right]U_{j-1}^n \\ &\quad +\left[\left(\frac{1}{Re}-\frac{1}{2}\right)c+\frac{1}{2}c^2\right]U_{j-2}^n \end{aligned} \tag{7.33}$$

2. Conservative Form

The numerical flux of the scheme is

$$F_{j+\frac{1}{2}}=\left(\frac{1}{Re}-\frac{1}{2}+\frac{c}{2}\right)F_{j-1}^a+\left(\frac{3}{2}-\frac{1}{Re}-\frac{c}{2}\right)F_j^a \tag{7.34}$$

Note that the $F_j^a = aU_j^n$ is the numerical advection flux.

For negtive speed a in equation (7.1) the corresponding three point scheme has flux

$$F_{j+\frac{1}{2}}=\left(\frac{1}{Re}+\frac{3}{2}+\frac{c}{2}\right)F_{j+1}^a-\left(\frac{1}{Re}+\frac{1}{2}+\frac{c}{2}\right)F_{j+2}^a \tag{7.35}$$

By unifying the two schemes we obtain a five-point method which can accommodate arbitrary wave speeds and has flux

$$F_{j+\frac{1}{2}}=\frac{1}{2}(F_j^n+F_{j+1}^n)-\frac{|a|}{2}\Delta U_{j+\frac{1}{2}}+|a|\left(\frac{1}{2}-\frac{1}{|Re|}-\frac{|c|}{2}\right)\Delta U_{j+L+\frac{1}{2}} \tag{7.36}$$

where

$$\Delta U_{j+L+\frac{1}{2}} = U_{j+L+1}-U_{j+L} \tag{7.37}$$

$$\begin{cases} L=-1 & if\ a>0 \\ L=1 & if\ a<0 \end{cases} \tag{7.38}$$

3. Stability

Applying equation (2.28) the amplification factor of the scheme (7.34) is defined as

$$\lambda = 1+\left(\frac{4}{Re}-4\right)c+2c^2 \tag{7.39}$$

Therefore the stability condition of the scheme is defined by

$$0\le c\le 2\left(1-\frac{1}{Re}\right) \tag{7.40}$$

Here, $1\le Re\le\infty$, and correspondingly $0\le c\le 2$.

The stability condition of the scheme (7.35) is:

$$-2\left(1+\frac{1}{Re}\right) \leq c \leq 0 \tag{7.41}$$

Here $-\infty \leq Re \leq -1$, and c is bounded by $-2 \leq c \leq 0$.

The stability condition of the unified method (7.36) now is:

$$|c| \leq 2\left(1-\frac{1}{|Re|}\right) \tag{7.42}$$

7.3.2 Fully Discrete Four-point Scheme

We can derive four-point schemes in the same way as above. But four-point schemes can not improve the temporal accuracy of numerical solutions (see equation (7.13)), therefore four-point schemes have first-order accuracy in time and third-order accuracy in space, i.e. order (1,3).

Upwind-biased Scheme

The upwind-biased scheme is denoted as $U_j^{n+1} = f(U_j^n, U_{j-1}^n, U_{j+1}^n, U_{j+2}^n)$. By repeating the same procedure as before, we have

1. Non – conservative Form

$$\begin{aligned} U_j^{n+1} &= \left[1+\left(\frac{1}{2}-\frac{2}{Re}\right)c-\left(1+\frac{3}{Re}\right)c^2-\frac{1}{2}c^3\right]U_j^n \\ &+\left[\left(\frac{1}{3}+\frac{1}{Re}\right)c+\left(\frac{1}{2}+\frac{1}{Re}\right)c^2+\frac{1}{6}c^3\right]U_{j-1}^n \\ &+\left[\left(\frac{1}{Re}-1\right)c+\left(\frac{1}{2}+\frac{3}{Re}\right)c^2+\frac{1}{2}c^3\right]U_{j+1}^n \\ &+\left(\frac{1}{6}c-\frac{1}{Re}c^2-\frac{1}{6}c^3\right)U_{j+2}^n \end{aligned} \tag{7.43}$$

(7.44)

2. Conservative Form

The numerical flux for the scheme is

$$F_{j+\frac{1}{2}} = \left[\frac{1}{3}+\frac{1}{Re}+\left(\frac{1}{2}+\frac{1}{Re}\right)c+\frac{c^2}{6}\right]F_j^a+\left[\frac{5}{6}-\frac{1}{Re}-\left(\frac{1}{2}+\frac{2}{Re}\right)c-\frac{c^2}{3}\right]F_{j+1}^a$$

$$-\left(\frac{1}{6}-\frac{1}{Re}c-\frac{c^2}{6}\right)F^a_{j+2} \tag{7.45}$$

Considering the opposite upwind-biased scheme (for wave speed $a \geq 0$), $U^{n+1}_j = f(U^n_j, U^n_{j+1}, U^n_{j-1}, U^n_{j-2})$ which has flux

$$\begin{aligned} F_{j+\frac{1}{2}} &= \left(\frac{c^2}{6}+\frac{c}{Re}-\frac{1}{6}\right)F^a_{j-1}+\left[\frac{5}{6}+\frac{1}{Re}+\left(\frac{1}{2}-\frac{2}{Re}\right)c-\frac{c^2}{3}\right]F^a_j \\ &\quad -\left[\frac{1}{Re}-\frac{1}{3}+\left(\frac{1}{2}-\frac{1}{Re}\right)c-\frac{c^2}{6}\right]F^a_{j+1} \end{aligned} \tag{7.46}$$

By unifying the two previous schemes we obtain a five-point method which can accommodates wave speeds of positive and negative sign and has flux

$$F_{j+\frac{1}{2}} = \frac{1}{2}(F^n_j + F^n_{j+1}) - \frac{|a|}{2}\Delta U_{j+\frac{1}{2}} + \left[|a|D_0\Delta U_{j+\frac{1}{2}} + |a|D_1\Delta U_{j+L+\frac{1}{2}}\right] \tag{7.47}$$

here

$$\begin{cases} D_0 = \frac{c^2}{6}+\left(\frac{1}{|Re|}-\frac{1}{2}\right)|c|+\frac{1}{3}-\frac{1}{|Re|} \\ D_1 = \frac{1}{6}-\frac{c}{Re}-\frac{c^2}{6} \end{cases} \tag{7.48}$$

with

$$\begin{cases} L=-1 & if \quad c>0 \\ L=1 & if \quad c<0 \end{cases}$$

3. Stability

From equation (2.28) the amplification factor of the scheme can be written as

$$\lambda = 1-\left(\frac{4}{3}+\frac{4}{|Re|}\right)|c|+\left(\frac{8}{|Re|}-2\right)c^2+\frac{4}{3}|c|^3 \tag{7.49}$$

For stability we require $|\lambda| \leq 1$. Since the explicit analytical solutin is very complicate, the stability condition of the scheme can be easily found by plotting equation (7.49) against different Re and c.

7.3.3 Fully Discrete Five-point Scheme

Five-point schemes are second-order in time and fourth-order in space, i.e. order (2,4).

Space-centered Scheme

We denote the five-point centered scheme as $U_j^{n+1} = f(U_{j-2}^n, U_{j-1}^n, U_j^n, U_{j+1}^n, U_{j+2}^n)$.

1. Non – conservative Form

$$\begin{aligned}
U_j^{n+1} &= \left[1 - \frac{5}{2Re}c + \left(\frac{3}{Re^2} - \frac{5}{4}\right)c^2 + \frac{3}{Re}c^3 + \frac{1}{4}c^4\right] U_j^n \\
&+ \left[\left(-\frac{1}{12} - \frac{1}{12Re}\right)c + \left(\frac{1}{2Re} - \frac{1}{24} + \frac{1}{2Re^2}\right)c^2 + \left(\frac{1}{12} + \frac{1}{2Re}\right)c^3 + \frac{1}{24}c^4\right] U_{j-2}^n \\
&+ \left[\left(\frac{2}{3} + \frac{4}{3Re}\right)c + \left(\frac{2}{3} - \frac{1}{Re} - \frac{2}{Re^2}\right)c^2 - \left(\frac{1}{6} + \frac{2}{Re}\right)c^3 - \frac{1}{6}c^4\right] U_{j-1}^n \\
&+ \left[\left(\frac{4}{3Re} - \frac{2}{3}\right)c + \left(\frac{2}{3} + \frac{1}{Re} - \frac{2}{Re^2}\right)c^2 + \left(\frac{1}{6} - \frac{2}{Re}\right)c^3 - \frac{1}{6}c^4\right] U_{j+1}^n \\
&+ \left[\left(\frac{1}{12} - \frac{1}{12Re}\right)c + \left(\frac{1}{2Re^2} - \frac{1}{24} - \frac{1}{2Re}\right)c^2\right. \\
&+ \left.\left(\frac{1}{2Re} - \frac{1}{12}\right)c^3 + \frac{1}{24}c^4\right] U_{j+2}^n
\end{aligned} \tag{7.50}$$

2. Conservative Form

The numerical flux of the scheme is

$$\begin{aligned}
F_{j+\frac{1}{2}} &= \frac{1}{2}\left(F_j^n + F_{j+1}^n\right) - \frac{|a|}{2}\Delta U_{j+\frac{1}{2}} \\
&+ |a| D_0 \Delta U_{j+\frac{1}{2}} + |a| D_{-1} \Delta U_{j+L+\frac{1}{2}} + |a| D_1 \Delta U_{j+M+\frac{1}{2}}
\end{aligned} \tag{7.51}$$

where

$$\begin{cases}
D_{-1} = \frac{1}{12} + \frac{1}{12|Re|} + \left(\frac{1}{24} - \frac{1}{2|Re|} - \frac{1}{2Re^2}\right)|c| - \left(\frac{1}{12} + \frac{1}{2|Re|}\right)c^2 - \frac{|c^3|}{24} \\
D_0 = \frac{1}{2} - \frac{7}{6|Re|} + \left(\frac{1}{Re^2} - \frac{7}{12}\right)|c| + \frac{c^2}{|Re|} + \frac{|c^3|}{12} \\
D_1 = \frac{1}{12|Re|} - \frac{1}{12} + \left(\frac{1}{24} + \frac{1}{2|Re|} - \frac{1}{2Re^2}\right)|c| + \left(\frac{1}{12} - \frac{1}{2|Re|}\right)c^2 - \frac{|c^3|}{24}
\end{cases} \tag{7.52}$$

and

$$\begin{cases}
L = -1, \quad M = 1 \quad if \quad c > 0 \\
L = 1, \quad M = -1 \quad if \quad c < 0
\end{cases}$$

3. Stability

The amplification factor of the scheme is:

$$\lambda = 1 - \frac{16}{3Re}c + \left(\frac{8}{Re^2} - \frac{8}{3}\right)c^2 + \frac{8}{Re}c^3 + \frac{2}{3}c^4 \tag{7.53}$$

For stability we require $|\lambda| \leq 1$. By plotting the function (7.53) the stability condition can be obtained.

7.4 Numerical Experiments

In this section some numerical experiments are used to illustrate the performance of the fully discrete high-order numerical schemes. To this end a smooth initial condition is selected

$$u(x,0) = sin\frac{\pi}{2}x \tag{7.54}$$

We are interested in evolving the solution for long times. The chosen computational domain is therefore large and varies according to the evolution time. We thus select a fixed mesh width $\Delta x = 0.1$ and a Courant number coefficient 0.7. Figure 6.1 shows the performance of different schemes. The lines presents the solutions of the 20-th order centered stencil scheme. Since the scheme hardly has any error at the shown time we take the solutions of the 20-th order method as the exact solutions. All of the solutions are obtained with Renold number $Re = 100$ ($\mu = 0.001$).

Figure 7.1 (a) shows a comparison between the numerical solution obtained by the three-point centered method (symbol) and the exact solution (line) after 800 time steps. The dispersive second-order spacial errors of the method are evident and result in a trailing numerical solution. Clearly three-point methods can be very inaccurate in modelling long time behaviour.

Figure 7.1 (b) shows a comparison between the numerical solution obtained by the four-point method and the exact solution after 4000 time steps. Although the solution looks more acceptable than the three-point solution evolved for only 800 time steps, the numerical diffusion of the first-order in time and third-order in space produces the inaccuracy observed.

Figure 7.1 (c) shows a comparison between the numerical solution obtained by the five-point centered method and the exact solution after 10000 time steps. The numerical solution still looks accurate at the shown time. This indicates that the accuracy of numerical solutions is improved dramatically by changing from three-point to five-point methods.

To summarize the situation figure 7.1 (d) shows the comparison of the three-point centered method (stars), the four-point method (crosses), the five-point centered method (boxes) and the very accurate (20-th order) solution (line) after 10000 time steps. The effects of dispersion and diffusion have made the solution of the three-point method meaningless. This justifies the necessity for higher-order numerical schemes for viscous problems which

involve long time evolution.

7.5 Summary

The fully discrete technique for the linear scalar advection-diffusion equation is established. Based on the technique the second-, third- and fourth-order, two-level, explicit, conservative numerical schemes are presented. The numerical experiments indicate that the three-point scheme is not good enough for long time evolution problems. In this case the higher-order schemes can give satisfactory solutions.

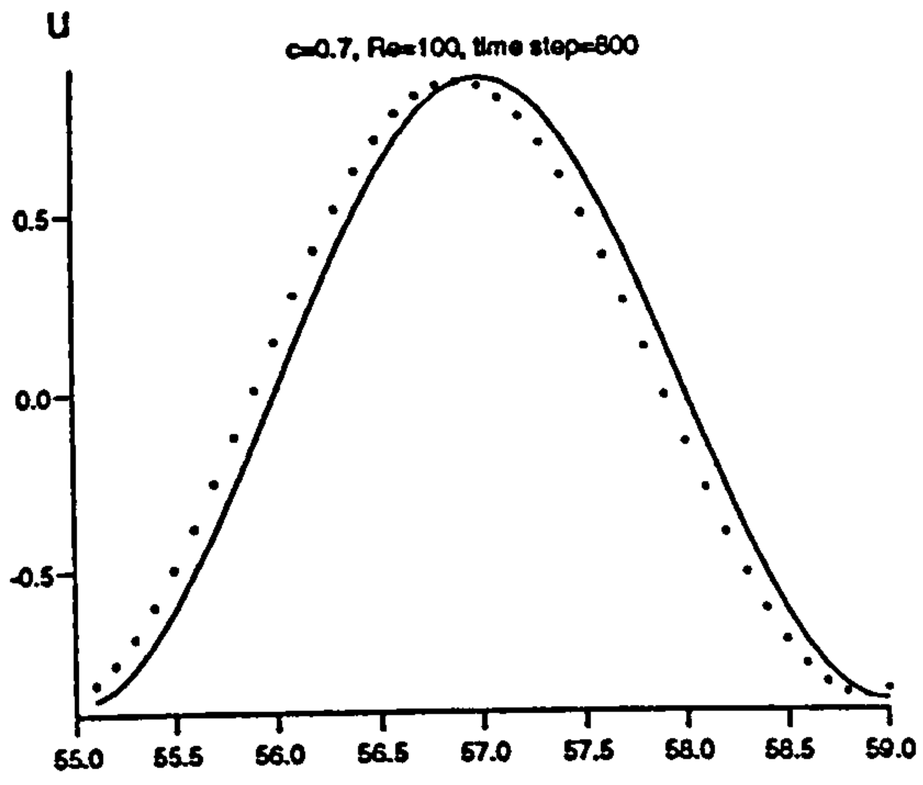

(a)

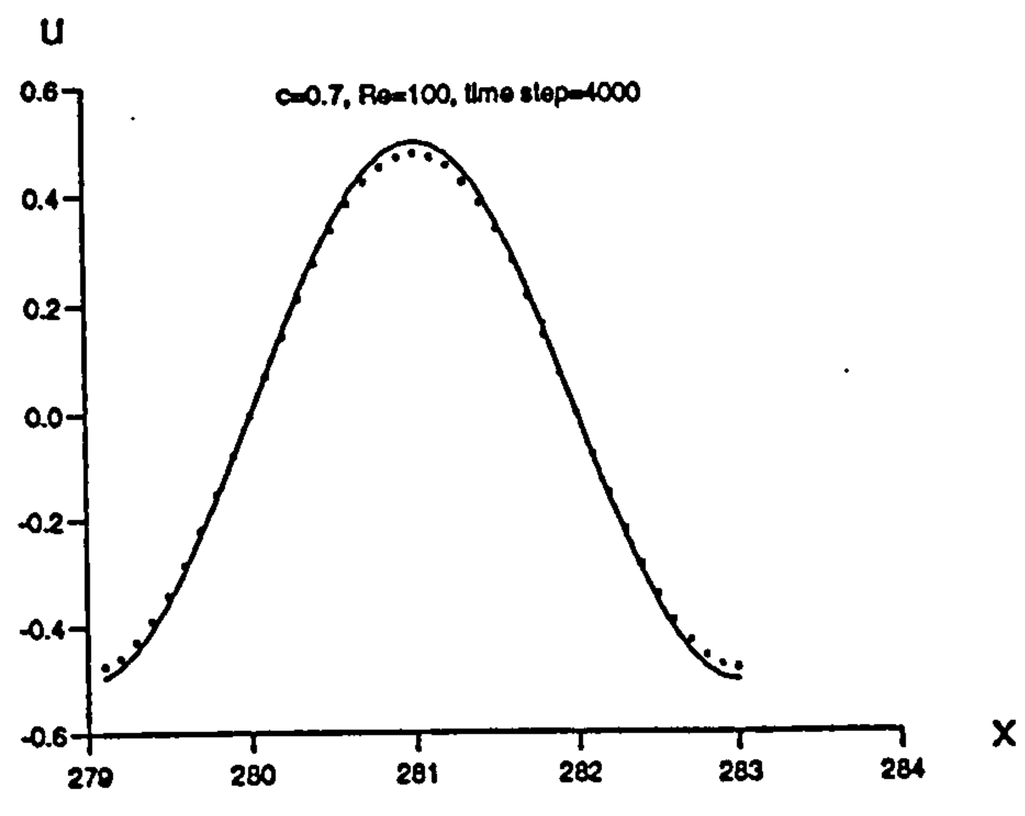

(b)

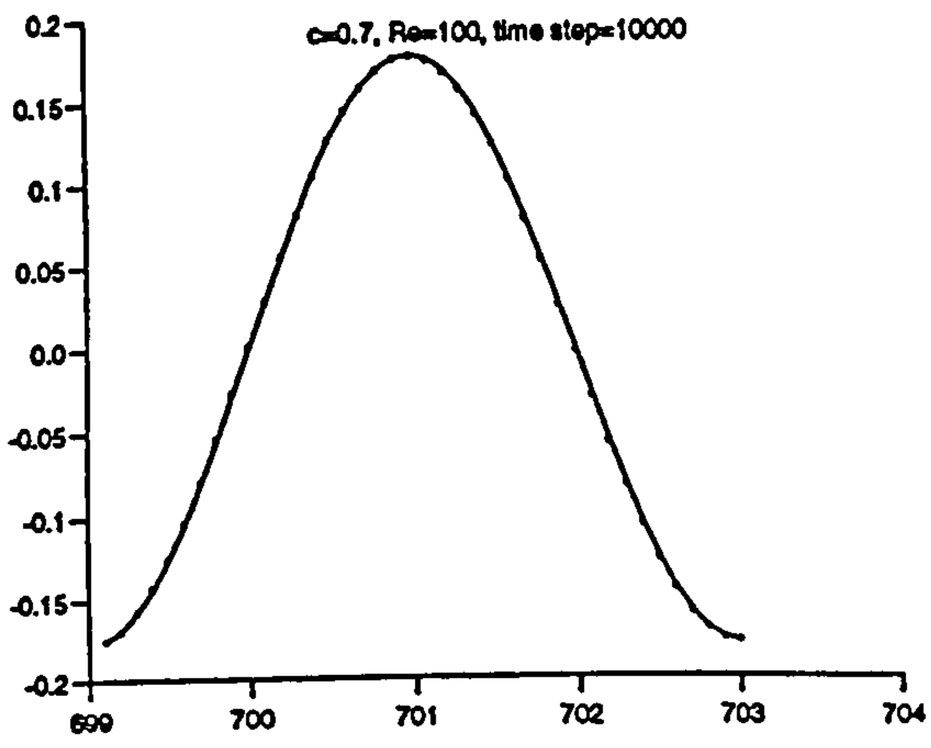

(c)

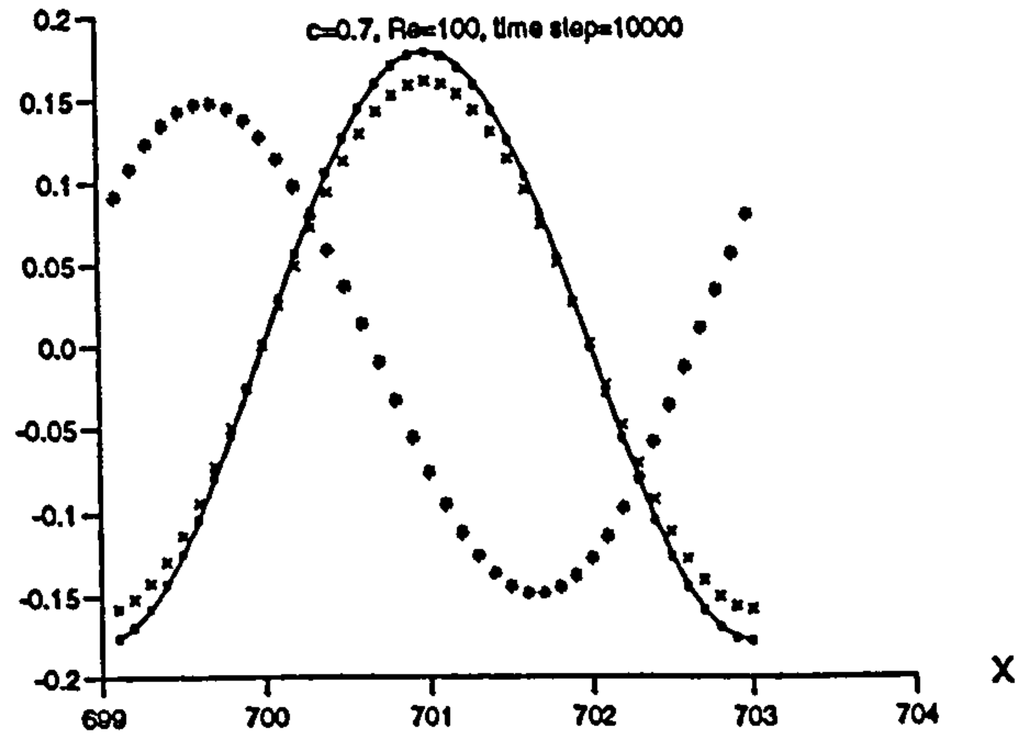

(d)

Figure 7.1: Comparison between the Numerical Solution (symbol) and the Exact Solution (line): (a) Three-point Space-centered Scheme; (b) Four-point Upwind-biased Scheme; (c) Five-point Space-centered Scheme; (d) Comparison between Three-, Four- and Five-point Schemes

Chapter 8

High-order Viscous Flux Limiters and TVD Schemes

8.1 Introductory Remarks

In the last decade the second-order, upwind, Riemann-based, shock-capturing schemes have been successfully applied to solve numerous hyperbolic problems. This popular approach is currently extended to solve transonic and supersonic viscous flows. Recently, some researchers reported their results for solving compressible Navier-Stokes (N-S) equations [67] [68]. They applied Riemann-problem based hyperbolic methods to deal with the convective part of the N-S equations and imposed a Total Variation Diminishing (TVD) property via the introduction of inviscid flux limiters. They found the solutions were different from what they expected. The failure may be due to the blind use of the inviscid flux limiters. In [69] Toro investigated the problem and indicated that second-order inviscid limiters might introduce excessive numerical viscosities in the computed viscous solutions. Therefore he introduced second-order viscous flux limiters into the Weigthed Average Flux method [58].

Based on the high-order viscous schemes developed in last chapter in this chapter high-order viscous flux limiter functions are investigated. A rigorous viscous TVD analysis for the fully discrete high-order numerical schemes are carried out. Second-, third-, and fourth-order viscous flux limiter functions are presented. These limiter functions are tested

and the results are compared with those using inviscid flux limiter functions. The results indicate that for viscous problems the viscous flux limiter functions can give satisfactory solutions. Therefore for solving viscous flows these viscous limiter functions should replace the inviscid limiter functions in the corresponding high-order hyperbolic schemes introduced in chapter 5 and 6.

The structure of the chapter is outlined as follows: section 2 analyses second-order viscous TVD regions and flux limiter functions; section 3 analyses third-order viscous TVD regions and flux limiter functions; section 4 analyses fourth-order viscous TVD regions and flux limiter functions; section 5 gives the results of numerical tests on one-dimensional Navier-Stokes equations using second- and third-order viscous limiters; section 6 is the summary.

8.2 Viscous Limiter Functions for Second-order Scheme

The numerical flux with viscous limiter function for the space-centered second-order scheme can be written as (refer to equation (7.23) for unlimited case)

$$F_{j+\frac{1}{2}} = \frac{1}{2}(F_j^n + F_{j+1}^n) - \frac{|a|}{2}\Delta U_{j+\frac{1}{2}} + |a|\left(\frac{1}{2} - \frac{1}{|Re|} - \frac{|c|}{2}\right)\Delta U_{j+\frac{1}{2}}\,\phi_j \qquad (8.1)$$

where ϕ_j is a viscous flux limiter function.

Applying the TVD theory introduced in chapter 5, the viscous flux limiter functions are defined as

$$\phi_j \leq \frac{2\theta_j}{\eta[1-2/((1-|c|)|Re|)]} \qquad (8.2)$$

$$\phi_j \leq \frac{2}{\eta[1-2/((1-|c|)|Re|)]} \qquad (8.3)$$

$$\phi_j \geq 0 \qquad (8.4)$$

here η is defined by equation (5.27) and θ_j is defined by equations (5.23) and (5.24).

The TVD region defined by the viscous limiter functions above is a function of Courant number c and cell Reynold number Re, i.e. Courant number and cell Reynold number dependent TVD region. In order to see the influence of individual factor c and Re on the viscous TVD regions, figure 8.1 (a) shows the viscous TVD regions against flow parameter θ_j with different Reynold numbers at Courant number $c = 0.5$. As showed in the figure when $|Re| = \infty$ the TVD region reduces to the inviscid TVD region which apply to the

pure convective flows. As the cell Reynold number decreases the upper boundary of the viscous TVD region goes up, which means that less limiting or numerical viscosity needed. This conforms the physical meaning, that is, the viscous flux limiter functions (8.2) and (8.3) have already concerned the physical viscosities contained in the original model A-D equation, which play a part to restrain the oscillation.

Figure 8.1 (b) shows the viscous TVD regions against flow parameter θ_j with different Courant numbers at cell Reynold number $Re = 100$ which shows that for a given $|Re|$ the upper boundary of the TVD region reaches the maximum at $|c| = 0.5$.

Analysing the viscous limiter functions we know that when the cell Reynold number satisfying

$$|Re| \leq \frac{2}{1 - |c|} \tag{8.5}$$

the physical viscosity is large enough to prevent any oscillations. Therefore there is no need of limiter functions at all. Here we have the same coclusion as that of Toro [69]. Figure 8.2 illustrates the numerical results without limiters for $Re = 20$ ($c = 0.9$) (a) and $Re = 4$ ($c = 0.5$) (b) after 25 time steps. The test problem has an initial discontinuity at $x = 0$. A mesh width $\Delta x = 0.05$ and a wave speed $a = 1$ are fixed in the test. Clearly, there are no visible oscillations in the figures.

Based on the viscous flux limiter functions (8.2), (8.3) and (8.5) two viscous limiters are introduced as follows.

8.2.1 FDV2A Limiter Function

The FDV2A (Fully Discrete Viscous 2-order A) limiter is defined as

$$\begin{aligned} \phi_j \;=\; max\left[0, min\left(1, \frac{2\theta_j}{1 - 2/((1-|c|)|Re|)}\right),\right. \\ \left. min\left(\theta_j, \frac{2}{1 - 2/((1-|c|)|Re|)}\right)\right] \end{aligned} \tag{8.6}$$

which is analogous to the inviscid SUPERBEE limiter for $|Re| = \infty$.

Figure 8.3 shows the the comparison between the exact solution (line) and the numerical results (symbol) for the SUPERBEE ((a) and (b)) and the FDV2A ((c) and (d)) after 1000 time steps. The cell Reynold number and Courant number used in the test are 100

and 0.8. As shown in the figures both of the limiters produce under-diffusive solutions which is typical for this kind of limiters.

8.2.2 FDV2B Limiter function

The FDV2B limiter function has the following form

$$\begin{aligned}\phi_j &= max\left[0, min\left(1, \frac{\theta_j}{\eta[1-2/((1-|c|)|Re|)]}\right),\right. \\ &\left. min\left(\theta_j, \frac{1}{\eta[1-2/((1-|c|)|Re|)]}\right)\right] \end{aligned} \tag{8.7}$$

which is analogous to the inviscid MINMOD limiter for $|Re| = \infty$.

Figure 8.4 shows the performance of the MINMOD ((a) and (b)) and the FDV2B ((c) and (d)) after 1000 time steps. Clearly shown in the figures the MINMOD is too diffusive and the FDV2B gives satisfactory results. Therefore when dealing with viscous flows using second-order method the FDV2B limiter function is recommanded.

For solving system of viscous equations the FDV2B limiter has the following form (refer to chapter 6)

$$\begin{aligned}\phi_j^{(p)} &= max\left[0, min\left(1, \frac{\theta_j^{(p)}}{\eta^{(p)}_{j+\frac{1}{2}}[1-2/((1-|c^{(p)}_{j+\frac{1}{2}}|)|Re^{(p)}_{j+\frac{1}{2}}|)]}\right),\right. \\ &\left. min\left(\theta_j^{(p)}, \frac{1}{\eta^{(p)}_{j+\frac{1}{2}}[1-2((1-|c^{(p)}_{j+\frac{1}{2}}|)|Re^{(p)}_{j+\frac{1}{2}}|)]}\right)\right] \end{aligned} \tag{8.8}$$

where $c^{(p)}_{j+1/2}$, $\theta^{(p)}_{j+1/2}$ and $\eta^{(p)}_{j+\frac{1}{2}}$ are defined by equations (6.11), (6.14), (6.15) and (6.16); $Re^{(p)}_{j+1/2}$ is determined by

$$Re^{(p)}_{j+\frac{1}{2}} = \frac{\lambda^{(p)}_{j+\frac{1}{2}}\, h}{\mu^{(p)}} \tag{8.9}$$

When dealing with viscous flows using the second-order scheme (6.10) the inviscid limiters FD2A or FD2B might be replaced by the FDV2B limiter.

8.3 Viscous Limiter functions for Third-order Scheme

The numerical flux with viscous limiter function for third-order scheme has the following form (refer to equation (7.47) for unlimited case)

$$F_{j+\frac{1}{2}} = \frac{1}{2}(F_j^n + F_{j+1}^n) - \frac{|a|}{2}\Delta U_{j+\frac{1}{2}} + \left(|a|D_0\Delta U_{j+\frac{1}{2}} + |a|D_1\Delta U_{j+L+\frac{1}{2}}\right)\phi_j \qquad (8.10)$$

where the coefficients D_0 and D_1 are given by equation (7.48).

The TVD function of the scheme is defined by

$$\phi_j \leq \frac{(1-|c|)\theta_j}{\eta(D_1\theta_j + D_0)} \qquad (8.11)$$

$$\phi_j \leq \frac{1-|c|}{\eta(D_1\theta_j + D_0)} \qquad (8.12)$$

$$\phi_j \geq 0 \qquad (8.13)$$

Figure 8.5 (a) shows TVD regions of this scheme with different cell Reynold numbers for $|c| = 0.5$. Figure 8.5 (b) gives TVD regions with different Courant numbers for $|Re| = 100$. These figures have similar features to those of the second-order scheme.

Based on the viscous TVD functions a viscous limiter called FDV3 (Fully Discrete Viscous 3-order) has the following form

$$\begin{cases} \phi_j = \frac{(1-|c|)\theta_j}{\eta(D_1\theta_j+D_0)} & if \;\; 0 \leq \theta_j < \theta^L \\ \phi_j = 1 & if \;\; \theta^L \leq \theta_j \leq \theta^R \\ \phi_j = \frac{1-|c|}{\eta(D_1\theta_j+D_0)} & if \;\; \theta_j > \theta^R \\ \phi_j = 0 & if \;\; \theta_j < 0 \end{cases} \qquad (8.14)$$

where

$$\theta^L = \frac{\eta D_0}{1-|c|-\eta D_1} \qquad (8.15)$$

$$\theta^R = \frac{1-|c|-\eta D_0}{\eta D_1} \qquad (8.16)$$

The shaded part in figure 8.5 (c) shows the FDV3 imiter for $|Re| = 100$. The upper boundary of the shaded area represents $|c| = 0.5$ and the lower boundary of it represents $|c| = 0$. For other values of $|c|$ the limiter varies in between.

Figure 8.6 shows the performance of the limiter after 1000 time steps. (a) and (b) are the results for Courant number $|c| = 0.5$; (c) and (d) are the results for $|c| = 0.8$. The solid

line is the exact solution. Clearly shown in the figures the numerical results (symbol) are very accurate.

For systems of viscous problems the FDV3 takes the form

$$\begin{aligned}
\phi_j^{(p)} &= \frac{(1-|c^{(p)}_{j+L+\frac{1}{2}}|)\ \theta_j^{(p)}}{\eta^{(p)}_{j+L+\frac{1}{2}}\left(D^{(p)}_{j+L+\frac{1}{2}}\theta_j^{(p)}+D^{(p)}_{j+\frac{1}{2}}\right)} \quad if \quad 0 \le \theta_j^{(p)} < \theta^L \\
\phi_j^{(p)} &= 1 \qquad\qquad if \quad \theta^L \le \theta_j^{(p)} \le \theta^R \\
\phi_j^{(p)} &= \frac{1-|c^{(p)}_{j+L+\frac{1}{2}}|}{\eta^{(p)}_{j+L+\frac{1}{2}}\left(D^{(p)}_{j+L+\frac{1}{2}}\theta_j^{(p)}+D^{(p)}_{j+\frac{1}{2}}\right)} \quad if \quad \theta_j^{(p)} > \theta^R \\
\phi_j^{(p)} &= 0 \qquad\qquad if \quad \theta_j^{(p)} \le 0
\end{aligned} \tag{8.17}$$

Here $\eta^{(p)}_{j+1/2}$ is defined by equation (6.16) and

$$D^{(p)}_{j+\frac{1}{2}} = \frac{1}{6}\left(c^{(p)}_{j+\frac{1}{2}}\right)^2 + \left(1/|Re^{(p)}_{j+\frac{1}{2}}| - \frac{1}{2}\right)|c^{(p)}_{j+\frac{1}{2}}| + \frac{1}{3} - 1/|Re^{(p)}_{j+\frac{1}{2}}| \tag{8.18}$$

$$D^{(p)}_{j+L+\frac{1}{2}} = \frac{1}{6} - c^{(p)}_{j+L+\frac{1}{2}}/Re^{(p)}_{j+L+\frac{1}{2}} - \left(c^{(p)}_{j+L+\frac{1}{2}}\right)^2 \tag{8.19}$$

$$\theta^L = \frac{\eta^{(p)}_{j+\frac{1}{2}} D^{(p)}_{j+\frac{1}{2}}}{1-|c^{(p)}_{j+\frac{1}{2}}| - \eta^{(p)}_{j+\frac{1}{2}} D^{(p)}_{j+L+\frac{1}{2}}} \tag{8.20}$$

$$\theta^R = \frac{1-|c^{(p)}_{j+\frac{1}{2}}| - \eta^{(p)}_{j+\frac{1}{2}} D^{(p)}_{j+\frac{1}{2}}}{\eta^{(p)}_{j+\frac{1}{2}} D^{(p)}_{j+L+\frac{1}{2}}} \tag{8.21}$$

$$\begin{cases} L=-1 & if \quad c^{(p)}_{j+\frac{1}{2}} > 0 \\ L=1 & if \quad c^{(p)}_{j+\frac{1}{2}} < 0 \end{cases} \tag{8.22}$$

When solving viscous flows using the third-order scheme (6.17) the inviscid limiter function FD3 might be replaced by the FDV3 limiter function.

8.4 Viscous Flux Limiter function for Fourth-order Scheme

The numerical flux with viscous limiter function for the fourth-order scheme is (see equation (7.51) for unlimited case)

$$F_{j+\frac{1}{2}} = \frac{1}{2}\left(F^n_j + F^n_{j+1}\right) - \frac{|a|}{2}\Delta U_{j+\frac{1}{2}}$$

$$+|a|\left(D_0\Delta U_{j+\frac{1}{2}}+D_{-1}\Delta U_{j+L+\frac{1}{2}}\right)\phi_j+|a|D_1\Delta U_{j+M+\frac{1}{2}}\,\phi_{j+M} \quad (8.23)$$

where D_{-1}, D_0 and D_1 are defined by equation (7.52); L and M are determined by equation (7.3.3).

The limiter functions are determined by

$$\phi_j \le \frac{(1-|c|)\,\theta_j}{\eta\,(D_{-1}\theta_j+D_0-D_1)} \quad (8.24)$$

$$\phi_j \le \frac{1-|c|+\eta D_1}{\eta\,(D_0+D_{-1}\theta_j)} \quad (8.25)$$

$$\phi_j \ge 0 \quad (8.26)$$

A limiter function called FDV4 is introduced which has the following form

$$\begin{cases} \phi_j = \frac{(1-|c|)\,\theta_j}{\eta\,(D_{-1}\theta_j+D_0-D_1)} & for\ \ 0 \le \theta_j < \theta^L \\ \phi_j = 1 & for\ \ \theta^L \le \theta_j \le \theta^R \\ \phi_j = \frac{1-|c|+\eta D_1}{\eta\,(D_0+D_{-1}\theta_j)} & for\ \ \theta_j > \theta^R \\ \phi_j = 0 & for\ \ \theta_j < 0 \end{cases} \quad (8.27)$$

$$\begin{cases} \phi_{j+M} = \eta\,\theta_{j+M} & for\ \ 0 \le \theta_{j+M} < 0.5 \\ \phi_{j+M} = 1 & for\ \ \theta_{j+M} > 0.5 \\ \phi_{j+M} = 0 & for\ \ \phi_j = 0 \end{cases} \quad (8.28)$$

where

$$\theta^L = \frac{\eta(D_0-D_1)}{1-|c|-\eta D_{-1}} \quad (8.29)$$

$$\theta^R = \frac{1-|c|+\eta(D_1-D_0)}{\eta D_{-1}} \quad (8.30)$$

Figure 8.7 shows the comparison between the exact solution (line) and the numerical results (symbol) after 1000 time steps. (a) and (b) are the results for Courant number $|c| = 0.5$; (c) and (d) are the results for $|c| = 0.8$. The results indicate that the FDV4 limiter function can give very satisfactory solution for viscous flows.

For viscous system of equations the FDV4 has exactly the same form as equations (6.30)-(6.33), however the coefficients $D^{(p)}_{j+1/2}$, $D^{(p)}_{j+L+1/2}$, $D^{(p)}_{j+M+1/2}$ are calculated by

$$D^{(p)}_{j+L+\frac{1}{2}} = \frac{1}{12}+\frac{1}{12|Re^{(p)}_{j+L+\frac{1}{2}}|}+\left(\frac{1}{24}-\frac{1}{2|Re^{(p)}_{j+L+\frac{1}{2}}|}-\frac{1}{2(Re^{(p)}_{j+L+\frac{1}{2}})^2}\right)|c^{(p)}_{j+L+\frac{1}{2}}|$$

$$- \left(\frac{1}{12} + \frac{1}{2|Re^{(p)}_{j+L+\frac{1}{2}}|} \right) (c^{(p)}_{j+L+\frac{1}{2}})^2 - \frac{|(c^{(p)}_{j+L+\frac{1}{2}})^3|}{24} \tag{8.31}$$

$$D^{(p)}_{j+\frac{1}{2}} = \frac{1}{2} - \frac{7}{6|Re^{(p)}_{j+\frac{1}{2}}|} + \left(\frac{1}{(Re^{(p)}_{j+\frac{1}{2}})^2} - \frac{7}{12} \right) |c^{(p)}_{j+\frac{1}{2}}| + \frac{(c^{(p)}_{j+\frac{1}{2}})^2}{|Re^{(p)}_{j+\frac{1}{2}}|} + \frac{|(c^{(p)}_{j+\frac{1}{2}})^3|}{12} \tag{8.32}$$

$$D^{(p)}_{j+M+\frac{1}{2}} = \frac{1}{12|Re^{(p)}_{j+M+\frac{1}{2}}|} - \frac{1}{12} + \left(\frac{1}{24} + \frac{1}{2|Re^{(p)}_{j+M+\frac{1}{2}}|} - \frac{1}{2(Re^{(p)}_{j+M+\frac{1}{2}})^2} \right) |c^{(p)}_{j+M+\frac{1}{2}}|$$

$$+ \left(\frac{1}{12} - \frac{1}{2|Re^{(p)}_{j+M+\frac{1}{2}}|} \right) (c^{(p)}_{j+M+\frac{1}{2}})^2 - \frac{|(c^{(p)}_{j+M+\frac{1}{2}})^3|}{24} \tag{8.33}$$

When solving viscous flows using the fourth-order scheme (6.26) the inviscid limiter function FD4 might be replaced by the FDV4 limiter function.

8.5 Numerical Test on One-dimensional Navier-Stokes Equations

In this section the simplest one-dimensional (1-D) Navier-Stokes equations is chosen to test the viscous flux limiters. If we ignore heat conduction the time dependent 1-D non-dimensionalized Navier-Stokes equations can be written as

$$U_t + (F^I + F^V)_x = 0 \tag{8.34}$$

where

$$U = \begin{pmatrix} \rho \\ \rho u \\ E \end{pmatrix}, \quad F^I = \begin{pmatrix} \rho u \\ \rho u^2 + p \\ u(E+p) \end{pmatrix}, \quad F^V = \begin{pmatrix} 0 \\ -\frac{4}{3Ro} u_x \\ -\frac{4}{3Ro} u u_x \end{pmatrix} \tag{8.35}$$

$$p = (\gamma - 1) \left(E - \frac{1}{2} \rho u^2 \right) \tag{8.36}$$

Here ρ, u, ρu, p, and E are the density, velocity, momentum, pressure, and total energy, respectively, which are non-dimensionalized by a characteristic length and velocity; the γ is the ratio of specific heats; Ro is the characteristic Reynolds number.

Roe's Riemann solver is used to find the inviscid flux F^I and second-order central differencing is applied to define the viscous flux F^V. Therefore the numerical flux of equation

(8.34) is

$$F_{j+\frac{1}{2}} = F^I_{j+\frac{1}{2}} + F^V_{j+\frac{1}{2}} \tag{8.37}$$

Note, it is the inviscid flux $F^I_{j+\frac{1}{2}}$ that needes to be limited. When applying viscous limiter functions the continuity equation is limited by an inviscid limiter function and the others are limited by a viscous limiter function.

A modified Sod's problem was selected to carry out the test. The problem consists of initial data:

$$\begin{cases} (\rho,\ u,\ p) = (0.42,\ 0.9275,\ 0.30313) & 0 \le x \le 0.5 \\ (\rho,\ u,\ p) = (0.125,\ 0,\ 0.1) & 0.5 < x \le 1.0 \end{cases} \tag{8.38}$$

Although we do not have the exact solution for this problem, we can define a very accurate solution for the problem by using very fine mesh. Therefore the domain was divided by 3000 cells and the Godunov first-order method was used for the advection flux and central difference for the viscous fluxes in order to obtain the accurate solution for the problem. These accurate results are used to compare with the numerical results. In figures 8.8 ($Ro = 1000$) and 8.9 ($Ro = 500$), the lines present the accurate solutions (density) and the symbols are the numerical solutions (density) which were computed in a domain which is divided by 100 cells at time 0.2 units. (a), (b) and (c) show the comparison between the accurate solution and numerical results obtained by the second-order method (6.10) with the inviscid MINMOD limiter, the second-order method with viscous FDV2B limiter function and the the third-order method with viscous FDV3 limiter function, respectively.

As expected the inviscid MINMOD limiter gives over-diffusive solutions (a). The solutions obtained by the second-order method with FDV2B are little better but still over-diffused (b). Clearly shown in the figures the third-order method with FDV3 can give much satisfactory results (c).

8.6 Summary

When applying high resolution schemes for hyperbolic conservation laws to deal with viscous flows, viscous flux limiters are needed, otherwise inviscid limiters will give under-diffusive solutions. In this chapter viscous TVD functions for second-, third-, and fourth-order schemes have been theoretically established for viscous flows. Viscous flux limiter functions have been proposed and tested via numerical experiments. When solving viscous problems using the second-order scheme the FDV2B limiter function is recommanded; for

third- and fourth-order schemes the FDV3 and FDV4 limiter functions can give satisfactory solutions.

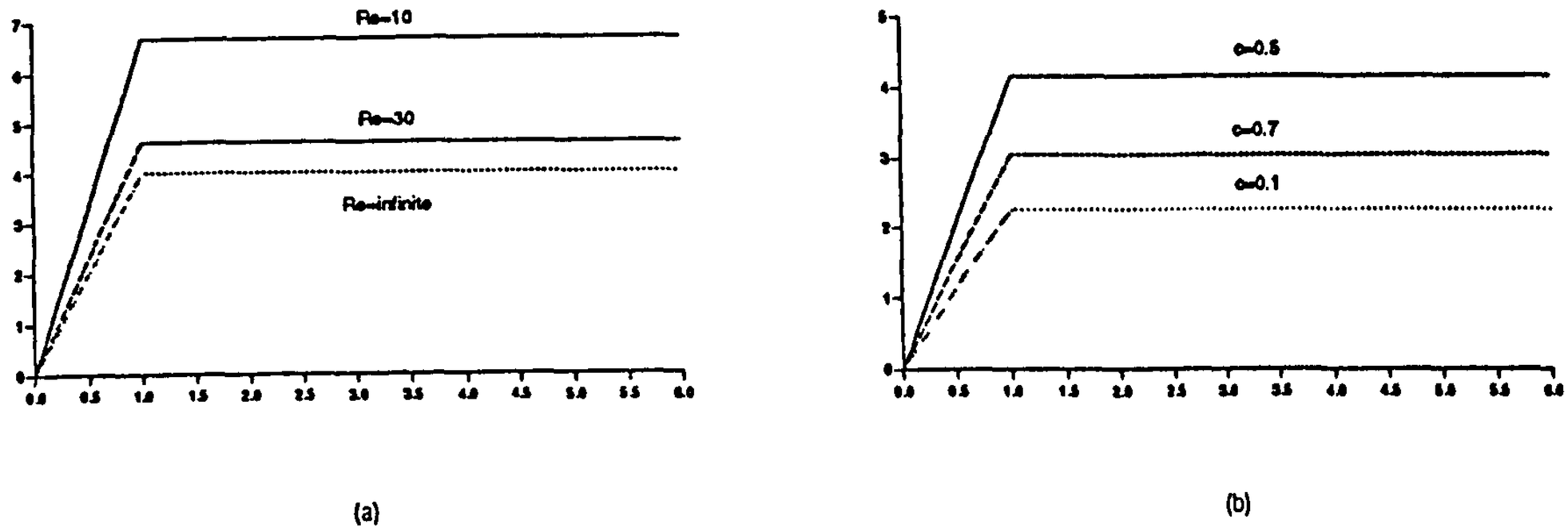

Figure 8.1: Viscous TVD Region of the Second-order Scheme for (a) $|c| = 0.5$ and (b) $|Re| = 100$.

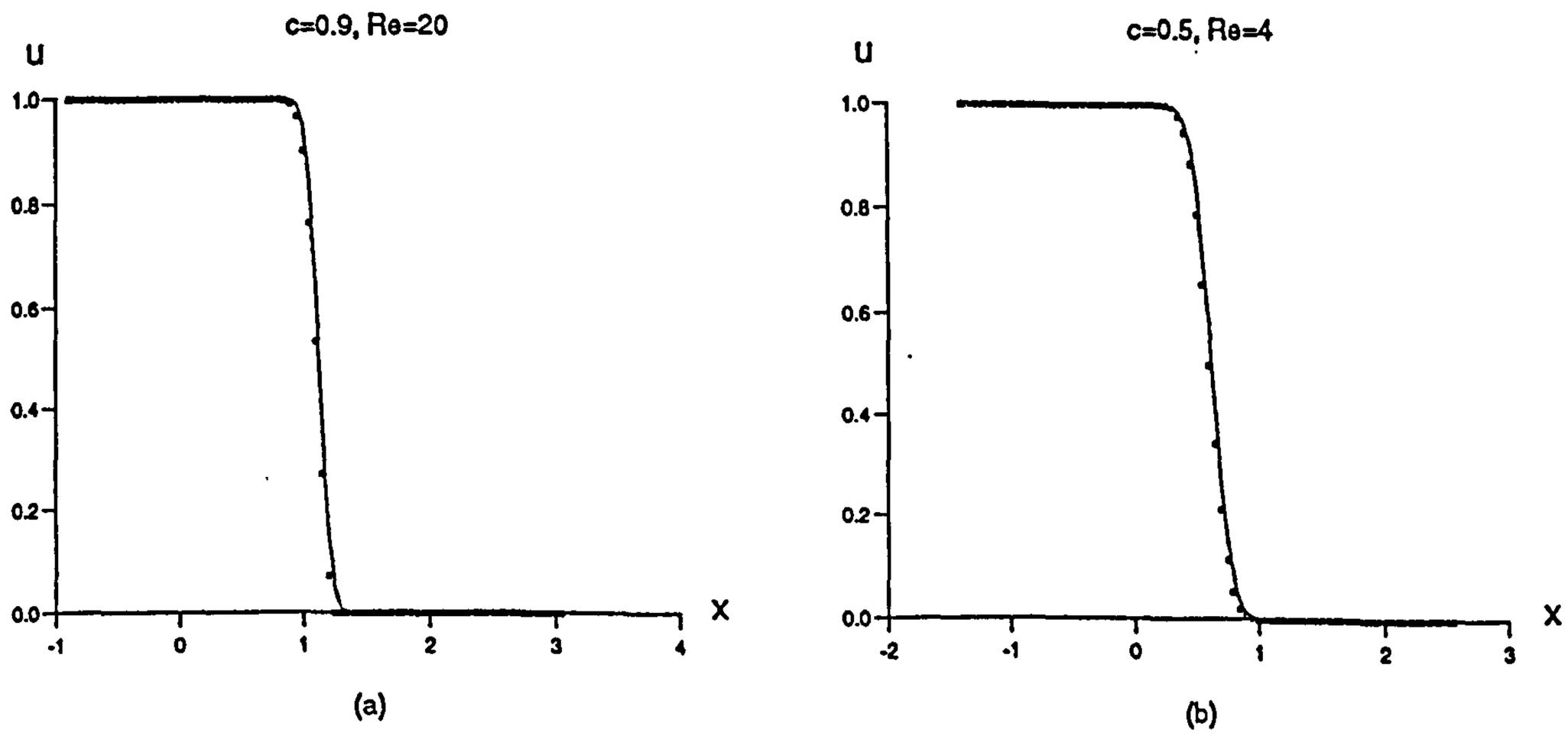

Figure 8.2: Numerical Solutions (symbol) of the Second-order Scheme without Limiter function; line is the exact solutions.

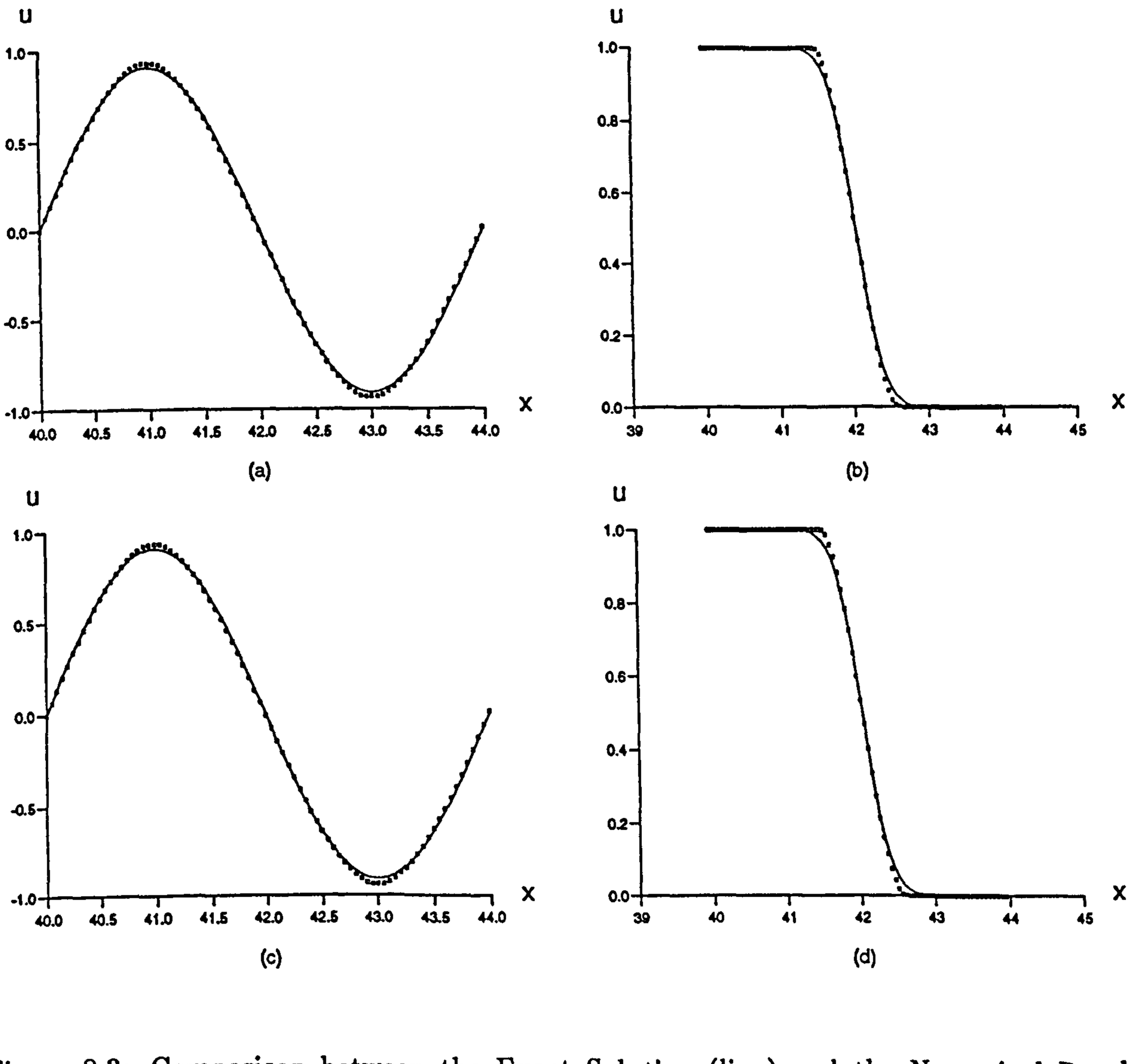

Figure 8.3: Comparison between the Exact Solution (line) and the Numerical Results (symbol) after 1000 Time Steps for $|Re| = 50$ and $|c| = 0.8$: (a) (b) by the Superbee; (c) (d) by the FDV2A Limiter function.

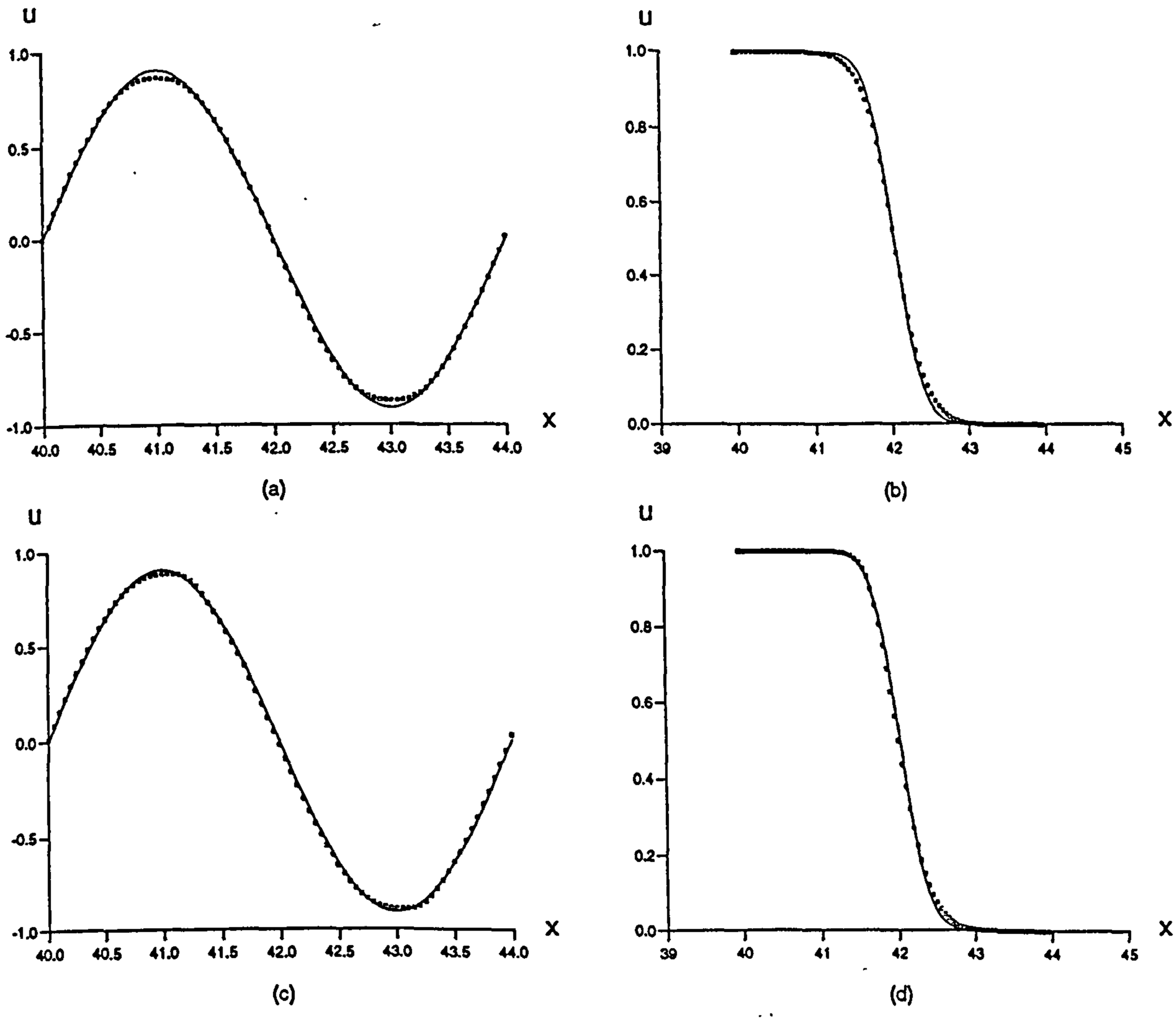

Figure 8.4: Comparison between the Exact Solution (line) and the Numerical Results (symbol) after 1000 Time Steps for $|Re| = 50$ and $|c| = 0.8$: (a) (b) by the Minmod; (c) (d) by the FDV2B Limiter function.

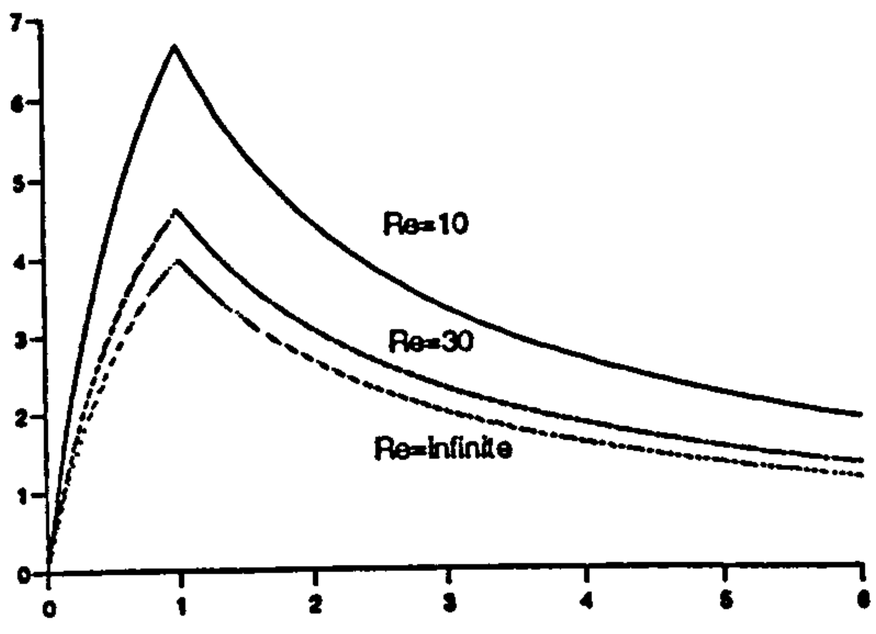

(a)

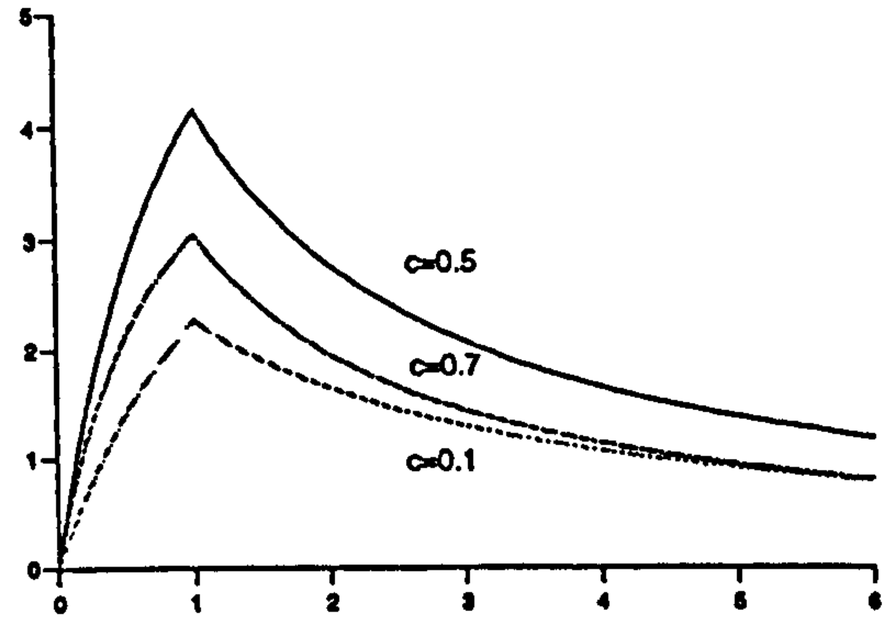

(b)

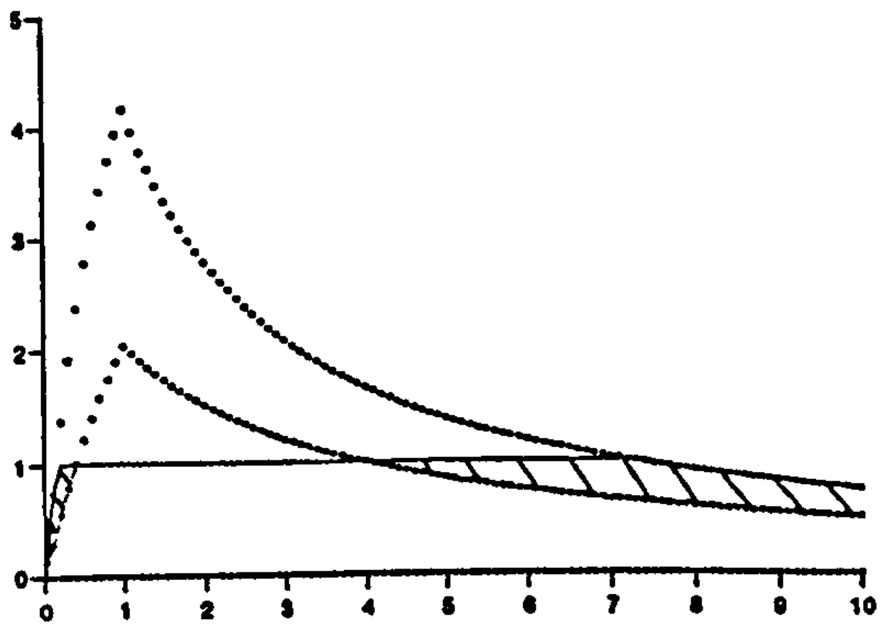

(c)

Figure 8.5: (a) Viscous TVD Region of the Third-order Scheme for $|c| = 0.5$; (b) Viscous TVD Region of the Third-order Scheme for $|Re| = 100$; (c) FD3V Limiter (shaded part).

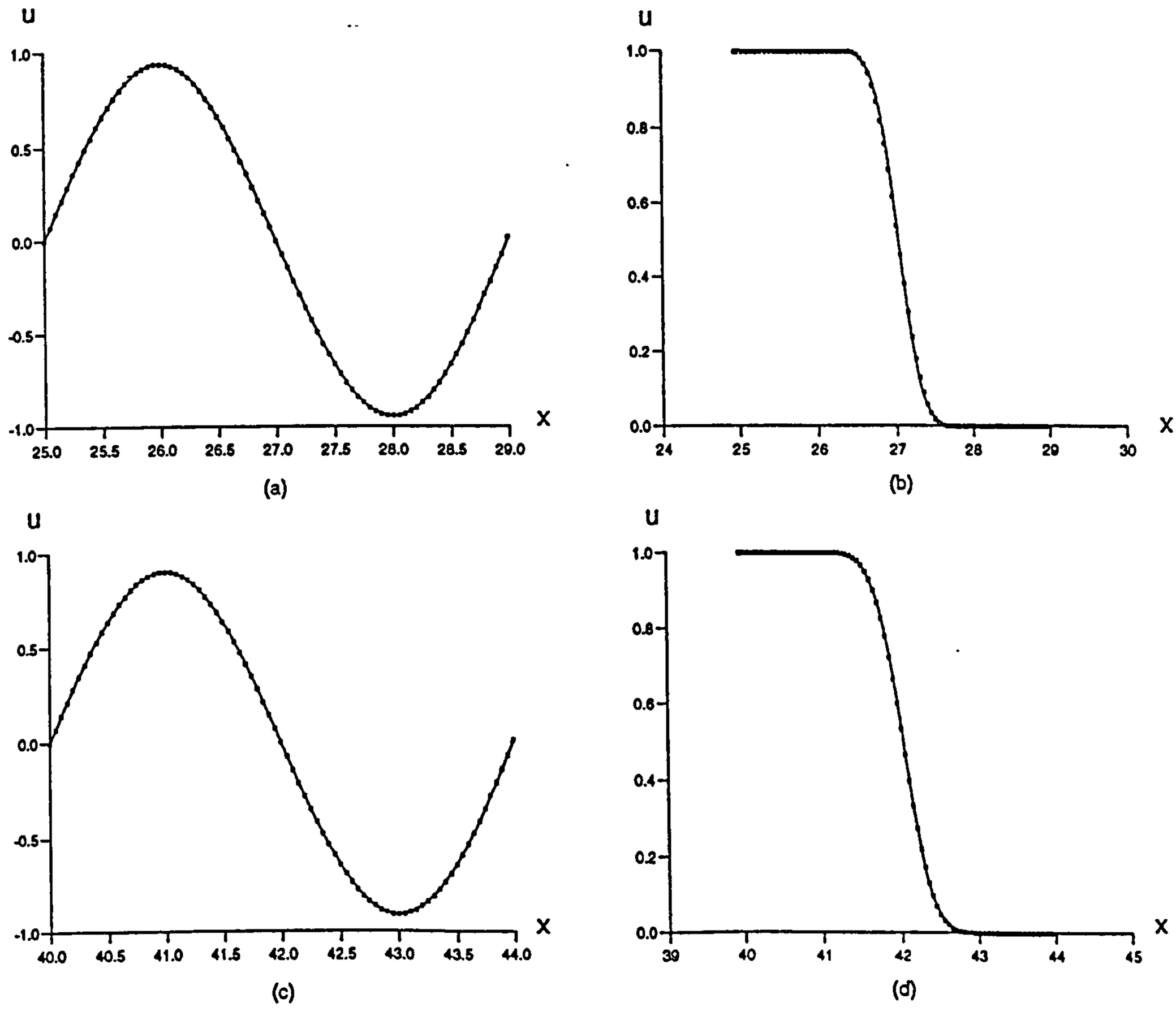

Figure 8.6: Comparison between the Exact Solution (line) and the Numerical Results (symbol) by the FDV3 Limiter function after 1000 Time Steps: (a) (b) for $|c| = 0.5$; (c) (d) for $|c| = 0.8$.

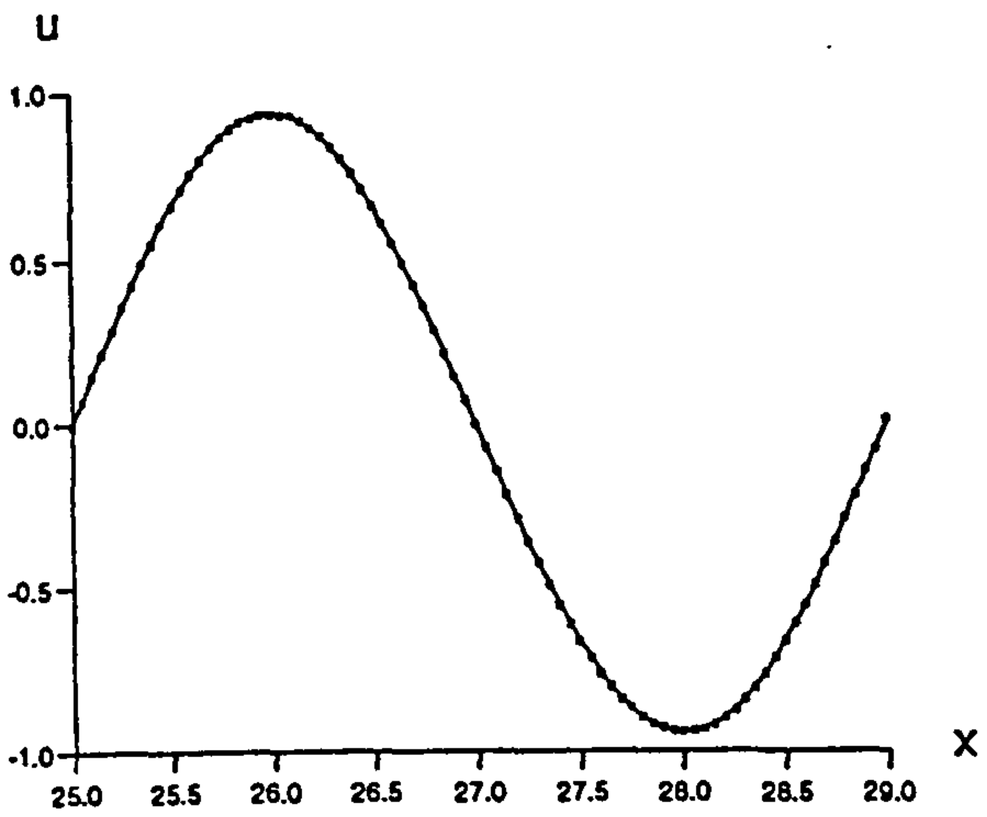

Figure 8.7: Comparison between the Exact Solution (line) and the Numerical Results (symbol) by the FDV4 Limiter function after 1000 Time Steps: (a) (b) for $|c| = 0.5$; (c) (d) for $|c| = 0.8$.

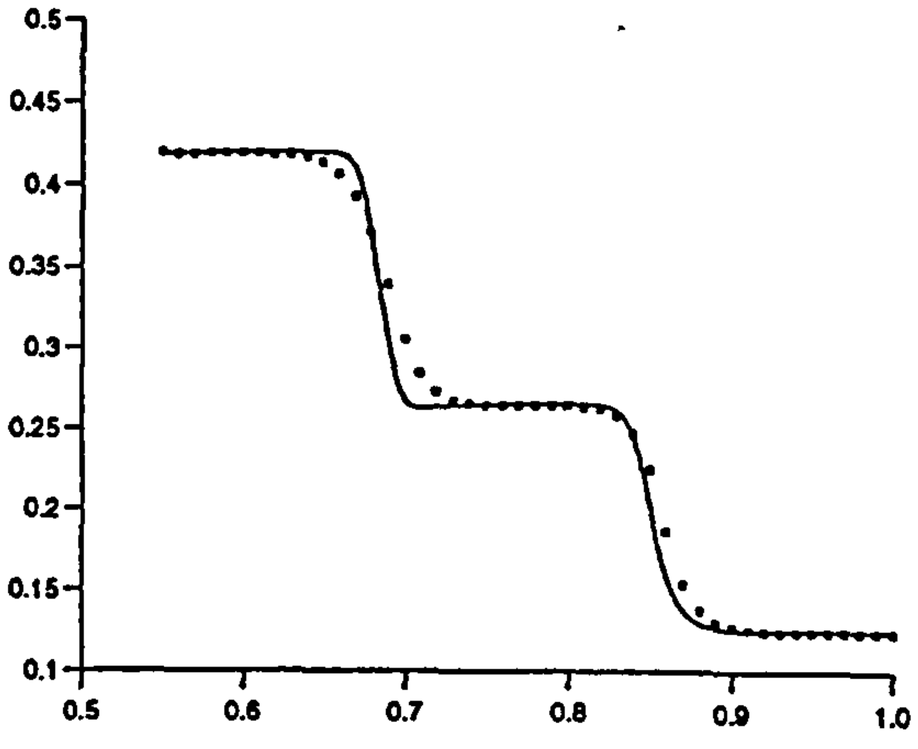

Figure 8.8: Comparison between the Numerical Solutions (symbol) and an Accurate Result (line) for $Ro = 1000$: (a) 2-order Method with the Inviscid Minmod limiter (symbol); (b) 2-order Method with the FDV2B Limiter function (symbol); (c) 3-order Method with the FDV3 Limiter function (symbol).

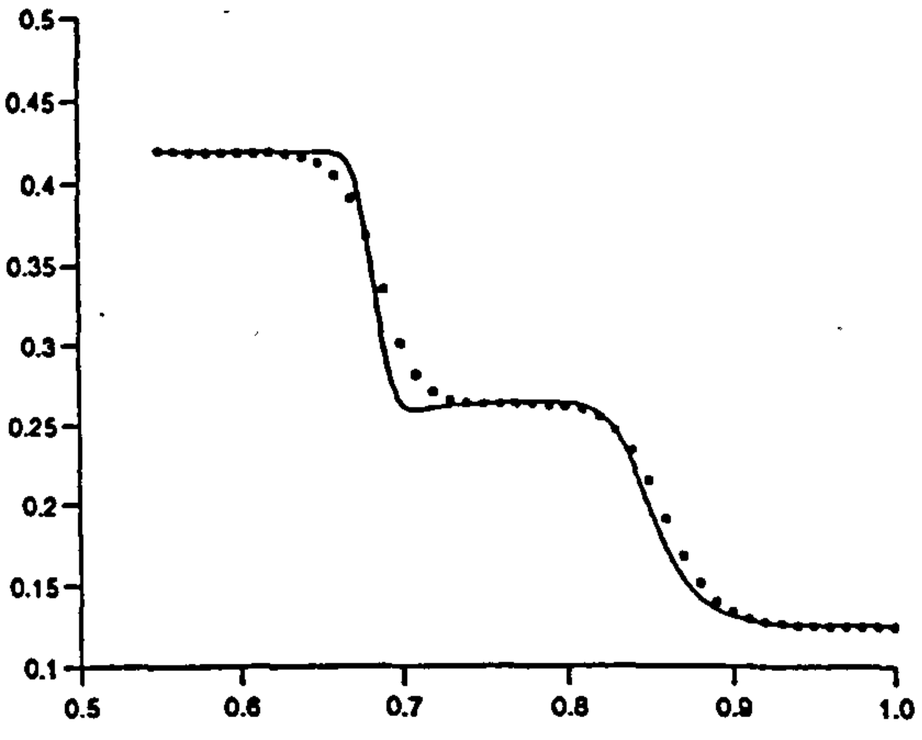

(a)

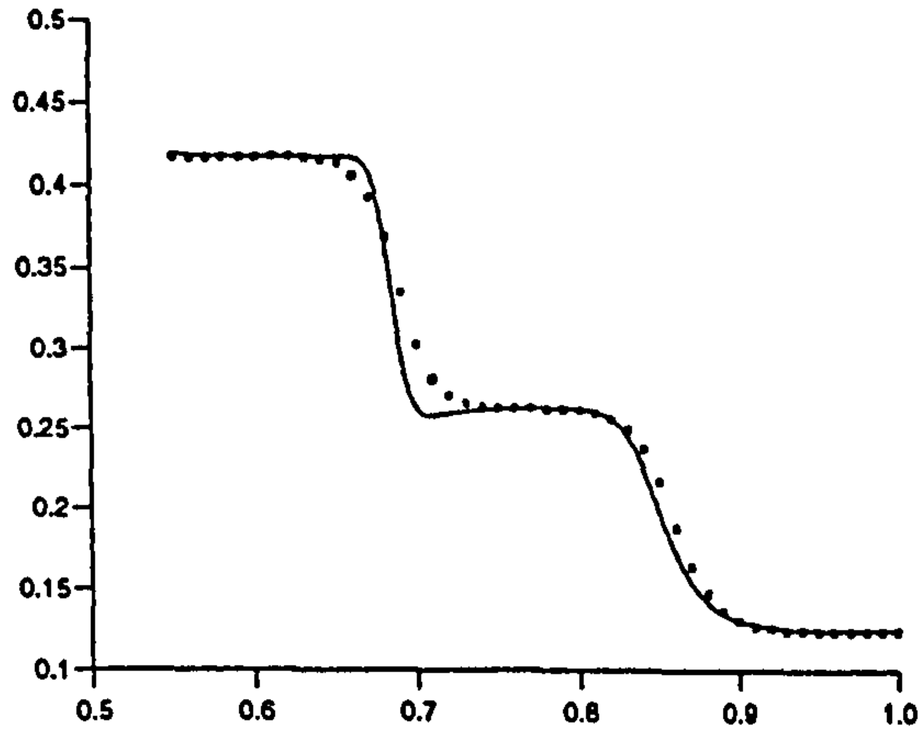

(b)

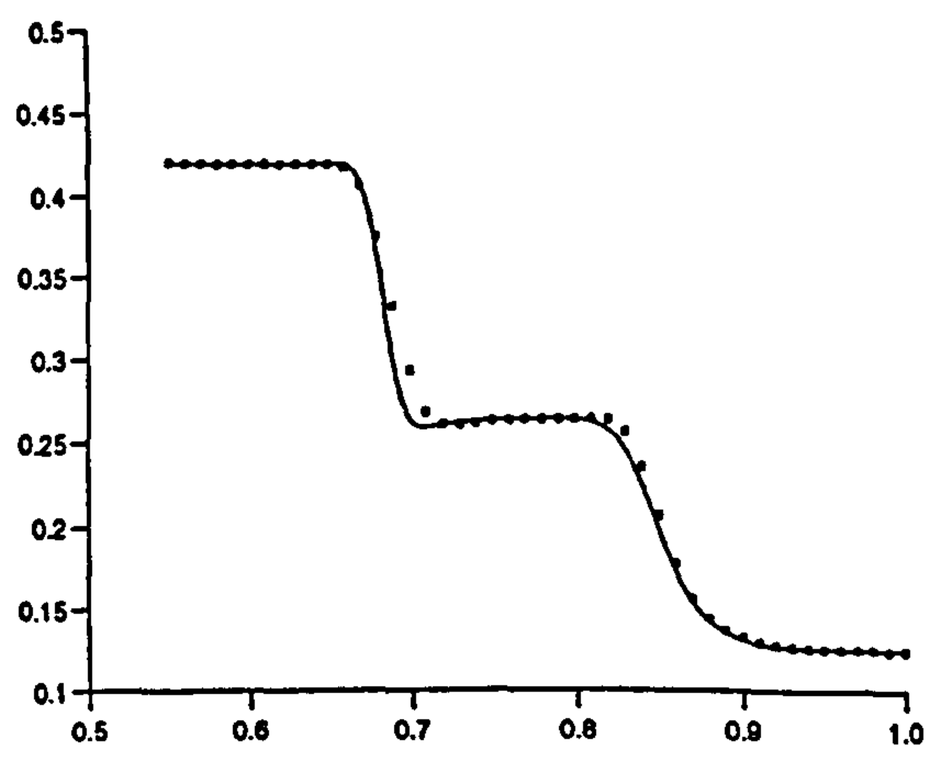

(c)

Figure 8.9: Comparison between the Numerical Solutions (symbol) and an Accurate Result (line) for $Ro = 500$: (a) 2-order Method with the Inviscid Minmod limiter (symbol); (b) 2-order Method with the FDV2B Limiter function (symbol); (c) 3-order Method with the FDV3 Limiter function (symbol).

Chapter 9

High-order Solutions for Steady Incompressible Flows

9.1 Introductory Remarks

In chapter 7 high-order fully discrete schemes for a model advection-diffusion equation are developed. In this chapter these schemes are extended to solve steady incompressible flows. Incompressible flows cover a wide variety of applications which include fluid motion of water and low speed air. Therefore the solution of the incompressible Navier-Stokes equations is of great interest in industry. The major difficulty for computation of the incompressible flows lies in the absence of the time derivative of density. Thus the pressure term can not be explicitly updated with the velocity marching advance. Hence the time-dependent methods suitable for compressible equations can not be applied without adaptation.

In order to overcome the problem great efforts have been made towards defining a way of coupling the pressure to the divergence-free velocity. Due to the means of coupling in the form of primitive variables these approaches may be classified into two categories: pressure correction methods [70] [71] and [72] and artificial compressibility methods [73] [74] [75] and [76]. The pressure correction methods first solve the time dependent momentum equations; by solving a Poissson equation the pressure is then corrected proportionally to the divergence of the velocity and in turn the true velocity is obtained by vanishing the

divergence of the velocity. Therefore the pressure correction methods can be used to solve unsteady and steady incompressible viscous flows.

The artificial compressibility method was initially introduced by Chorin [73] as an efficient approach to solve a steady-state problem of viscous incompressible flows. The principle of this method is to replace the divergence-free continuity equation by a pseudo-time dependent equation with a pseudo-time derivative of the pressure which is designed to vanish as steady state is reached, where the divergence-free condition is satisfied. One remarkable feature of the approach is that the pseudo-compressible Navier-Stokes equation possesses the hyperbolic character with pseudo-pressure waves propogating with finite speed. It is the pseudo-hyperbolic nature that enables us to take advantage of the robust, upwind, Riemann-problem based techniques for viscous incompressible flows.

In this chapter a new approach for the steady incompressible viscous fluid flows is investigated. This is based on the high-order viscous numerical schemes introduced in chapter 7 and a modified artificial compressibility continuity equation which is different from that introduced by Chorin. The feature of the approach is that the steady incompressible Navier-stokes equation is solved in the similar manner as hyperbolic conservation laws. Therefore all techniques suitable for hyperbolic systems can be similarly extended to the incompressible viscous system. To illustrate the approach the numerical experiments of the driven cavity problem proposed by Shih [80] are presented. The computational results agree with the exact solution well.

The rest of the chapter is organised as follows: Section 2 discusses the governing incompressible Navier-Stokes equations and the modified artificial compressibility incompressible Navier-Stokes equations used in the chapter; section 3 discusses the linear system of advection-diffusion equations and extends the scalar high-order viscous numerical schemes introduced in chapter 7 to linear advection-diffusion systems; section 4 discusses the nonlinear advection-diffusion systems and presents Riemann solvers for the artificial compressibility incompressible Navier-Stokes equations; section 5 applies the high-order, Riemann-problem based schemes to solve the steady incompressible two-dimensional driven cavity flows; and section 6 is the summary.

9.2 Artificial Compressibility Navier-Stokes Equations

The system of incompressible Navier-Stokes equations in a vector form reads

$$\frac{\partial u}{\partial t} + u \cdot \nabla u + \nabla p = \frac{1}{Ro} \nabla^2 u \tag{9.1}$$

$$\nabla \cdot u = 0 \tag{9.2}$$

where u, p, t are the velocity, pressure, real time, respectively, which are non-dimensionlized by a characteristic lengh and a velocity. Ro is the characteristic Reynolds number.

To apply the artificial compressibility method the continuity equation (9.2) is replaced by the following pseudo-time dependent equation [73]

$$\frac{\partial p}{\partial t} + \delta^2 \nabla \cdot u = 0 \tag{9.3}$$

where δ is the constant artificial compressibility parameter. Note that in such a definition the time t in the pseudo-compressibility system (9.1) and (9.3) has become a pseudo time. Thereby the solution of the transient behaviour loses its physical meaning until the steady state is approached asymptotically in the pseudo-time, where the time derivatives in the pseudo-system vanish so that the divergence-free velocity is satisfied.

For a reason which will be explained in a due course equation (9.3) is modified to the following form

$$\frac{\partial p}{\partial t} + \delta^2 \nabla \cdot u = \frac{1}{Ro} \nabla^2 p \tag{9.4}$$

As is known that for flows with low Reynolds number the pressure approximately satisfies the Laplace equation, i.e. $\nabla^2 p \doteq 0$, while for relatively large Reynolds number flows the magnitude of coefficient $\frac{1}{Ro}$ is small. Therefore when steady state is reached the right hand side of the equation is always very small.

Combining equation (9.1) with equation (9.4) the two dimensional pseudo-compressible Navier-Stokes equations in cartesian coordinates take on the following form

$$U_t + F(U)_x + G(U)_y = N \nabla^2 U \tag{9.5}$$

$$U = \begin{pmatrix} p \\ u \\ v \end{pmatrix}, \quad F(U) = \begin{pmatrix} \delta^2 u \\ u^2 + p \\ uv \end{pmatrix}, \quad G(U) = \begin{pmatrix} \delta^2 v \\ uv \\ v^2 + p \end{pmatrix} \tag{9.6}$$

$$N = \begin{pmatrix} \frac{1}{Ro} & 0 & 0 \\ 0 & \frac{1}{Ro} & 0 \\ 0 & 0 & \frac{1}{Ro} \end{pmatrix} \tag{9.7}$$

Here u and v are the velocity components in x and y direction respectively.

One way of treating multi-dimensional problems is to apply the method of fractional steps or operator splitting [77]. In this approach the viscous system (9.5) can be split into two augmented one-dimensional viscous systems

$$U_t + F(U)_x = N\ U_{xx} \tag{9.8}$$

and

$$U_t + G(U)_y = N\ U_{yy} \tag{9.9}$$

then the solution of (9.5) can be obtained by solving equations (9.8) and (9.9) using *Strang splitting* (see chapter 6). Note that since the final solution is in a steady-state, there is no effect of time accuracy in the splitting approach. Therefore it is reasonable that from now on we turn our attention to study the system of one-dimensional advection-diffusion equations.

9.3 Linear Advection-diffusion Systems

In the last section the nonlinear parabolic system was derived. In order to understand the solution structure of the system and justify the Riemann-problem based approach, for convenience we first study the initial-value problem for a one-dimensional linear advection-diffusion system with constant coefficients.

$$\begin{aligned} &U_t + AU_x = N\ U_{xx} \\ &U(x,0) = U_0(x) \end{aligned} \tag{9.10}$$

where, U are vector functions of m conserved variables, $A = F'(U)$ is a m by m constant matrix, and Q is a m by m diagonal diffusive coefficient matrix.

If we ignore the viscous terms on the right hand side of equation (9.10), then equation (9.10) reduces to a system of conservation laws with only advective flux function $F(U) = AU$. We know that the system is hyperbolic if A is diagonalizable with real eigenvalues, i.e. the matrix A can be expressed by equation (6.2) or (6.3).

9.3.1 Characterestic Variables

We can decouple the linear systems into m independent scalar equations in terms of the *characteristice variables* which is defined by

$$V = R^{-1}U \tag{9.11}$$

However with the viscous terms on the right hand side of equation (9.10) the system is parabolic. Nevertheless we still adopt the definition of equation (9.11) and transform the viscous system (9.10) into characteristic variables by multiplying equation (9.10) by R^{-1}

$$R^{-1}U_t + \Lambda R^{-1}U_x = R^{-1}N\ U_{xx} \tag{9.12}$$

i.e.

$$V_t + \Lambda V_x = N\ V_{xx} \tag{9.13}$$

since $R^{-1}N\ R = N$. Note that the viscous system (9.10) is absolutely decoupled into m independent scalar advection-diffusion equations

$$\begin{cases} v_t^{(p)} + \lambda^{(p)} v_x^{(p)} = \nu\ v_{xx}^{(p)} \\ p = 1, 2, \ldots, m \end{cases} \tag{9.14}$$

Recall that in the artificial compressibility equation (9.5) $\nu = 1/Ro$, This is why the artificial compressibility equation is modified in the form of equation (9.4).

Applying the viscous numerical schemes introduced in chapter 7 the solutions of $v^{(p)}(x,t)$ for each of these scalar advection-diffusion equations can be computed. Then the original solution of equation (9.10) can be transformed back via

$$U(x,t) = RV(x,t) \tag{9.15}$$

i.e.

$$U(x,t) = \sum_{p=1}^{m} v^{(p)}(x,t)\ r^{(p)} \tag{9.16}$$

The analysis procedure and the solution (9.16) looks much like that of hyperbolic conservation laws except that the values of $v^{(p)}$ no longer hold constant along characteristic lines for each scalar equation, in other words they no longer simply advect with the initial values since

$$\begin{aligned} \frac{dv^{(p)}}{dt} &= v_t^{(p)} + \frac{dx}{dt} v_x^{(p)} \\ &= v_t^{(p)} + \lambda^{(p)} v_x^{(p)} \\ &= \nu v_{xx}^{(p)} \end{aligned} \tag{9.17}$$

Instead of the right hand side being zero, it is $\nu v_{xx}^{(p)}$. This means that apart from advection the values of $v^{(p)}$ are diffused with time evolution at the rate of $\nu v_{xx}^{(p)}$. However, the characteristic curve is still a straight line since

$$\frac{dx}{dt} = \lambda^{(p)} \tag{9.18}$$

i.e.

$$x = \lambda^{(p)} t + x_0$$

here $x = x_0$ when $t = 0$.

Therefore the solution of equation (9.16) can be viewed as the superposition of m waves, each of which is not only advected independently with propagating speed $\lambda^{(p)}$, but also diffused independently at the dissipating rate $\nu v_{xx}^{(p)}$.

9.3.2 High-order Viscous Schemes for Linear Systems

In this section we extend the scalar viscous schemes developed in chapter 7 to the system of advection-diffusion equations. The strategy of the extension is exactly the same as we did in Chpter 6.

Three-point Centered Viscous Scheme for Systems

Applying equation (6.7) the three-point viscous flux (see equation (7.23)) which has first-order accuracy in time and second-order in space, i.e. order (1,2), can be extended to systems as follows.

$$\begin{aligned} F_{j+\frac{1}{2}} &= \frac{1}{2}(F_j^n + F_{j+1}^n) - \frac{1}{2}\sum_{p=1}^{m} |\lambda_{j+\frac{1}{2}}^{(p)}|\ \alpha_{j+\frac{1}{2}}^{(p)}\ r_{j+\frac{1}{2}}^{(p)} \\ &+ \sum_{p=1}^{m} \left(\frac{1}{2} - 1/|Re_{j+\frac{1}{2}}^{(p)}| - |c_{j+\frac{1}{2}}^{(p)}|/2\right) |\lambda_{j+\frac{1}{2}}^{(p)}|\ \alpha_{j+\frac{1}{2}}^{(p)}\ r_{j+\frac{1}{2}}^{(p)} \end{aligned} \tag{9.19}$$

Here recall

$$\begin{cases} c_{j+\frac{1}{2}}^{(p)} = \dfrac{\lambda_{j+\frac{1}{2}}^{(p)}\ k}{h} \\ Re_{j+\frac{1}{2}}^{(p)} = \dfrac{\lambda_{j+\frac{1}{2}}^{(p)}\ h}{\nu} \end{cases}$$

Five-point Upwind-baised Viscous Scheme for Systems

Similarly the numerical flux of the four-point scheme (7.47) (order (1,3)) for systems is

$$F_{j+\frac{1}{2}} = \frac{1}{2}(F_j^n + F_{j+1}^n) - \frac{1}{2}\sum_{p=1}^{m} |\lambda_{j+\frac{1}{2}}^{(p)}|\ \alpha_{j+\frac{1}{2}}^{(p)}\ r_{j+\frac{1}{2}}^{(p)}$$
$$+ \sum_{p=1}^{m}\left(D_{j+\frac{1}{2}}^{(p)}\ |\lambda_{j+\frac{1}{2}}^{(p)}|\ \alpha_{j+\frac{1}{2}}^{(p)}\ r_{j+\frac{1}{2}}^{(p)} + D_{j+L+\frac{1}{2}}^{(p)}\ |\lambda_{j+L+\frac{1}{2}}^{(p)}|\ \alpha_{j+L+\frac{1}{2}}^{(p)}\ r_{j+L+\frac{1}{2}}^{(p)}\right) \quad (9.20)$$

Here $D_{j+1/2}^{(p)}$ and $D_{j+L+1/2}^{(p)}$ are defined by equations (8.18) and (8.19); L is determined by equation (8.22).

Five-point Centered Viscous Scheme for Systems

The scalar five-point scheme (7.51) (order (2,4)) can be extended to systems to give

$$F_{j+\frac{1}{2}} = \frac{1}{2}(F_j^n + F_{j+1}^n) - \frac{1}{2}\sum_{p=1}^{m} |\lambda_{j+\frac{1}{2}}^{(p)}|\ \alpha_{j+\frac{1}{2}}^{(p)}\ r_{j+\frac{1}{2}}^{(p)}$$
$$+\sum_{p=1}^{m}\left(D_{j+\frac{1}{2}}^{(p)}\ \lambda_{j+\frac{1}{2}}^{(p)}\ \alpha_{j+\frac{1}{2}}^{(p)}\ r_{j+\frac{1}{2}}^{(p)} + D_{j+L+\frac{1}{2}}^{(p)}\ \lambda_{j+L+\frac{1}{2}}^{(p)}\ \alpha_{j+L+\frac{1}{2}}^{(p)}\ r_{j+L+\frac{1}{2}}^{(p)}\right.$$
$$\left.+D_{j+M+\frac{1}{2}}^{(p)}\ \lambda_{j+M+\frac{1}{2}}^{(p)}\ \alpha_{j+M+\frac{1}{2}}^{(p)}\ r_{j+M+\frac{1}{2}}^{(p)}\right) \quad (9.21)$$

Here $D_{j+L+1/2}^{(p)}$, $D_{j+1/2}^{(p)}$ and $D_{j+M+1/2}^{(p)}$ are defined by equations (8.31), (8.32) and (8.33); L and M are determined by equation (6.38).

9.4 Nonlinear Advection-diffusion Systems

In this section we extend our discussion to nonlinear system of advection-diffusion equations

$$U_t + F(U)_x = N\ U_{xx} \quad (9.22)$$

where, $U(x,t)$ is column vector of m conserved variables; $F(U)$ is a vector-valued physical advection flux function of m components; N is a diagonal diffusive coefficient matrix.

It is said that the parabolic system of equations (9.22) has hyperbolic character if the m by m Jacobian matrix

$$A(U) = F'(U) \tag{9.23}$$

is diagonalizable with real eigenvalues $\lambda^{(1)}(U), \lambda^{(2)}(U), \ldots, \lambda^{(m)}(U)$.

Let us take the one-dimensional artificial compressibility Navier-Stokes equations (9.8) introduced in section 9.2 for example. The eigenvalues of the Jocabin matrix $F'(U)$ of equation (9.8) are

$$\lambda^{(1)}(U) = u - a, \quad \lambda^{(2)}(U) = u, \quad \lambda^{(3)}(U) = u + a \tag{9.24}$$

where

$$a = \sqrt{u^2 + \delta^2} \tag{9.25}$$

is analogous to the sound speed in the Euler equations. The corresponding right eigenvectors are

$$r^{(1)}(U) = \begin{pmatrix} -(a+u) \\ 1 \\ -v/a \end{pmatrix}, \quad r^{(2)}(U) = \begin{pmatrix} 0 \\ 0 \\ 1 \end{pmatrix}, \quad r^{(3)}(U) = \begin{pmatrix} a-u \\ 1 \\ v/a \end{pmatrix} \tag{9.26}$$

The eigenvalues are not constant. The strategy for solving systems of the nonlinear equations utilizing the Riemann problem solutions was discussed in chapter 6. Therefore we need Riemann solvers for the artificial compressibility Navier-Stokes equations.

9.4.1 Flux Riemann Solvers

For the artificial compressibility Navier-Stokes equations (9.8) Roe's eigenvalues and eigenvectors are evaluated at the average state $\bar{U}$ which for the two-simensional case takes the following form

$$\bar{u} = \tfrac{1}{2}(u_j + u_{j+1}), \quad \bar{v} = \tfrac{1}{2}(v_j + v_{j+1}), \quad \bar{a} = (\bar{u}^2 + \delta^2)^{1/2} \tag{9.27}$$

The wave strengths $\bar{\alpha}^{(p)}$ are determined by

$$\begin{cases} \bar{\alpha}^{(1)} = \Delta p(\bar{u} + \bar{a})/2\bar{a}\delta^2 - \Delta u/2\bar{a} \\ \bar{\alpha}^{(2)} = \Delta v - \Delta p\bar{v}/\bar{a}^2 - \Delta u\bar{v}\bar{u}/\bar{a}^2 \\ \bar{\alpha}^{(3)} = \Delta u/2\bar{a} - \Delta p(\bar{u} - \bar{a})/2\bar{a}\delta^2 \end{cases} \tag{9.28}$$

here

$$\Delta u = u_{j+1} - u_j, \quad \Delta v = v_{j+1} - v_j, \quad \Delta p = p_{j+1} - p_j$$

For splitting system (9.9) in the y direction the corresponding eigenvalues and eigenvectors can be obtained by interchanging the roles of u and v.

From the observation of the eigenvalues (9.24) we know that the eigenvalue $\lambda^{(1)}$ is always negative and the $\lambda^{(3)}$ always positive, i.e. there is no sonic point in the Riemann solution. This is indeed a very pleasant feature of the artificial compressibility Navier-Stokes equations because there is no fear of failure caused by entropy-violating when applying an approximate Riemann solver.

9.4.2 State Riemann Solvers

Two state Riemann solvers, the exact solver and the approximate linearized solver, are given in the section, which is introduced by Darling in [78].

Exact Riemann Solver

The exact Riemann solver has the following form

$$f_j(u_j, u^*) + f_{j+1}(u_{j+1}, u^*) - \Delta p = 0 \tag{9.29}$$

$$f_k(u_k, u^*) = \begin{cases} \frac{1}{2}\left[u_k^2 + u_k\left(\delta^2 + u_k^2\right)^{1/2} + \delta^2\, arcsinh(\frac{u_k}{\delta})\right. \\ \left. -\left(u^{*2} + u^*\left(\delta^2 + u^{*2}\right)^{1/2} + \delta^2\, arcsinh(\frac{u^*}{\delta})\right)\right] \\ \quad (for\ \ rarefactions) \\ \frac{1}{2}(u_k - u^*)\left[\left((u_k + u^*)^2 + 4\delta^2\right)^{1/2} + (u_k + u^*)\right] \\ \quad (for\ \ shocks) \end{cases} \tag{9.30}$$

Here $k = j$ or $j+1$.

$$v_L^* = \frac{v_j(u_j - S_j)}{u^* - S_j} \tag{9.31}$$

$$v_R^* = \frac{v_{j+1}(u_{j+1} - S_{j+1})}{u^* - S_{j+1}} \quad (for\ \ shocks) \tag{9.32}$$

where

$$S_k = \frac{\delta^2 u_k}{p_k - p^*} \tag{9.33}$$

$$\frac{v_L^*}{v_j} = \frac{u_j + (\delta^2 + u_j^2)^{1/2}}{u^* + (\delta^2 + u^{*2})1/2} \tag{9.34}$$

$$\frac{v_R^*}{v_{j+1}} = \frac{u^* + (\delta^2 + u^{*2})^{1/2}}{u_{j+1} + (\delta^2 + u_{j+1}^2)1/2} \tag{9.35}$$

(for rarefactions)

$$p^* = p_k + f_k(u_k, u^*) \tag{9.36}$$

Applying an iterative method (e.g. Newton-Raphson) the solution of equations (9.29) and (9.30) gives the value of u^*, the values of v_L^*, v_R^* and p^* are then obtained by equations (9.31)-(9.36). Once the star values at each cell interface are calculated the flux jump $\Delta F_{j+1/2}^{(p)}$ for each wave can be easily defined.

Linearized Riemann Solver

The linearized Riemann solver has the following simple form

$$p^* = \frac{1}{2\bar{a}}\left[(\bar{a}^2 - \bar{u}^2)(u_{j+1} - u_j) + (\bar{a} - \bar{u})\, p_j + (\bar{a} - \bar{u})\, p_{j+1}\right] \tag{9.37}$$

$$u^* = u_{j+1} + (p_{j+1} - p^*)/(\bar{a} + \bar{u}) \tag{9.38}$$

$$v_L^* = v_j + \frac{\bar{v}}{\bar{a}}(u_j - u^*) \tag{9.39}$$

$$v_R^* = v_{j+1} + \frac{\bar{v}}{\bar{a}}(u^* - u_{j+1}) \tag{9.40}$$

Here the $\bar{u}$, $\bar{v}$ and $\bar{a}$ are defined by equation (9.27).

9.5 Application to the Driven Cavity Problem

Because incompressible viscous flow in a driven cavity has a simple geometry and can present some interesting complex fluid dynamic features, such as vortex development and boundary-layer formation (high Reynolds number) near the walls of the cavity, the driven cavity problem has been accepted as a ideal test problem for evaluating an optimum numerical scheme for solving the incompressible Navier-Stokes equations [79].

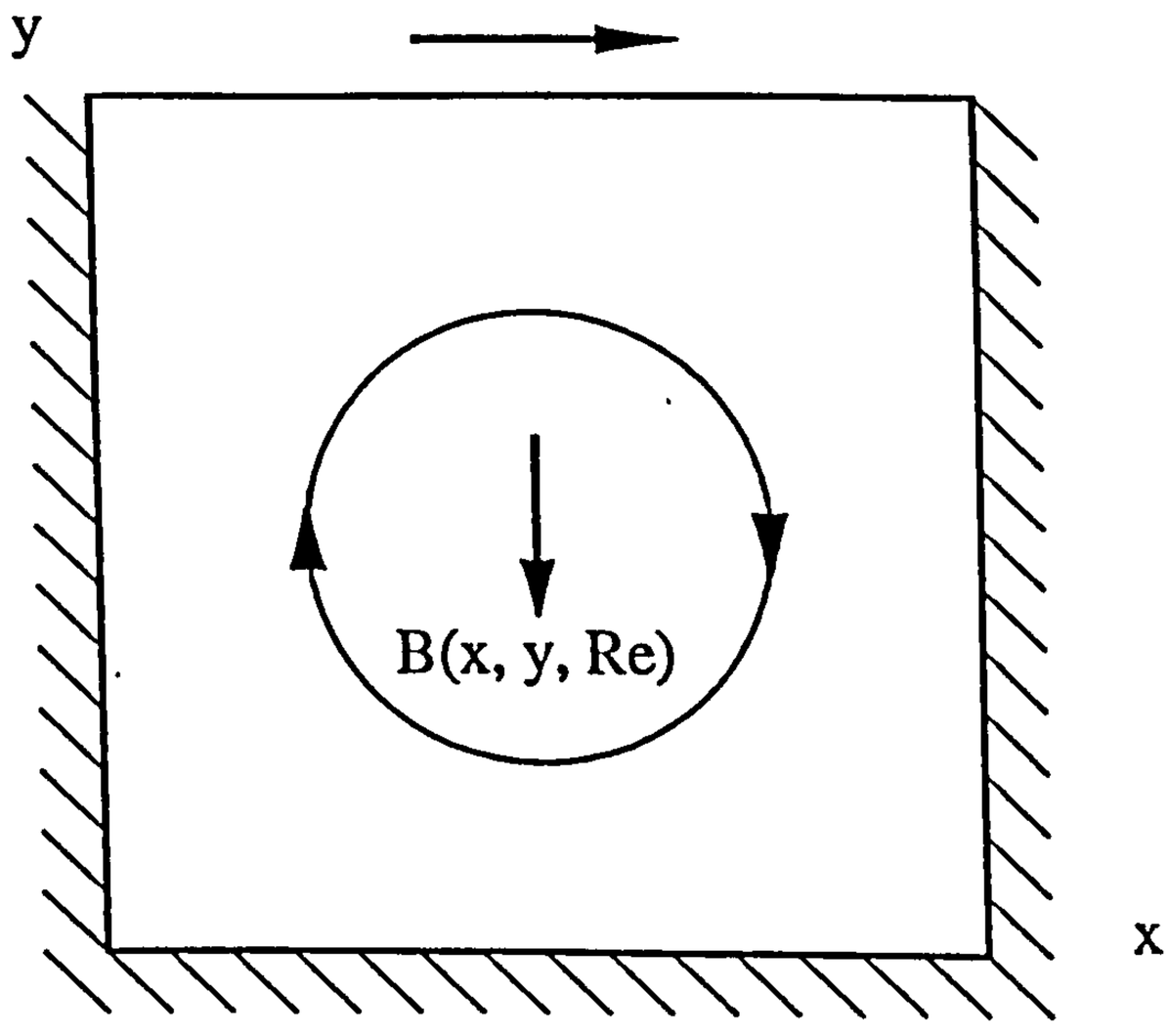

Figure 9.1: Shis's Driven Cavity Problem

The specific driven cavity problem considered in this chapter is proposed by Shih et al. [80]. Instead of the classical lid-driven cavity flow this flow is driven by combined shear and body forces. The advantage of Shih's problem is that the exact solution is known, therefore provides a reliable base to compare with.

9.5.1 The Shih's Driven Cavity Problem

The Shih's driven cavity problem considers the steady two-dimensional flows in the square cavity shown schematically in figure 9.1. The non-dimensionalized cavity size is 1 by 1. The Dirichlet boundary conditions on velocities u and v is applied, i.e. zero everwhere except the upper wall which moves in the positive x-direction with speed

$$u(x,1) = 16\left(x^4 - 2x^3 + x^2\right) \tag{9.41}$$

Differing from the classical lid-driven flow problem the Shih's problem is driven not only by the upper lid but also by a body force which is designed to give an exact solution to the Shih's problem.

The body force is present in the normal direction to the lid (y-direction in figure 9.1) and

has the following form

$$\begin{aligned} B(x,y,Ro) &= -\frac{8}{Ro}\left[24F(x)+2f_x(x)g_{yy}(y)+f_{xxx}(x)g(y)\right] \\ &\quad -64\left[F_2(x)G_1(y)-g(y)g_y(y)F_1(x)\right] \end{aligned} \tag{9.42}$$

where

$$\begin{aligned} f(x) &= x^4-2x^3+x^2 \\ g(y) &= y^4-y^2 \\ F(x) &= 0.2x^5-0.5x^4+x^3/3 \\ F_1(x) &= -4x^6+12x^5-14x^4+8x^3-2x^2 \\ F_2(x) &= 0.5[f(x)]^2 \\ G_1(y) &= -24y^5+8y^3-4y \end{aligned}$$

The exact solution to this problem is known to be

$$u(x,y) = 8\left(x^4-2x^3+x^2\right)\left(4y^3-2y\right) \tag{9.43}$$

$$v(x,y) = -8\left(4x^3-6x^2+2x\right)\left(y^4-y^2\right) \tag{9.44}$$

$$\begin{aligned} p(x,y,Ro) &= \frac{8}{Ro}\left[F(x)g_{yyy}(y)+f_x(x)g_y(y)\right] \\ &\quad +64F_2(x)\left\{g(y)g_{yyy}(y)-[g_y(y)]^2\right\} \end{aligned} \tag{9.45}$$

As shown in equations (9.43) and (9.44) the velocities u and v in the exact solution are independent of the Reynolds number and only the pressure solution is associated with the Reynolds number (see equation (9.45)).

9.5.2 The Boundary Condition

The boundary conditions specify a particular environment for a problem solved. Since the precision of the boundary conditions directly affects the quality of the computed solutions, it is worthwile considering carefully the boundary conditions.

The boundary condition imposed on the driven cavity problem is a Dirichlet condition, which simply states that the velocities of fluid and the surface of solid walles are equal at the boundary, i.e. no-slip for the flow variables on the solid walls. The boundary conditions of the driven cavity problem is defined as follows.

The Boundary Condition for Normal Velocity

To satisfy the no-slip condition, For example, along the boundary $x = 0$ the normal velocity u can be set as follows

$$\begin{aligned} u_{0,j} &= -u_{1,j} \\ u_{-1,j} &= -u_{2,j} \\ u_{-2,j} &= -u_{3,j} \\ &\vdots \end{aligned} \tag{9.46}$$

and along the boundary $x = 1$

$$\begin{aligned} u_{m+1,j} &= -u_{m,j} \\ u_{m+2,j} &= -u_{m-1,j} \\ u_{m+3,j} &= -u_{m-2,j} \\ &\vdots \end{aligned} \tag{9.47}$$

Likewise along the boundaries $y = 0$ and $y = 1$ for v.

The Boundary Condition for Tangential Velocity

Here we consider the velocities on the boundaries tangential to moving or stationary walls. To satisfy the no-slip boundary condition, for example, along $x = 0$ the tangential velocity v can be set as

$$\begin{aligned} v_{0,j} &= 2v_w - v_{1,j} \\ v_{-1,j} &= 2v_w - v_{2,j} \\ v_{-2,j} &= 2v_w - v_{3,j} \\ &\vdots \end{aligned} \tag{9.48}$$

and along the boundary $x = 1$

$$\begin{aligned} v_{m+1,j} &= 2v_w - v_{m,j} \\ v_{m+2,j} &= 2v_w - v_{m-1,j} \\ v_{m+3,j} &= 2v_w - v_{m-2,j} \\ &\vdots \end{aligned} \tag{9.49}$$

where v_w is the velovity of wall.

Likewise along the boundaries $y = 0$ and $y = 1$ for u.

Another way to obtain the boundary codnition for the tangential velocities is to solve the Riemann problems exactly in the boundary cells. In this approach the interface values in the boundary cells U^* of Riemann problems are known as, for example along $x = 0$, $u^* = 0$, $v^* = v_w$ and $p^* = p_w$.

From equations (9.31) - (9.35), after some manipulations, along boundary $x = 0$ the tangential velocities v are defined as

$$\begin{aligned} v_{0,j} &= \frac{v_w S_{0,j}}{S_{0,j} - u_{0,j}} && (for\ \ shocks) \\ v_{0,j} &= \frac{v_w \delta}{u_{0,j} + \left(\delta^2 + u_{0,j}^2\right)^{1/2}} && (for\ \ rarefactions) \end{aligned} \tag{9.50}$$

where

$$S_{0,j} = \frac{-2\delta^2}{\left(u_{0,j}^2 + 4\delta^2\right)^{1/2} + u_{0,j}}$$

and along boundary $x = 1$ the tangential velocities are

$$\begin{aligned} v_{m+1,j} &= \frac{v_w S_{m+1,j}}{S_{m+1,j} - u_{m+1,j}} && (for\ \ shocks) \\ v_{m+1,j} &= \frac{v_w \left(u_{m+1,j} + \left(\delta^2 + u_{m+1,j}^2\right)^{1/2}\right)}{\delta} && (for\ \ rarefactions) \end{aligned} \tag{9.51}$$

where

$$S_{m+1,j} = \frac{2\delta^2}{\left(u_{m+1,j}^2 + 4\delta^2\right)^{1/2} - u_{m+1,j}}$$

Note that the boundary conditions for tangential velocities are determined by the normal velocities. Since the boundary conditions for normal velocities can be explicitly defined by equations (9.46) and (9.47), the boundary conditions for tangential velocities can also be defined. This boundary conditions are used for the driven cavity problem.

The Boundary Condition for Pressure

We need the pressure at the wall to calculate the numerical fluxes across the normal boundaries. One technique for deriving the boundary pressure is to find the relationship for the pressure gradient normal to the boundary in terms of the normal velocity gradient. This can be done by applying the governing momentum equations at the boundaries. For example, along the boundary $x = 0$ where $u = v = 0 = u_t = v_t = u_y = v_y = 0$. The momentum equation in x-direction

$$\frac{\partial u}{\partial t} + \frac{\partial u^2}{\partial x} + \frac{\partial uv}{\partial y} + \frac{\partial p}{\partial x} = \frac{1}{Ro}\left(\frac{\partial^2 u}{\partial x^2} + \frac{\partial^2 v}{\partial y^2}\right) \tag{9.52}$$

reduces to

$$\left(\frac{\partial p}{\partial x}\right)_{0,j} = \frac{1}{Ro}\left(\frac{\partial^2 u}{\partial x^2}\right)_{0,j} \tag{9.53}$$

Expanding both sides of equation (9.53) about the boundary point $0, j$ in the Taylor series

$$p(x-\Delta x, y) = p - \Delta x\frac{\partial p}{\partial x} + \frac{1}{2}\Delta x^2\frac{\partial^2 p}{\partial x^2} - \ldots \tag{9.54}$$

$$u(x+\Delta x, y) = u + \Delta x\frac{\partial u}{\partial x} + \frac{1}{2}\Delta x^2\frac{\partial^2 u}{\partial x^2} + \ldots \tag{9.55}$$

From equation (9.54) and (9.55) we have

$$\left(\frac{\partial p}{\partial x}\right)_{0,j} = \frac{1}{\Delta x}(p_{0,j} - p_{-1,j}) \tag{9.56}$$

$$\left(\frac{\partial^2 u}{\partial x^2}\right)_{0,j} = \frac{1}{\Delta x}\left[\left(\frac{\partial u}{\partial x}\right)_{1,j} - \left(\frac{\partial u}{\partial x}\right)_{0,j}\right] \tag{9.57}$$

Therefore equation (9.53) can be written as

$$p_{-1,j} = p_{0,j} - \frac{1}{Ro}\left[\left(\frac{\partial u}{\partial x}\right)_{1,j} - \left(\frac{\partial u}{\partial x}\right)_{0,j}\right] \tag{9.58}$$

Here

$$\left(\frac{\partial u}{\partial x}\right)_{1,j} = \frac{u_{2,j} - u_{0,j}}{2\Delta x} \tag{9.59}$$

$$\left(\frac{\partial u}{\partial x}\right)_{0,j} = \frac{u_{1,j} - u_{0,j}}{\Delta x} \tag{9.60}$$

Finally, the boundary pressure along $x = 0$ is defined as

$$p_{-1,j} = p_{0,j} - \frac{u_{2,j} - 2u_{1,j} + u_{0,j}}{2\Delta x\ Ro} \tag{9.61}$$

or

$$p_{0,j} = p_{1,j} - \frac{u_{3,j} - 2u_{2,j} + u_{1,j}}{2\Delta x\ Ro} \tag{9.62}$$

Similarly along $x = 1$ boundary

$$p_{m+1,j} = p_{m,j} - \frac{u_{m-2,j} - 2u_{m-1,j} + u_{m,j}}{2\Delta x\ Ro} \tag{9.63}$$

Likewise along other boundaries.

9.5.3 Convergence Criterion

We are interested in a steady-state solution. After finite iterations the artificial compressibility approach will approximately converge to the steady-state solution. The residual error is measured by a parameter, which monitors the convergence rate of the solution to the steady-state. One parameter introduced by Peyret and Taylor [81] has the following form

$$R = \frac{1}{N} \sum_{i,j} \left| U_{i,j}^{n+1} - U_{i,j}^{n} \right| \tag{9.64}$$

Here N is the number of computational cells; U is the flow variables.

Another parameter

$$R = \frac{\sum_{i,j} \left| U_{i,j}^{n+1} - U_{i,j}^{n} \right|}{\sum_{i,j} \left| U_{i,j}^{n+1} \right|} \tag{9.65}$$

is also widely used. If the magnitude of R is less than a pre-set tolerance, then the solution is said to have converged to the stead-state solution.

In the driven cavity simulation the first parameter (9.64) was used. The convergence criterion or the average residual tolerance is set to be 1 x 10^{-5}.

9.5.4 The Numerical Results

To illustrate the approach, Reynolds numbers $Ro = 100$ and $Ro = 500$ are chosen for the tests. The domain is discretized with 40 x 40 uniform cells. Flux Riemann solver (9.27)-(9.28) is applied to carry out these tests. The pre-numerical experiments indicate that the artificial compressibility parameter δ not only affects the convegence rate but also affects the accuracy of the solution [82]. When determining the value of δ, the first priority is put on the accuracy and then the convegence rate.

Figure 9.2 shows the exact solutions given by equations (9.43)-(9.45), which are presented for comparison with the numerical results. In figure 9.2, (a) presents contours of isovelocity u; (b) presents the isovelocity v; (c) is contours of iso-pressure for $Ro = 100$ and (d) is contours of iso-pressure for $Ro = 500$.

Case 1: $Ro = 100$

Figure 9.3 shows the numerical solutions by the three-point centered scheme (9.19). The artificial compressibility parameter $\delta = 2$ was used in the case. The convergence rate is fast: the number iterations 1119 and the CPU time used is 7.58 minutes (DECstation 5000/200). In figure 9.3, (a) is the isovelocity u; (b) is the isovelocity v; (c) presents the computed iso-pressure and (d) shows the comparison between the exact solution (line) and the numerical solution (symbol) for the velocity v at $y = 0.5$. As shown in the figures the numerical results have good agreement with the exact solutions.

Figure 9.4 shows the numerical solutions by the five-point centered scheme (9.21). The arrangement of the figure is the same as figure 9.3. Comparing with three-point scheme, the five-point scheme used nearly twice the CPU time as that of the three-point scheme, which is due to the complexity of the algebra of the scheme. Again there is a good agreement between the numerical results and the exact solutions.

Case 2: $Ro = 500$

As in case 1, figures 9.5 and 9.6 show the numerical solutions by the three- and five-point centered schemes, respectively. In this case the artificial compressibility parameter $\delta = 1$ was used. The numerical results of velocity u and pressure have good agreements with the exact solution. However the velocity v have a little different from the exact solution (see (b) and (d) in the figures).

9.6 Summary

A approach for solving steady incompressible Navier-Stokes equations is presented in this chapter. This method extends the Riemann-problem based techniques to viscous flows, which is obtained by applying a modified artificial compressibility Navier-Stokes equations and the high-order numerical schemes for systems of advection-diffusion equations. In this approach, utilizing the local Riemann solutions the steady incompressible viscous flows can be solved in the same way as that of inviscid hyperbolic conservation laws. Numerical experiments on the driven cavity problem indicate that this approach can give satisfactory solutions.

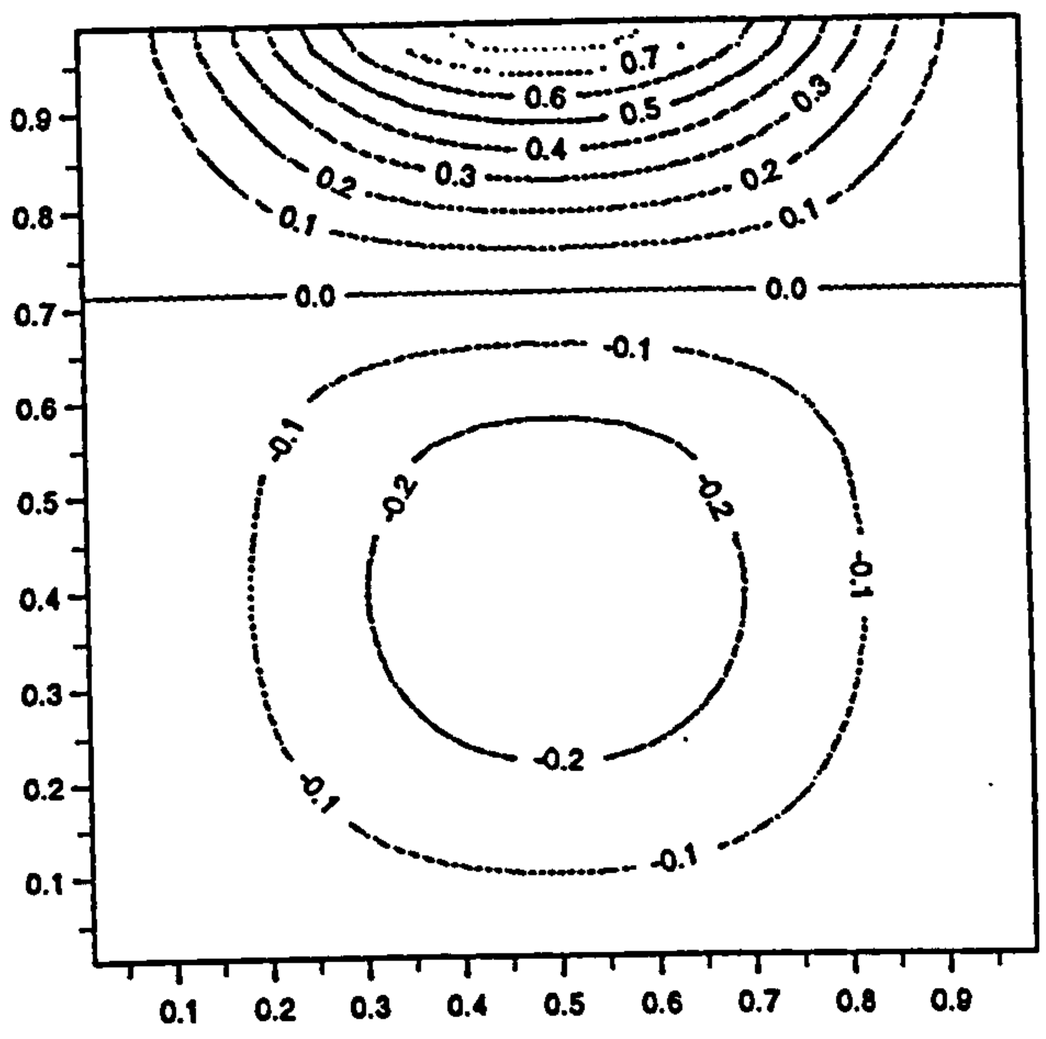

(a)

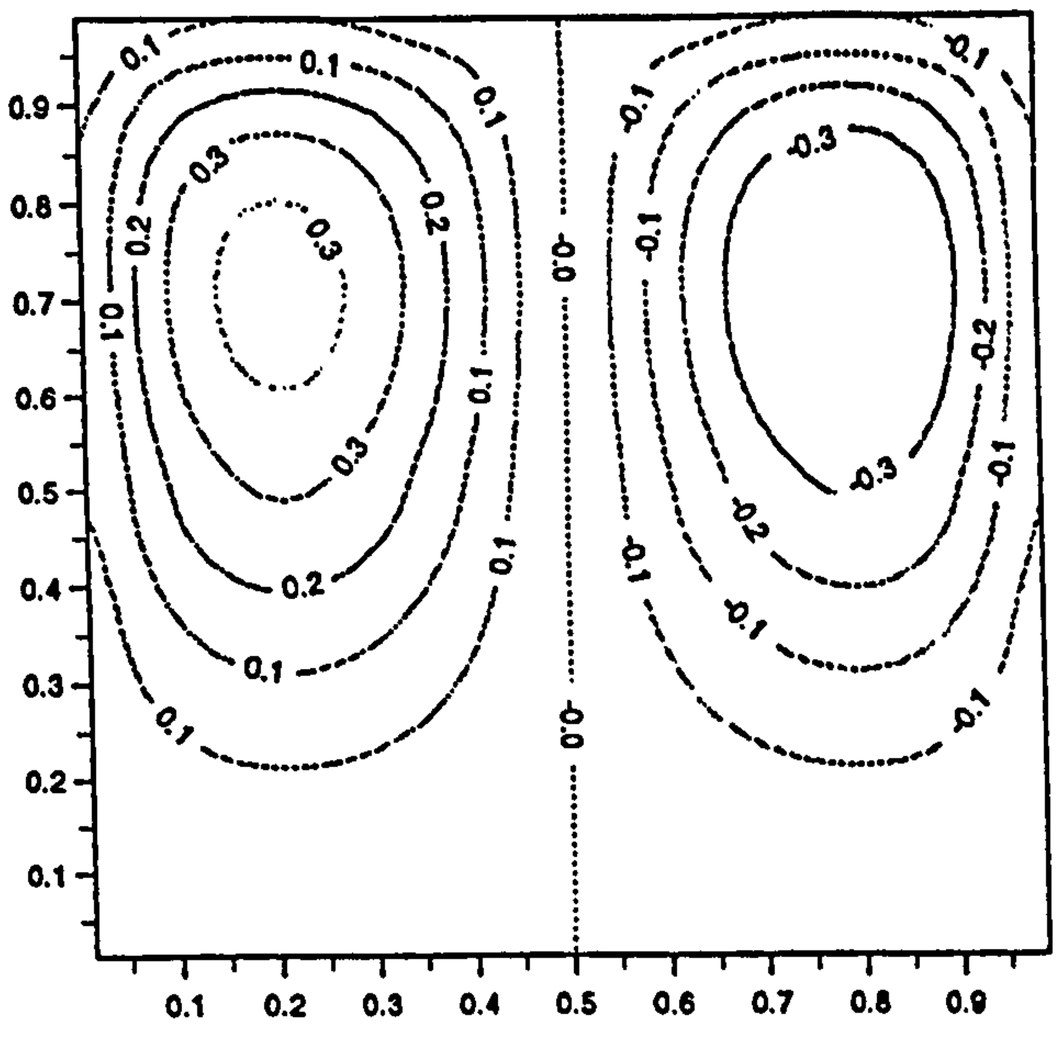

(b)

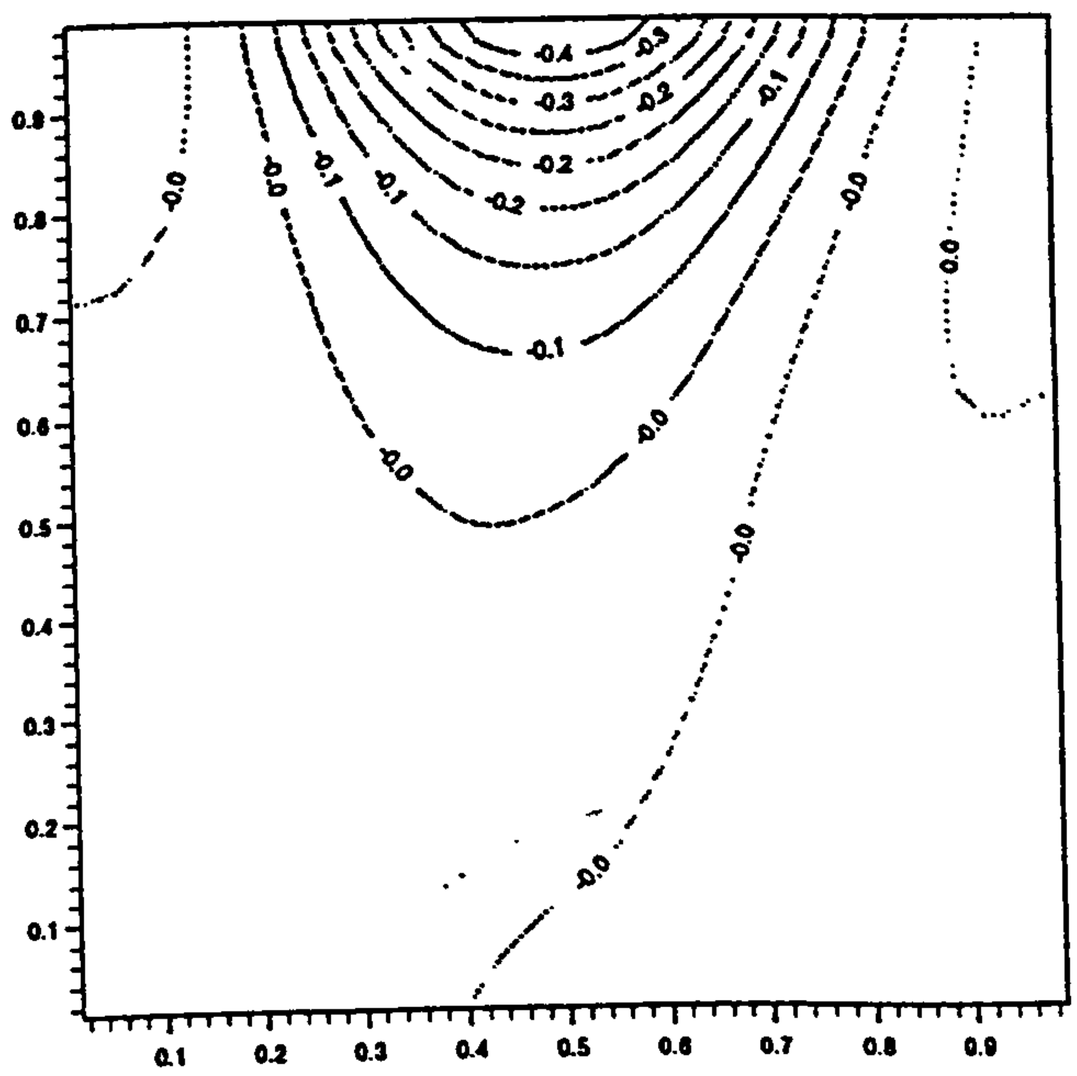

(c)

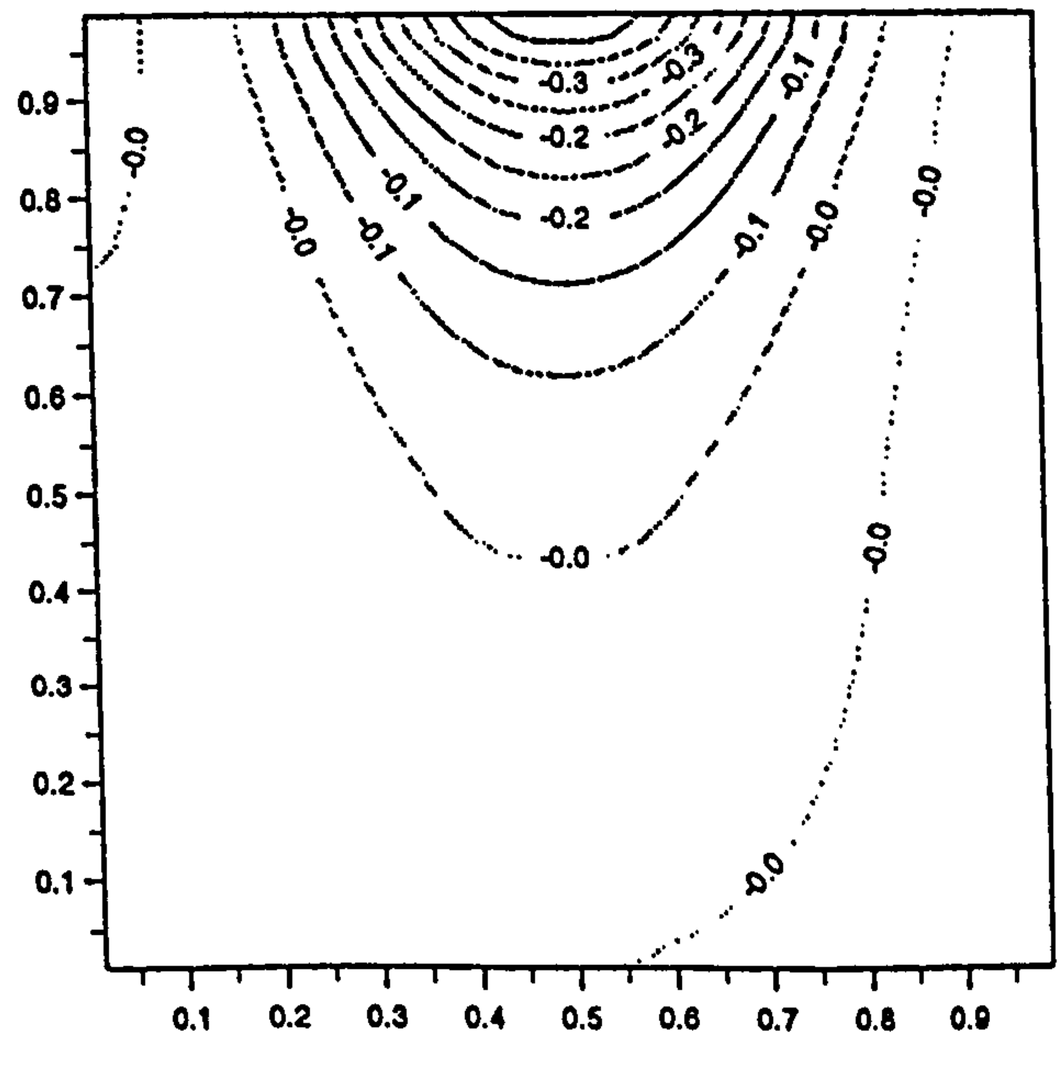

(d)

Figure 9.2: The Exact Solution of the Driven Cavity Problem: (a) Velocity u; (b) Velocity v; (c) Pressure for $Ro = 100$; (d) Pressure for $Ro = 500$.

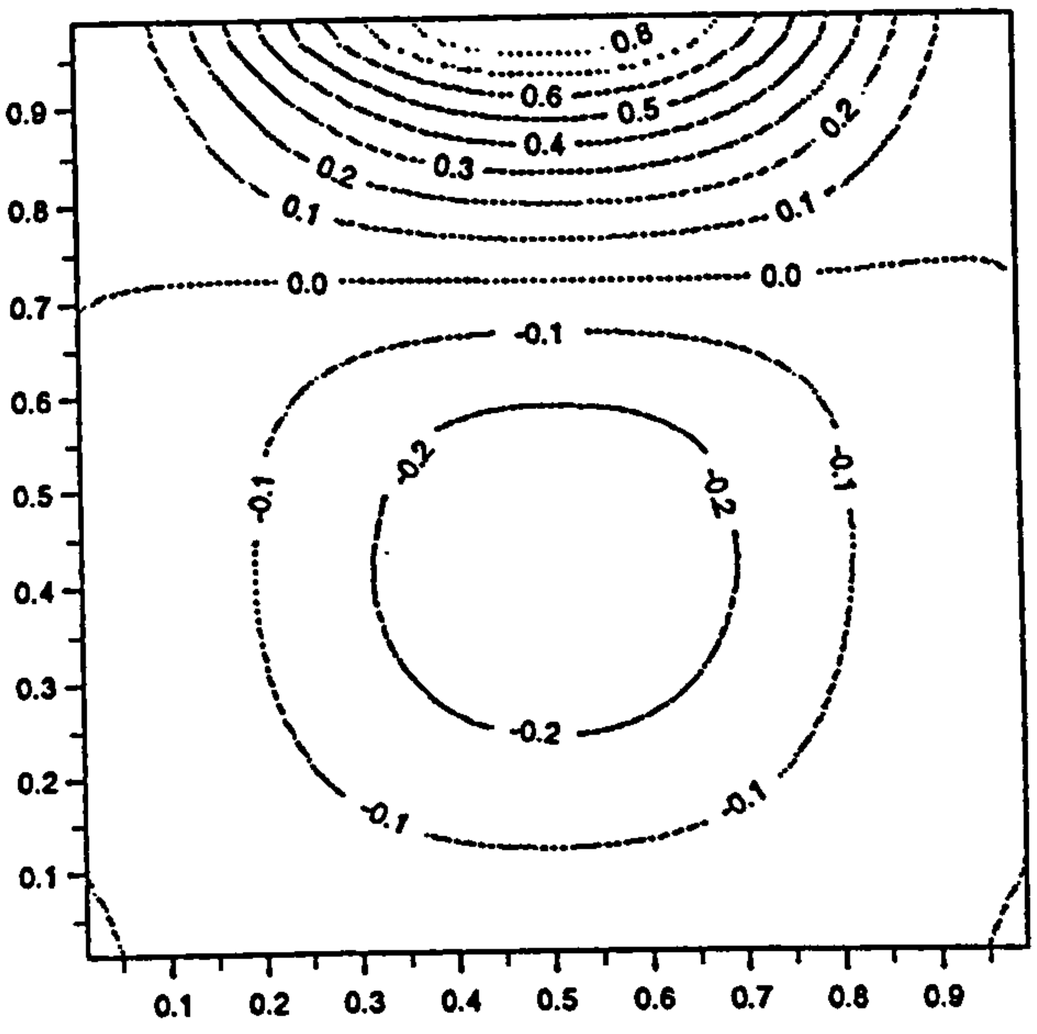

(a)

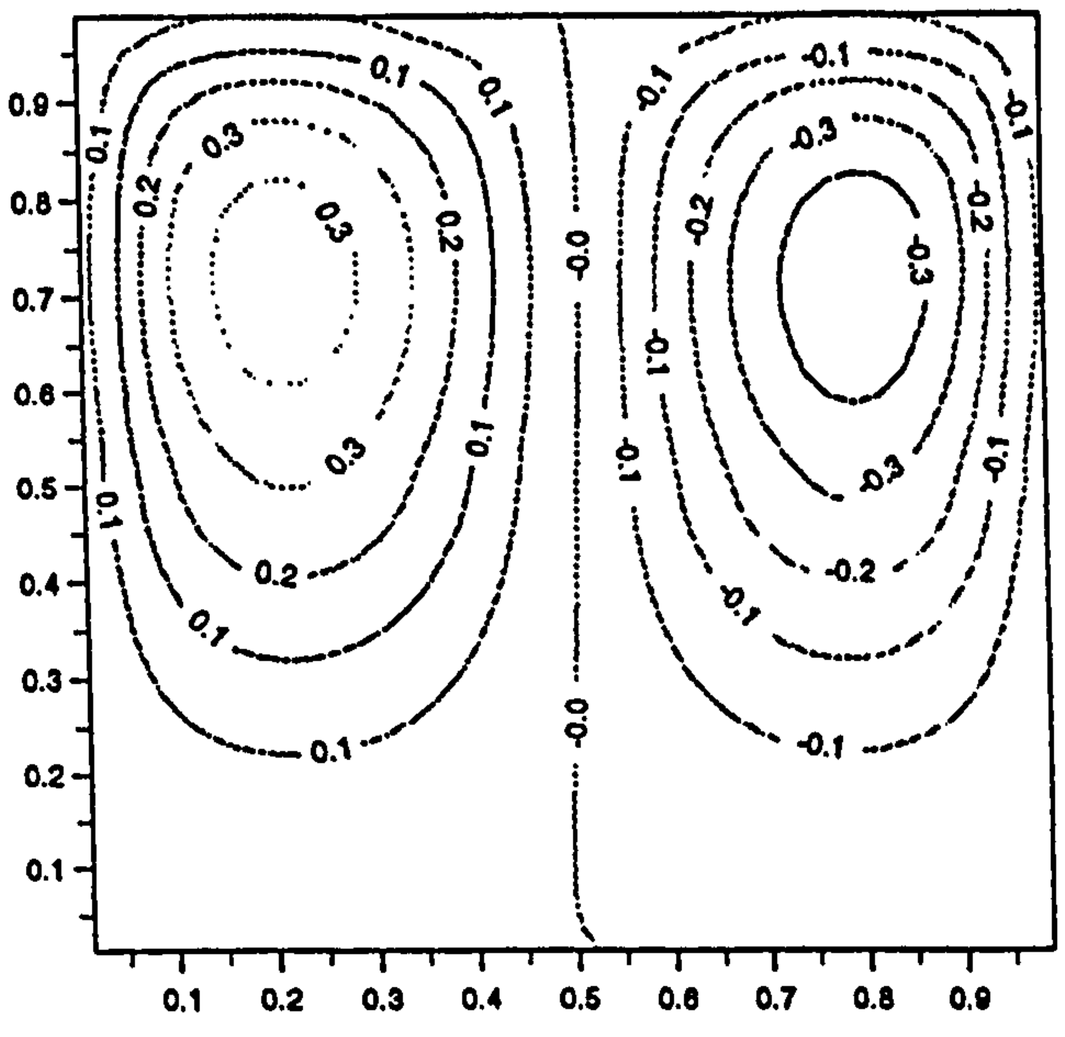

(b)

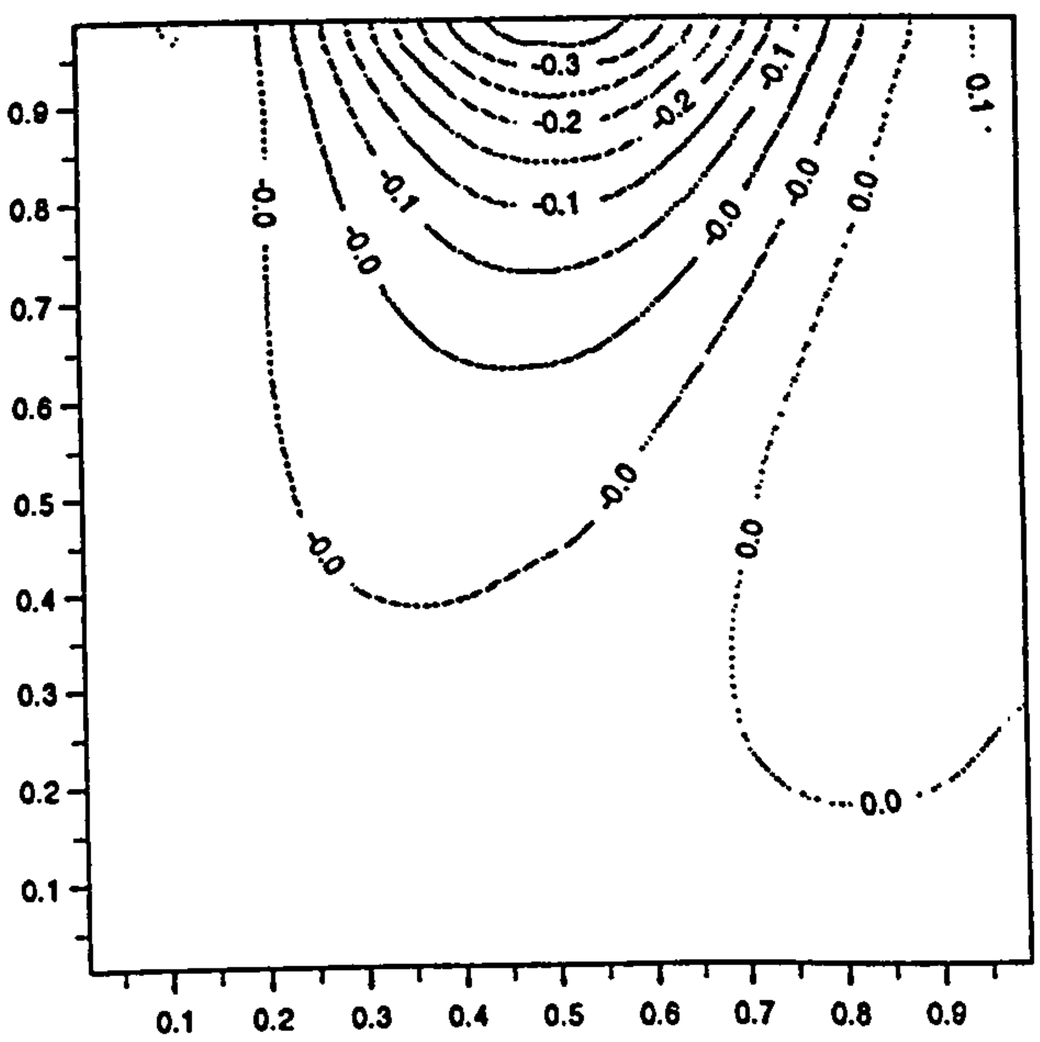

(c)

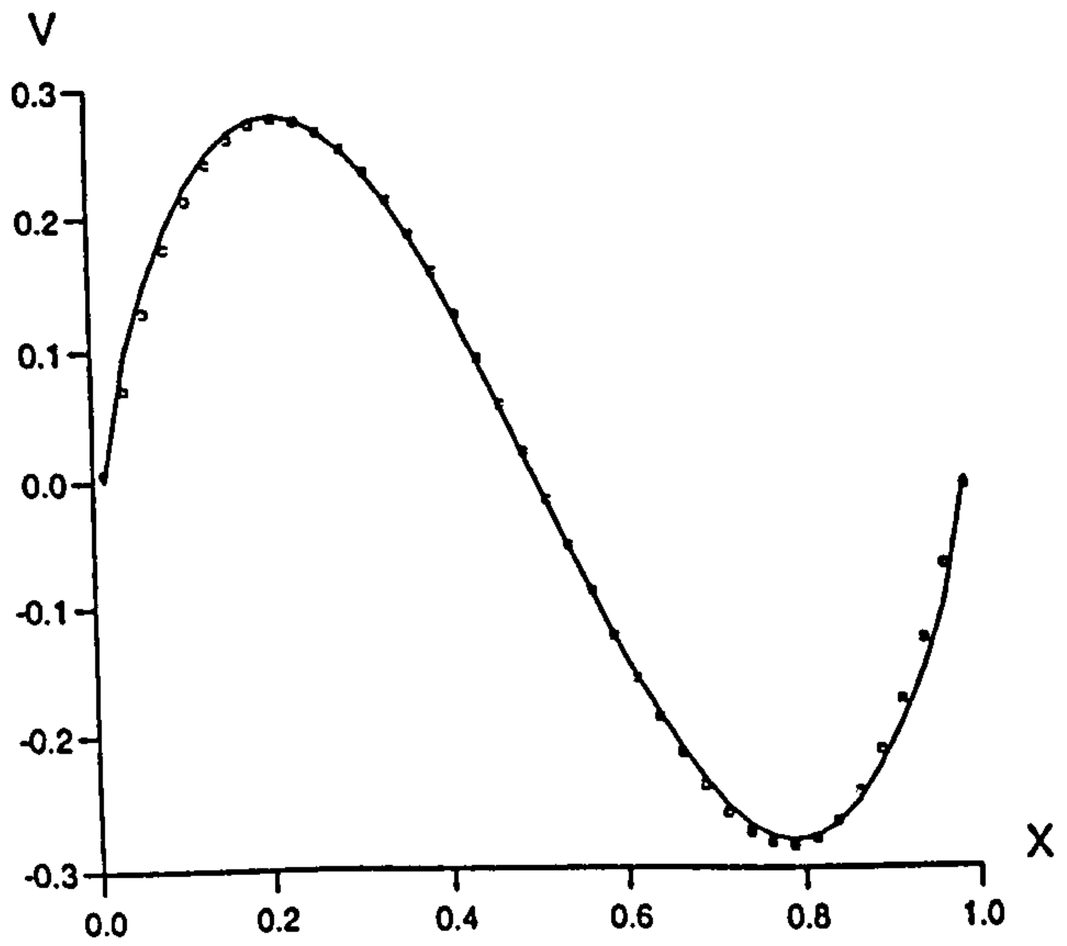

(d)

Figure 9.3: Numerical Solutions by the Three-point Scheme for $Ro = 100$: (a) Velocity u; (b) Velocity v; (c) Pressure; (d) Comparison between the Exact Solution (line) and the Numerical Solution (symbol) for the Velocity v at $y = 0.5$.

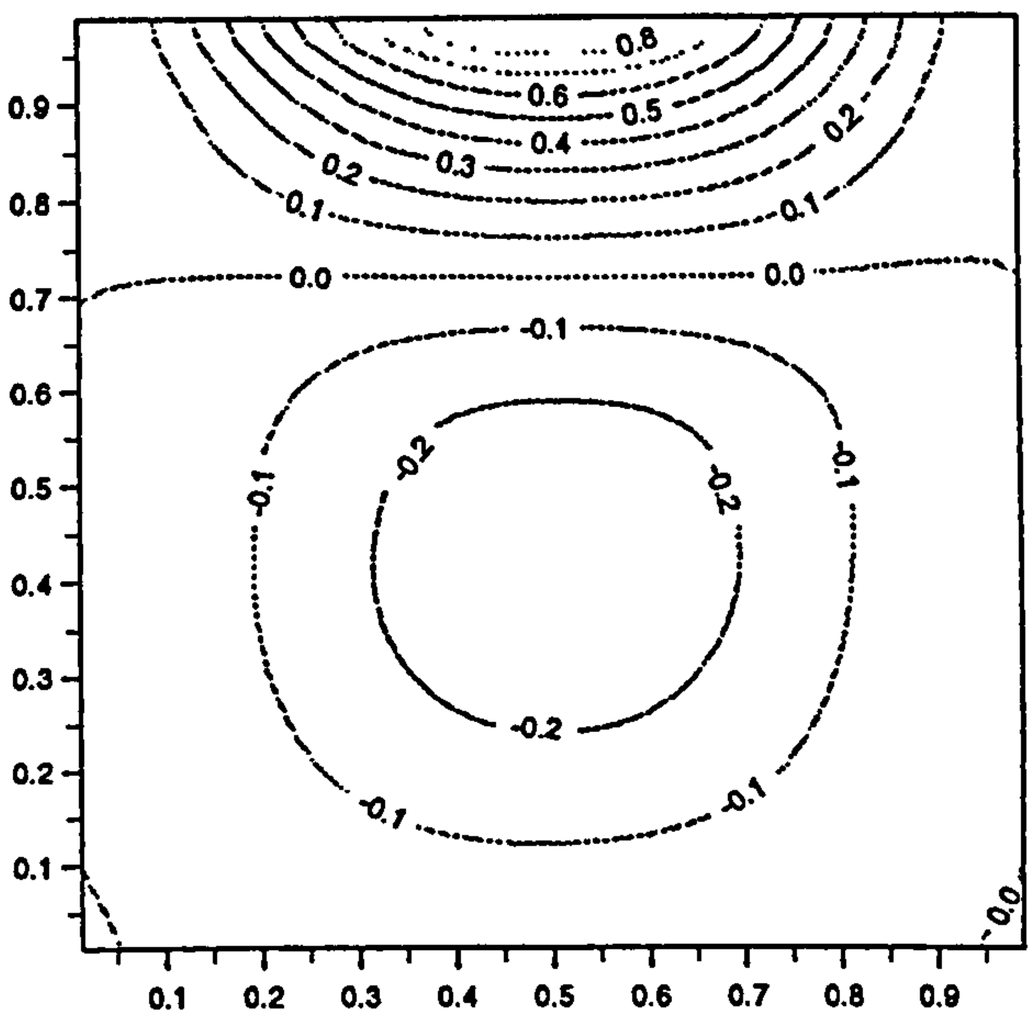

(a)

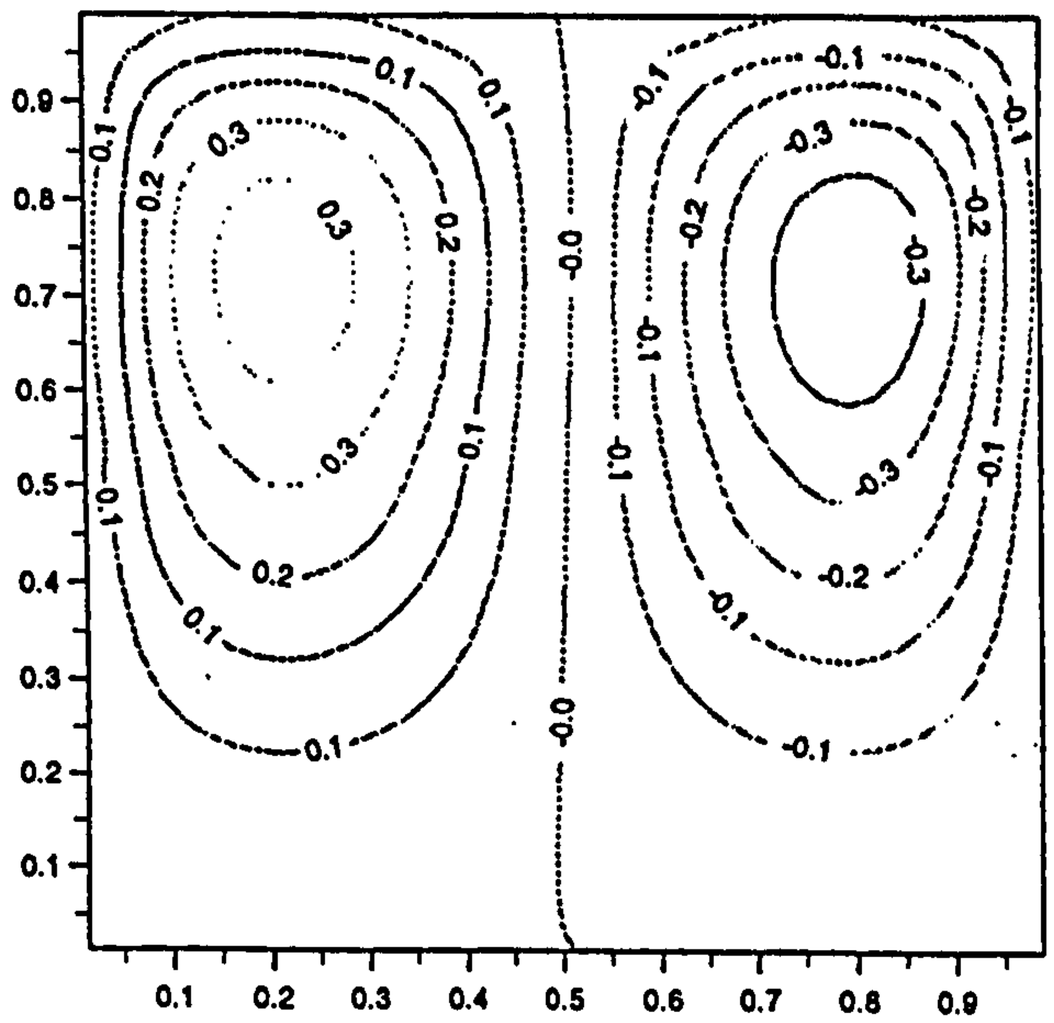

(b)

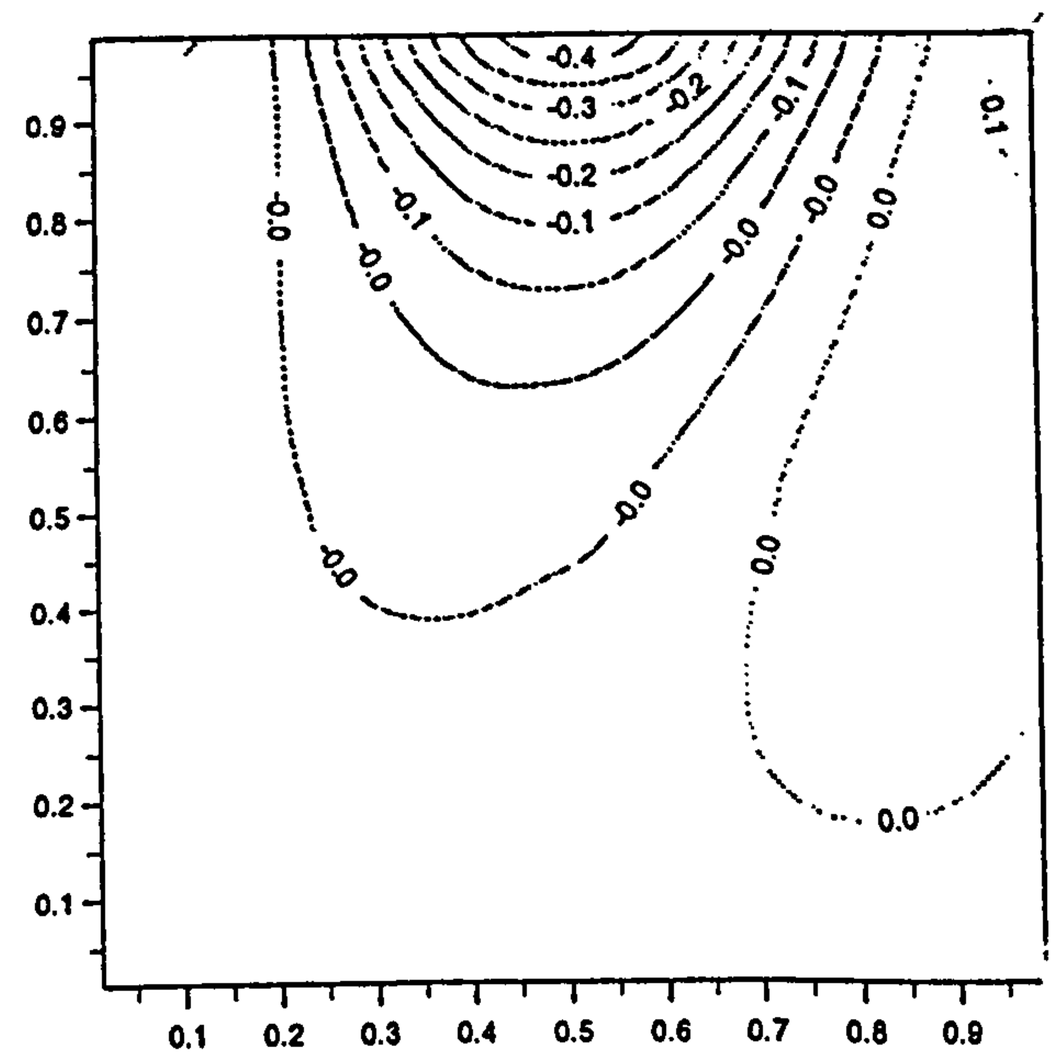

(c)

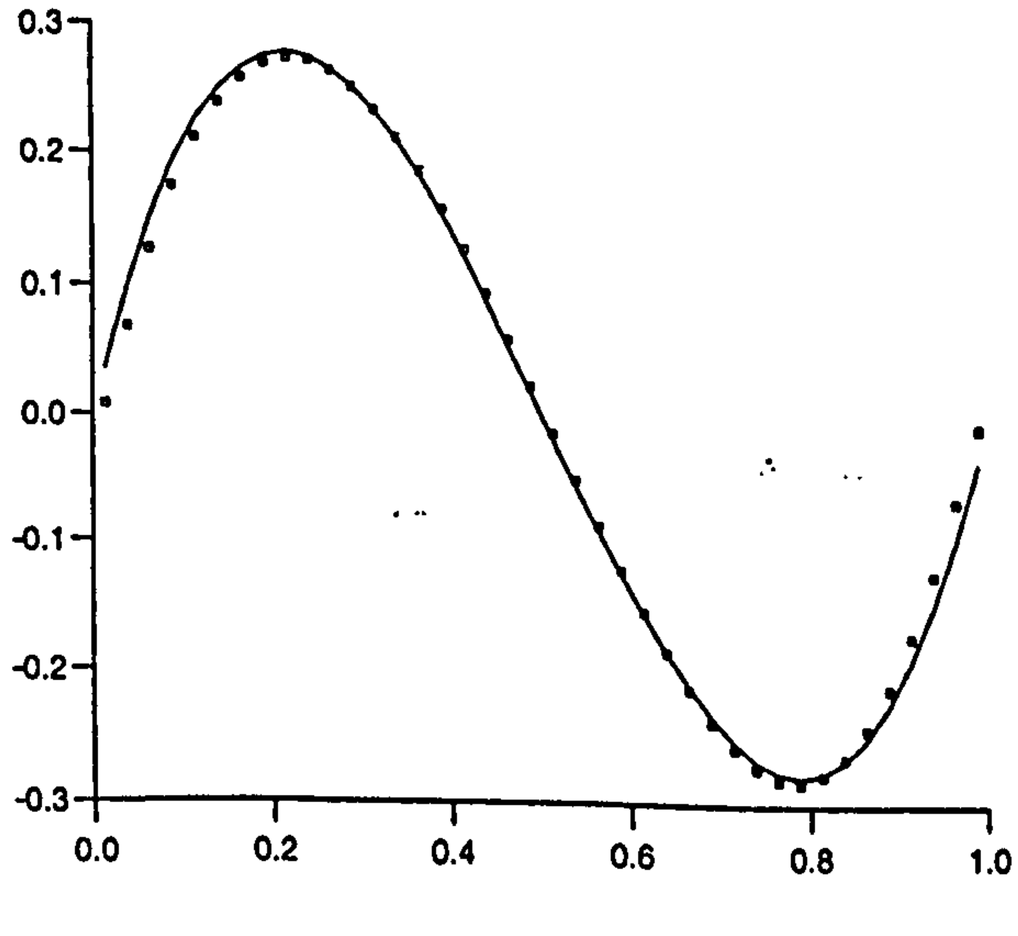

(d)

Figure 9.4: Numerical Solutions by the Five-point Scheme for $Ro = 100$: (a) Velocity u; (b) Velocity v; (c) Pressure; (d) Comparison between the Exact Solution (line) and the Numerical Solution (symbol) for the Velocity v at $y = 0.5$.

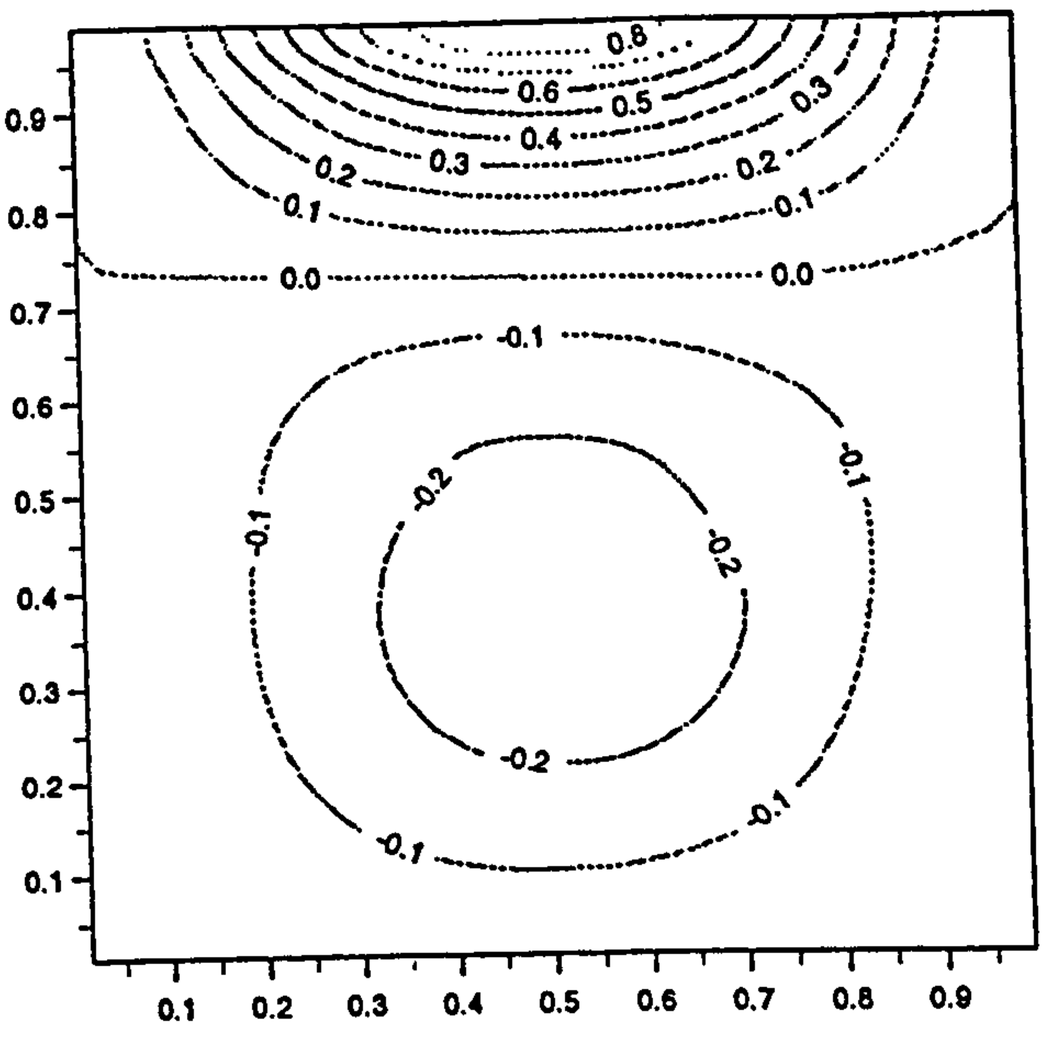

(a)

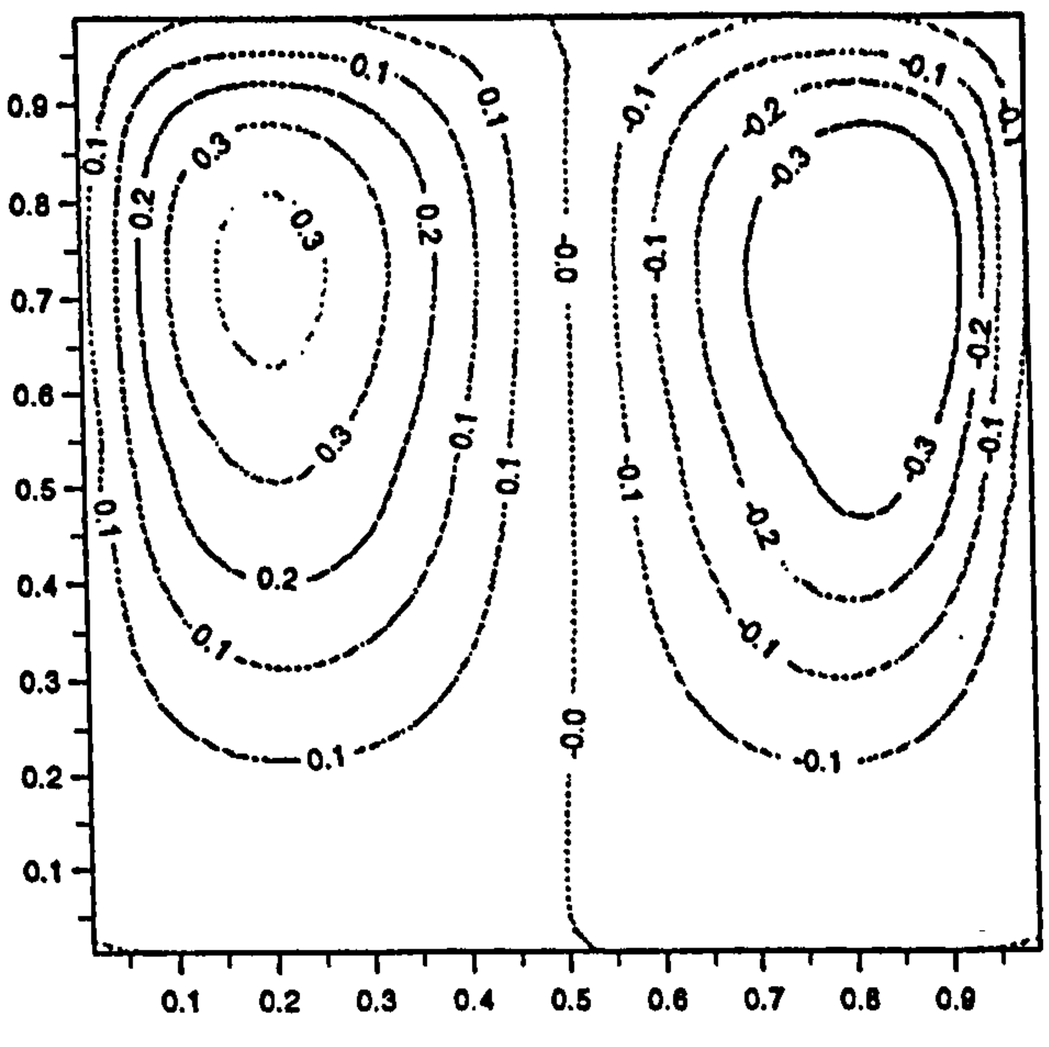

(b)

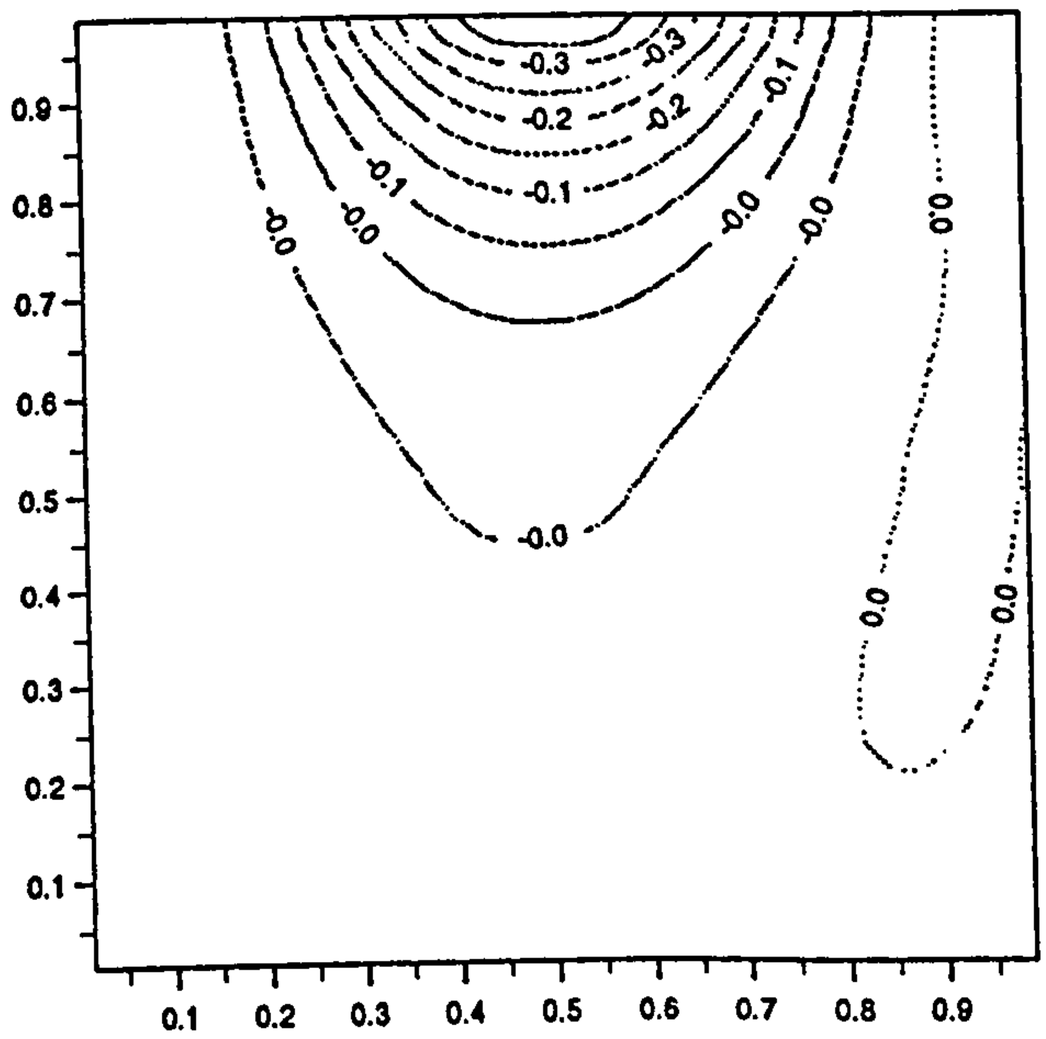

(c)

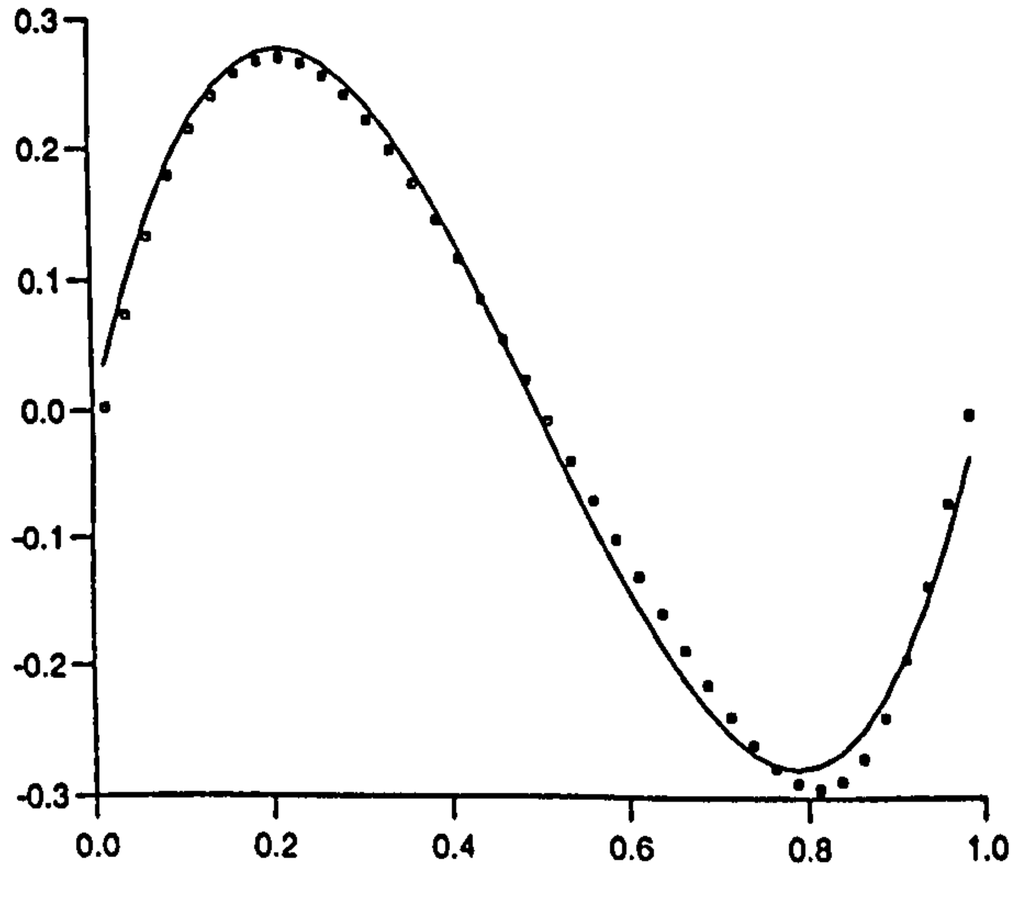

(d)

Figure 9.5: Numerical Solutions by the Three-point Scheme for $Ro = 500$: (a) Velocity u; (b) Velocity v; (c) Pressure; (d) Comparison between the Exact Solution (line) and the Numerical Solution (symbol) for the Velocity v at $y = 0.5$.

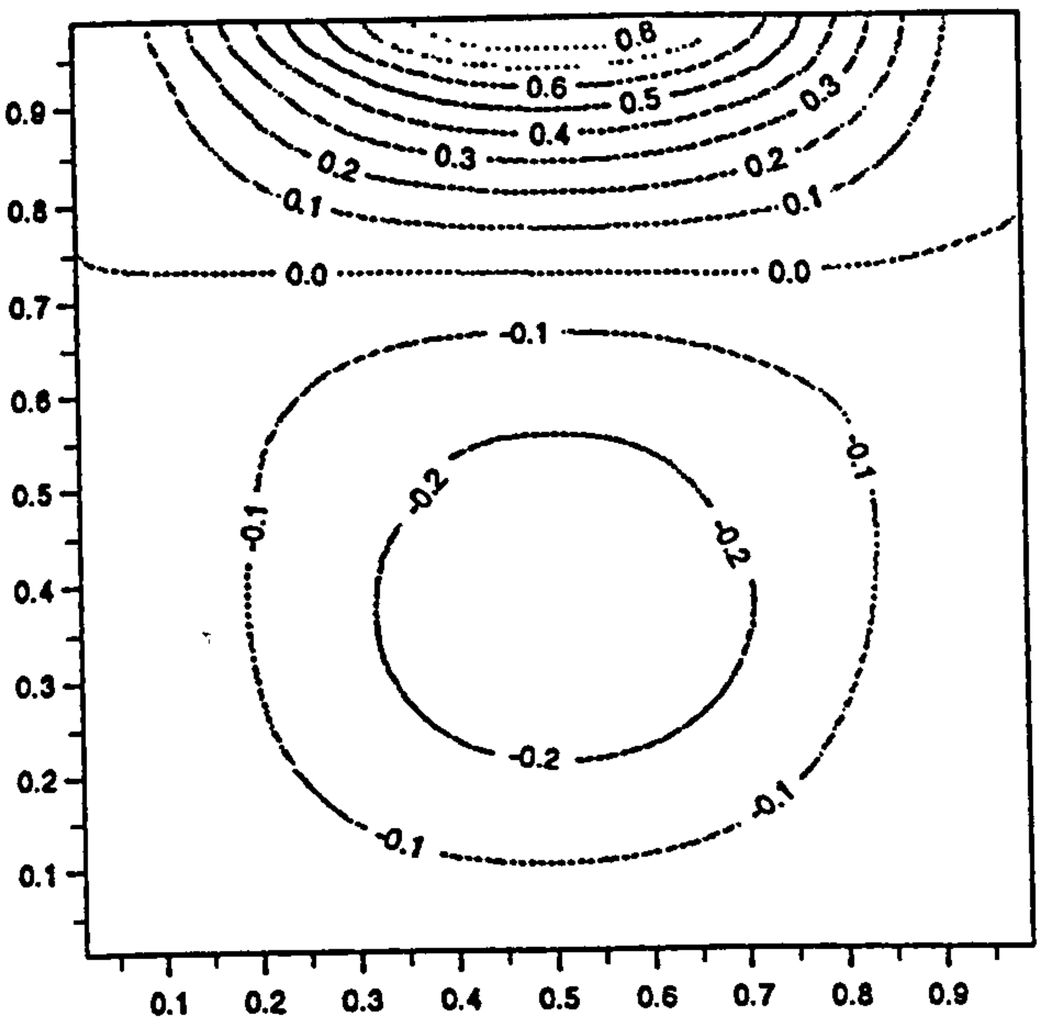

(a)

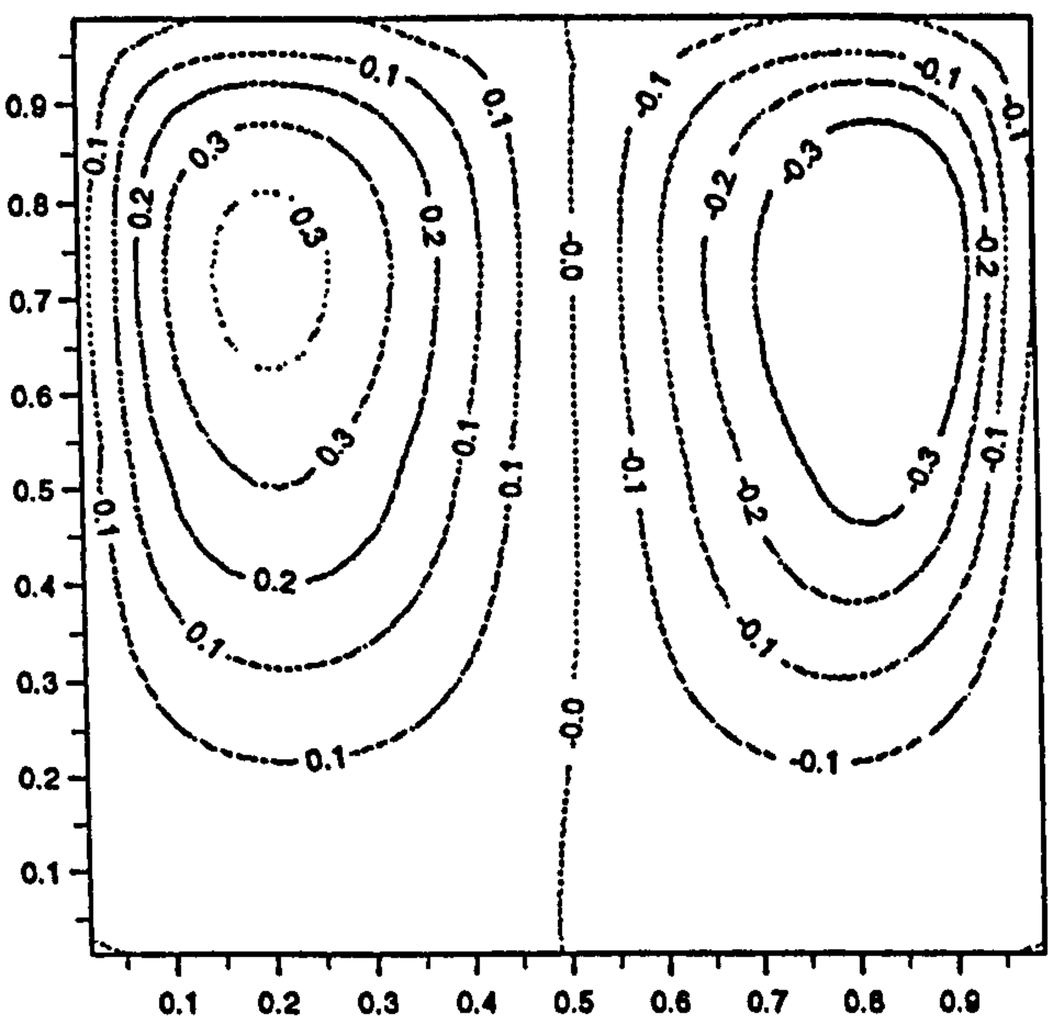

(b)

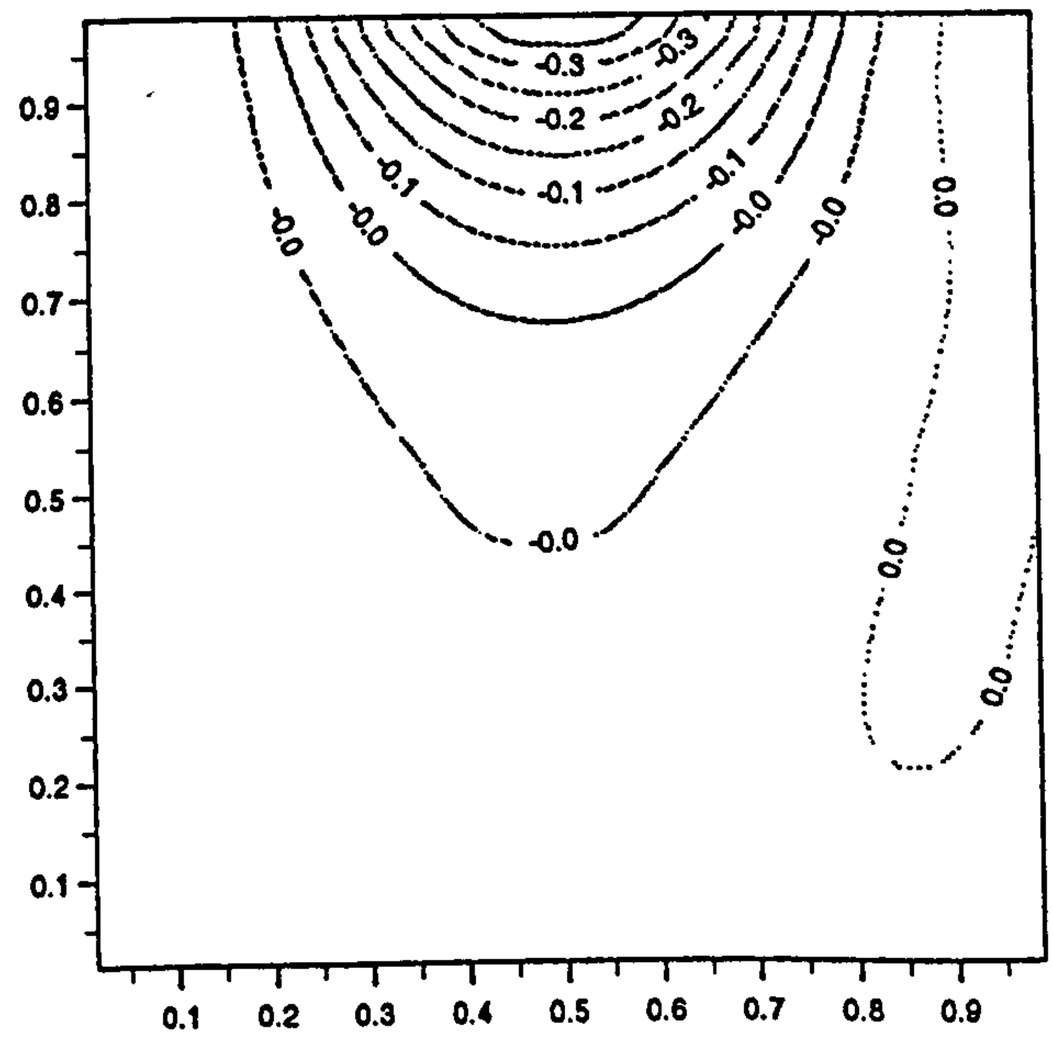

(c)

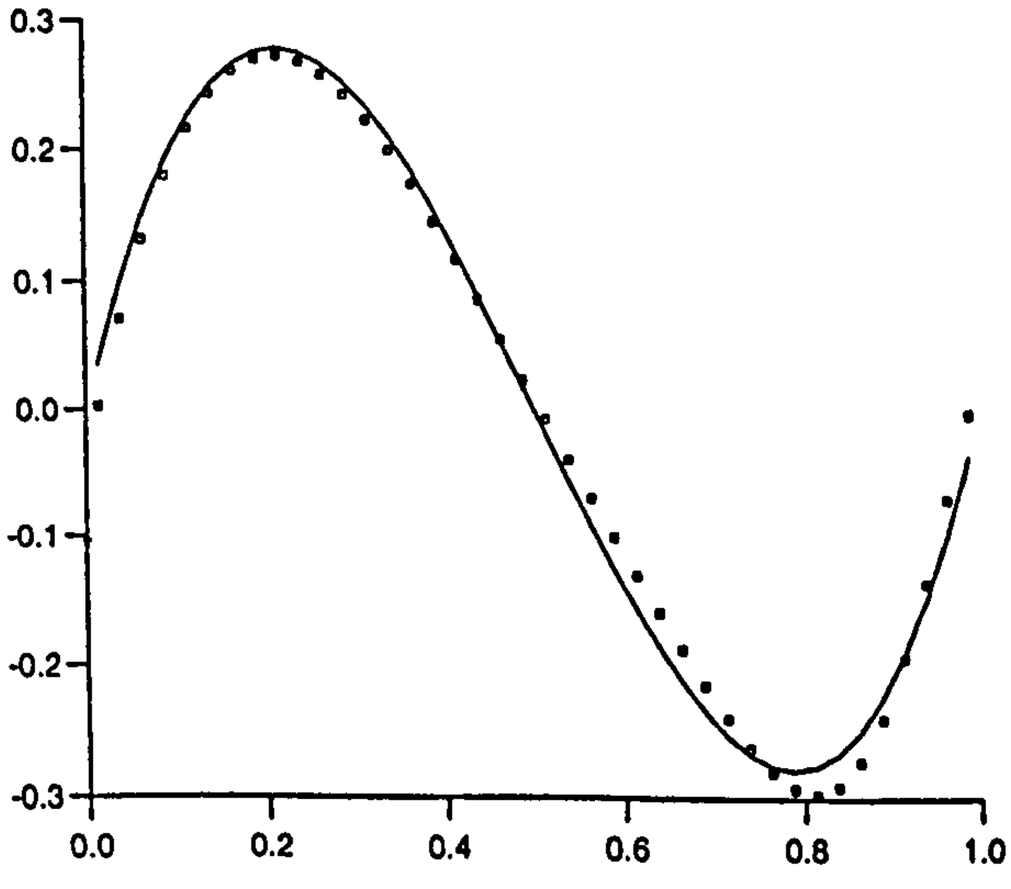

(d)

Figure 9.6: Numerical Solutions by the Five-point Scheme for $Ro = 500$: (a) Velocity u; (b) Velocity v; (c) Pressure; (d) Comparison between the Exact Solution (line) and the Numerical Solution (symbol) for the Velocity v at $y = 0.5$.

Chapter 10

Closure

In this chapter we close our discussions by giving suggestions for further work and drawing the conclusions.

10.1 Suggestions for Further Work

Although the high resolution schemes for solving Euler equations and the incompressible Navier-Stokes equations have only been demonstrated in this thesis, these high-order schemes can also be applied to deal with other nonlinear scalar or system of conservation laws. For example, considering time-dependent viscous compressible flows, the compressible Navier-Stokes equations can be decoupled in terms of the advection part and the diffusion part. Then the advection part (Euler equations) can be solved by applying the high-order hyperbolic schemes with the viscous limiter functions, and the diffusion part (Stokes equations) can be solved by using the high-order viscous schemes. A similar approach can also be applied to deal with the time-dependent unsteady incompressible flows. These applications are of great importance for the future work.

For the two-dimensional time-dependent Euler equations, the Strang's *operator splitting* approach [77] was applied. In this method the schemes still keep high-order spacial accuracy. However accurate the scheme is, in time it is reduced to second-order. This highlights a need to investigate a method in order to recover the temporal high-order accuracy.

The high resolution schemes are obtained by imposing TVD properties via the introduction of flux limiters. Although high-order for smooth flow, at extrema the TVD schemes reduce to only first-order. In order to overcome this shortcoming, some interesting works in different approaches in the literature have been presented [40] and [83]. Therefore it is worthwile pursuing the research further in order to obtain high-order at extrema.

10.2 Conclusions

Fully discrete high resolution numerical schemes for viscous and inviscid flows were developed. A new approach to deal with linear stability analysis for one-dimensional numerical schemes were discussed. When developing high-order or complicated numerical schemes, this approach is very useful for stability analysis. Fully discrete techniques for model advection and model advection-diffusion equations were presented. The principle behind these techniques is the Taylor series expansion. A way to formulate conservative high-order schemes was given. In this way any finite difference schemes can be reformulated into a conservative forms. This is essential because it is the conservative schemes that one needs to use for nonlinear problems in Fluid Dynamics. A general TVD function for second-, third-, and fourth-order schemes with stability condition $c \leq 1$ was established. Based on the TVD function, flux limiter functions for these high-order schemes can be designed. The second-, third-, and fourth-order viscous and inviscid flux limiter functions have been proposed and tested. These limiter functions can be coupled to the corresponding high-order schemes to solve viscous and inviscid flows. Numerical experiments indicate that these limiter function give satisfactory solutions. Two methodologies have been introduced. One is the method which extends the high-order (higher than second-order) scalar schemes to systems of conservation laws; another is the approach for solving steady incompressible viscous flows. These methods have been successfully applied, for example, in solving some popular test problems for the one and two dimensional Euler equations and the incompressible Navier-Stokes equations.

Bibliography

[1] **FLORES, J., CHADERJIAN, N.M. and SORENSON, R.L.,** (1987), *AIAA paper, 87-1197.*

[2] **RAI, M.M.,** (1989), *AIAA J. Prpulsion and Power, 3.*

[3] **RIGGINS, D. and McCLINTON, C.** (1991), *AIAA paper, 91-5093.*

[4] **LING, R.T.,** (1987), Application of Computational Fluid Dynamics (CFD) Method to Numerical Study of Electromagnetic Wave Scattering Phenomena, *AIAA-87-0487,* AIAA 25th Aerospace Sciences Meeting.

[5] **CHEUNG, S., EDWARDS, T. and LAWRENCE, S.,** (1990), Application of CFD to Sonic Boom Near-and Mid-Field Prediction, *AIAA-90-3999,* AIAA 13th Aeroacoustics Conference.

[6] **STURGESS, G.J.,** (1988), Application of CFD to Gas Turbine Engine Secondary Flow Systems - The Labyrinth Seal, *AIAA-88-3203,* AIAA/ASME/SAE/ASEE 24th Joint Propulsion Conference.

[7] **HAWKINS, R. and DILLEY, A.,** (1992), CFD Comparisons with Wind Tunnel and Flight Data for the X-15, *AIAA-92-5047,* AIAA 4th International Aerospace Planes Conference.

[8] SNYDER, J.R., (1990), CFD Needs in Conceptual Design, *AIAA-90-3209,* AIAA/AHS/ASEE Aircraft Design systems and Operations Conference.

[9] LAI, H.T. and RAJU, M.S., (1993), CFD Validation of Subsonic Turbulent Planar Shear Layers, *AIAA-93-1773,* AIAA/SAE/ASME/ASEE 29th Joint Propulsion Conference and Exhibit.

[10] **KIM, J., MOIN, P. and MOSER, R.,** (1987), *J. Fluid Mech., 177.*

[11] **HIRSCH, C.,** (1988), Numerical Computation of Internal and External Flows, *Volume 1 and 2, John Wiley and Sons Ltd..*

[12] **LAX, P.D.,** (1957), Hyperbolic Systems of Conservation Laws 2, *Comm. Pure and Applied Mathematics, 10, 537-66.*

[13] **LAX, P.D. and WENDROFF, B.,** (1960), Systems of Conservation Laws, *Comm. Pure and Applied Mathematics, 13, 217-37.*

[14] **LAX, P.D. and WENDROFF, B.,** (1964), Difference Schemes for Hyperbolic Equations with High Order of Accuracy, *Comm. Pure and Applied Mathematics, 17, 381-98.*

[15] **RICHTMYER, R.D. and MORTON, K.W.,** (1967), Difference Methods for Initial Value Problems, 2nd edn, *London: Wiley-Interscience.*

[16] **MacCORMARK, R.W.** (1969), The Effect of Viscosity in Hypervelocity Impact Cratering, *AIAA paper, 69-354.*

[17] **MacCORMARK, R.W.** (1981), A Numerical method for Solving the Equations of Compressible Viscous Flow, *AIAA paper, 81-0110, AIAA 19th Aerospace Science Meeting.*

[18] **LERAT, A. and PEYRET, R.,** (1974), Non Centered Schemes and Shock Propagation Problems, *Computers and Fluids, 2, 35-52.*

[19] **JAMESON, A., SCHNIDT, W. and TURKEL, E.,** (1981), Numerical Simulation of the Euler Equations by Finite Volume Methods Using Runge-Kutta Time Stepping Schemes, *AIAA paper, 81-1259, AIAA 5th Computational Fluid Dynamics Conference.*

[20] **VON NEUMANN, J. and RICHTMYER, R.D.,** (1950), A method for the Numerical calculations of Hydrodynamical Skocks, *J. Math. Phy., 21.*

[21] **JAMESON, A.,** (1982), Transonic Aerafoil calculations Using the Euler Equations, In P.L. RO(ed.), *Numerical Methods in Aeronautical Fluid Dynamics, New Yoyk: Academic Press.*

[22] **PULLIAM, T.H.,** (1984), Euler and Thin Layer Navier-Stokes Codes: ARC2D, ARC3D., Proc. Computational Fluid Dynamics User's Workshop, *The University of Tennessee Space Institute, Tullahoma, Tennessee.*

[23] **PULLIAM, T.H. and STEGER, J.L.,** (1985), Recent Improvements in Efficiency, Accuracy and Convergence for Implicit Approximate Factorization Algorithms, *AIAA paper, 85-0360, AIAA 23rd Areospace Science Meeting.*

[24] **COURANT, R., ISAACSON, E. and REEVES, M.,** (1952), On the Solution of Nonlinear Hyperbolic Differential Equations by Finite Differences, *Comm. Pure and Applied Mathematics, 5, 243-55.*

[25] **STEGER, J.L. and WARMING, R.F.,** (1981), Flux Vector Splitting of the Inviscid Gas-Dynamic Equations with Application to Finite Difference Methods, *J. Comput. Phy., 40, 263-93.*

[26] **VAN LEER, B.,** (1982), Flux Vector Splitting for the Euler Equations, *In Proc. 8th International Conference on Numerical Methods in Fluid Dynamics, Springer Verlag.*

[27] **GODUNOV, S.K.,** (1959), A Difference Scheme for Numerical Computation of Discontinuous Solution of Hydrodynamic Equations, *Math. Sbornik, 47, 271-306 (in Russian), Translated US Joint Publ. Res. Service, JPRS 7226.*

[28] **ENGQUIST, B. and OSHER, S.,** (1980), Stable and Entropy satisfying Approximations for Transonic Flow Calculations, *Mathematics of Computation, 24, 45-75.*

[29] **OSHER, S.,** (1982), Shock Modelling in Aeronautics, *In, K.W. Morton and M.J. Baines(eds), Numerical Methods for Fluid Dynamics, pp. 179-218, London: Academic Press.*

[30] **ROE, P.L.,** (1981a), The Use of the Riemann Problem in Finite Difference Schemes, *Lecture Notes in Physics, Vol. 141, 354-9, Berline: Springer Verlag.*

[31] **ROE, P.L.,** (1981b), Approximate Riemann Solvers, Parameter Vectors and Difference Schemes, *J. Comput. Phy., 43, 357-72.*

[32] **TORO, E.F.,** (1991), A Linearized Riemann Solver for the Time Dependent Euler Equations of Gas Dynamics, *Proc. R. Soc. Lond. A 434 pp 683-693.*

[33] **ENGQUIST, B. and OSHER, S.,** (1981), One-side Difference Approximations for Nonlinear Conservation Laws, *Mathematics of Computation, 36, 321-52.*

[34] **OSHER, S.,** (1982), Riemann Solvers, the Entrop Condition and Difference Approximations, *SIAM J. Numerical Analysis, 21, 217-35.*

[35] **BORIS, J.P. and BOOK, D.L.,** (1973), Flux Corrected Transport I., SHASTA, A Fluid Transport Algorithm That Works, *J. Comput. Phy., 11, pp. 38-69.*

[36] **VAN LEER, B.,** (1974), Towards the Ultimate Conservative Difference Scheme : 2. Monotinicity and Conservation Combined in a Second Order scheme, *J. Comput. Phy., 14, 361-70.*

[37] **HARTEN, A.,** (1983), High Resolution Schemes for Hyperbolic Conservation Laws, *J. Comput. Phy., 49, 357-93.*

[38] **SWEBY, P.K.,** (1984), High Resolution Schemes Using Flux Limiters for Hyperbolic Conservation Laws, *SIAM J. Num. Anal., 21, pp 995-1011.*

[39] **RAI, M.M. and MOIN, P.,** (1991), Direct Simulation of Turbulent Flow Using Finite-Difference Schemes, *J. Comput. Phy., 96, 15-53.*

[40] **HARTEN, A. and OSHER, S.,** (1987), Uniformly High-order Accurate Nonoscillatory Schemes 1, *SIAM J. Num. Anal., 24, pp. 279-309.*

[41] **SHU, S. and OSHER, S.,** (1988), Efficient Implementation of Essentially Nonoscillatory Shock Capturing Schemes, *J. Comput. Phys., 77, pp. 439-471.*

[42] **HARTEN, A.,** (1989), ENO Schemes with Subcell Resolution, *J. Comput. Phys., 83, pp. 148-184.*

[43] **LAX, P.D. and RICHTMYER, R.D.,** (1956), Survey of the Stability of Linear Finite Difference Equations, *Comm. on Pure and Applied Math., Vol.9.*

[44] **CRANK, J. and NICHOLSON, P.,** (1947), A Practical method for Numerical Evaluation of Solutions of Partial Differential equations of the Heat Conduction Type, *Proceeding of the Cambridge Philosophical Society, 43, 50-67.*

[45] **CHARNEY, J.G., FJORTOFT, R. and VON NEUMANN, J.,** (1950), Numerical Integration of the Barotropic Vorticity Equation, *Tellus, 2, 237-54.*

[46] **LEVEQUE, R.J.,** (1990), Numerical Methods for Conservation Laws. *Birkhauser.*

[47] **VAN LEER, B.,** (1974), (1977), (1977), (1979), Towards the Ultimate Conservative Difference Scheme. 2, 3, 4, 5, *J. Comput. Phys..*

[48] **ROE, P.L.,** (1987), Numerical Algorithms for the Linear Wave Equation, *Royal Aircraft Establishment Technical Report 81047.*

[49] **WARMING, R.F. and BEAM, R.M.,** (1976), Upwind Second-order Difference Schemes and Applications in Aerodynamic Flows, *J. AIAA, Vol. 14, No. 9, pp. 1241-1249.*

[50] **LAX, P.D.,** (1973), Hyperbolic Systems of Conservation Laws and the Mathematical Theory of shock waves, *Philadelphia: AIAM publications.*

[51] **VILA, J.P.,** (1988), High-order Schemes and Entropy Condition for Nonlinear Hyperbolic Systems of Conservation Laws, *Mathematics of Computation, Vol.50, No.181.*

[52] **TREFETHEN, L.N.** (1982), Group Velocity in Finite Difference Schemes, *SIAM Review, 24, pp. 113-136.*

[53] **HARTEN, A.,** (1983), High Resolution Schemes for Hyperbolic Conservation Laws. *J. Comput. Phys., 49, pp. 357-393.*

[54] **DAVIS, S.F.,** (1984), TVD Finite Difference Schemes and Artificial Viscosity, *ICASE Report 84-20, NASA CR-172373,* NASA Langley Research Center.

[55] **ROE, P.L.,** (1984), Generalized Formulation of TVD Lax-Wendroff Schemes. *NASA Contractor Report No. 84-53.*

[56] **ROE, P.L.,** (1985), Some Contributions to the Modelling of Discontinuous Flows, *Proc. 1983 AMS-SIAM Summer Seminar on Large Scale Computing in Fluid Mechanics, Leture in Applied Mathematics, Vol. 22, pp. 163-93,* SIAN Philadelphia.

[57] **CHAKRARTHY, S.R. and OSHER, S.,** (1983), High Resolution Applications of the Osher Upwind Scheme for the Euler Equations, *AIAA paper 83-1943, Proc. AIAA 6th Computational Fluid Dynamics Conference, pp. 363-73.*

[58] **TORO, E.F.,** (1989), A Weighted Average Flux Method for Hyperbolic Conservation Laws, *Proc. R. Soc. Lond. A 423 pp 401-418.*

[59] **LEONARD, B.P.,** (1988), Universal Limiter for Transient Interpolation Modeling of the Advective Transport Equations: The ULTIMATE Conservative Difference Scheme. *NASA Technical Memorandum 100916.*

[60] **HARTEN, A. and HYMAN, J.M.,** (1983), Self-adjusting grid methods for One-dimensional Hyperbolic Conservation Laws, *J. Comput. Phys., 50, pp. 235-269.*

[61] **EINFELDT, B., MUNZ, C.D., ROE, P.L. and SJOGREEN, B.,** (1991), On Godnov-type Methods Near Low Densities, *J. Comput. Phys., 92, 273-295.*

[62] **HARTEN, A., LAX, P.D. and VAN LEER, B.,** (1982), Upstream Differencing and Godunov Type Schemes for Hyperbolic Laws, *ICASE..*

[63] **SOD, G.,** (1978), A Survey of Several Finite Difference Methods for Systems of Nonlinear Hyperbolic Conservation Laws, *J. Comput. Phy., 27, pp. 1-31.*

[64] **WOODWARD, P. and COLELLA, P.,** (1984), The Numerical Simulation of Two-dimensional Fluid Flow with Strong Waves, *J. Comput. Phys., 54, 115-173.*

[65] **COLELLA, P. and GLAZ, H. M.,** (1983), Efficient Algorithms for the Solution of the Riemann Problem for Real Gases, *Lawrence Berkeley Laboratory Report LBL-15776.*

[66] **GLAZ, H. M. and COLELLA, P.,** (1985), A Numerical Study of Oblique Shock-wave Reflections with Experimental Comparisons, *Proc. R. Soc. Lond. A 398, 117-140.*

[67] **HANEL, D.,** (1989), On the Numerical Solution of the Navier-Stokes Equations for Compressible Fluids, *VKI Lecture Series on Computational Fluid Dynamics.*

[68] **WANG, Z.,** (1991), High Resolution Schemes for Steady Flow Computation, *J. Comput. Phys., 97, pp. 53-72.*

[69] **TORO, E.F.,** (1991), Viscous Flux Limiters, *Proceedings of the Ninth GAMM-Conference on Numerical Methods in Fluid Mechanics, Lausanne.*

[70] **HARLOW, F.H. and WELCH, J.E.,** (1965), Numerical Calculation of Time-dependent Viscous Incompressible Flow of Fluid with Free Surface, *Physics of Fluids, 8, 2182-9.*

[71] **CHORIN, A.J.,** (1968), Numerical Solution of the Navier-Stokes Equations, *Mathematics of Computation, 23, 341-54.*

[72] **TEMAM, R.,** (1977), Navier-Stokes Equations, Amsterdam: North Holland Publishing Co. Thomasset, F. (1981), *Implementation of Finit Element Methods for*

Navier-Stokes Equations, Springer Series in Computational Physics, New York: Springer Verlag.

[73] **CHORIN, A.J.,** (1967), A Numerical method for Solving Incompressible Viscous Flow Problems, *J. Comput. Phys., 2, pp. 12-26.*

[74] **STEGER, J.L. and KUTLER, P.,** (1977), Implicit Finite Difference Procedures for the Computation of Vortex Wakes, *AIAA Journal, 15, 581-90.*

[75] **CHANG, J.L., KWAK, D., DAO, S.C. and ROSEN, R.,** (1985a,), A Three-dimensional Incompressible Flow Simulation Method and its Application to the Space Shuttle Main Engine - Part 1 - Laminar Flow, *AIAA 23rd Aerospace Sciences Meeting.*

[76] **CHANG, J.L., KWAK, D., DAO, S.C. and ROSEN, R.,** (1985b,), A Three-dimensional Incompressible Flow Simulation Method and its Application to the Space Shuttle Main Engine - Part 1 - Turbulent Flow, *AIAA Paper 85-1670,* AIAA 18th Fluid Dynamics, Plasmadynamics and Lasers Conference.

[77] **STRANG, G.,** (1968), On the Construction and Comparison of Difference Schemes, *SIAM J. Numer. Anal. 5, pp 506-517.*

[78] **DARLING, P.S.,** (1992), An Implementation of the Method of Artificial Compressibility Using Numerical Schemes Based on Riemann Problems, *M.sc. Thesis 1991-2,* COA, Cranfield Institute of Technology.

[79] **NASA REPORT,** (1975), Numerical Techniques for the Solution of the Driven cavity problem, *NASA SP-378.*

[80] **SHIH, T.M. and TAN, C.H.,** (1989), Effects of Grid Staggering on Numerical Schemes, *Int. J. Numer. Methods in Fluids, 9, 193-212.*

[81] **PRYRET, R. and TAYLOR, T.D.,** (1983), Computational Methods for Fluid Flow, *Springer.*

[82] **TURKEL, E.,** (1987), *J. Comp. Phys., Vol 72, 277-298.*

[83] **MAO, D.K.,** (1992), A Treatment of Discontinuities for Difference Methods, *J. Comput. Phy., 103, pp. 359-360.*

Appendix A

The 20th-Order Numerical Method

The 20th order method takes the following form

$$\begin{aligned} U_j^{n+1} &= B_0 U_j^n + B_{-10} U_{j-10}^n + B_{-9} U_{j-9}^n + B_{-8} U_{j-8}^n + B_{-7} U_{j-7}^n \\ &+ B_{-6} U_{j-6}^n + B_{-5} U_{j-5}^n + B_{-4} U_{j-4}^n + B_{-3} U_{j-3}^n + B_{-2} U_{j-2}^n \\ &+ B_{-1} U_{j-1}^n + B_1 U_{j+1}^n + B_2 U_{j+2}^n + B_3 U_{j+3}^n + B_4 U_{j+4}^n \\ &+ B_5 U_{j+5}^n + B_6 U_{j+6}^n + B_7 U_{j+7}^n + B_8 U_{j+8}^n + B_9 U_{j+9}^n \\ &+ B_{10} U_{j+10}^n \end{aligned} \tag{A.1}$$

where the coefficients obtained by using a computational program are as follows.

$$\begin{aligned} B_{-10} &= -5.4125441274697011E-07\ C - 5.4125442193536856E-08\ C^2 \\ &+ 8.3340607714097 44E-07\ C^3 + 8.3340608286850486E-08\ C^4 \\ &- 3.4882441781009 31E-07\ C^5 - 3.4882441891155766E-08\ C^6 \\ &+ 6.2018699671233378E-08\ C^7 + 6.2018699781630719E-09\ C^8 \\ &- 5.6212428632890577E-09\ C^9 - 5.6212428695281 8E-10\ C^{10} \\ &+ 2.8337919393891736E-10\ C^{11} + 2.8337919414809486E-11\ C^{12} \\ &- 8.2180457465338512E-12\ C^{13} - 8.2180457507619695E-13\ C^{14} \\ &+ 1.3541852441707 44E-13\ C^{15} + 1.3541852446737389E-14\ C^{16} \\ &- 1.1714405226362 76E-15\ C^{17} - 1.1714405229588017E-16\ C^{18} \end{aligned}$$

$$+ 4.1103176232824669E-18\ C^{19} + 4.1103176241380932E-19\ C^{20}$$

$$\begin{aligned} B_{-9} = {} & 1.2027875799663232E-05\ C + 1.3364306711344411E-06\ C^2 \\ & - 1.8491921508798121E-05\ C^3 - 2.0546579573255938E-06\ C^4 \\ & + 7.7085597515460868E-06\ C^5 + 8.5650664136481394E-07\ C^6 \\ & - 1.3605424588926793E-06\ C^7 - 1.5117138455282181E-07\ C^8 \\ & + 1.2190162084810 73E-07\ C^9 + 1.3544624551725358E-08\ C^{10} \\ & - 6.0415222193403872E-09\ C^{11} - 6.7128024702854551E-10\ C^{12} \\ & + 1.7100969895060985E-10\ C^{13} + 1.9001077669921326E-11\ C^{14} \\ & - 2.7243020794222938E-12\ C^{15} - 3.0270023115029691E-13\ C^{16} \\ & + 2.2491658034449778E-14\ C^{17} + 2.4990731155980741E-15\ C^{18} \\ & - 7.3985717218632879E-17\ C^{19} - 8.2206352482552116E-18\ C^{20} \end{aligned}$$

$$\begin{aligned} B_{-8} = {} & -1.2854792258442681E-04\ C - 1.6068490601938150E-05\ C^2 \\ & + 1.9721086119309995E-04\ C^3 + 2.4651357766736245E-05\ C^4 \\ & - 8.1743718940279278E-05\ C^5 - 1.0217964890385482E-05\ C^6 \\ & + 1.4280653553870 14E-05\ C^7 + 1.7850816965332447E-06\ C^8 \\ & - 1.2592043798505395E-06\ C^9 - 1.5740054761137869E-07\ C^{10} \\ & + 6.0977941920976703E-08\ C^{11} + 7.6222427444841 52E-09\ C^{12} \\ & - 1.6720311077765168E-09\ C^{13} - 2.0900388856030767E-10\ C^{14} \\ & + 2.5554272136247108E-11\ C^{15} + 3.1942840180820 11E-12\ C^{16} \\ & - 2.0055061746993 82E-13\ C^{17} - 2.5068827190492179E-14\ C^{18} \\ & + 6.2476827872381071E-16\ C^{19} + 7.8096034858409144E-17\ C^{20} \end{aligned}$$

$$\begin{aligned} B_{-7} = {} & 8.8147147022441235E-04\ C + 1.2592449720362899E-04\ C^2 \\ & - 1.3480868260251767E-03\ C^3 - 1.9258383301538196E-04\ C^4 \\ & + 5.5414611748462071E-04\ C^5 + 7.9163731210419160E-05\ C^6 \\ & - 9.5373632669074515E-05\ C^7 - 1.3624804681203933E-05\ C^8 \\ & + 8.2182136755446 77E-06\ C^9 + 1.1740305258767458E-06\ C^{10} \\ & - 3.8533056741743935E-07\ C^{11} - 5.5047223943406495E-08\ C^{12} \\ & + 1.0134817956397296E-08\ C^{13} + 1.4478311371637456E-09\ C^{14} \end{aligned}$$

$$
\begin{aligned}
&- 1.4754246524325741E-10\,C^{15} - 2.107749504109896 4E-11\,C^{16}\\
&+ 1.1020912436507576E-12\,C^{17} + 1.5744160627642396E-13\,C^{18}\\
&- 3.2800334632538536E-15\,C^{19} - 4.6857620914379306E-16\,C^{20}
\end{aligned}
$$

$$
\begin{aligned}
B_{-6} = \; & -4.3706293678705118E-03\,C - 7.2843823472016191E-04\,C^2\\
&+ 6.6520539913242586E-03\,C^3 + 1.1086756682913929E-03\,C^4\\
&- 2.6992754360052182E-03\,C^5 - 4.4987923993807736E-04\,C^6\\
&+ 4.5398869824749103E-04\,C^7 + 7.5664783101954 85E-05\,C^8\\
&- 3.7788748938689926E-05\,C^9 - 6.2981248265185162E-06\,C^{10}\\
&+ 1.6925148814571187E-06\,C^{11} + 2.8208581368916746E-07\,C^{12}\\
&- 4.2229287043591243E-08\,C^{13} - 7.0382145095313115E-09\,C^{14}\\
&+ 5.8407602736300839E-10\,C^{15} + 9.7346004587333441E-11\,C^{16}\\
&- 4.1700939722246099E-12\,C^{17} - 6.9501566220910104E-13\,C^{18}\\
&+ 1.1948693330177068E-14\,C^{19} + 1.9914488888179928E-15\,C^{20}
\end{aligned}
$$

$$
\begin{aligned}
B_{-5} = \; & 1.6783216790265943E-02\,C + 3.3566433739730434E-03\,C^2\\
&- 2.5338759119334336E-02\,C^3 - 5.0677518335719013E-03\,C^4\\
&+ 1.0061219734637984E-02\,C^5 + 2.0122439488629 76E-03\,C^6\\
&- 1.6287905249829739E-03\,C^7 - 3.2575810519266637E-04\,C^8\\
&+ 1.2838263606553 36E-04\,C^9 + 2.5676527224143184E-05\,C^{10}\\
&- 5.3947515886538981E-06\,C^{11} - 1.0789503180983456E-06\,C^{12}\\
&+ 1.2690531937984211E-07\,C^{13} + 2.5381063883369351E-08\,C^{14}\\
&- 1.6710964543258815E-09\,C^{15} - 3.3421929095318834E-10\,C^{16}\\
&+ 1.1470745596579926E-11\,C^{17} + 2.2941491198815431E-12\,C^{18}\\
&- 3.1863182212735747E-14\,C^{19} - 6.3726364440528092E-15\,C^{20}
\end{aligned}
$$

$$
\begin{aligned}
B_{-4} = \; & -5.2447552382367639E-02\,C - 1.3111888163451239E-02\,C^2\\
&+ 7.8003552315233024E-02\,C^3 + 1.9500888102217392E-02\,C^4\\
&- 2.9733434540143964E-02\,C^5 - 7.4333586397198753E-03\,C^6\\
&+ 4.4892831985170432E-03\,C^7 + 1.1223208001032861E-03\,C^8\\
&- 3.2421435340729 9E-04\,C^9 - 8.1053588378368919E-05\,C^{10}
\end{aligned}
$$

$$
\begin{aligned}
&+ 1.264303113397633 2E-05\, C^{11} + 3.160757784373409 4E-06\, C^{12} \\
&- 2.807336257411514 1E-07\, C^{13} - 7.018340645293100 7E-08\, C^{14} \\
&+ 3.539489732800221E-09\, C^{15} + 8.848724334095519 8E-10\, C^{16} \\
&- 2.351502847218736 3E-11\, C^{17} - 5.878757119392987 6E-12\, C^{18} \\
&+ 6.372636442317502 5E-14\, C^{19} + 1.593159110938033 1E-14\, C^{20}
\end{aligned}
$$

$$
\begin{aligned}
B_{-3} = \; & 0.139860139932248 9\, C + 4.662004667119901 8E-02\, C^2 \\
&- 0.201210716043007 4\, C^3 - 6.707023872630438 2E-02\, C^4 \\
&+ 6.993300459807978 7E-02\, C^5 + 2.331100154196980 4E-02\, C^6 \\
&- 9.156660441459236E-03\, C^7 - 3.052220148102620 2E-03\, C^8 \\
&+ 5.953787597353935 5E-04\, C^9 + 1.984595866319347 1E-04\, C^{10} \\
&- 2.159727972875519 8E-05\, C^{11} - 7.199093244698960 5E-06\, C^{12} \\
&+ 4.560971098645676E-07\, C^{13} + 1.520323699908324 2E-07\, C^{14} \\
&- 5.550120256401079 6E-09\, C^{15} - 1.850040085897812 1E-09\, C^{16} \\
&+ 3.594166953249646 1E-11\, C^{17} + 1.198055651352440 E-11\, C^{18} \\
&- 9.558954662846919 4E-14\, C^{19} - 3.186318221699014 9E-14\, C^{20}
\end{aligned}
$$

$$
\begin{aligned}
B_{-2} = \; & -0.340909090774096 2\, C - 0.170454545545684 0\, C^2 \\
&+ 0.443102635528962 7\, C^3 + 0.221551317843336 0\, C^4 \\
&- 0.114180608750391 3\, C^5 - 5.709030439213017E-02\, C^6 \\
&+ 1.271439638198280 9E-02\, C^7 + 6.357198192775930 3E-03\, C^8 \\
&- 7.525655006654334 4E-04\, C^9 - 3.762827504347923E-04\, C^{10} \\
&+ 2.575040825035399 3E-05\, C^{11} + 1.287520412861062 9E-05\, C^{12} \\
&- 5.233979019443609E-07\, C^{13} - 2.616989510420843 3E-07\, C^{14} \\
&+ 6.205243213563923E-09\, C^{15} + 3.102621607623997 8E-09\, C^{16} \\
&- 3.945458536665811 5E-11\, C^{17} - 1.972729268881239 9E-11\, C^{18} \\
&+ 1.035553421686128 2E-13\, C^{19} + 5.177767109908796 4E-14\, C^{20}
\end{aligned}
$$

$$
\begin{aligned}
B_{-1} = \; & 0.909090908934087 1\, C + 0.909090909158730 3\, C^2 \\
&- 0.499788846365348\, C^3 - 0.499788846531162 8\, C^4 \\
&+ 0.100094533932304 1\, C^5 + 0.100094533971566 6\, C^6
\end{aligned}
$$

$$
\begin{aligned}
&- 9.9309289012765676E-03\ C^7 \ - \ 9.9309289056588156E-03\ C^8 \\
&+ 5.5217668611212 7E-04\ C^9 \ + \ 5.5217668637241141E-04\ C^{10} \\
&- 1.8201402847760972E-05\ C^{11} \ - \ 1.8201402856741592E-05\ C^{12} \\
&+ 3.6126371888276745E-07\ C^{13} \ + \ 3.6126371906854591E-07\ C^{14} \\
&- 4.2155308676830449E-09\ C^{15} \ - \ 4.2155308699409659E-09\ C^{16} \\
&+ 3.6510167586153395E-11\ C^{17} \ + \ 2.6510167600918578E-11\ C^{18} \\
&- 6.9036894753918626E-14\ C^{19} \ - \ 6.9036894793773 23E-14\ C^{20}
\end{aligned}
$$

$$
\begin{aligned}
B_1 \ = \ & -0.9090909089982441\ C \ + \ 0.9090909090107639\ C^2 \\
&+ 0.4997888467038099\ C^3 \ - \ 0.4997888464761192\ C^4 \\
&- 0.1000945340215663\ C^5 \ + \ 0.1000945339597436\ C^6 \\
&+ 9.9309289117927961E-03\ C^7 \ - \ 9.9309289044145661E-03\ C^8 \\
&- 5.5217668675993216E-04\ C^9 \ + \ 5.5217668630038223E-04\ C^{10} \\
&+ 1.8201402870649327E-05\ C^{11} \ - \ 1.8201402854301842E-05\ C^{12} \\
&- 3.6126371936227 73E-07\ C^{13} \ + 3.6126371901919222E-07\ C^{14} \\
&+ 4.2155308735369533E-09\ C^{15} \ - \ 4.2155308693570004E-09\ C^{16} \\
&- 2.6510167624410223E-11\ C^{17} \ + \ 2.6510167597207196E-11\ C^{18} \\
&+ 6.9036894856845310E-14\ C^{19} \ - \ 6.9036894784028248E-14\ C^{20}
\end{aligned}
$$

$$
\begin{aligned}
B_2 \ = \ & 0.3409090911590382\ C \ - \ 0.1704545454095551\ C^2 \\
&- 0.4431026357790551\ C^3 \ + \ 0.2215513177642915\ C^4 \\
&+ 0.1141806088171811\ C^5 \ - \ 5.7090304375038911E-02\ C^6 \\
&- 1.2714396389902835E-02\ C^7 \ + \ 6.3571981909751434E-03\ C^8 \\
&+ 7.5256550115547 71E-04\ C^9 \ - \ 3.7628275033047855E-04\ C^{10} \\
&- 2.5750408267719344E-05\ C^{11} \ + \ 1.2875204125074939\ C^{12} \\
&+ 5.2339790230882308E-07\ C^{13} \ - \ 2.6169895097051142E-07\ C^{14} \\
&- 6.2052432180178555E-09\ C^{15} \ + \ 3.1026216067765952E-09\ C^{16} \\
&+ 3.9454585395780889E-11\ C^{17} \ - \ 1.9727292683423773E-11\ C^{18} \\
&- 1.0355534224698324E-13\ C^{19} \ + \ 5.1777671084932366E-14\ C^{20}
\end{aligned}
$$

$$
B_3 \ = \ -0.1398601398680919\ C \ + \ 4.6620046550289472E-02\ C^2
$$

$$
\begin{aligned}
&+ 0.2012107161932965\,C^3 - 6.7070238657622 28E-02\,C^4 \\
&- 6.9933004638802393E-02\,C^5 + 2.3311001527102117E-02\,C^6 \\
&+ 9.1566604463335817E-03\,C^7 - 3.0522201465355389E-03\,C^8 \\
&- 5.9537876003893763E-04\,C^9 + 1.9845958654107830E-04\,C^{10} \\
&+ 2.1597279739557117E-05\,C^{11} - 7.1990932416161747E-06\,C^{12} \\
&- 4.5609711009187323E-07\,C^{13} + 1.5203236992836355E-07\,C^{14} \\
&+ 5.5501202591831552E-09\,C^{15} - 1.8500400851574985E-09\,C^{16} \\
&- 3.5941669550703171E-11\,C^{17} + 1.1980556508912785E-11\,C^{18} \\
&+ 9.5589546677486802E-14\,C^{19} - 3.1863182204603885E-14\,C^{20}
\end{aligned}
$$

$$
\begin{aligned}
B_4 = \;& 5.2447552542760158E-02\,C - 1.3111888087354322E-02\,C^2 \\
&- 7.8003552387288705E-02\,C^3 + 1.9500888059841 91E-02\,C^4 \\
&+ 2.9733434559988135E-02\,C^5 - 7.4333586305919156E-03\,C^6 \\
&- 4.4892832009135923E-03\,C^7 + 1.1223207991417077E-03\,C^8 \\
&+ 3.2421435355727 75E-04\,C^9 - 8.1053588322611519E-05\,C^{10} \\
&- 1.2643031139325643E-05\,C^{11} + 3.1607577824812954E-06\,C^{12} \\
&+ 2.8073362585376238E-07\,C^{13} - 7.0183406414589029E-08\,C^{14} \\
&- 3.5394897341775433E-09\,C^{15} + 8.8487243295521279E-10\,C^{16} \\
&+ 2.3515028481189938E-11\,C^{17} - 5.8787571165019582E-12\,C^{18} \\
&- 6.3726364447379082E-14\,C^{19} + 1.5931591101781878E-14\,C^{20}
\end{aligned}
$$

$$
\begin{aligned}
B_5 = \;& -1.6783216790265943E-02\,C + 3.3566433397294302E-03\,C^2 \\
&+ 2.5338759146446066E-02\,C^3 - 5.0677518143916545E-03\,C^4 \\
&- 1.0061219742240127E-02\,C^5 + 2.0122439447458 93E-03\,C^6 \\
&+ 1.6287905259103595E-03\,C^7 - 3.2575810475890017E-04\,C^8 \\
&- 1.2838263612394298E-04\,C^9 + 2.5676527198963036E-05\,C^{10} \\
&+ 5.3947515907457231E-06\,C^{11} - 1.1789503172426883E-06\,C^{12} \\
&- 1.2690531942398 74E-07\,C^{13} + 2.5381063866006513E-08\,C^{14} \\
&+ 1.6710964548665981E-09\,C^{15} - 3.3421929074718 48E-10\,C^{16} \\
&- 1.1470745600117163E-11\,C^{17} + 2.2941491185692477E-12\,C^{18} \\
&+ 3.1863182222250577E-14\,C^{19} - 6.3726364406004012E-15\,C^{20}
\end{aligned}
$$

$$
\begin{aligned}
B_6 \;=\;& 4.37062937989995E-03\,C \;-\; 7.28438223517004 58E-04\,C^2 \\
& - 6.6520539990204087E-03\,C^3 \;+\; 1.1086756619139275E-03\,C^4 \\
& + 2.699275438196650 1E-03\,C^5 \;-\; 4.4987923857653351E-04\,C^6 \\
& - 4.5398869851632942E-04\,C^7 \;+\; 7.5664782958773701E-05\,C^8 \\
& + 3.778874895566 16E-05\,C^9 \;-\; 6.2981248182117565E-06\,C^{10} \\
& - 1.6925148820651 63E-06\,C^{11} \;+\; 2.8208581340692872E-07\,C^{12} \\
& + 4.2229287056413 8E-08\,C^{13} \;-\; 7.0382145038040535E-09\,C^{14} \\
& - 5.8407602751987296E-10\,C^{15} \;+\; 9.7346004519377128E-11\,C^{16} \\
& + 4.1700939732493913E-12\,C^{17} \;-\; 6.9501566177616943E-13\,C^{18} \\
& - 1.1948693332930086E-14\,C^{19} \;+\; 1.0014488876789506E-15\,C^{20}
\end{aligned}
$$

$$
\begin{aligned}
B_7 \;=\;& -8.8147147022441235E-04\,C \;+\; 1.2592449419145932E-04\,C^2 \\
& + 1.3480868276531 46E-03\,C^3 \;-\; 1.9258383147415187E-04\,C^4 \\
& - 5.5414611795211459E-04\,C^5 \;+\; 7.9163730883412 4E-05\,C^6 \\
& + 9.5373632726828108E-05\,C^7 \;-\; 1.3624804646819964E-05\,C^8 \\
& - 8.2182136792058245E-06\,C^9 \;+\; 1.1740305238792094E-06\,C^{10} \\
& + 3.8533056754888451E-07\,C^{11} \;-\; 5.5047223875425271E-08\,C^{12} \\
& - 1.0134817959171436E-08\,C^{13} \;+\; 1.4478311357821706E-09\,C^{14} \\
& + 1.4754246527719211E-10\,C^{15} \;-\; 2.1077495024685307E-11\,C^{16} \\
& - 1.1020912438723225E-12\,C^{17} \;+\; 1.5744160617175219E-13\,C^{18} \\
& + 3.2800334638485865E-15\,C^{19} \;-\; 4.6857620886819089E-16\,C^{20}
\end{aligned}
$$

$$
\begin{aligned}
B_8 \;=\;& 1.2854792233381353E-04\,C \;-\; 1.6068490020642247E-05\,C^2 \\
& - 1.9721086142894054E-04\,C^3 \;+\; 2.4651357511000552E-05\,C^4 \\
& + 8.1743719009019 58E-05\,C^5 \;-\; 1.0217964836322332E-05\,C^6 \\
& - 1.4280653562422396E-05\,C^7 \;+\; 1.7850816908452 2E-06\,C^8 \\
& + 1.2592043803954657E-06\,C^9 \;-\; 1.5740054728028971E-07\,C^{10} \\
& - 6.0977941940620429E-08\,C^{11} \;+\; 7.6222427331900794E-09\,C^{12} \\
& + 1.6720311081924454E-09\,C^{13} \;-\; 2.0900388833025625E-10\,C^{14} \\
& - 2.5554272141348674E-11\,C^{15} \;+\; 3.1942840153432374E-12\,C^{16} \\
& + 2.0055061750332314E-13\,C^{17} \;-\; 2.5068827172994957E-14\,C^{18} \\
& - 6.2476827881359847E-16\,C^{19} \;+\; 7.8096034812267166E-17\,C^{20}
\end{aligned}
$$

$$
\begin{aligned}
B_9 \;=\; & -1.202787583098989E-05\,C \;+\; 1.336430620353620 1E-06\,C^2 \\
& +\; 1.849192153014139E-05\,C^3 \;-\; 2.054657931070433 7E-06\,C^4 \\
& -\; 7.708559757771679E-06\,C^5 \;+\; 8.565066358162 45E-07\,C^6 \\
& +\; 1.360542459667721 5E-06\,C^7 \;-\; 1.511713839685359 2E-07\,C^8 \\
& -\; 1.219016208973139 6E-07\,C^9 \;+\; 1.354462451768992 5E-08\,C^{10} \\
& +\; 6.041522221103627 7E-09\,C^{11} \;-\; 6.712802458673577 4E-10\,C^{12} \\
& -\; 1.710096989876961E-10\,C^{13} \;+\; 1.900107764627499 5E-11\,C^{14} \\
& +\; 2.724302079874297 5E-12\,C^{15} \;-\; 3.027002308689194 4E-13\,C^{16} \\
& -\; 2.249165803739125 1E-14\,C^{17} \;+\; 2.499073113801424 1E-15\,C^{18} \\
& +\; 7.398571722650669 6E-17\,C^{19} \;-\; 8.220635243519829E-18\,C^{20}
\end{aligned}
$$

$$
\begin{aligned}
B_{10} \;=\; & 5.412544117680119 9E-07\,C \;-\; 5.412543987124321 4E-08\,C^2 \\
& -\; 8.334060780487603 6E-07\,C^3 \;+\; 8.334060701484447 3E-08\,C^4 \\
& +\; 3.488244180760358 3E-07\,C^5 \;-\; 3.488244162312832 3E-08\,C^6 \\
& -\; 6.201869970452416 8E-08\,C^7 \;+\; 6.201869949947851 8E-09\,C^8 \\
& +\; 5.621242865414646 4E-09\,C^9 \;-\; 5.621242853075977 4E-10\,C^{10} \\
& -\; 2.833791940155249 3E-10\,C^{11} \;+\; 2.833791935858306E-11\,C^{12} \\
& +\; 8.218045748154272 2E-12\,C^{13} \;-\; 8.218045739289542 9E-13\,C^{14} \\
& -\; 1.354185244369300 2E-13\,C^{15} \;+\; 1.254185243305919 4E-14\,C^{16} \\
& +\; 1.171440522766124 3E-15\,C^{17} \;-\; 1.171440522083842 8E-16\,C^{18} \\
& -\; 4.110317623631571E-18\,C^{19} \;+\; 4.110317621828286 9E-19\,C^{20}
\end{aligned}
$$

$$
\begin{aligned}
B_0 \;=\; & 1 \;+\; 9.643184E-09\,C \;-\; 1.549768\,C^2 \;-\; 4.8558619E-09\,C^3 \\
& +\; 0.6598717\,C^4 \;+\; 2.192701E-10\,C^5 \;-\; 0.121028\,C^6 \\
& +\; 3.0618016E-10\,C^7 \;+\; 1.1531415E-02\,C^8 \;+\; 1.6614871E-11C^9 \\
& -\; 6.2741595E-04\,C^{10} \;-\; 4.3139212E-13\,C^{11} \;+\; 2.0418935E-05C^{12} \\
& +\; 2.4922193E-14\,C^{13} \;-\; 4.0202718E-07\,C^{14} \;-\; 1.3142628E-16C^{15} \\
& +\; 4.6662447E-09\,C^{16} \;+\; 3.0843404E-19\,C^{17} \;-\; 2.9237123E-11C^{18} \\
& -\; 7.3362479E-22\,C^{19} \;+\; 7.5940576E-14\,C^{20}
\end{aligned}
$$

where, C is the CFL number.

The amplification factor of the method is

$$\begin{aligned}\lambda \;=\; & 1 \;-\; 2\,(-2.1820901E-08\,C \;+\; 1.91839\,C^2 \;+\; 2.2592523E-08C^3 \\ & -\; 1.144243\,C^4 \;-\; 6.8021899E-09\,C^5 \;+\; 0.2509956\,C^6 \\ & +\; 1.1990592E-09\,C^7 \;-\; 2.6645366E-02\,C^8 \;+\; 4.4792958E-11C^9 \\ & +\; 1.5550008E-03\,C^{10} \;+\; 2.3386265E-13\,C^{11} \;-\; 5.3070333E-05C^{12} \\ & -\; 1.5452447E-14\,C^{13} \;+\; 1.0802879E-06\,C^{14} \;+\; 4.9565642E-16C^{15} \\ & -\; 1.2842341E-08\,C^{16} \;-\; 4.3901846E-18\,C^{17} \;+\; 8.1889627E-11C^{18} \\ & +\; 4.1853998E-21\,C^{19} \;-\; 2.1549903E-13\,C^{20}) \end{aligned} \tag{A.2}$$